An Assessment of Different Optimisation Schemes for Hybridising a Battery Electric Vehicle with a Supercapacitor Pack

Rebecca C. Carter

Submitted for the Degree

of

Doctor of Philosophy

Institute for Energy and Environment

Department of Electronic and Electrical Engineering

University of Strathclyde

Glasgow, G1 1XW

United Kingdom

2010

Abstract

Electric vehicles offer an opportunity to greatly reduce the air pollution caused by the transport sector in the UK. However, uptake of electric vehicles is limited, largely due to the limited driving range and the expense of replacing aged batteries. This thesis investigates the possibility of addressing these limitations by hybridising battery-powered vehicles with supercapacitors.

A methodology for comparing optimisation strategies for a battery/supercapacitor hybrid vehicle is presented. Such a comparison between optimisation strategies is novel to the field of battery/supercapacitor electric vehicle research. Two optimisation strategies are investigated: one to maximise the efficiency of the vehicle and hence increase its range, and the second to minimise peak battery currents, with the goal of increasing battery life. This analysis demonstrates that the most effective hybridisation strategy for the Strathclyde vehicle is to minimise peak battery currents, and a method for determining the optimal supercapacitor pack size for this purpose is demonstrated.

The optimisation strategies are demonstrated using a novel power flow control strategy, developed to be 'tuneable' to allow the investigation of the different options for optimisation, e.g. increased yield (km travelled per kWh used) or reduced peak battery currents. The simulations of this control strategy demonstrate that the optimal points for maximising yield and for minimising peak battery currents are typically not the same, and hence that the choice of optimisation strategy has a significant impact on the effectiveness of a hybrid vehicle.

A novel battery model for use in the simulations of the hybrid system is also presented. This model was created to provide an accurate simulation of the Strathclyde electric vehicle's battery pack while remaining simple to implement within the framework of existing vehicle modelling software, i.e. ADVISOR. A verification of the model is presented, and the novel battery model is shown to offer improved performance to that of the standard ADVISOR battery models.

Acknowledgements

I would like to thank my supervisor, Dr Andy Cruden, for giving me the chance to work on this project, and for his guidance and support throughout. This has been a fantastic start to my research career, and I am truly grateful for this opportunity.

I would also like to thank the rest of the Supergen Energy Storage Consortium, especially my second supervisor Prof Peter Hall, and my colleagues Dr Mojtaba Mirzaean and soon-to-be Dr Fiona Sillars.

Thank you to Mr Bob Baird, for his assistance in all things Cobra-related. Thank you to everyone who has supported me in this work with advice, loans of equipment and assistance with recalcitrant computers.

Many thanks and hugs to my friends who have supported me in this venture, and in particular the ever-patient David Dolliver, who has tolerated epic levels of whingeing and who is also very good at cleaning up messy diagrams.

Most of all, thank you to my husband Greg. None of this would matter without you.

List of Symbols

Symbol	Definition	Units
a	Acceleration	m/s^2
C	Capacitance	F
C1, C2	Smoothing capacitances in a half-bridge converter	F
C_o	Parallel capacitor in a Randle's Cell	F
E	Energy	J
I	Current	A
i_{Co}	Current in parallel capacitor in a Randle's Cell	A
i_{Ro}	Current in parallel resistor in a Randle's Cell	A
N	Number of batteries in a pack	
m	Mass	kg
P	Power	W
$P_{droploss}$	Power losses in a battery due to the V_{drop} term	W
P_{loss}	Power losses in a battery	W
R	Resistance	Ω
R_{app}	Apparent internal resistance of a battery, following Ohm's Law	Ω
R_o	Parallel resistor in a Randle's Cell	Ω
s	Speed	mph
t	Time	s
v	Velocity	m/s
V	Voltage	V
V1, V2	Measured voltages on either side of a DC/DC converter	V
V_{Co}	Voltage across parallel capacitor in a Randle's Cell	V
V_{drop}	Constant voltage drop in Cobra batter model	V
$V_{initial}$	Initial voltage on a capacitor	V
V_{meas}	Voltage measured at the terminals of an energy storage pack	V
V_{OC}	Open Circuit Voltage	V
V_{Ro}	Voltage across parallel resistor in a Randle's Cell	V

δ	Duty cycle	%
η	Efficiency	%
τ	Time Constant	s

List of Abbreviations

Abbreviation	Definition
ADVISOR	Advanced Vehicle Simulator
ANN	Artificial Neural Net
Batt.	Battery
cRIO	Compact Reconfigurable Input/Output Device
ECE	Economic Commission for Europe
EV	Electric Vehicle
FIFO	First In, First Out
FPGA	Field Programmable Gate Array
FTV	Frequency to Voltage
HEV	Hybrid Electric Vehicle
ICE	Internal Combustion Engine
KE	Kinetic Energy
MTBF	Mean Time Between Failures
NREL	National Renewable Energy Laboratories
PCh	Charging Power from Cobra Batteries to Supercapacitors
PE	Power Electronics
PMin	Minimum Power Supplied by Cobra Batteries
PReq	Power Required by Cobra Motor
Regen.	Regeneration
RT	Real Time
S-Caps	Supercapacitors
SOC	State of Charge as a Percentage of Energy
SOC_V	State of Charge as a Percentage of Voltage
SOH	State of Health
VRLA	Valve-Regulated Lead Acid

Table of Contents

List of Figures

List of Tables

1 Introduction

1.1 Electric Vehicles and the Environment

Road transport in the UK accounts for a substantial percentage of the country's emissions of greenhouse gases and other pollutants. For example, in 2006 road transport was responsible for 21% of carbon dioxide emissions and was one of the largest sources of particulate matter [1]. Furthermore, carbon emissions from vehicles have remained relatively constant over the past fifteen years, as illustrated in Figure 1.1, in spite of the fact that most other pollutants have dramatically decreased. Carbon dioxide pollution is inherent to traditional vehicles, as it is a natural by-product of fossil fuel combustion [2]. New technology is necessary to reduce carbon emissions; this naturally leads one to consider electric vehicles, which have zero emissions at point of use and which could be recharged by renewable electricity sources.

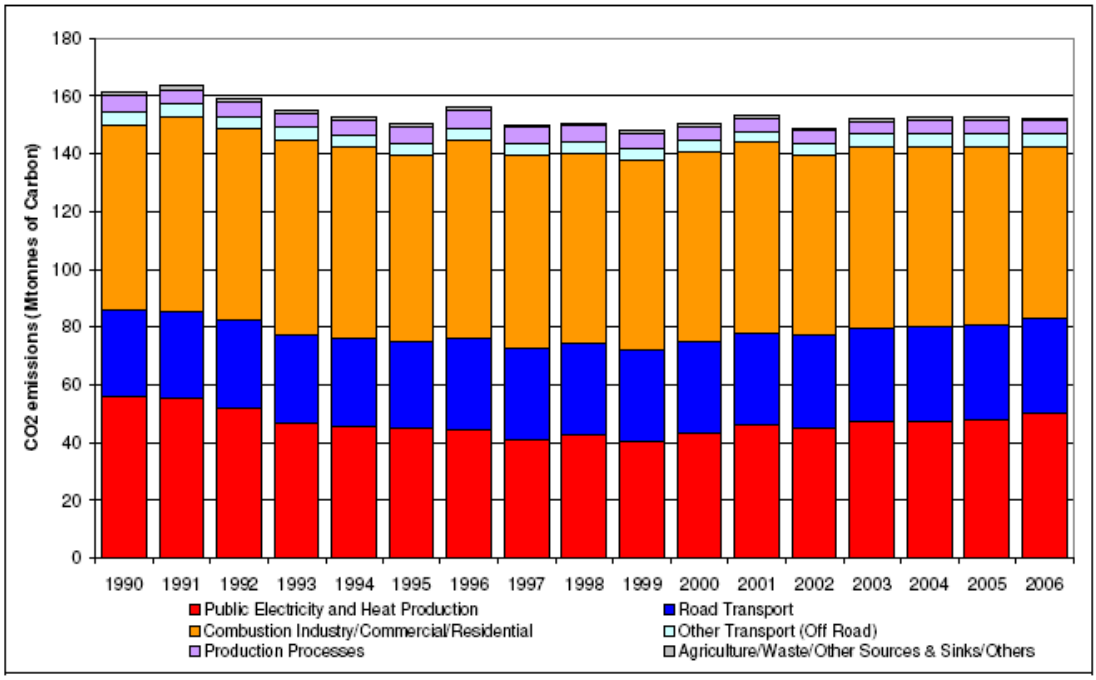

Figure 1.1: CO_2 emissions in the UK from different sectors since 1990 [1].

Electric vehicles (EVs) can also provide substantially higher well-to-wheel efficiencies than are available from internal combustion engine (ICE) vehicles. Calculations by the United States Department of Energy [3] give a well-to-wheel

efficiency for light vehicles powered by petrol engines of just 11.4%, while diesel vehicles fare slightly better at 15.6%. Most of the losses occur due to the inefficiency of the combustion engines themselves, with a fuel tank-to-wheel efficiency of 14.1% for the petrol car and 18.5% for the diesel. By contrast, batteries and electric motors are highly efficient. Estimates of the overall efficiency of battery-powered vehicles range from 70% to 86% [4-6], while the efficiency of transmission and recharging is estimated to be between 80% and 92% [4-6]. Using the most conservative of these estimates gives a plant-to-wheel efficiency of 56%. This shows that EVs have the potential to far outperform the total efficiency of ICE vehicles, depending on the electricity source used to recharge them. The largest fuel source for electricity generation in the UK is natural gas; in 2007 it supplied 43% of the country's electricity [7]. The efficiency of obtaining electricity from natural gas is approximately 55% [4], which gives the electric vehicle a well-to-wheel efficiency of 30.8% - approximately double the efficiency of an ICE vehicle. Clearly, battery-powered electric vehicles have a lot to offer.

1.2 The Current Electric Vehicle Market

A number of electric vehicles are already available for purchase, but their uptake has been hindered by the necessity of trading vehicle performance for affordability, and by the limited lifespan of the battery packs. For example, the high performance Tesla Roadster could be purchased in America for a base price of $109,000 in early 2009, equivalent to about £77,000 [8]. The manufacturer advertises a driving range of 220 miles per charge and a top speed of 125mph. By contrast, the Indian electric vehicle REVA, which is available in the UK under the name 'G-Wiz', cost a much more affordable £8000 [9]. This car has a peak range of 48 miles and a top speed of 50mph. The substantial discrepancy in price and performance between the Tesla and the G-Wiz is largely due to the expense of installing a large battery pack that features both high power capability and high energy storage. The Tesla Roadster features a lithium-ion battery pack with a nominal voltage of 375V, a capacity of 53kWh and a peak power capability of 200kW [10], while the G-Wiz uses flooded lead acid batteries (as of 2010 a lithium-ion version is also available at twice the original price – technical details of this pack are not known) with a nominal voltage of 48V and a capacity of 9.6kWh, while the G-Wiz motor is rated for just 6kW [9].

It is worth noting that both cars compare poorly with ICE vehicles of similar types. For example, a person looking for a two-seater city vehicle such as the G-Wiz might instead choose a Smart ForTwo, which has a base price of just £7000, a top speed of 90mph and a range of approximately 500 miles in urban conditions [11], plus like all ICE vehicles it has the ability to be easily refuelled. A person in the market for a sports car might choose a Lotus Elise, on which the chassis of the Tesla Roadster was based. The Elise [12] has a base cost of $46,000, a range of 220-285 miles and a top speed of at least 150mph. The 0 to 60mph time is 4.9s for the Elise, not quite as impressive as the Roadster's 3.9s [8], but upgrading to the Lotus Exige 240 will give a 4.0s 0 to 60mph time, and at $66,000, its base price will still be less than 2/3 the price of the Roadster.

Electric vehicles also suffer from the limited lifespan of the batteries. The lead-acid batteries of the G-Wiz have an advertised battery life of two to three years [9]. The pack costs £1895 to replace, and it is worth noting that the flooded-type batteries are cheaper than modern valve-regulated lead acid (VRLA) batteries and require regular topping up with de-ionised water. The Tesla Roadster's lithium ion batteries are expected to last somewhat longer, with an expected life of five or seven years, depending on which part of the website one reads [8]. In 2009 Tesla Motors announced that the battery pack cost approximately $36,000, or about £25,500. The company encouraged customers to buy the replacement pack at the time of purchasing the vehicle, in anticipation of the batteries' failure some years down the line, for a reduced price of $12,000.

Some electric car companies have addressed the battery life issue by leasing the batteries rather than selling them as part of the car. While this would increase the total cost for the customer, it would spread the cost out over several years in a predictable fashion. For example, the Norwegian electric car company Think suggested in 2007 that their vehicle would cost $15,000-$17,000 to buy, with the battery leased at $100-$200 each month [13]. Nissan is considering a similar scheme for its 2012 plug-in hybrid vehicles [14]. When the batteries become too old to be

used in electric vehicles, they could be sold for continued use in stationary applications [13, 14] or recycled, potentially at a profit [15].

Another option for battery leasing is to have a battery pack which when discharged can be easily swapped out for a freshly charged pack. This could be performed at a station equivalent to today's petrol stations. Some such stations, built by the company Better Place, are currently under construction in Hawaii as part of an ambitious plan to make the islands independent of foreign oil [16]. For this to work on a large scale, car companies will have to agree on a standardised battery pack. At present, the Better Place stations can service only two makes of electric vehicle [16].

As these examples illustrate, currently available electric vehicles offer an uneconomic cost/performance trade-off. Although electric vehicles offer the possibility of cheaper refuelling (the G-Wiz is estimated to cost just 1p per mile to refuel [9]) this is offset by the high cost of replacing the old batteries. It will be very difficult for electric vehicles to break into the mass market without further technological improvements that offer better value for money.

1.3 Supercapacitors: A Potential Solution

There are a number of possible ways to address the detrimental aspects of battery electric vehicles. One option which has proved to be commercially viable is to hybridise batteries with an ICE, as in the Toyota Prius and Honda Insight [17]. The ICE provides increased range and power capability, but at the cost of continued air pollution. Another alternative is to use a fuel cell vehicle. Fuel cells have the same easy refuelling capability as do ICEs, while also creating no emissions at their point of use except for water vapour [18, 19]. However, fuel cells have a typical electric efficiency of less than 50% [18, 19], and furthermore would require an extensive hydrogen infrastructure that does not currently exist. This is a serious weakness as in the early stages of adoption, there will be nowhere to refuel the vehicles. Battery-powered vehicles may be charged from standard outlets if necessary, and while a major increase in EV usage would require upgrades to the grid, these may be performed as needed without preventing early adoption of EVs [20].

An alternative approach is to hybridise the batteries with a second energy storage device which can deliver high power, thereby improving the performance of the batteries while protecting them from damage and extending their lifespan. This is the method chosen for further examination in this thesis, with a focus on supercapacitors. These devices are a developing technology which are just beginning to emerge on the market in transport applications.

Supercapacitors are an energy storage device that can deliver very high power capability: about 10 times larger than that of batteries. Supercapacitors also have a higher energy cycle efficiency - up to 98%, [21] while lead-acid batteries typically have an efficiency of 82.5% and the much more expensive lithium ion batteries have an energy cycle efficiency up to 90% [22]. These traits allow supercapacitors to provide improved acceleration and to recapture energy from regenerative braking more efficiently. They also degrade much more slowly, and if used in an electric vehicle would have a lifetime of about 10 years [21]. However, the energy density of supercapacitors is far below that of batteries, with even the most advanced supercapacitors containing no more than 10Wh/kg [23]. This means that supercapacitors cannot be used as the sole energy storage mechanism for an electric vehicle, as the range would be unacceptably limited. A comparison of battery and supercapacitor traits is presented in Table 1.1.

Supercapacitors acting as part of a hybrid vehicle system can provide high bursts of power even when the vehicle's battery capabilities have decreased due to a low state of charge, maintaining the accelerative performance of the vehicle. Supercapacitors can also protect the batteries from high currents, which can damage them [24-26], by taking on the high power requirements of a vehicle. Therefore using supercapacitors in a hybrid system with batteries can extend the batteries' lifetime. This will be beneficial if the cost of replacing the batteries is greater than the cost of the additional supercapacitors and associated interface electronics. The greater efficiency of supercapacitors, along with their ability to accept high currents from regenerative braking, can lead to an increase in overall vehicle efficiency and thereby increase the driving range.

Table 1.1: Battery and Supercapacitor Characteristics

Type	Power Density (W/kg)	Energy Density (Wh/kg)	Eff'cy (%)	Life (cycles)	~Cost* (USD/Wh)
S-Caps	100-10k [23]	1-10 [23]	85-98 [21]	100k-500k [27]	10.3 [28]
Pb-Acid	80-300 [22]	25-30 [22]	82.5 [22]	500 [22]	0.5 [29]
NiMH	200-1500 [22]	60-70 [22]	70 [22]	1350 [22]	1.2 [29]
Li-ion	80-2000 [22]	60-150 [22]	90 [22]	1000 [22]	>3.7 [29]

Alternatively, one can attempt to preserve vehicle functionality but reduce capital costs by replacing some batteries with supercapacitors. This is possible if the number of batteries necessary to meet the vehicle's power requirements is larger than the number needed to meet its energy requirements. In this case some batteries can be replaced with supercapacitors. Again, this will be worthwhile only if the cost of adding the supercapacitor pack is lower than the cost of the batteries it is replacing.

Supercapacitors may be used as part of a battery/supercapacitor hybrid system in an electric vehicle for one or more of four possible purposes, as identified by the author:

1) to improve vehicle acceleration
2) to improve overall drive efficiency, increasing the driving range
3) to reduce lifecycle costs by extending the life of the batteries
4) to reduce capital costs by direct replacement of some batteries

This thesis will demonstrate that each of these purposes is to some extent exclusive of the others, as reported in papers by the author [30, 31].

1.4 Thesis Contributions

This research has involved the modelling, hybrid energy strategy development and scenario analysis of a battery/supercapacitor vehicle, based on a model of an existing battery-powered electric vehicle at the University of Strathclyde. This vehicle is made from an AC Cobra kit car ("the Cobra", pictured in Figure 1.2), and is a low-

* The costs given in the table should only be used for general comparisons between devices and not as a rigid indicator of price. The cost of energy storage devices is highly variable and depends not only on the specific devices (which may be specialised for some aspect of performance such as power or which may be a low-cost device with comparatively poor performance) but also on the price of materials and the overall economic climate. For example, in early 2007 a 650F Maxwell supercapacitor optimised for power cost £33.44/Wh, roughly equivalent at the time to $60.19/Wh. This is far higher than the $10.30/Wh quoted as the average for all supercapacitors on the market, including small, mass-produced devices for mobile applications. In 2009, after the credit crunch and decline of the British pound, the cost of the 650F units increased to £58.56/Wh, or about $83.13/Wh.

budget car suitable for urban commuting. It uses six 12-volt 70 Ah gel type VRLA batteries from Hawker Genesis. The Cobra runs using a 9kW liquid-cooled induction motor and has a top speed of about 40 mph, with a range of about 15 miles.

Figure 1.2: The Cobra, driven by the author and accompanied by some of the Strathclyde SUPERGEN Energy Storage Consortium members.

A model of the Cobra's energy storage system was created, based on the vehicle simulation programme ADVISOR. ADVISOR was developed by the National Renewable Energy Laboratory in Colorado and is now commercially available through AVL [32]. The author modified the standard ADVISOR battery and supercapacitor models, and inserted power electronics and power control elements, to create the new hybrid energy storage system model.

The author's final model involves three physical elements:

1) a novel battery model, which represents the vehicle's batteries with an error of less than 3%.
2) a simple supercapacitor model, which allows a wide variety of commercial supercapacitors to be modelled, as well as theoretical devices.

This model was tested and validated using commercial supercapacitors and found to have an error of less than 5%.

3) a power electronics architecture consisting of two half bridge DC/DC converters, which were simulated separately to create efficiency maps. The efficiency maps are used in the system model to allow fast, modular simulations.

These physical elements are combined with a novel power flow control strategy designed by the author to be tuneable for different optimisations.

Of the four possible purposes for hybridisation defined in section 1.3, two were selected as being suitable for the Cobra and developed by the author, specifically improving overall drive efficiency and reducing lifecycle costs. Both of these attributes are highly important to a low-budget commuter vehicle, which should have as large a range as possible given its relatively small battery pack, and which ideally would not incur additional costs due to the necessity of replacing batteries. The option to replace some batteries with supercapacitors was not investigated for the Cobra, as a reduced battery pack size would excessively limit the range. The option to increase the vehicle acceleration capability was also not investigated, as this is currently limited by the installed motor power rather than being limited by the battery capabilities. However, both costs and vehicle acceleration were considered in the analysis. The costs of the supercapacitors and the associated electronics were tracked to ensure that they were in keeping with the costs of the vehicle as a whole. The vehicle acceleration capabilities were also monitored to determine if an optimisation for efficiency or for battery life resulted in a decline in vehicle performance.

The relationship of each of these variables and the trade-offs they require has been analysed. This analysis is new to the field of battery/supercapacitor vehicle development, as past vehicles have used a single, pre-chosen optimisation strategy with no consideration or analysis of the relative merits of one optimisation strategy over another. The analysis has been used to develop a novel hybrid control strategy, which may be tuned to achieve different optimisations.

This thesis therefore presents four aspects of novelty as accomplished by the author:

1) A methodology for comparing optimisation strategies for a battery/supercapacitor hybrid vehicle. This consists of two elements: to identify the most effective optimisation strategy for an electric vehicle, and to identify the optimal supercapacitor pack size for that strategy from a range of commercially available supercapacitor packs. The optimisation methodology encompasses both technical attributes of the supercapacitors (voltage, capacitance, and internal resistance) and the cost of the supercapacitors; this ensures that the hybridisation is both technically suitable and financially viable.

2) The application of this methodology to assess the hybridisation options for the Cobra. The options to focus on maximising efficiency or to focus on minimising peak battery currents are analysed and compared, and a recommendation made for use in the Cobra, including the selection of a suitable supercapacitor pack.

3) A novel control strategy for managing the power flow in the hybrid system. This strategy was developed to allow the investigation of the different options for optimisation, and thus has been created by the author to be 'tuneable' to achieve different effects, e.g. increased yield (km travelled per kWh drawn from the energy storage) or lower peak battery currents.

4) A novel battery model for use in the simulations of the hybrid system. This model was created by the author to provide an accurate simulation of the Cobra battery pack behaviour, while remaining simple to implement within the framework of the existing vehicle simulation program, ADVISOR. The model provides improved accuracy compared to the default models provided by ADVISOR, without introducing unnecessary complexity.

1.5 Thesis Review

This work was funded by the EPSRC initiative, SUPERGEN, and is a part of the SUPERGEN Energy Storage Consortium[*]. This consortium involves research into materials, modelling and applications for supercapacitors and lithium-ion batteries. The role of this rsearch within the consortium was to provide information on the use of supercapacitors in transport applications, with the objective of providing specifications for supercapacitors optimised for use in an electric vehicle.
The remaining body of this thesis is divided into the following chapters:

- Chapter 2 presents control strategy optimisation options in further detail. It provides a review of supercapacitors and batteries used in electric vehicles, including aspects of control, past vehicles and control strategies, modelling techniques and power electronics. It further describes ADVISOR and the default ADVISOR models for batteries and supercapacitors.

- Chapter 3 describes the battery-powered Cobra, and verifies the battery model developed by the author to accurately characterise the batteries in a modular framework suitable for use in ADVISOR. It also discusses the use of regenerative braking, and the development of the drive cycles used in the simulations of the hybrid Cobra.

- Chapter 4 discusses the current supercapacitor market, including technical specifications and cost of commercially available supercapacitors. It describes the aspects of designing a battery/supercapacitor system using different optimisation strategies, and the sizing methodology for each optimisation. It also describes the development of the supercapacitor and power electronics models, and their integration into a complete hybrid system model, including the control strategy.

- Chapter 5 provides a comparison of the different optimisation schemes and their cost effectiveness using commercially available supercapacitors. This

[*] Grant ref: EP/D031672/1. More information is available at www.energystorage.org.uk

includes results optimised for each drive cycle as well as generalised results for other drive cycles. The effects of battery SOC and of the availability of regenerated energy from braking are also discussed, and lastly the effectiveness of combining different optimisation strategies is investigated.

- Chapter 6 presents the thesis conclusions, supporting the author's claims of novel contributions to the field of battery/supercapacitor hybridisation for EV applications. Finally, it suggests avenues for further work.

1.6 Publications

The following papers have been written based on the work presented in this thesis.

Journal Papers Submitted for Publication:

1) S I Fletcher, F B Sillars, R C Carter, A J Cruden, M Mirzaeian, N E Hudson, J A Parkinson, P J Hall, "The Effects of Temperature on the Performance of Electrochemical Double Layer Capacitors", submitted to the Journal of Power Sources, February 2010.

2) P Hall, A Rennie, F Sillars, M Mirzaeian, R Carter, A Cruden, G Wilson, G Shitta-Bey, S I Fletcher, "Energy storage in electrochemical capacitors: Engineering materials to improve device performance", submitted to the Journal of Energy and Environmental Science, January 2010.

Journal Papers to be Submitted:

1) R Carter, F Sillars, A Cruden, P Hall, "Supercapacitor voltage measurement – biased against applications?", to be submitted to the Journal of Energy and Environmental Science, Summer 2010.

Peer-Reviewed Conference Papers:

1) S I Fletcher, F B Sillars, R Carter, A Cruden, M Mirzaeian, N E Hudson, J Parkinson, P J Hall, "The Effects of Temperature on the Performance of Electrochemical Double Layer Capacitors.", in the Proceedings of the

Electrical Energy Storage Applications and Technologies Conference (EESAT 2009), Seattle, Washington, October 2009.

2) R Carter, A Cruden, "Strategies for control of a battery/supercapacitor system in an electric vehicle", in the Proceedings of the International Symposium on Power Electronics, Electrical Drives, Automation and Motion (SPEEDAM 2008), Ischia, Italy, June 2008, pp 727-732.

3) R Carter, A Cruden, "Strategies for maximising battery lifetime in a battery/supercapacitor system for an electric vehicle", in the Proceedings of the 3rd European Ele-Drive Transportation Conference (EET-2008), Geneva, Switzerland, March 2008, Session 3B - Batteries and Super Capacitors, CD-ROM.

4) R Carter, A Cruden, "The effects of AC current on supercapacitor performance", in the Proceedings of the 234th National Meeting of the American Chemical Society, Boston, MA, August 2007.

Poster Presentation:

1) R Carter, A Cruden, "Rating a supercapacitor bank for a battery/supercapacitor electric vehicle", EPSRC Energy Programme Meeting, Oxford, UK, May 2008.

2 The Use of Supercapacitors in Electric Vehicles

The limitations of battery electric vehicles are well-known, and some investigation has already taken place into the potential for hybridising such vehicles with supercapacitors. This chapter will review the different purposes which such a hybridisation can serve, and some of the battery/supercapacitor vehicles which have previously been built. The different aspects involved in battery/supercapacitor hybridisation are considered, including the physical construction of the hybrid system, and the modelling of the vehicle and the different energy storage elements. This chapter will also indicate the gaps in the literature which require further investigation.

2.1 Background

Electric vehicles which operate solely on batteries suffer limited performance due to the low power density of batteries, which tend to have a specific power in the range of 50-2000 W/kg [22]. Vehicles require high power to accelerate, hence the battery must be capable of delivering high power bursts. If the vehicle is to make use of regenerative braking, then the energy storage system must be capable of receiving high power spikes as well. Furthermore, when batteries are exposed to high currents their lifespan is reduced, decreasing the reliability of the vehicle.

Figure 2.1 shows the ECE-15 cycle, which was specified by the United Nations Economic Commission for Europe (hence 'ECE') to assess the performance of vehicles in Europe, including battery lifespan and emissions tests. From Figure 2.1 it is clear that the maximum power for a small vehicle on this cycle is much higher than the average power. This is the case for almost all drive cycles, and it suggests that a high power system, such as a pack of supercapacitors, operating in conjunction with the batteries would be a more effective system than batteries alone. The supercapacitors would supply the peak power demands of the vehicle and receive the power available from regenerative braking (indicated as a negative power in the figure). The power demands on the batteries would be reduced; their limited power density would no longer be a problem, and their reliability would be improved.

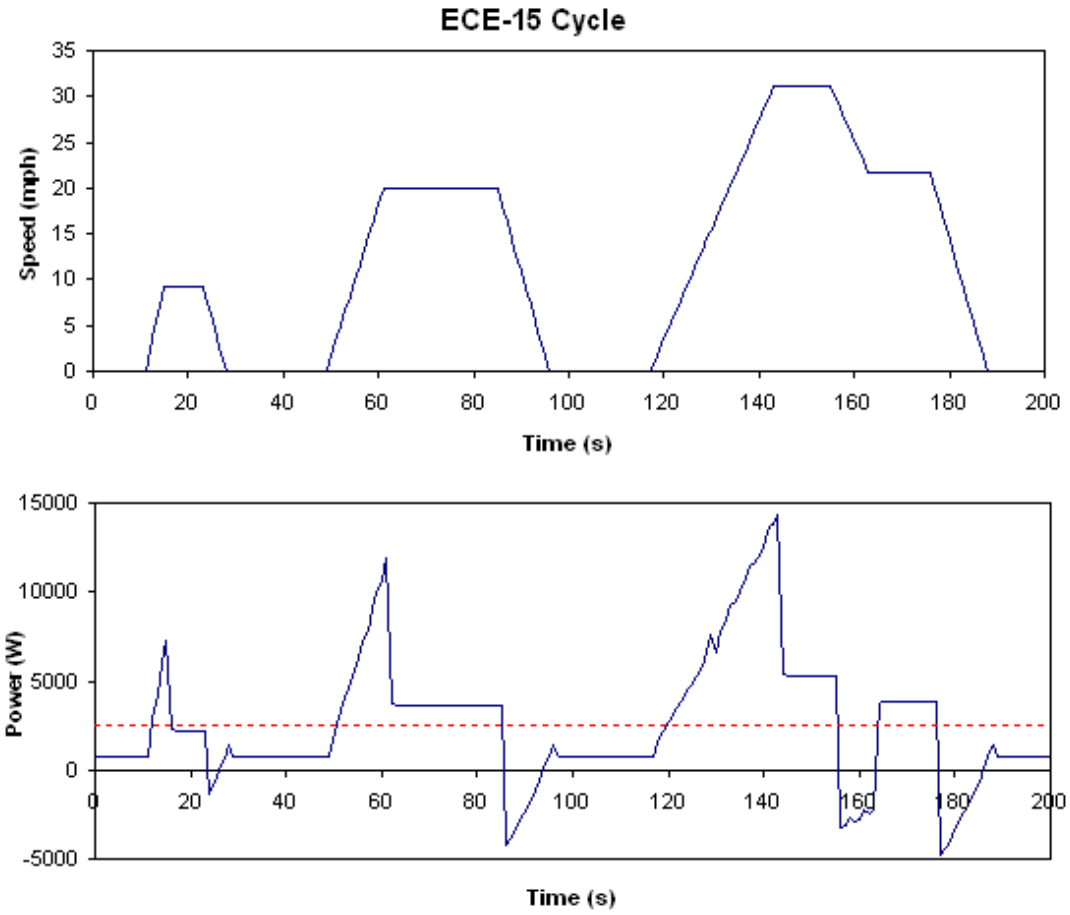

Figure 2.1: Speed and Power of a small vehicle in the ECE-15 drive cycle – data from ADVISOR. The red dashed line shows the average power for the cycle.

The simplest way to add a supercapacitor pack is to directly connect it electrically in parallel to the battery pack, as in reference [33]. However, studies have shown that far better results can be achieved by employing power electronics to control the supercapacitors and batteries separately, in terms of increasing maximum power output [34], reducing battery current [34, 35], and extracting useful energy from the supercapacitors [35]. To design a hybrid system one must determine an appropriate pack size, the best physical means of relating the two energy sources, and a control strategy to determine when and to what extent each should be used. This, in turn, requires the identification of the specific reasons for adding the supercapacitors. Then the best method of hybridisation for the purpose can be determined.

2.2 Elements of a Control Strategy

A new control strategy for a battery/supercapacitor vehicle can consider one or more of the following elements:

1) to improve vehicle acceleration
2) to improve overall drive efficiency, increasing the driving range
3) to reduce lifecycle costs by extending the life of the batteries
4) to reduce capital costs by direct replacement of some batteries

These elements are inter-related and may work together or in opposition to each other, as described in more detail below. The primary goal of a control strategy must be identified in advance, otherwise the strategy will lack focus and may not achieve any benefit at all.

2.2.1 Vehicle Acceleration

For a vehicle to have good acceleration, it must be capable of handling high power demands. The high power capabilities can be limited by the motor, which will have maximum voltage, current and power ratings, and may also have a minimum voltage rating. The capabilities may also be limited by the battery, which will need to be protected from high temperatures and high currents. As the battery state of charge (SOC) decreases, its voltage also decreases while its resistance goes up. This further reduces its power capabilities, because a lower current is needed to push the battery voltage below the acceptable minimum limit.

Supercapacitors, by contrast, can supply very high power as listed in Table 1.1. They are also not harmed by working at a low voltage as long as their voltage polarity does not reverse. The supercapacitors can continue to supply high power even when the battery SOC is low, as long as they can be recharged from regenerative braking or low power recharges from the batteries. Using the supercapacitors for acceleration can therefore maintain the vehicle performance even when a low battery SOC or a somewhat aged battery pack has limited the batteries' ability to supply power.

2.2.2 Vehicle Range

The range of the vehicle is determined by two parameters: the total energy losses in the system, and the total energy which can be withdrawn from the battery. The former is down to the overall efficiency of the system, including the energy storage systems, power electronics and motor, as well as losses due to friction and air resistance. The latter may be influenced by the magnitude of battery currents. Operation at high currents reduces the effective energy capacity of batteries – this phenomenon is described by Peukert's Law [36-38].

Peukert's Law states that for a battery

$$C_x = C_n \left(I_n / I_x \right)^{p-1}, \tag{2-1}$$

where C_n (Ah) is the nominal capacity, I_n (A) is the discharge current which corresponds to the nominal capacity, I_x (A) is some other discharge current, C_x (Ah) is the apparent capacity at that current, and p is the Peukert coefficient. For a lead acid battery p will typically be between 1 and 2 [38, 39]. This effect is caused by diffusion rates in the pores in the battery's active material [36]. When the battery is discharged slowly, acid in the pores is replenished through diffusion. When the battery is discharged quickly, only acid near the pore opening is replenished, while the acid deeper in the pores is used up. When a region is depleted of acid, no more reactions can take place in that region, limiting the available charge.

Peukert's Law works well to describe the behavior of a flooded battery, but works less well for modern valve-regulated lead acid (VRLA) batteries, such as those found in the Cobra [36, 37]. VRLA batteries do not have a large reservoir of acid to replenish the acid in the pores. Their discharge behaviour cannot be fully described with a constant value of p; instead p tends to increase with higher discharge currents [36, 37, 40]. This means that a VRLA battery will experience a more dramatic reduction of capacity at high currents. After a discharge at high currents, some acid will be replenished and the battery may subsequently be discharged further at a lower rate [38]. Although there will still be a small net loss in capacity as the lead sulphate

formed near the pore entrance will increase the resistance of the battery [36, 38], using Peukert's Law does not give an accurate picture of battery SOC in cases where the current varies and the battery is rested in between uses.

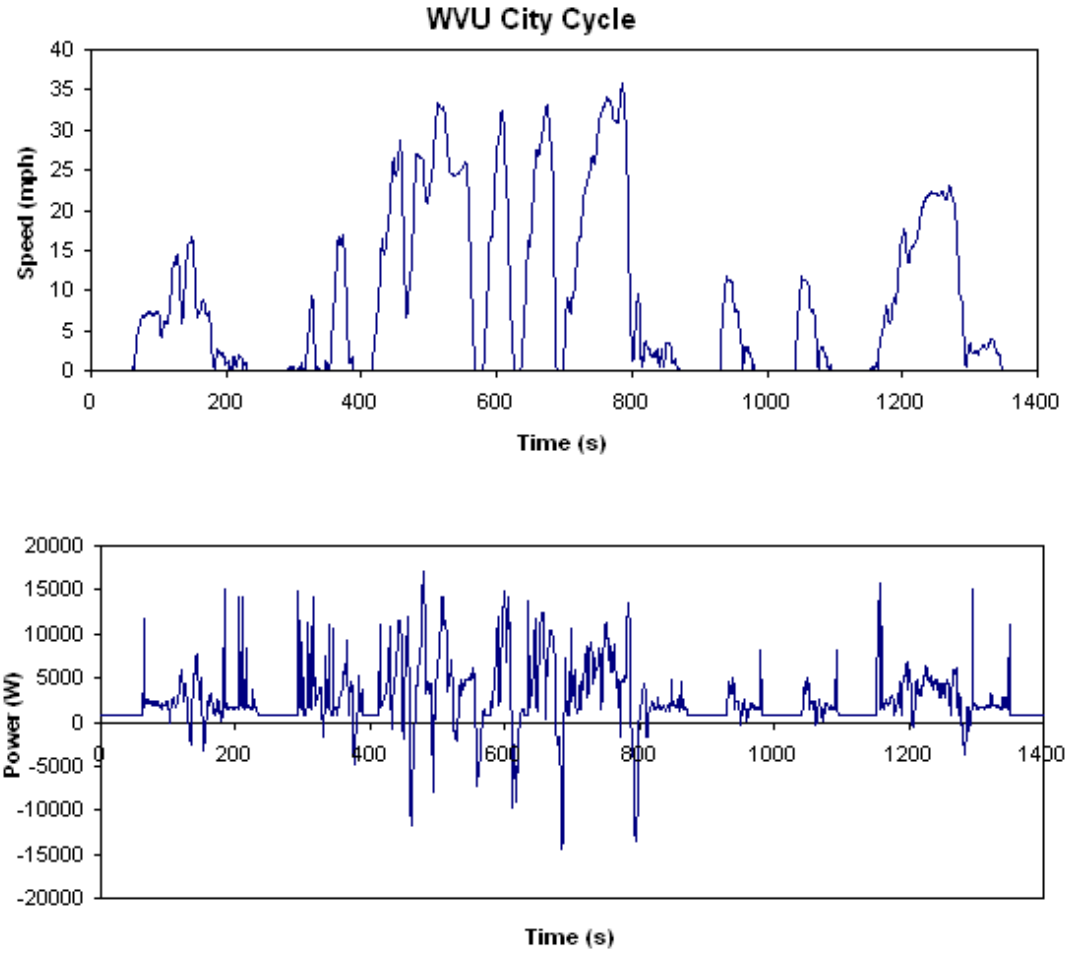

Figure 2.2: Speed and power of a small vehicle in an urban drive cycle developed at the University of West Virginia and available from ADVISOR.

The second and more important factor in determining vehicle range is efficiency. The efficiency of an electric vehicle is calculated using the yield, defined as the kilowatt-hours used per kilometre travelled. Recapturing some of the vehicle's kinetic energy during braking is a good way to increase the overall vehicle efficiency. High power spikes may be available from regenerative braking; this may be seen in the drive cycles and power profiles in Figures 2.1 and 2.2. Figure 2.2 shows the power requirements of a small vehicle driving an urban cycle without using its friction brakes. The cycle was developed at the University of West Virginia

and is now available through ADVISOR. The profile shows that power spikes of more than 10kW may be available if the full braking power is returned to the energy storage. However, the full power may not be returned to the battery as the battery charging currents must be limited to prevent out-gassing [41].

For example, the Hawker Genesis batteries used in the Cobra may not have a voltage above 15.0V [40]. For an internal resistance of 0.03Ω (a typical value for the charging resistance) and an open circuit voltage of 12.5V, this gives a peak charging current of 83.3A. There are six batteries in the Cobra, so this translates to a peak regenerating power of 6*15*83.3 = 7.5kW. The actual peak power which it is possible to absorb at any given time will vary depending on the batteries' state of charge. Nevertheless, it is clear that on some occasions it is impractical to recapture all of the available regenerative braking power.

Supercapacitors, on the other hand, are capable of accepting charging currents of up to a few thousand Amps [42]. Even a small pack of supercapacitors could accept the full regenerative power, assuming they were not already fully charged. A strategy optimised for efficiency should capture as much regenerated energy as possible. The state of charge of the supercapacitors must be considered to ensure they are capable of receiving the incoming energy.

Adding a supercapacitor to a battery-powered vehicle means also adding further power electronics to relate the two power sources, and this will create additional losses. In particular, any power which is sent from the batteries to the supercapacitors will undergo losses first within the batteries themselves, then from the power electronics and finally from the internal losses in the supercapacitors. If efficiency is to be a primary concern then this will limit the usefulness of the supercapacitors.

2.2.3 Lifecycle Costs

Lead acid batteries such as those used in the Cobra have a lifetime of at most 500 full cycles [22]. The number of years which a battery will last depends on a number of factors including the frequency of use, depth of discharge, and the currents and

temperatures to which it is subjected. In a battery-powered electric vehicle, it is the latter two factors which can be controlled - high currents can cause high temperatures as well as being damaging in and of themselves. A battery in an electric vehicle will typically last about 3-5 years, depending on the type of battery used [8, 9, 21]. This could potentially be extended, and if the battery needed to be replaced less frequently then long-term costs would be reduced.

The battery costs may also be reduced by improving their mean time between failures (MTBF). The MTBF describes the failure rate of batteries in the middle of their lifecycle – in other words, how likely a battery is to fail *before* it reaches the end of its life [43]. Some companies have suggested leasing electric and plug-in hybrid vehicle batteries to consumers [13, 14], and a more reliable battery would be less expensive to lease even if the battery life expectancy remained the same. Reliable batteries are also essential for battery-swap stations like those being built by Better Place [16].

Lead acid batteries in high power applications such as electric vehicles are primarily damaged by a mechanism known as 'sludging' which is caused by high discharge currents [24]. The positive plate of a lead acid battery consists of lead dioxide which forms $PbSO_4$ on discharge. This material is supported by a metal grid. High discharge currents cause a dense layer of $PbSO_4$ to form near the surface of the cathode grid [25, 26]. On recharge, the dioxide reforms on the surface of this layer, away from the grid. Over repeated cycles, the mass moves away from the grid and eventually electronic contact may be lost. This material may also collect at the edges of the grid and cause a short circuit.

The rate of sludging depends highly on the peak currents applied to the battery. This was confirmed by Papazov et. al. [44] using life cycle tests on the positive plates of lead-acid batteries. The plates were tested with an electric vehicle drive cycle, varying only the value of the peak current in the cycle and keeping all lower current values the same. These tests suggested that the lifetime of the positive active mass was directly proportional to the value of the peak current, although this could not be

stated conclusively due to an insufficient number of test samples. The ageing of a cathode in a test rig will not be exactly the same as the ageing of a positive plate encased in a VRLA battery, as the construction of the battery will put pressure on the plate and physically hold the active mass in place [26, 45]. However, this test illustrates the importance of the maximum current value in determining battery lifetime.

2.2.4 Capital Costs

In some systems there could be a reduction in the capital cost while maintaining the same performance by substituting some of the batteries with supercapacitors - although it would not be practical to substitute all the batteries with supercapacitors, due to the supercapacitors' insufficient energy density. In order for this strategy to be effective, the cost of the supercapacitors plus their electronics and any further installation costs must be less than the cost of the batteries being replaced. The final capital cost relates to the design of the physical system. Capital costs can also be reduced by choosing the smallest supercapacitors necessary. The option to replace some batteries will not be explored with the Cobra, nor in this thesis. However, the costs of the supercapacitors and electronics are very much in mind, and will be discussed in more detail in Chapter 4.

2.3 Existing Vehicles

There are many ways a vehicle can be hybridised. Several commercially available hybrids combine an electric motor and batteries with an internal combustion engine (ICE) [17]. A variety of experimental hybrid vehicles exist; these may combine batteries [46-48], supercapacitors [49, 50], flywheels [46], solar panels [48], ICEs [50] or fuel cells [47, 49], among other possibilities. A few combine batteries with supercapacitors, and these are of the most relevance to this thesis. The strategies for other types of vehicle are not directly applicable as they must consider additional constraints, for example a desire to conserve fuel or the need to convert between electric and mechanical systems.

2.3.1 Catholic University of Chile

A battery/supercapacitor pick-up truck was built at the Catholic University of Chile [51-53]. A 300V (nominal voltage), 20F supercapacitor bank was added to a truck powered with a 356V pack of 50Ah lead acid batteries [54]. These batteries were later replaced with ZEBRA batteries containing 24kWh of energy [55]. Two control strategies were devised for this vehicle, one a heuristic strategy and one that uses an Artificial Neural Net (ANN) [53]. These strategies were both intended to increase the efficiency of the system, with the heuristic strategy found to be 5% more efficient, in terms of yield, than the truck using the battery alone in a specific urban cycle, and the ANN-based strategy being 8.9% more efficient than the battery alone.

After the ZEBRA batteries were added, vehicle performance was also assessed. Simulations showed that the acceleration of the vehicle would be improved [55]. Both lead acid batteries and ZEBRA batteries were expected to have a longer life span when hybridised with the supercapacitors, but no actual life cycle tests were performed to confirm this [51, 52, 55].

Using the heuristic strategy, the supercapacitor voltage was maintained at a level determined by the vehicle speed and the battery state of charge. A lower speed meant a higher voltage, anticipating an acceleration; likewise a high speed meant a low voltage so the supercapacitors would be ready to accept energy from regenerative braking. The voltage was also higher if the battery state of charge was lower, and vice versa. The supercapacitors were charged or discharged via the battery to maintain the correct voltage. This relationship of supercapacitor state of charge to vehicle speed is shown in Figure 2.3.

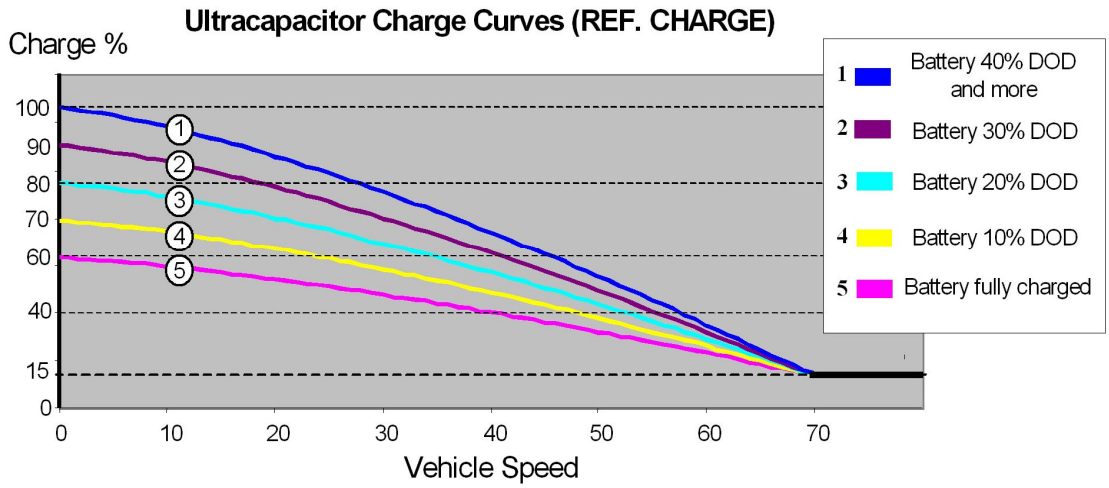

Figure 2.3: Supercapacitor state of charge vs. vehicle speed, taken from [52]. DOD means depth of discharge.

The ANN strategy [53] focused on the efficiency of the components, particularly the DC/DC converter. It tried to calculate the means of achieving the minimum energy expenditure at any time, and was somewhat more efficient than the heuristic method, as this strategy could be more closely tailored to the demands of the vehicle.

2.3.2 EVermont

An American battery/supercapacitor vehicle was designed by a group called EVermont and built by a consortium involving EVermont, Solectria Coporation and others [56-59]. The lead-acid battery pack had a nominal voltage of 156V and a capacity of 86.4Ah, while the supercapacitor pack had a voltage of 120 V and a total capacitance of 47.5F. The supercapacitor voltage was controlled to be inversely proportional to the vehicle speed, down to an unspecified minimum speed. Below that the supercapacitor voltage was kept at maximum. The control strategy also ensured that the battery voltage and supercapacitor current remained within specified boundaries. The strategy seems to have been intended to optimise for several variables simultaneously, namely efficiency, vehicle performance and battery lifetime.

The vehicle's performance with and without supercapacitors was compared [57]. The addition of supercapacitors was found to noticeably decrease the battery currents in all situations. For example, on one drive test the battery-only vehicle experienced

a peak battery current of about 240A, while the hybrid vehicle had a peak battery current of only 140A. Similarly, an acceleration test showed battery currents reduce from about 200A in the battery-only vehicle to about 150A in the hybrid. It also allowed more energy to be extracted from the battery before performance fell off.

However, the supercapacitor did not always increase the range of the vehicle or the efficiency of the system. This was heavily dependent on drive cycle. Efficiency was more likely to be improved when the drive cycle had a lot of stops and starts; even so, some urban drive cycles had a decrease in efficiency when the supercapacitors were present, due to additional losses in the DC/DC converter. Even when more energy was extracted from the battery, the vehicle range was not always increased as the extra energy was lost due to low efficiency.

Battery lifetime tests were also performed by using two strings of 13 batteries each, identical to the battery packs used in the vehicle [58]. The packs were cycled repeatedly, with one pack subjected to a current profile recorded from the battery-only vehicle, and the other receiving a current profile recorded from the hybrid vehicle driving the same cycle. The batteries were recharged by identical charging units. The hybrid current cycle had a peak current of about 150A; 29% lower than that of the battery-only cycle, which was about 225A. Nevertheless, the lifetime tests of the batteries showed that the battery life was not noticeably extended by the addition of the supercapacitors [58]. Note also that a full assessment of battery life and reliability is not possible given the small number of batteries used in the test.

2.3.3 Karlsruhe University

A battery/supercapacitor van was built at Karlsruhe University in Germany [60]. The supercapacitor bank had a voltage of 241.5V and a capacitance of 14.8F. The battery pack consisted of zinc-air batteries; two different models were tested, both manufactured by ZOXY. This company appears to be defunct and data sheets for the batteries are no longer available, thus the voltage and capacity of the battery packs is not known. Zinc-air batteries have a very low specific power of no more than 10 W/kg, but a high specific energy of more than 100 Wh/kg.

The control strategy called for the battery pack to output a constant current for as long as the supercapacitor voltage was below a certain level, while the supercapacitors handled any necessary deviations in power. The low power density of the batteries meant that if the vehicle demanded power in excess of what the supercapacitors could provide, then the battery pack was not capable of temporarily increasing its power output. The research team stated that a higher power battery would have enabled them to alter the control strategy based on vehicle speed, similar to the strategy employed by the previous two groups. In this vehicle, the battery could not be used alone due to its very low power capabilities. Thus the addition of the supercapacitors could be seen as having the goal of decreasing the size of the battery pack, which would have needed to be much larger had the supercapacitors not been present. Due to the nature of the vehicle drive train, no direct comparison could be made of the supercapacitor's usefulness; the conclusion was simply that this is a feasible system.

2.3.4 Cranfield University

At Cranfield University, a go-kart powered by a battery and supercapacitor system has been built [61, 62]. The go-kart used a pack of 27Ah lead acid batteries with a nominal voltage of 48V, and a supercapacitor pack with a voltage of 45V and a capacitance of 58F. The control strategy is based on a modular structure with three management shells: an Energy Management Shell handling long-term effects ("strategy"), a Power Management Shell handling medium term effects ("policy") and a Power Electronics Shell handling short term actions ("process"). The Energy Management Shell regulated the supercapacitor voltage by creating a reference state using the following relation:

$$E_{uc} + E_{kin} = K, \qquad (2\text{-}2)$$

where E_{uc} (J) is the energy stored in the supercapacitors, E_{kin} (J) is the kinetic energy of the vehicle, and K (J) is a constant. It then ensured that the supercapacitors would trend toward the reference state by raising or lowering the maximum allowable power from the battery. The Power Management Shell determined what power should be drawn from the batteries and the supercapacitors at any given time. The

load power was drawn from the battery up to the maximum allowable power (which could have a range of values as dictated by the Energy Management Shell), and then from the supercapacitors. Energy from regenerative braking was sent to the supercapacitors only, and if this was not possible then friction brakes were used. The batteries also charged the supercapacitors whenever the load power was less than the average load power. Finally, the Power Electronics Shell controlled the switches that caused the appropriate powers to be delivered. Simulations showed that the hybrid go-kart was more efficient than the battery-only version, although the efficiencies were not quantified. It was predicted that the battery life would also be extended.

2.3.5 National Science Council of Taiwan

A battery/supercapacitor motorcycle was built by a consortium funded by the National Science Council of Taiwan [63, 64]. The motorcycle had a 'gearshift' which changed the configuration of the batteries and the supercapacitors depending on the speed of the vehicle. The four 12V, 15.6Ah lead-acid batteries could be connected in parallel, in series, or with two parallel branches of two batteries. The batteries were connected to a DC motor, which required low voltage and high currents at start-up and vice versa at high speeds. There were eleven supercapacitors of 1700F each, arranged in two groups of five with one standing alone – the specific reasons for this configuration were not given. The supercapacitors could also be connected in a variety of configurations at different voltages, and were connected to the motor. If the supercapacitor pack voltage was higher than the battery voltage, then it supplied all the current. Once the supercapacitor voltage dropped below that of the batteries, then the battery pack supplied all current. The supercapacitors could also be completely disconnected from the motor, and were recharged only by regenerative braking.

This is a very complicated architecture, but it gave a good improvement to efficiency. A set of test cycles showed that the hybrid system had a range 18.5% greater than that of the batteries alone [63]. It was also speculated that the battery life span would be increased, although this was not confirmed with life cycle tests.

2.3.6 CR-ENEA

CR-ENEA refers to the Italian Governmental Agency for the Environment and Alternative Energy – Electric Vehicle division. In conjunction with the University of Rome and Semikron Italy, they developed a battery/supercapacitor vehicle and entered it into the Formula ATA 2008 competition [33]. This vehicle used a single pack of 6V, 180Ah lead-acid batteries with a total voltage of 48V, in parallel with two supercapacitor packs, each with 48.6V peak voltage and 47F capacitance. Each supercapacitor pack was connected to a different inverter and AC motor. The two drive motors were rated at 4kW and the use of two motors was intended to increase the overall reliability of the vehicle.

As the supercapacitors were directly connected to the batteries, the hybrid vehicle could not have a deliberate control strategy to direct the power flow. Nevertheless, the addition of the supercapacitors increased the acceleration of the vehicle, reducing the time to go from 0km/h to 50km/h by 5 seconds [33]. They also improved the overall efficiency of the vehicle by 11.1%. The researchers suggested that the battery life would also be increased.

2.3.7 Educational Vehicles

Two different battery/supercapacitor vehicles have been built as educational projects for undergraduate students: one at MIT [65] and another at the University of Manchester [66]. Neither vehicle was assessed in a systematic way to determine the benefits of battery/supercapacitor hybridisation.

2.3.8 Proposed Battery/Supercapacitor Vehicles

Several other groups have proposed control strategies to be used in battery/supercapacitor vehicles [35, 67-69]. Two of these [35, 68] are described qualitatively and are very similar: the supercapacitors should be fully charged prior to acceleration, and during acceleration should handle the bulk of the power demand while the battery current slowly rises. The battery should eventually take over any steady current demand. One group [68] adds that the battery should send a small current to the supercapacitors to make up for efficiency losses and maintain the supercapacitor voltage. During braking, regenerated energy should be sent to the

supercapacitors to protect the battery from high charging currents. This strategy did not have a clearly stated purpose, but suggested that the strategy could be refined to produce improved vehicle performance, battery lifetime and total efficiency. One strategy [35] also specifies that during braking the supercapacitor should send a small current to recharge the battery. The intent of this strategy was to protect the batteries from damaging currents.

The strategy suggested by [69] is closely related to the two strategies described above, but is more specific in the means by which the battery current is determined. Here, the load is split into five components: accessories, rolling resistance, aerodynamic drag, gravitational load and inertial load. Assuming that the first four elements are slow-changing, while the inertial load is fast-changing, they provide calculations to determine the inertial load while braking and accelerating and assign that to the supercapacitors. Supercapacitor voltage is also maintained such that the energy that the supercapacitors can accept is equal to the kinetic energy of the vehicle; this is a lower-priority rule. The purpose of this strategy is to minimise losses in the batteries, in the hope that reducing the stress on the batteries in this manner will extend their life. The range of the vehicle was found in simulations to be extended somewhat, but the researchers concluded that it was not by a sufficient margin for the supercapacitors to be cost-effective if added for this reason alone [69]. Improved acceleration of the vehicle was considered and rejected as a suitable factor for optimisation.

A fourth group [67] used two constraints to control the system: Pb_{max} (W), the maximum power through the battery, and dPb/dt_{max} (W/s), the maximum rate of change of the power through the battery. The qualitative aspects of this system were much the same as the other three. This group simulated their system with a range of values for the two constraints, and also tested the system with a fuel cell added to provide a small constant power. The strategy was intended to increase the lifetime of the batteries by minimising dPb/dt_{max}. Lifecycle tests were not performed on the batteries, and the group concluded that further work was needed to fully optimise the strategy and assess its benefits.

2.3.9 Supercapacitor packs

Most attempts to size a supercapacitor pack for a hybrid system involve the use of a specific cycle to optimise the sizing, or a somewhat arbitrary criterion to establish the needs of the supercapacitors.

A simple control strategy for a battery/supercapacitor vehicle is to use the battery to supply the mean power and the supercapacitor to supply or receive all the variations in power. Such a strategy is suggested in [70]. The obvious problem with this strategy is that every cycle will have a different average power, and it is impossible to know in advance exactly when the supercapacitors will be needed to provide or sink power. It also requires a large supercapacitor pack – a problem which [70] acknowledges.

Other papers suggest specific goals which the supercapacitor pack is to achieve. For example, the electric vehicle constructed by EVermont used a supercapacitor pack designed to have sufficient power and energy to accelerate the vehicle from 12 to 50 miles per hour [71]; this calculation used the kinetic energy of the vehicle without taking into account the losses in the drive train, nor those due to friction and air resistance. The vehicle built at the Catholic University of Chile had a supercapacitor pack which was intended to be able to accelerate the vehicle from 0 to 60 kilometres per hour, followed by powering the car up a hill of 30 metres height [51]. Again, this was calculated using kinetic and potential energy, neglecting losses. A battery/supercapacitor/photovoltaic vehicle currently under construction at the Polytechnic Institute of Coimbra, called 'VEIL,' used a specific drive cycle to size the components [72]. The battery power was first determined by calculating the power needed for the vehicles maximum speed, including mechanical and electrical losses. The supercapacitor power was then determined as the power needed to meet the drive cycle's initial acceleration, using the batteries and supercapacitors together. The supercapacitors were also sized to have power and energy capabilities to receive and store all the regenerative braking energy. The power needed to climb a 6^{o} slope was calculated, but treated as a battery requirement and not that of the supercapacitors. A similar but more generic approach is given in [73]: to choose a

constant power value for a specified time and determine the required supercapacitor size from these values. Each of these methods is somewhat arbitrary in the choice of criteria. In fact, the sizing method used in [71] was ultimately described in the same paper as being unsuitable for the purpose.

Two sizing regimes were considered for the supercapacitors in the Cranfield University vehicle [62]. The first was to consider the amount of energy that will be available due to regenerative braking, and size the pack to be able to accept all of this energy. The second is to analyse a drive cycle to determine the maximum interval of discharge followed by the maximum interval of charge that the supercapacitors will experience. This requires an *a priori* knowledge of the drive cycle, and furthermore some advance knowledge of what the control strategy will be, although the details of the control strategy will itself depend on the size of the supercapacitor pack. The usefulness of the drive cycle analysis method will depend on how typical the chosen drive cycle is for the vehicle in question. It is not clear which, if either, of these methods was used to choose the supercapacitor pack ultimately used in the Cranfield vehicle.

The chosen power electronics architecture also needs to be considered when sizing the supercapacitor pack, as it will place limits on the operating voltage. For example, one proposed battery/supercapacitor/ICE vehicle uses the supercapacitors to provide the main bus voltage for the vehicle [74]. In other words, the supercapacitor voltage is the same as the main DC voltage source for the motor controller. The supercapacitor pack for this vehicle must be large enough to operate at the bus voltage, which in this case is 600V DC. Alternatively, if the supercapacitors connect to the bus via power electronics then, depending on the nature of the electronics, the supercapacitor voltage will need to be maintained above or below the bus voltage. This question was visited in the design of a fuel cell/supercapacitor vehicle described in [75]. The supercapacitors in this vehicle were also constrained by size, as they needed to be small enough to fit in the available space and to have minimal mass [75]. In this case, a higher operating voltage was chosen to limit the currents.

Another method of sizing is to analyse a sample drive cycle by frequency analysis as in [76]. As with the drive cycle analysis method described in [62], the usefulness of this method is determined by whether the chosen drive cycle is typical for the vehicle. Finally, the vehicle can be modelled in different drive cycles using different configurations of supercapacitor, as in [77]. This allows a verification of the chosen pack, but limits the options to those actively tested. A more suitable pack size might be overlooked.

2.4 Power Electronics

When using an active control strategy, there must be some physical means of connecting the battery pack and the supercapacitor pack to each other and to the main bus using a DC/DC converter. A survey of converter types for hybrid electric vehicles was conducted by a group at the University of Arkansas [78]. They surveyed the half-bridge, Cúk, and SEPIC/Luo configurations. These are shown in Figure 2.4, with V1 and V2 representing the voltages at either end of the converters, and the other labels indicating components within the converters. The researchers concluded that the half-bridge type required the lowest current ratings for the switches and a smaller inductor. They also found that the half-bridge converter had the highest potential efficiency, having lower conduction and switching losses.

The actual efficiency of any converter depends on the details of the system, including peak power, working voltages and permissible current and voltage ripples, so the benefits of the different configurations are given as comparisons and not enumerated.

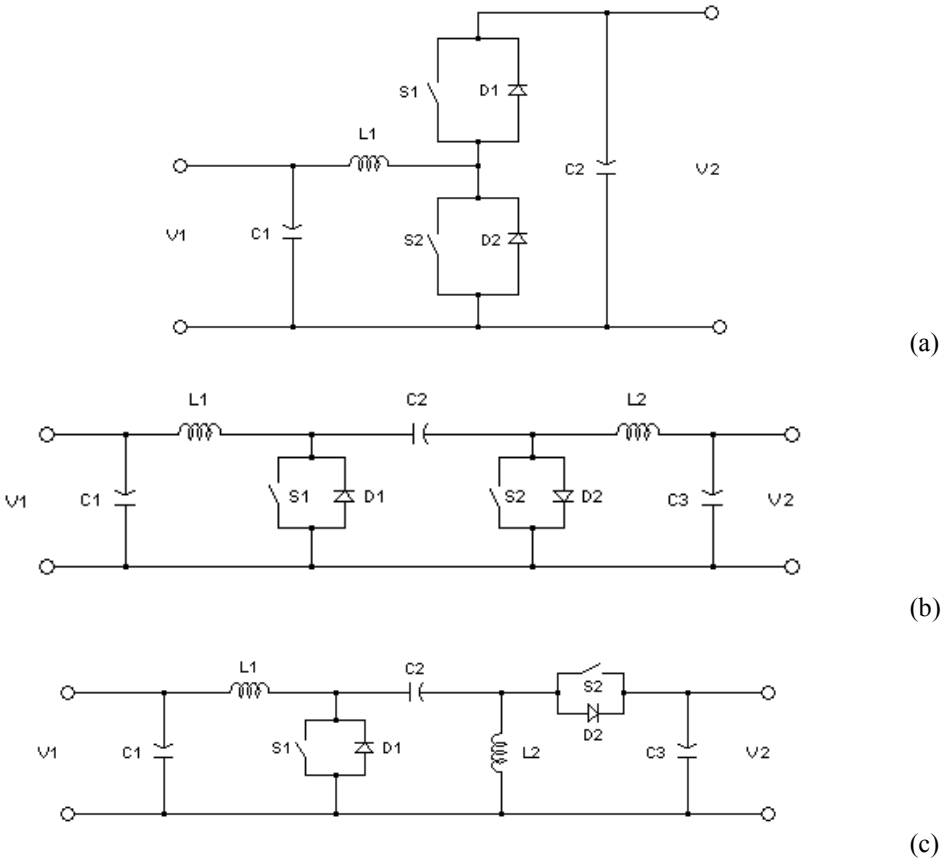

Figure 2.4 (a) Half-bridge converter, (b) Cúk converter, (c) SEPIC/Luo converter

Other architectures are possible, and a number of possibilities have been proposed for use in fuel cell/supercapacitor vehicles. One architecture featured three interleaved coupled-inductor boost converters, and achieved a high efficiency of 95.6% at full load [79]. A second option featured two inverter/rectifiers connected with a high frequency transformer [80]. Two options were investigated for the low voltage side of the converter: an L-type half-bridge converter and a full bridge converter. The converter featuring an L-type half-bridge architecture had a peak efficiency of 89% for discharging and 90% for charging, while the full-bridge version's efficiency was 94% for discharging and 95% for charging. Finally, a bidirectional forward converter was studied in [81], however a value for the converter efficiency was not given. These converters, pictured in Figure 2.5, are efficient but also very complex and hence expensive, and are not well-established in battery/supercapacitor literature. It was decided to focus on a simpler, more common and cheaper architecture for the Cobra.

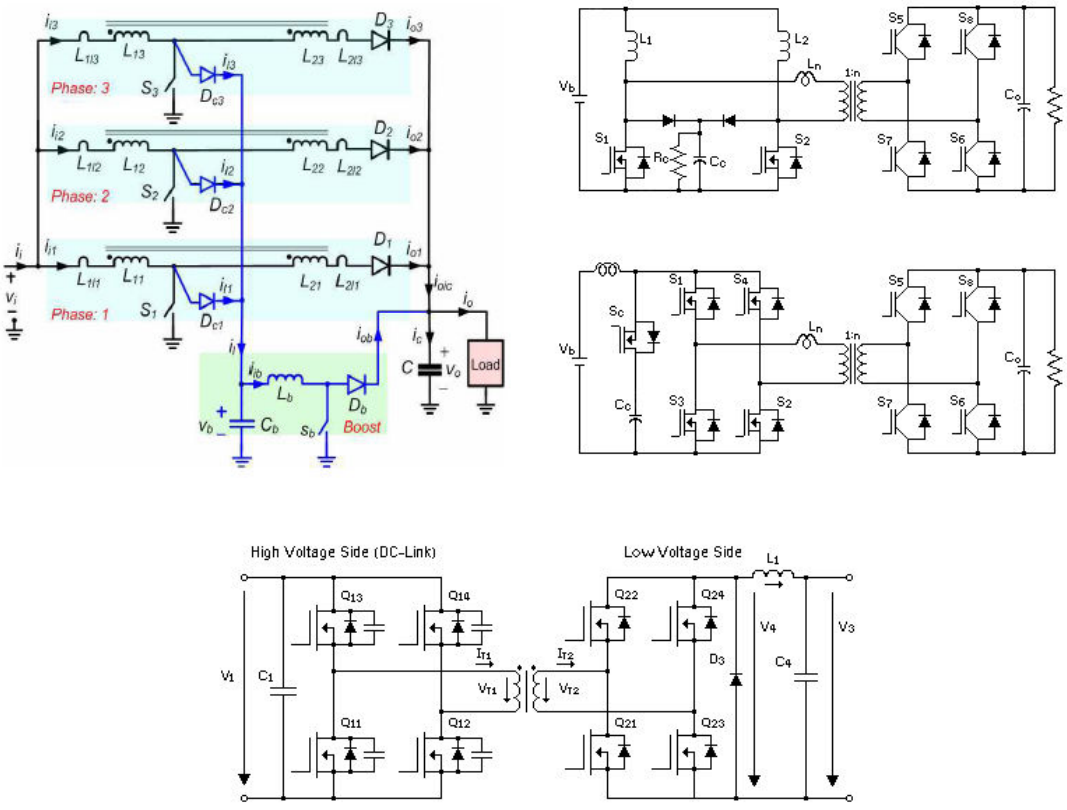

Figure 2.5: Diagrams of the converters from [79] (top left), [80] (top right) and [81] (bottom).

For battery/supercapacitor vehicles, some form of half bridge converter is the most commonly used architecture. The half-bridge DC/DC converter, shown in Figure 2.4a, is a two-quadrant converter – so called because the current can flow in two directions, but the voltage is always positive. This is illustrated in Figure 2.6.

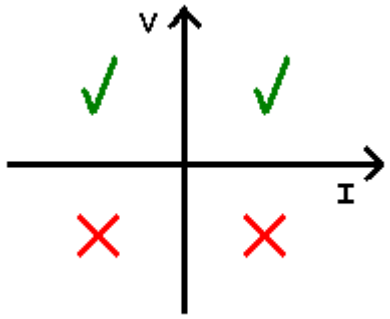

Figure 2.6: The operating regions of a half-bridge DC/DC converter

To transfer power from V2 to V1, switch 1 is used and switch 2 is kept open. When the converter is operated in this fashion,

$$V1 = \delta V2, \tag{2-3}$$

where δ, the duty cycle, is the fraction of time that the switch spends closed within the switching period. For power flow from V1 to V2, switch 2 is used and switch 1 is kept open. In this case,

$$V1 = (1-\delta)V2. \tag{2-4}$$

These equations are derived later in Appendix A. For now, it is sufficient to note that because δ must be between 0 and 1, V2 must always be higher than V1. Also note that the capacitors, C1 and C2, will have the same voltage as V1 and V2. Their purpose is to buffer the current from their respective ends of the converter, and they are not essential to the converter. The operation of the half bridge converter is illustrated in Figure 2.7.

The half-bridge converter is typically used with the supercapacitor in the V1 position and either the battery pack or the DC bus as V2; for examples see references [35, 67, 82, 83]. This architecture is used in both the vehicle built in Chile [51, 52] and that built by Solectria Corp [56, 57]. In these two cars, the battery pack is found at V2 and is used as the main DC bus for the motor drive, and the supercapacitor pack is at V1.

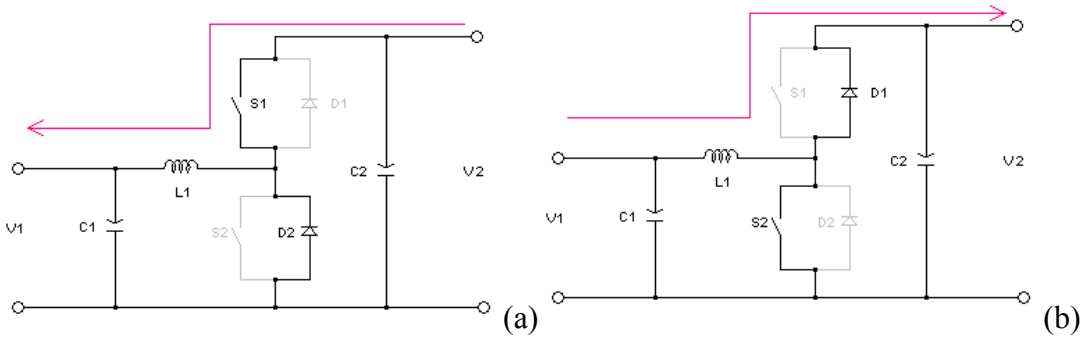

Figure 2.7 (a) Half bridge converter operating in first quadrant – power flow from V2 to V1. (b) Half bridge converter operating in second quadrant – power flow from V1 to V2.

It is also possible to use the supercapacitors on the V2 side of the converter: this was done in a battery/supercapacitor test bench built at the University of Sheffield [84].

In this case the supercapacitor also acts as the main bus to the motor. The test bench features a half-bridge converter, using smoothing capacitors on both the battery and supercapacitor sides. Two such converters were built, each testing a different type of supercapacitor and battery. The converters use parallel switches to reduce the current requirements of each switch and allow for high power through the converters.

Another option is to use neither energy storage element as the main bus. The MIT vehicle used the supercapacitor pack in series with the battery half-bridge converter, as shown in Figure 2.8.

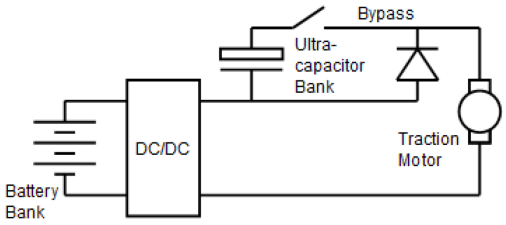

Figure 2.8: The power electronics configuration used in [65].

The Cranfield University go-kart used two half-bridge converters [61, 62], one for the batteries and one for the supercapacitors, connecting both to the DC motor bus (see Figure 2.9). The Karlsruhe University van also used this architecture [60]. The two converters allow greater flexibility of battery and supercapacitor control, as the energy storage elements do not need to have any particular voltages with respect to each other. However, as both converters will create efficiency losses, using two converters is inherently less efficient than using a single converter.

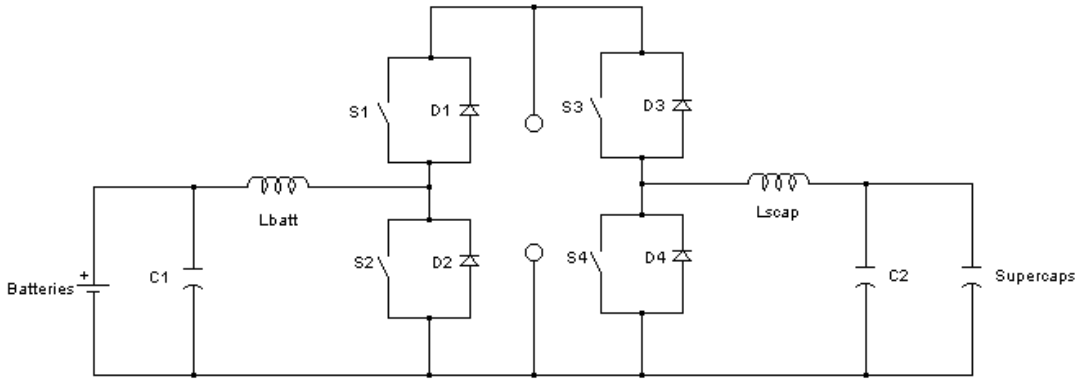

Figure 2.9: Two half bridge converters as described in [61].

Taking this a step further, the Coimbra-based VEIL vehicle is planned to have three half-bridge converters [85]. The converters will connect three power sources to the DC motor: batteries, supercapacitors and solar cells. Currently the VEIL vehicle uses only batteries, and the converter boosts the 96V battery pack to the 600V required by the motor. Another example of a proposed vehicle with three half-bridge converters uses fuel cells, batteries and supercapacitors in the V1 position of each converter, with the main bus at each V2 [86].

The choice of main bus voltage remains a topic of debate. If an energy storage element is to provide the bus voltage, then the batteries are most commonly used instead of the supercapacitors – and furthermore the bus voltage will be found on the V2 side of the converter [35, 52, 67, 87]. Almost always, the input voltage required by the motor is similar to or higher than the voltage of the energy storage systems. This means that the motor must be found on the V2 side of the converter, unless an additional set of power electronics is to be added.

The supercapacitor voltage varies based on the state of charge: a supercapacitor with 25% of the total available energy remaining will have an open circuit voltage that is half the voltage it would have at full state of charge. But a battery's voltage does not vary as highly: at 25% SOC the open circuit voltage will typically be within 10% of the voltage at 100% SOC. If the supercapacitors are located at V2 then they will either need to have a much higher voltage than the batteries at V1 (so that even when mostly depleted they exceed the battery voltage) or else they will need to be prevented from discharging fully, thus rendering much of their stored energy inaccessible.

However, researchers at the Illinois Institute of Technology argue that it is preferable to use the supercapacitors as the main bus for a battery/supercapacitor system [88]. They reason that this allows the battery currents to be controlled and the stress on the battery minimised. This group went on to assess three power electronic architectures. The first used batteries and supercapacitors in parallel, with a buck-

boost converter connecting the paralleled energy storage systems to the motor. The second used a buck-boost converter between the batteries and supercapacitors; due to the wide voltage swings of the supercapacitors, an additional converter was used between them and the motor bus. The third architecture used similar converters, one each to connect the supercapacitors and the batteries to the bus. Their analysis found that the third option was best for efficiency, flexibility and total power [88], with the numerical value for each quantity unspecified as it would depend on the specific equipment and power profile used.

2.5 Modelling a Vehicle

Most of the hybridisation options described in the previous sections were developed with the help of simulations using vehicle models. There are several software products that might be used to build a computer model of a vehicle.

This research uses a model based on the Advanced Vehicle Simulator (ADVISOR), which runs using Matlab/Simulink. This software was developed by the NREL in 1994 and until 2003 it was made freely available for download. During that time, ADVISOR was regularly updated. The final update performed by the NREL was in 2002, by which point the software had been downloaded approximately 5000 times [89]. Licensing rights for ADVISOR were then sold to the company AVL (www.avl.com), which expanded the capabilities of the software and released a version for purchase in 2004.

ADVISOR is primarily a backward-facing simulator, with a forward-facing component [90]. A backward-facing simulator starts by assuming a certain performance from the vehicle, and then determines the demands that would be placed on the various components to make that performance. By contrast, a forward-facing simulator starts with an input from a driver, and then determines what performance this would cause.

ADVISOR combines these elements by starting with a certain drive cycle which specifies speed and road gradient over time and calculating the behaviour of the individual components leading to this performance, as in a standard backward-facing

simulator. However, it also incorporates a forward-facing element by placing limits on the capabilities of the vehicle, and if the drive cycle demands a performance beyond the car's capabilities, then the simulator will flag a warning and will simulate the vehicle performing as closely as possible to what was asked of it.

ADVISOR models vehicles using a specified drivetrain, and specifications for each part of the drivetrain. A range of component specifications are provided, but custom components can be added. The specification takes the form of two files: one an m-file defining a range of parameters, and one a Simulink model tracing the power through the component and recording appropriate variables, such as current, voltage, power loss, etc. In this way an existing model can be used with altered parameters, or an entirely new model substituted. Some components present a choice of model. For instance, a supercapacitor is modelled as a simple resistor and capacitor in series, but the resistance and capacitance may vary with respect to temperature plus either SOC or applied current depending on the choice of model. Each component is related to the other components by tracing power flow through the vehicle, so if a certain power is needed to accelerate the vehicle then this demand can be traced through the wheels, transmission, motor and energy storage, with efficiency losses at each stage adding to the power demanded from subsequent stages.

Figure 2.10 shows an example of the component specification screen in ADVISOR 2002. To the left is a simple diagram of the vehicle, and below that a contour plot showing the efficiency of the motor at different torques and speeds. Other contour plots can be shown here as appropriate, for instance a vehicle with an internal combustion engine could show the engine efficiency. To the right is a list of possible drivetrain components. Those which are greyed out do not appear on this vehicle, while those in black have drop-down menus to choose which model and which parameters to use.

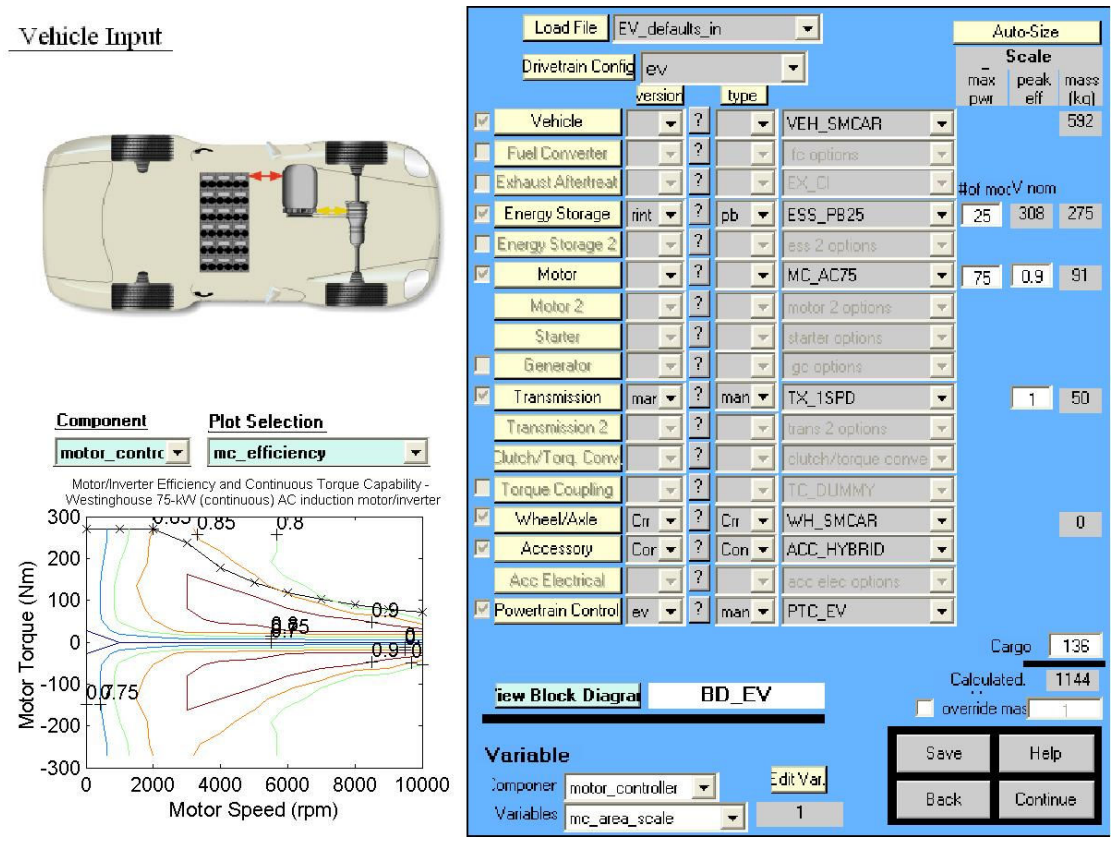

Figure 2.10: A screen shot from ADVISOR 2002 showing the components of a battery-powered electric vehicle.

Having defined a vehicle, the next step is to select a drive cycle. A wide range of drive cycles are provided, including the standard emissions test cycles for America and for the UK, and a selection of real-life cycles both urban and highway. Custom drive cycles may also be added. The cycle defines the speed at which the vehicle will (or should) travel at any given time, and some cycles also include changes in road gradient. The behaviour of each component of the defined vehicle is determined as it follows the cycle, and any failure to follow the cycle is flagged. The researcher can then examine the state of the vehicle over time. Figure 2.11 shows a sample result from such a simulation, using the battery car as defined in Figure 2.10. The top plot shows the required speed of the vehicle along with the actual speed of the vehicle. In this case the vehicle was capable of completing the cycle with no problems, so these two lines appear as one. The next plot shows the state of charge of the battery during vehicle operation. Below that is a plot showing the power supplied by the battery at each stage of the journey. The final plot shows the power losses in the battery.

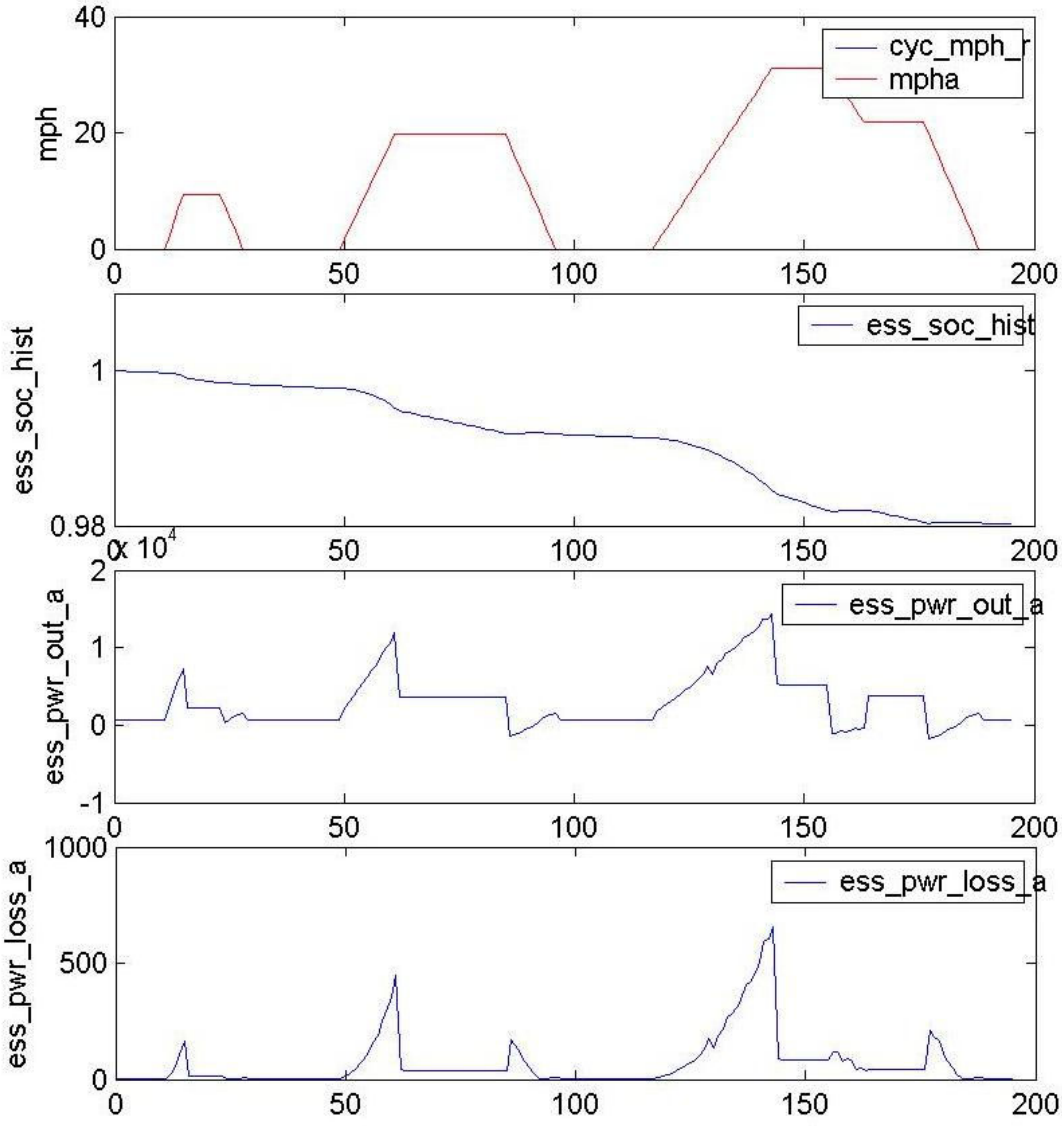

Figure 2.11: A screenshot from ADVISOR 2002 showing the outputs for a battery powered vehicle on a drive cycle which is defined in the top-most plot. The remaining plots, from top to bottom, show the battery state of charge, the power output of the battery and the power losses in the battery.

ADVISOR has been used to assess the effectiveness of supercapacitors in a range of ICE hybrid vehicles [91] and in a fuel cell hybrid vehicle [92]. ADVISOR can also receive new models for components if necessary – for example a fuel cell vehicle was modelled in ADVISOR using a more advanced fuel cell model created by the researchers themselves [93]. Another group updated ADVISOR's regenerative braking calculations for their model of a battery/ICE hybrid electric vehicle [94].

ADVISOR models can also be used outside the ADVISOR framework, to be combined with bespoke models created in Matlab/Simulink, as in the Cobra model.

Of particular interest to this review is an investigation by researchers at the Illinois Institute of Technology, using ADVISOR to model a hybrid car including a battery pack, supercapacitor pack and an internal combustion engine [21]. They first used ADVISOR's basic parallel hybrid drivetrain to model a vehicle with a battery pack and ICE. They then modified this vehicle to include a supercapacitor pack and related power electronics. The battery/ICE vehicle used 26 lead-acid batteries with a capacity of 26Ah, and the battery/supercapacitor/ICE vehicle used 18 of the same batteries. Different numbers of 2500F supercapacitors were used, and the capital cost was calculated to be lower for the supercapacitor vehicle using up to 45 supercapacitors. However, the cost of the power electronics was not included. The supercapacitors reduced the peak battery current by up to 50%, and the researchers speculated that the battery life would be extended. The ADVISOR tests of grade-ability and maximum speed were also used to assess the performance of the vehicles. The performance remained approximately the same, with the battery/ICE vehicle having slightly worse grade-ability and slightly better top speed. This illustrates both the uses to which ADVISOR can be put, and that battery/supercapacitor systems in HEVs as well as in pure EVs follow similar patterns of optimisation.

Other modelling options exist. A model for the vehicle built at Cranfield University was created with the electromechanical modelling software SIMPLORER. The National Instruments software LabVIEW has also been used to create a vehicle model [95]. Some groups have even created bespoke software to further their research. A group at the University of South Carolina created a virtual test bed environment which could relate models from different languages (e.g. SPICE, ASCL and SABER) for the different components of their vehicle [96].

The different vehicle models are all modular to some extent – the individual components can be altered and their effects monitored. The following sections will look at the different models available for supercapacitors and for batteries. The

interplay of these energy storage elements remains at the heart of any control strategy development for a hybrid vehicle.

2.6 Modelling Supercapacitors

2.6.1 The Physical Properties of Supercapacitors

Ordinary capacitors store energy as an electrical charge which has built up on a pair of conducting plates separated by a gap containing an insulating material. The energy stored in a capacitor is given by:

$$E = \tfrac{1}{2} CV^2, \tag{2-5}$$

where E is the energy (J), C is the capacitance (F) and V is the voltage difference (V) between the two plates. The capacitance can be determined if the physical properties of the capacitor are known, using the relation:

$$C = \varepsilon A / d, \tag{2-6}$$

where ε is permittivity (F/m) of the insulator, A is the surface area (m^2) of each plate, and d is the distance (m) between the plates. Note that the voltage decreases sharply as energy decreases, in contrast to batteries which maintain most of their peak voltage. This is illustrated in Figure 2.12.

A supercapacitor works on the same principle as an ordinary capacitor. Supercapacitors consist of charged electrodes placed in an electrolyte. Ions in the electrolyte crowd against the electrode of opposite charge, and there is no electrical conductance between the electrode and the electrolyte. The boundary of the electrode and electrolyte therefore forms a kind of capacitor, and as they are so close together - in the order of a few nanometres - and because the porous electrodes have a surface area of a few thousand m^2/g, a very high capacitance results [97]. The energy stored in a supercapacitor is almost entirely due to this capacitance, with a negligible contribution from chemical effects* [98].

* A closely related technology, the pseudocapacitor, stores energy in both electrical and chemical forms. These devices are outwith the scope of this thesis.

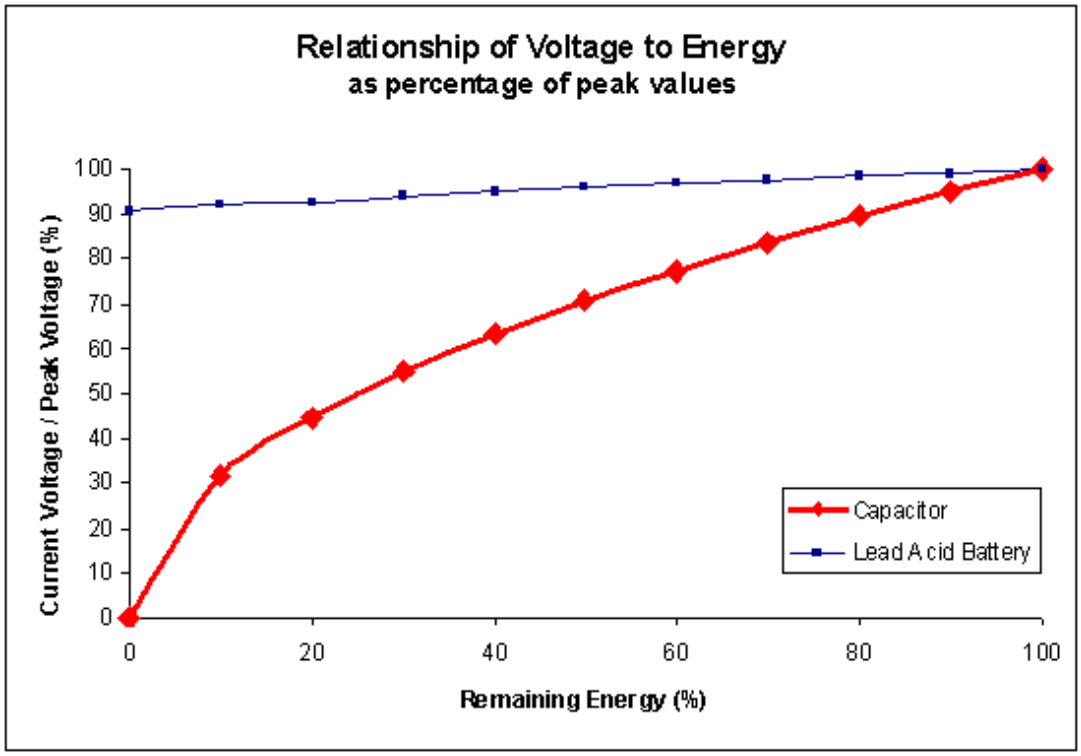

Figure 2.12: The relationship of voltage to energy for lead acid batteries and capacitors. The lead acid battery data is from ADVISOR.

The electrolyte ions which are close to an oppositely-charged electrode move up against it as they are attracted to the opposite charge. Ions which are further away experience a different effect: they are attracted to the electrode, but repelled by the layer of ions which has formed in front of it. Therefore, in the bulk of the electrolyte the ions are fairly evenly distributed, although there is a small capacitance effect from the diffuse ions near, but not immediately beside, the electrodes [99]. A rough sketch of the ion distribution can be seen in Figure 2.13.

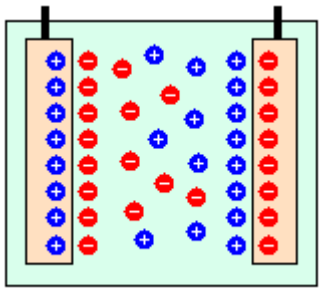

Figure 2.13: Diagram of a supercapacitor.

The porous structure of supercapacitors is worth investigating in further detail. A simple model of an individual pore of a supercapacitor can be found by assuming each pore to be an infinite cylinder [100]. In this case, it can be modelled as a transmission line of capacitors and resistors. Figure 2.14 shows a model of a pore proposed by [101].

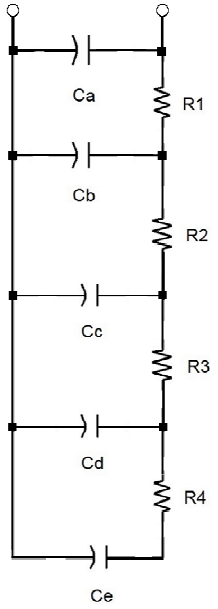

Figure 2.14: A model of a supercapacitor pore as proposed by [101].

These pores mean that the 'history' of the supercapacitor becomes important. Consider Figure 2.15, which shows the behaviour of a pore as modelled in Figure 2.14 as it is steadily charged to 9V and then discharged to 0V. The outermost capacitor, C_a, cycles along with the charging and discharging current, but the innermost capacitor, C_e, is slowly rising. It takes 10-12 cycles to achieve a 'steady-state' in which all the capacitors cycle in a regular fashion. Clearly the history of the pore makes a difference to its internal state. In fact, a supercapacitor with a non-zero initial voltage must be left in short circuit for as long as six weeks in order to ensure that, upon removal of the short circuit, the measured voltage will rise to no more than 1% of the maximum voltage [102]. This is due to charge redistribution in the pores; long after the outermost capacitors in the transmission line model have shed all their charge, the deeper capacitors retain a charge. Similarly, if a capacitor is quickly

charged to a certain voltage and then left in open circuit, a later measurement will show a lower voltage, partly due to self-discharge, and partly due to the charge migrating deeper into the pores. The pore model can be taken as the basis for a model of the full capacitor [103].

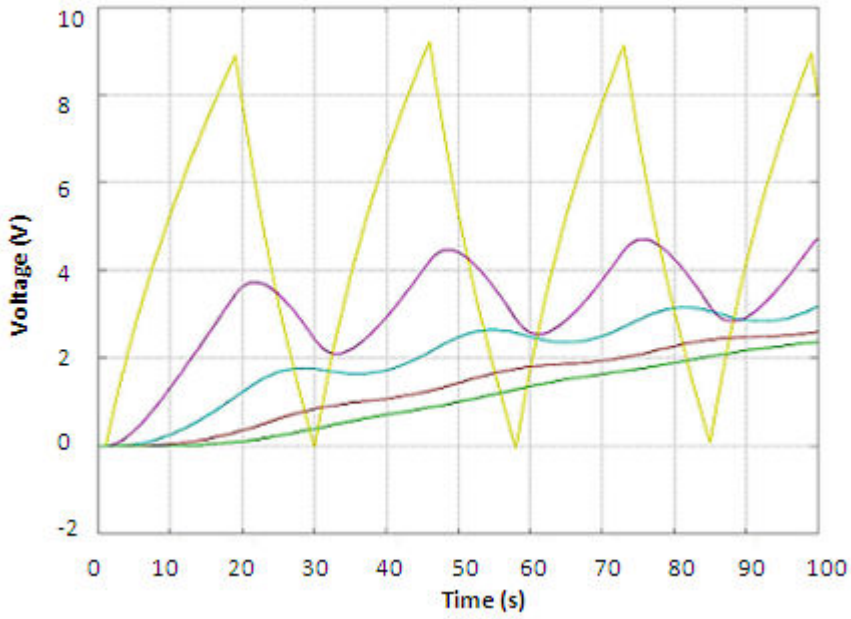

Figure 2.15: A pore charged with a steady current to 9V and then discharged with a steady current to 0V. The coloured lines represent the different capacitors in the model as follows: yellow – Ca, purple – Cb, blue – Cc, red – Cd, green – Ce.

Supercapacitor modelling is further complicated by a relationship of charge to potential [104, 105], which occurs because of interfacial tension between the electrode and the electrolyte. Interfacial tension is an adhesive force between two substances of different phases – it is the same effect which causes the capillary action of water climbing a narrow glass tube. In a supercapacitor, interfacial tension means that the electrolyte and the electrode tend to cling to each other. As the potential across the capacitor terminals increases, the attraction between the electrode and electrolyte also increases due to the increased density of charged ions in the electrolyte and of opposite charges in the electrodes at the boundary between them. This ensures better contact between the electrode and electrolyte, increasing surface area, decreasing distance, and thereby increasing capacitance.

2.6.2 Supercapacitor Models from Literature

A variety of supercapacitor models have been developed. A model may be expressed as an equivalent circuit or as a mathematical equation which attempts to fit the behaviour of a supercapacitor without relating it to a set of circuit elements. Often a physical model has a mathematical approximation, and vice versa.

The simplest physical model is just an ordinary capacitor in series with a resistor, and this is sufficient for some situations. More complex models focus on an arrangement of capacitors and resistors, often with variable values, to more accurately characterise the supercapacitor behaviour. Some models also include a small inductor in series with the resistor/capacitor network [98, 102, 106-109], but as the inductance of a supercapacitor is quite small, typically less than 50nH, others choose to neglect it [99, 110, 111].

One of the earliest models was created at the University of Toronto [102, 104] in the late 90s, using 470F and 1500F carbon-based supercapacitors. This is called the 'three branch model' although it is often used with only two branches, leaving out the 'long-term' branch (described below). It is depicted in Figure 2.16

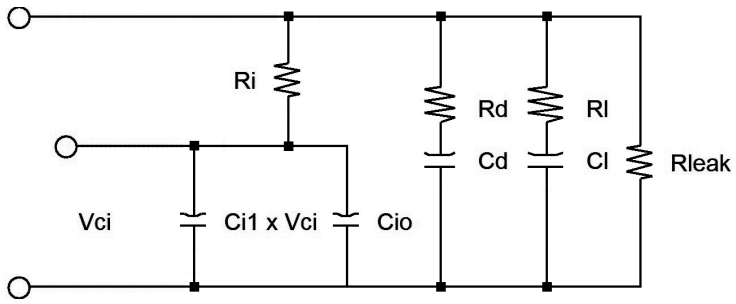

Figure 2.16: The three-branch model.

The first branch of the model consists of the resistor R_i in series with parallel capacitors C_{io} and $C_{i1}*V_{ci}$. This is called the 'immediate' branch as it represents the supercapacitor's immediate response to a current, with a time constant in the order of a few seconds. The variable capacitance represents the effect of interfacial tension as discussed in section 2.6.1. The second branch, consisting of R_d and C_d, is called the 'delayed' branch; it represents the supercapacitor's response in the order of a few

minutes. Finally, R_l and C_l comprise the third, 'long-term' branch, used to describe the supercapacitor's response in the order of tens of minutes. This model also includes a leakage resistor, R_{leak}, representing the self-discharge behaviour of the supercapacitor. If necessary, further branches can be added to describe longer term responses. The model was reported to have a very low error (not quantified) at voltages higher than 40% of the peak voltage, but at lower voltages peak error rose to 10% [104]. The model's creators speculated that the accuracy would be improved by including variable capacitances in the second and third branches as well, however the methods for determining these parameters were not specified.

Some closely related models have been developed by other groups. One [99] used a transmission line of *n* branches, the first with a variable capacitance which is associated with a look-up table relating capacitance to voltage. It is not clear what value of *n* was used in the simulation. A mathematical expression for the transmission line impedance was also calculated, although it was not used in simulations. At the University of California, Davis, a 5-branch model with non-variable capacitors was developed for use by the United States Department of Energy [103]. This model was identical to the pore model shown in Figure 2.14, with the addition of an inductor in series, and a parallel resistor to model self-discharge. Unlike the two previous models, this was fitted to a set of impedance spectra to get the parameter values. Finally, a group at the University of Bordeaux [107, 112] created a transmission line model using a small inductance, resistance and capacitance in series followed by four branches of identical resistors and capacitors. The four identical branches featured variable capacitors to take into account the voltage-dependence of the capacitance. None of these models have stated error margins, so they cannot be compared directly.

A team at the University of South Carolina created a new model, based on the U.C. Davis model, using non-variable capacitors and *n* branches, where *n* was determined based on frequency [106]. At a given frequency the minimum number of branches necessary for an error of no more than 1% were used – the lower the frequency, the lower the number of branches. The values for the elements in each branch were

calculated based on the number of branches used, as was the time step used in the simulation. This sped up the simulations.

Some models focus on calculating the supercapacitor impedance numerically, although they may also be associated with approximate physical models. At the Aachen University of Technology [108, 109] a 1400F supercapacitor was modelled as a resistor, an inductor and an impedance designated '$Z_{p,}$' all in series, with

$$Z_p = \frac{\tau \coth(\sqrt{j\omega\tau})}{C\sqrt{j\omega\tau}}, \tag{2-7}$$

where C (F) is the capacitance, ω (rad/s) is the angular frequency, and τ (s) is a modelling parameter found using a look-up table relating it to temperature and voltage. This is known as a Warburg impedance. An equivalent circuit approximating the impedance Z_p was also developed, using resistors and capacitors whose parameters were calculated using C and τ. This model was compared to a supercapacitor in a dynamic load cycle and found to have a peak voltage error of about 5%, and an error in energy efficiency calculations of 0.75%. This model was developed for use in dynamic applications such as HEVs. Finally, the supercapacitor manufacturing company cap-XX modelled the supercapacitors as a resistor followed by a constant phase element [110], which has an impedance:

$$Z = {}^{1}\!\!\diagup\!\!{}_{T(j\omega)^P} \tag{2-8}$$

where T (s^p/Ω) and p (dimensionless) are defining parameters of constant phase elements; they are derived through a mathematical fit and do not correspond to physical attributes. Error values were not given for this model.

2.6.3 Temperature and Age

Supercapacitor models may also include the effects of operating temperature and age. Temperature effects include the ambient temperature around the supercapacitor as well as the self-heating caused by current flow through the device. A temperature which exceeds the upper bound of the supercapacitor can be very damaging to the

electrolyte and should be strictly avoided; for an acetonitrile supercapacitor, the maximum working temperature is about 60°C [112].

A team at the University of Franche-Comté [105] performed a study of the DC behaviour of a 2700F and a 3700F supercapacitor over a temperature range of -40 to 40°C, using a two-branch equivalent circuit model of the form proposed in [102, 104] and discussed above in its three-branch incarnation (Figure 2.16). They found that the initial resistance (R_i) decreases as temperature increases – the difference in the resistance value at -25°C and at 25°C was 50%, with most of the variation occurring at temperatures below 0°C. They modelled this as a third-degree polynomial; the error for this model was less than 4%. They also found that the total initial capacitance (C_{i0}) increased with temperature, with an increase of 21% as the temperature rose from -35°C to 25°C. Meanwhile, the voltage-dependant part of the capacitance (C_{i1}) decreased by 17% across the same temperature range. These were also modelled with third-degree polynomials, and again most of the variation occurred at temperatures below 0°C. The same team developed an artificial neural network model, including thermal effects, of the DC behaviour of the same types of supercapacitors plus a 325F module [113]. More recently, this group developed a full model of a supercapacitor involving impedance spectroscopy, voltage dependence and temperature effects [114]. The comparative accuracy of these models is unknown.

At the University of Bordeaux [112] a 2600F, 2.5V Maxwell supercapacitor was subjected to cycles of constant current, 100A alternating with -100A. They chose to disregard the differences in behaviour during charge and discharge and to analyse the thermal situation as being equivalent to a constant current equalling the root-mean-square of the cycled current. They found that the temperature at the terminals increased by about 18°C after 40 minutes, and by about 22°C after 80 minutes (in both cases from a starting temperature of 25°C). Based on this they developed a thermal model (Figure 2.17), which describes how the temperature of a supercapacitor changes when subjected to currents.

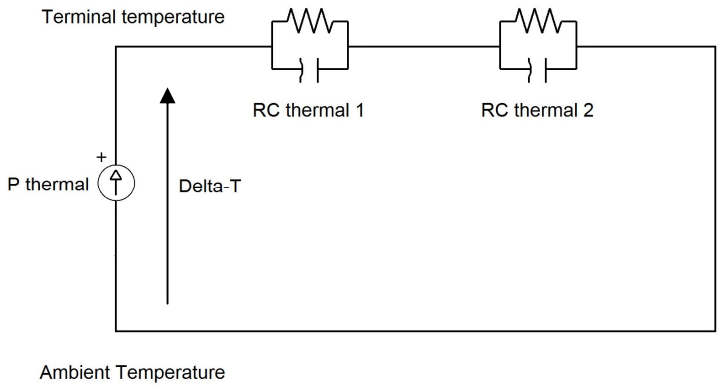

Figure 2.17: A thermal model of a supercapacitor developed by [112]. Resistor-analogues have units of K/W and capacitor-analogues have units of J/K.

The research team also performed impedance spectroscopy at a variety of ambient temperatures. They found that the resistance of a supercapacitor is not affected by temperature in the range of 25-60^{o}C at any frequency, which does not contradict the findings in [105] as they also found very little change in this region. The Bordeaux team also confirmed that chemical effects are not involved in the thermal behaviour of the supercapacitor. The effect of temperature on impedance spectroscopy was also studied by a group working at the Paul Scherrer Institute in Switzerland, together with Maxwell Technologies [115]; their findings match those of previous groups: decreasing resistance and increasing capacitance with increasing temperature.

Realistically, a supercapacitor in use in a vehicle will not be subjected to regular current cycles, but to varying cycles depending on the demands of the vehicle. At the Paul Scherrer Institute, researchers built a fuel cell car with power boosts supplied by a bank of supercapacitors [49]. They created a power profile for the supercapacitors based on a recorded drive cycle they made through the mountains, and subjected a 12.5V supercapacitor module to the power profile for 40 minutes. During this time the temperature of the module rose by 3.5^{o}C with no cooling. In the actual vehicle they used two 180V supercapacitor modules, cooled by fans. The modules were placed in the vehicle and charged and discharged at a constant power of 30kW. After 45 minutes the temperature rose by a maximum of 15^{o}C. The

cycling was stopped and the modules rested for 30 minutes, still cooled by the fans; during this time the temperature dropped by 10°C.

Temperature also contributes to supercapacitor ageing. An Epcos product sheet shows the relationship between ambient temperature, operating voltage and lifetime (Figure 2.18).

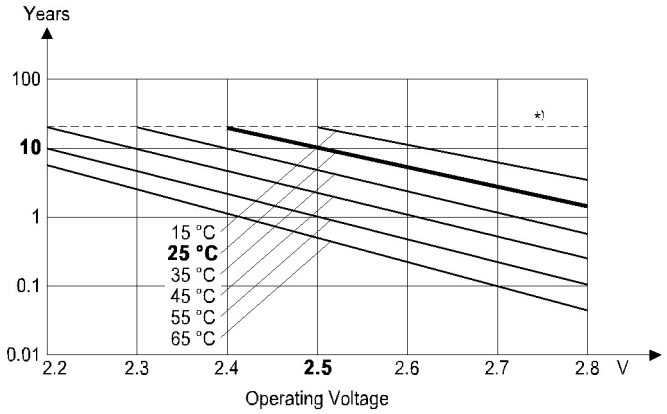

Figure 2.18: Supercapacitor lifetime vs. operating voltage and ambient temperature[116]. *Note: the lifetime is shown up to 20 years, as beyond this time fatigue of materials becomes significant.

Note that a typical supercapacitor with an operating voltage of 2.5V in an ambient temperature of 25°C will have a lifetime of 10 years.

Supercapacitors do not rely on chemical reactions for their operation, and so they are much less affected by age than batteries. Still, given enough time their performance does degrade. Impedance spectroscopy tests performed at the University of Bordeaux [112, 117] show that the resistance of a supercapacitor increases at all frequencies as the supercapacitor ages, and the capacitance decreases at low frequencies. They used a 2500F, 2.7V supercapacitor from Maxwell for these tests.

2.6.4 Modules

In an electric vehicle, supercapacitors will need to be combined in packs to increase their effective voltage rating. If there are no charge balancing mechanisms in place, the voltage might not be shared evenly between the supercapacitors and some will overcharge due to small differences in the capacitances of the individual

supercapacitors [109]. This problem is exacerbated over time as the different voltages cause temperature differences in the individual supercapacitors, which in turn lead to a greater divergence of voltage [118]. Overcharging causes a supercapacitor's electrolyte to decompose, so most modules use charge balancing electronics to prevent this from occurring.

The charge balancing electronics can take many forms [108, 119]. A simple method of charge balancing is to place resistors in parallel with the individual capacitors. As this reduces efficiency, a better option is to use actively switched resistors instead of passive resistors. The resistors are activated when the capacitors reach a certain upper voltage, and are deactivated if the capacitors drop below a certain lower voltage. However, energy is lost through the resistors when they are activated. Care must be taken to ensure that the minimum amount of energy is lost, while also ensuring that the equalising resistors are sufficient to prevent overcharge of all the supercapacitors. Another method is to use Zener diodes, which will start conducting current when the capacitors reach an upper voltage limit. This also causes energy loss. Furthermore, Zener diodes have a temperature dependency which is an important consideration in a vehicle environment. Finally, an active circuit involving DC/DC converters can be used. This is more efficient than the other methods, although it still involves losses; it is also very expensive.

Commercial charge balancing kits are available from Maxwell, and these were used for this research. The physical construction of the charge-balancing kits is proprietary information owned by Maxwell. However, it can be stated that they are an active charge balancing mechanism which is not in the path of normal charging and discharging currents. The kits can operate in temperatures up to 65^{o}C, with a leakage current of 50μA at 25^{o}C and 100μA at 50^{o}C. The kits cost £50.40 for a pack of 3, and one kit is needed for every two supercapacitors in a pack.

To model a module, one can model a set of supercapacitors connected in series, and if necessary including an appropriate component to account for the losses in the connecting electronics. The complexity of this method will depend on the

complexity of the models for the individual supercapacitors. For example, at Auburn University in Alabama a module of supercapacitors used to supply a constant power load was modelled simply by a capacitor and a resistor in series [120, 121]. The capacitance was determined from the equivalent of the nominal capacitances of the component supercapacitors according to their electrical arrangement (which was not specified) and the resistance modelled the combined resistances of the supercapacitors and the connecting electronics. The supercapacitors were connected to a DC/DC converter, which was modelled as having a constant efficiency. The results worked well for high voltages, but as the supercapacitor voltage fell the actual output increasingly deviated from the prediction, until finally the voltage fell below the converter's capabilities.

In general, this simple model is much better suited to constant power scenarios, where the supercapacitors are discharged over a period of several seconds, than it is to pulsed power situations such as those found in a vehicle [111]. However, the Auburn University model was put to use by researchers at the University of Idaho for modelling their ICE/supercapacitor hybrid vehicle, the Future Truck, in ADVISOR [122]. One additional complexity was included: the capacitance of the individual supercapacitors was found using a random number generator to create a uniform distribution within the manufacturing tolerance of ±10% of the rated capacitance. This had the effect that the total capacitance varied slightly from simulation to simulation. Simulations which calculated the supercapacitor voltage of the truck as it was driven on a certain cycle showed significant discrepancies from the actual voltage of the supercapacitors on test drives. This was attributed to an inaccurate engine model.

The Aachen University team [108, 109] modelled modules for vehicles by combining individual supercapacitors modelled with Warburg impedances (as described in section 2.6.2) in series, and using a look-up table to account for the losses in the balancing electronics. The U.C. Davis team also used their model to describe modules in a vehicle [103], however it does not appear that the model was altered for this purpose apart from the numerical values of the total capacitance and

the voltage. It is not clear what charge balancing electronics, if any, were present in this module.

2.6.5 Standard Supercapacitor Models Within ADVISOR

ADVISOR provides two supercapacitor models, which both take the same basic form of a resistor and capacitor in series. The 'Rint' model uses look-up tables for the resistance and capacitance, with the option to use different values corresponding to state of charge and temperature. However, the default 'Rint' model uses the same value for R (0.206mΩ) and capacitance (2.1Ah, or 5040F) at all SOCs and temperatures. The 'RC' model also uses look-up tables for the resistance and capacitance, but in this model the values correspond to different applied currents and temperatures, rather than to different SOCs. The default values for the 'RC' model are illustrated in Figure 2.19.

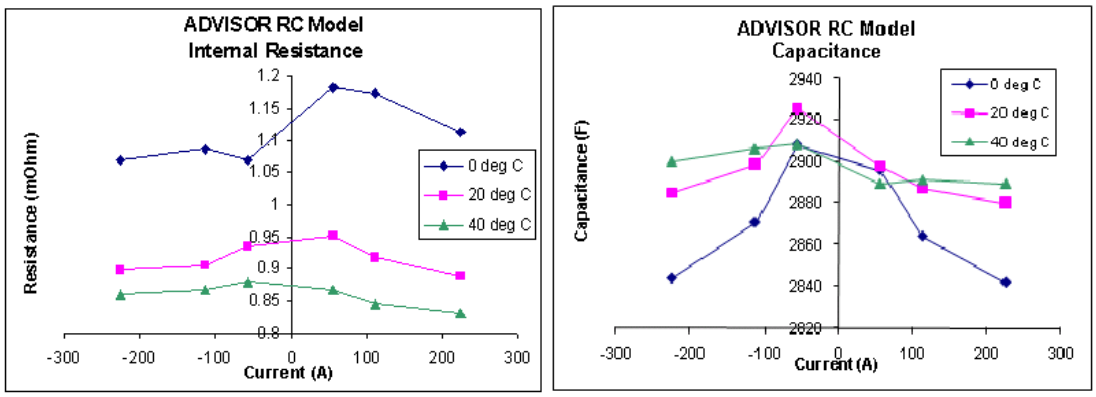

Figure 2.19: The default values for internal resistance and capacitance for the ADVISOR 'RC' supercapacitor model.

The RC model is purpose built based on a Maxwell 2500F capacitor from 2004, with a peak rated voltage of 2.5V. The Rint model is drawn from the Rint battery model, but with values appropriate for a generic 5000F supercapacitor with a peak voltage of 3V (0.3V higher than commercially available 5000F capacitors). The developers of the ADVISOR software (NREL and AVL) do not offer a comparison of the accuracy of these two models. However, the Rint model more strongly resembles actual supercapacitor behaviour. As discussed in section 2.6.1, capacitance and state of charge are strongly correlated, whereas capacitance and applied current are not [107].

2.7 Modelling Batteries

2.7.1 The Physical Properties of Batteries

Batteries derive electrical energy from spontaneous chemical reactions occurring between the electrodes and the electrolyte. The electrodes are made of metal and when immersed in an appropriate electrolyte, the metal ions begin to dissolve into the electrolyte while ions in the electrolyte will be deposited on the electrode. This tendency is described by the system's chemical potential. The difference in charge between the electrode and the electrolyte is defined as the electrical potential. The combination of these two effects is the electrochemical potential. At some point an equilibrium will be reached when the rate of ions leaving the metal equals the rate of ions being deposited on the metal. If two different electrodes in equilibrium with their electrolytes are connected to each other by a voltmeter, a potential difference between them will be measured.

For example, consider an electrode of lead dioxide (PbO_2) placed in an electrolyte of sulphuric acid (H_2SO_4), as in the case of the positive plate of a lead acid battery. The interaction of the electrode and electrolyte will reach an equilibrium of the reaction:

$$PbO_2 + 4H^+ + SO_4^{2-} + 2e^- \rightleftharpoons PbSO_4 + 2H_2O \qquad (2\text{-}9)$$

at a potential of 1.685V. Now consider an electrode of lead (Pb) which is also in an electrolyte of sulphuric acid, as in the case of the negative plate of a lead acid battery. This will reach an equilibrium of the reaction:

$$Pb + SO_4^{2-} \rightleftharpoons PbSO_4 + 2e^- \qquad (2\text{-}10)$$

at a potential of -0.356V. There will therefore be a total potential difference of 2.041V between these two electrodes when placed in the same electrolyte. These electrodes form a lead-acid battery cell – the PbO_2 forms the positive electrode, and the Pb forms the negative electrode (see Figure 2.20). A number of lead acid battery cells can be placed electrically in series within a single physical case to make a single battery of higher voltage. Typically one extra negative plate will be added; a lead acid battery of 12V nominal voltage will have six positive plates and seven negative

plates, for a total voltage of 12.602V [123, 124]. The overall battery reaction when discharging is:

$$Pb + PbO_2 + 2H_2SO_4 \rightarrow 2PbSO_4 + 2H_2O. \quad (2\text{-}11)$$

When discharging, the lead in the negative electrode splits into positively charged lead ions and free electrons, and the lead ions in turn combine with the SO_4^{2-} to form $PbSO_4$. The electrons travel to the positive electrode, where they combine with the PbO_2 and the hydrogen in the electrolyte to form lead ions and water – these lead ions also combine with SO_4^{2-} to form $PbSO_4$. In this state the positive electrode is called a cathode and the negative electrode is the anode. When charging, the reactions run in reverse, and the negative electrode acts as the cathode (receiving electrons) while the positive plate becomes the anode.

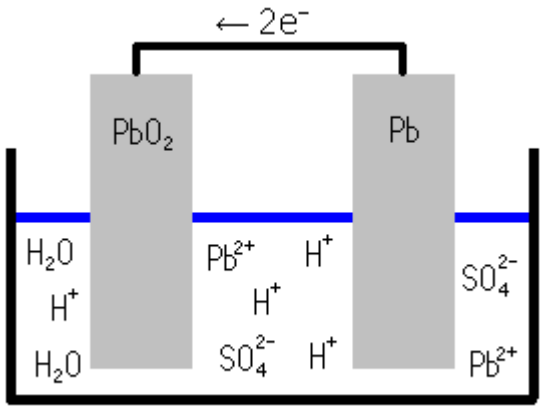

Figure 2.20: A discharging lead acid battery.

There are many types of battery possible, using different combinations of metals and electrolytes. A good candidate for a battery system should use a lightweight metal that has a high equilibrium potential in its electrolyte. This is why lithium batteries have a very good performance – not only is lithium a very light atom (atomic number 3, while lead has atomic number 82) but when placed in an aqueous solution it produces a high potential of -3.045V. However, lithium is a highly reactive element and must be treated with care. Lithium-ion cells may explode if overcharged [125], which means that each individual cell must have voltage control and hence multiple cells cannot be combined into a single casing [126]. Extra circuitry is needed to

combine the batteries into high-voltage units and to protect the batteries from failure, which contributes to the high cost of lithium batteries. Another common battery type uses nickel with other metals such as cobalt or manganese. These are also more expensive than lead acid batteries, mostly due to the relatively low cost of lead. The Strathclyde Cobra is a low-budget vehicle, and this is the main reason why it uses lead acid batteries.

Lead acid batteries do have problems of their own. As the battery discharges, water is created. When the battery is recharged, however, not all of the hydrogen and oxygen recombines with the lead and sulphur to recreate the original state. Instead, the water electrolytically breaks down and the separate hydrogen and oxygen gases bubble up through the electrolyte and escape. For many years this problem meant that lead acid batteries needed to be topped up with water periodically, or else the electrolyte would dry up. This original type of lead acid battery is known as a flooded battery. Approximately twenty years ago [45] a variant on the flooded battery was invented which did not need additional water. This technology is today called a valve-regulated lead acid battery (VRLA), but has also been known as a sealed battery, a maintenance-free battery and a fully recombinant battery.

VRLA batteries use a separator made of gel or of matted glass fibres in between the positive and negative plates [123]. A thin layer of electrolyte is in between the separator and each plate, but unlike in a flooded battery the electrolyte does not extend above or below the separator. The electrolyte is found in the pores of the separator and when the battery is discharged the electrolyte is absorbed into the electrodes. This removes the pool of electrolyte through which gas can bubble up and escape, as in a flooded battery. VRLA batteries are therefore described as ‘electrolyte starved.’ When the battery is recharging, the emitted gases instead travel through the porous separator. Internal pressure is maintained to promote homogeneous recombination of the gases with the lead and sulphur. However, if the battery is recharged too aggressively, the pressure can rise to dangerous levels. In this situation, valves on the battery release the excess gas. VRLA batteries are lower maintenance than the original ‘flooded’ form of battery, and they are also safer

because they do not contain an excess amount of acid which might spill. Therefore, the Cobra uses VRLA batteries, balancing cost with safety.

2.7.2 Battery Models from Literature

Batteries may be modelled simply using an ideal voltage source in series with a resistor. This is possible because the battery open circuit voltage does not change much even when state of charge is very low – unlike supercapacitors which have a great deal of voltage variation, as shown in Figure 2.12 and repeated for convenience in Figure 2.21. The battery open circuit voltage is based on the equilibrium potentials of its electrodes, and this varies very slowly. This model is suitable for short-term modelling with a steady current. The model may be improved by varying the internal resistance with respect to SOC, temperature, and/or current [127, 128].

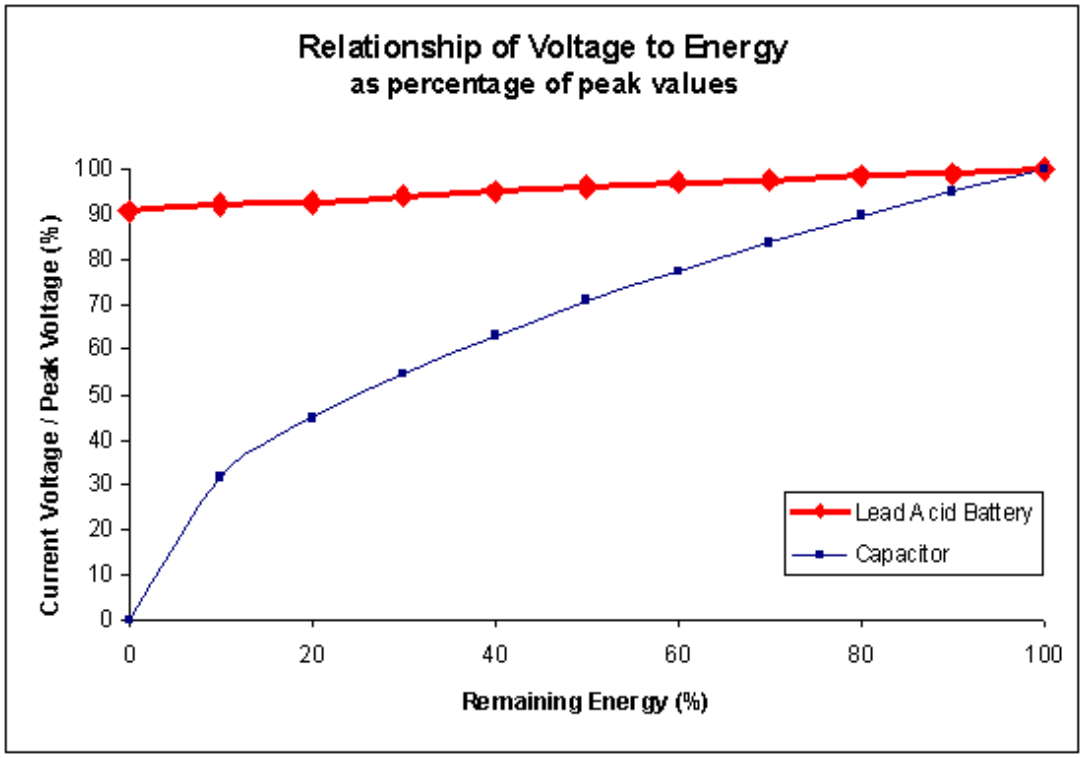

Figure 2.21: The relationship of voltage to energy for lead acid batteries and capacitors. The lead acid battery data is from ADVISOR.

Another common model, known as the Thevenin model or Randle's cell, is shown in Figure 2.22. This model adds an additional RC block to the basic model, representing the capacitance created between the parallel plates that form the battery

electrodes, and the resistance between the plates and the electrolyte [128, 129]. In the model's basic form these values are all constant, however, they can be varied to produce a more rigorous and detailed model. For example, one proposed model for a lead acid battery [128] uses a Randle's cell model as a starting point, but varies the voltage with respect to SOC. The resistances also vary depending on whether the battery is charging or discharging, and there is an additional self-discharge resistance in parallel with the voltage source. A model created at the University of Strathclyde builds on this by also varying the resistances with respect to SOC and proposing an alternate calculation for the voltage [129]. Yet another variation on the Randle's cell model uses multiple RC-blocks and a 'parastic reaction branch' to represent gassing of the electrolyte [130]. The Strathclyde model had a maximum error of less than 1% on discharge tests [129], but the errors of the other models were not enumerated.

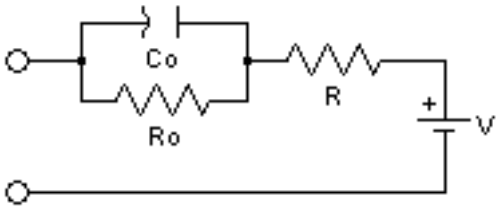

Figure 2.22: Randle's cell model for a battery.

The electrochemistry of the batteries can also be used as the basis for a model. For example, a VRLA battery model developed at the Aachen University of Technology uses the physical structure of the plates and electrolyte to form a mathematical model. This model includes the changes in the structure as the battery charges and discharges, the transport of electrolyte in the pores and of currents in the electrodes, and currents travelling between the electrodes and the electrolyte [131]. The accuracy of this model is not stated.

Another option is to use impedance spectroscopy to form a model of the battery. One such model was developed in the labs of Korea Kumho Petrochemical [132]. Impedance spectroscopy data was used to develop a mathematical model of the battery, which tests found to have an average error of less than 1%. The researchers found that at high frequencies their model was superior to a basic model with resistor

and capacitor, although they agreed closely between 20mHz and 1kHz. They tested their model with various lithium-ion batteries and a NiMH battery, but not with a lead-acid battery.

2.7.3 Ageing

As described in section 2.2.3, a battery pack used in an electric vehicle is expected to last for 3-5 years before needing to be replaced, and one reason for combining them with supercapacitors is to extend their lifetime. The major ageing processes which occur in lead acid batteries are [25, 26, 45]:

-corrosion of the positive grid
-shedding or sludging of the positive mass
-formation of defects in the negative mass
-defects in the separator (affects only flooded batteries)
-loss of water (affects only VRLAs)

These processes are gradual ageing effects which occur throughout the lifetime of the battery and degrade its performance. However they may lead to sudden catastrophic failures by causing an internal short circuit. The extent to which each ageing process occurs is dependent on a range of variables including charging and discharging regimes and temperature, and they are also interdependent to an extent. Different failure modes are more prevalent in flooded batteries and others in VRLA batteries. The Cobra uses VRLAs with a gel separator, and so this review will focus on VRLA ageing.

Corrosion of the positive grid (i.e. the current collector) is a major ageing process in both flooded and VRLA batteries [26]. The corrosion reaction is [26]:

$$2\beta\text{-}PbO_2 + 2H_2SO_4 + Pb \rightarrow \alpha\text{-}PbO_2 + 2PbSO_4 + 2H_2O. \qquad (2\text{-}12)$$

The two different forms of PbO_2, α and β, refer to different physical structures; the α form is more compact, with slightly lower capacity per kg [133]. This corrosion does not take place at the negative electrode because typically it is at a potential below that at which the $Pb/PbSO_4$ reaction occurs spontaneously. When the battery is discharging some corrosion occurs at the negative plate, but it reverses during

charging. At the positive plate, corrosion is slowed by the formation of a layer of PbO_2 and $PbSO_4$ which covers the Pb and separates it from the sulphuric acid. Corrosion is more severe in float applications and in car starter batteries, in which the battery is often at a high state of charge [26]. Figure 2.23 shows the corroded positive grid from a car starter battery after 5 years of service. Corrosion is also a major factor in the degradation of deep cycling batteries such as would be found in an electric vehicle [45]. Overcharging of the battery causes a particularly high rate of corrosion [45]. Fast recharging can decrease the rate of corrosion by promoting the formation of a protective dioxide layer [25]. High temperatures increase the rate of corrosion as does low acidity [25, 26]. (That low acidity increases corrosion is counter-intuitive, but it is an observed phenomenon and may be due to increased solubility of the protective layer [26].)

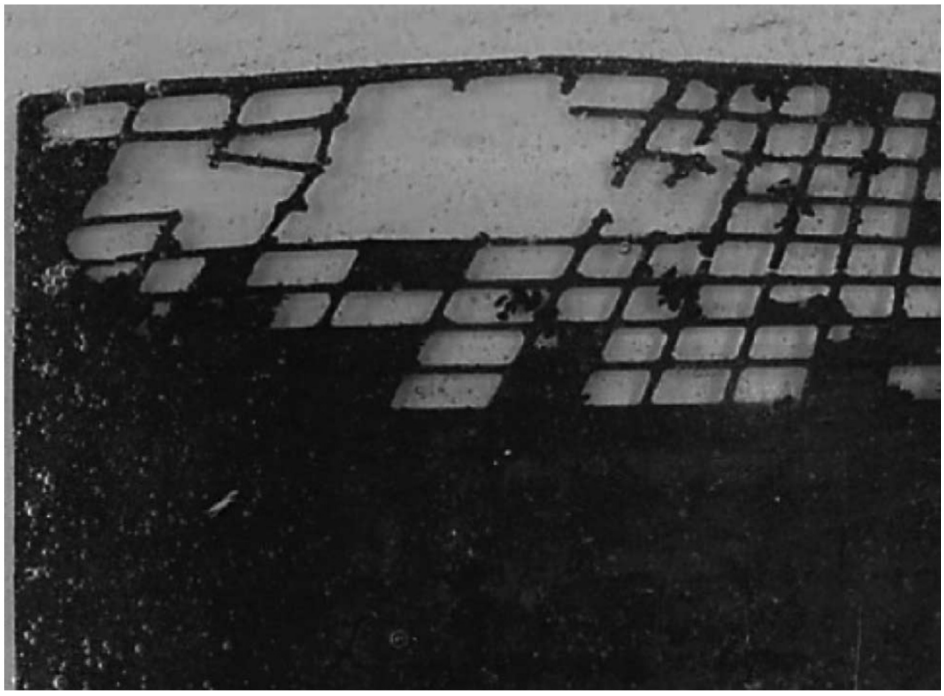

Figure 2.23: A corroded positive plate from a car starter battery after 5 years of service [26].

Another major ageing process is the degradation of the positive active mass in a process known as shedding or sludging. This occurs when the active material at the positive plate ceases to adhere to the grid. Sludging affects flooded batteries far more than VRLAs because the VRLA grids are compressed against the separator,

which helps to physically hold the active mass in place [26, 45]. However it can still affect VRLAs, particularly when the battery is subjected to frequent cycling [26]. For example, the starter battery in a city bus is subjected to frequent shallow charge/discharge cycles, and sludging is a major cause of failure in these batteries. Figure 2.24 shows the positive grid from a city bus starter battery after 6 months of use.

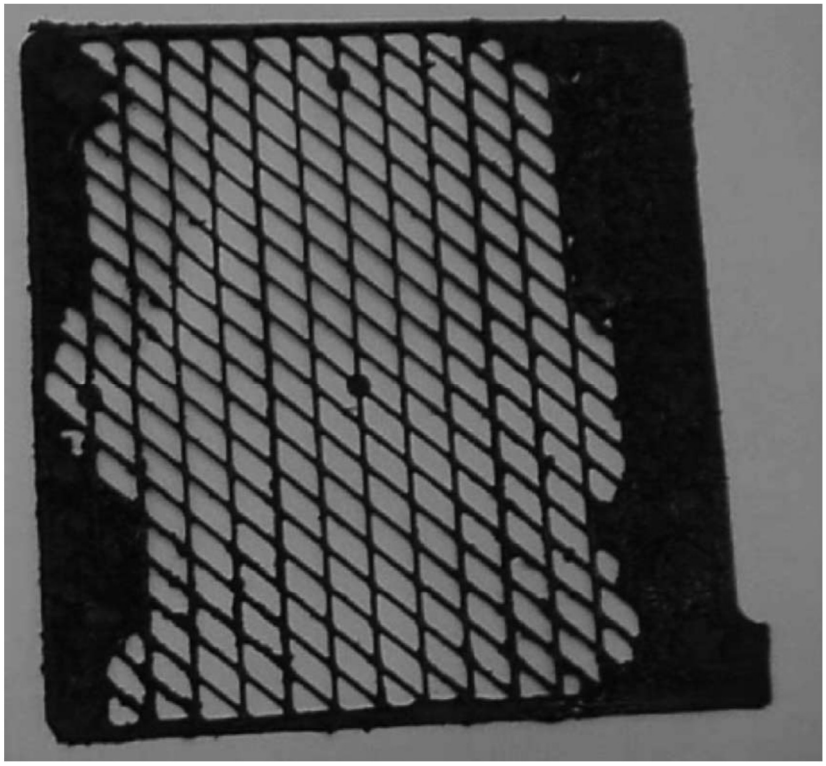

Figure 2.24 The positive plate of a starter battery from a city bus, showing severe sludging after 6 months of use [26].

Sludging is promoted by high rates of discharge [25, 26]. High currents cause a dense layer of $PbSO_4$ to form near the surface of the grid. On recharge, the dioxide reforms on the surface of this layer, away from the grid. Over repeated cycles, the mass moves away from the grid and eventually electronic contact may be lost. This material may collect at the edges of the grid and cause a short circuit. The rate of sludging is also increased by low temperatures and high acidity. Fast charging may inhibit sludging, possibly by raising temperatures [26].

The negative mass can cause failure of the batteries through a process called 'sulphation.' This occurs when the lead sulphate ($PbSO_4$), which is created when the battery discharges, enters a hard crystalline state which resists recharging [25, 26, 45]. Sulphation is especially likely to occur when a battery is left standing for a long time while discharged or partially charged; likewise a long, slow discharge can lead to sulphation. High operating temperatures and high acidity will also increase sulphation. In tall batteries, acid stratification can cause sulphation [26, 45]. Acid becomes concentrated at the bottom of the battery, and when the battery charges the top part becomes fully charged while the bottom part does not. This is particularly a problem with flooded batteries and can be counteracted by deliberate gassing of the battery, which churns up the electrolyte and remixes it. VRLA batteries are less prone to sulphation [45] but it may occur if a patch dry of electrolyte forms in between the separator and the negative plate [26]. This may be aggravated if oxygen enters a faulty valve.

Another negative mass fault that can occur is called 'leading through.' This can occur in both flooded and VRLA batteries in a situation of over-discharge or prolonged deep discharge [26, 45]. It occurs when lead sulphate precipitates into the pores of the separator and then forms a dendrite of metallic lead when the battery is recharged. This can cause a short circuit of the battery.

Flooded batteries can suffer from degradation of the separator, which is made of a porous polymer [25, 45]. The purpose of the separator is to prevent short circuiting of the positive and negative grids and to hold the active material in place. It may suffer mechanical failure due to construction defects, which may be exacerbated by persistently high temperature or the ingress of contaminants. VRLA batteries use a glass mat or gel separator in place of the traditional polymer, and these are not susceptible to this type of failure [45].

Finally, VRLA batteries can be affected by water loss [26, 45], which is not considered an ageing effect in flooded batteries as proper maintenance of these batteries includes topping up with water. This is more of a problem in cycled

batteries rather than float batteries, and can also be exacerbated by overcharging or excessively rapid charging. Water loss increases the acidity of the electrolyte, which as discussed above contributes to sulphation and sludging [26].

2.7.4 Modelling Battery State of Health

The lifetime prediction of batteries is very complicated and involves many different factors. Those models that do exist tend to focus on predicting the remaining life of a battery which is regularly measured – in other words, they do not model a battery throughout its life, but attempt to predict how much life is left in a physical battery based on a few key measurements. For example, work performed at the University of Sheffield used a mathematical model of a VRLA to determine SOC and state of health (SOH) based on voltage measurements [134]. The model predicted the SOC of a battery for a hybrid electric vehicle with a peak error 2%, and predicted the capacity loss over time to within 4%.

There have been some attempts to model the lifetime of batteries based on simulated cycles. One method of doing so is called 'weighted Ah throughput', which counts the total Ah that have passed through the battery, and multiplies them by a factor that depends on the conditions at the time – for example high temperature, high current, etc. An example of such a model [135] uses the weighted Ah calculations to estimate the degradation of the positive active mass and the formation of sulphate crystals, to model the reduction in battery performance. This model was used for flooded lead acid batteries in stationary applications, so acid stratification was also considered. A numerical value for the error was not available. Another example of a weighted Ah throughput model used depth of discharge and rate of discharge to modify the Ah count for a NiCd battery [136]. This model was hindered by a lack of data on how rate of discharge affects battery life, so the accuracy of the model could not be calculated.

Other models include artificial neural networks [137] and equivalent circuit diagrams [138]. These also suffer from a lack of data – especially the ANN which needs a large amount of data to properly train the model [41]. A more successful model has been developed using fuzzy logic. Fuzzy logic was used to model NiMH batteries,

allowing a determination of SOC and capacity without prior knowledge of the battery's charging history or age, using impedance measurements [139]. The battery SOC was correctly modelled to within ±5%, even after repeated cycling caused available capacity to reduce by 20%.

In spite of the lack of details about modelling battery age, there is a consensus on the most important factors. In high power applications, high discharge currents have the biggest effect on battery lifetime [24]. These currents can directly contribute to battery ageing by increasing the degradation of the positive active mass. However, the construction of VRLA batteries limits the damage caused by sludging because the active mass is firmly held in place. It remains to be seen whether preventing high current spikes will have a sufficient effect on the sludging rate to noticeably improve the battery lifetime. Sludging can cause short circuits, so it may be that the chance of catastrophic failure of the batteries is reduced. Alternatively, high current spikes could raise the temperature of the batteries; higher temperature is associated with a lower rate of sludging, but a higher rate of corrosion and sulphation.

Tests which directly assess the impact of supercapacitors on battery life have been mixed. For the EVermont vehicle discussed in section 2.3.2, the supercapacitors did not substantially increase the battery life [58]. The current profiles used in these tests showed approximately a 35% decrease in peak battery current for the hybrid system as compared to the battery-only vehicle, from 225A to 150A. On the other hand, a battery/supercapacitor test bench at the University of Hawaii did create a significant reduction in battery currents when subjected to a cycle of pulses [140]. The batteries alone received currents of over 100A, while the batteries in the hybrid system experienced currents of no more than 20A – an 80% reduction. The supercapacitors extended the life of their battery pack by 253%. A third study involving the positive plates of experimental lead acid batteries also found that reducing peak battery currents resulted in an increase to the life span of the plates [44]. This study found the plate life extended by up to 50% for a current reduction of 33%, and life extended by 137% for a current reduction of 83%.

For the positive plate study, the life was reduced at high currents due to softening of the positive active mass [44]. Unfortunately, neither the batteries from the EVermont vehicle nor the batteries tested at the University of Hawaii were subjected to a post-mortem after their lifetime testing, and so the ageing mechanisms in those batteries are not known. The Hawaii batteries were also not traction batteries but starter batteries for an ICE vehicle, and thus the life extension of EV batteries cannot be directly extrapolated from these results.

2.7.5 Standard Battery Models Within ADVISOR

ADVISOR supplies four different battery models to choose from. The simplest model is called 'Rint' and it models the battery as a voltage source and a resistor in series. The voltage and resistance vary by SOC, with the option to vary by temperature (although temperature-based variations to the characteristics are not provided in the default model), and are determined by use of a look-up table. The resistance also depends on whether the current is charging or discharging the battery. The values for the charging and discharging resistances and the open circuit voltage with respect to SOC are shown in Figure 2.25. This model was tested by NREL on a range of battery types, including VRLA batteries. The primary weaknesses of the Rint model, as identified by the NREL, are an overly strong voltage response to loading, and the fact that the internal resistance does not vary with current [127].

A more complex model is called 'RC'. This models the battery as a set of capacitors and resistors whose values vary by SOC and by temperature, as shown in Figure 2.26. The main capacitance, Cb, is very large and represents the energy stored in the battery. The secondary capacitance, Cc, has a much smaller value and represents surface effects due to diffusion and chemical reactions. The NREL's tests on batteries using the Rint and RC models showed that the Rint model had a maximum error of 12%, while the RC model had a maximum error of 4% [127]. The RC model was tested with a lithium ion battery and with a NiMH battery.

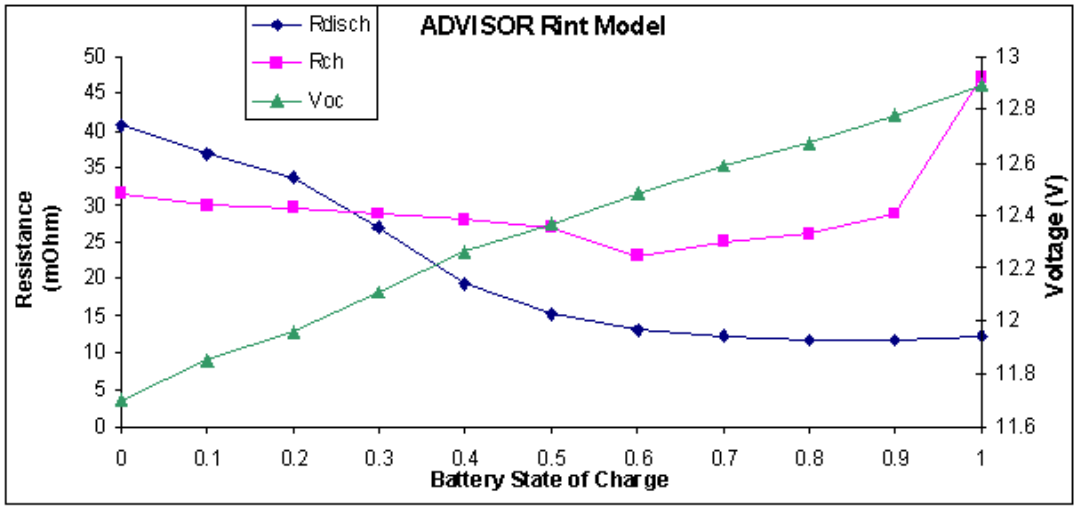

Figure 2.25: Charging and discharging resistances and open circuit voltage of a 25Ah battery in the default ADVISOR 'Rint' lead-acid battery model.

Two ADVISOR models were developed for specific batteries. The first of these models is called the 'Fundamental Lead Acid Battery' model, and was developed based on the chemical reactions and material properties of a lead acid battery from Optima. This model was found to have a peak voltage error of 3%. The second is a neural network model created for a lead acid battery from Hawker Genesis. The neural network model was trained with powers up to 1.2kW and at SOC of 0.27-0.74 [127], and had a peak voltage error of 5%. Unlike the other models, it does not contain a thermal component.

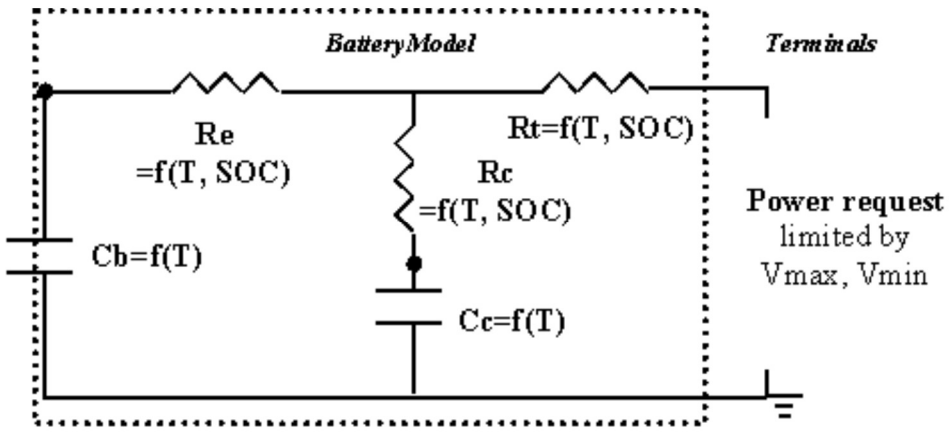

Figure 2.26: RC battery model from ADVISOR [127].

For those models which include a thermal component, the temperature of the batteries is calculated based on the heat that is generated due to the Coulombic losses and internal resistance losses of the batteries, the thermal resistance of the battery case, and the ambient air temperature. A fan may be used if the battery temperature exceeds a set value.

A fifth battery model is described in literature as being under development, called the 'PNGV' model [127]; PNGV refers to the Partnership for a New Generation of Vehicles, which operated as a consortium between the US government and various car companies from 1993 to 2001. However, this model has not been implemented in ADVISOR.

These models have been developed for simulating individual drive cycles, and their primary purpose is to determine the performance of the vehicle over the course of the cycle; in other words, they determine how much power the battery can supply at any given time, based on the voltage and current limits. They are not suitable for simulating the performance of the vehicle over several cycles with recharges in between, because they do not track the state of health of the battery. This means these models cannot be used to directly assess the benefits of a battery lifetime extension strategy.

2.8 Chapter Summary

This work has identified four elements which may be used as the objective for a control strategy for a battery/supercapacitor vehicle:

1) to improve vehicle acceleration
2) to improve overall drive efficiency, increasing the driving range
3) to reduce lifecycle costs by extending the life of the batteries
4) to reduce capital costs by direct replacement of some batteries

A number of battery/supercapacitor hybrid vehicles have been proposed and several have been completed. Each of them attempted to optimise their control strategy for one or more of the listed elements. A van built at Karlsruhe University in Germany used the supercapacitors as a means to reduce the size of their battery pack, at the

cost of flexibility of control [60]. Cranfield University [61, 62], the Catholic University of Chile [51-53], and the National Science Council of Taiwan all chose to optimise their vehicles for efficiency [63, 64]. These groups speculated that battery life would be extended, but it was not used a specific criterion. Meanwhile a vehicle proposed by researchers at the Norwegian University of Science and Technology rejected efficiency as a criterion for optimisation and focused on battery life [69]. The Italian CR-ENEA car did not have a control strategy as such, since the supercapacitors were connected in parallel with the batteries [33]. Nevertheless they achieved increased efficiency and acceleration, while anticipating an increase in battery life. In none of these cases was a battery lifecycle test possible. Finally, the EVermont vehicle tried to achieve each of the first three options – improving efficiency, acceleration and battery life. Their results were disappointing, and lifecycle tests did not show a significant increase in battery life. Each of these groups made a decision about optimisation and designed their hybrid vehicle using models and assessments based on that decision, however the relative merits of different optimisations were not investigated.

Supercapacitors are added to a battery EV to improve the vehicle in one or more of the listed ways, and this should guide the design of the hybrid vehicle. If the optimisation strategy is not well-defined in advance, the hybrid version of a vehicle may not offer a significant advantage over the battery-only version. To achieve the best results, it is important to analyse the potential benefits of the supercapacitors before committing to a strategy and pack size. This requires a robust model of the vehicle.

For this research, the Cobra model is based on the Advanced Vehicle Simulator, (ADVISOR), developed at the National Renewable Energy Laboratory [90]. The key elements for accurately modelling the Cobra are the batteries, supercapacitors and the connecting power electronics. A variety of power electronics models were investigated, with two half-bridge converters being chosen as offering the best combination of flexibility and efficiency. A range of models for the two types of energy storage device have also been investigated.

Supercapacitors may be modelled simply with a resistor and capacitor in series. A number of models take the form of some sort of 'transmission line', with several branches of resistors and capacitors to reflect the porous nature of the electrodes [99, 103, 104, 106, 107]. Some of these models also account for the voltage dependence of the capacitance [99, 104, 107] Other models do not have the transmission line format, but focus on modelling the impedance of supercapacitors with a Warburg impedance [108] or a constant phase element [110]. The thermal behaviour of supercapacitors has also been modelled [105, 112, 113, 115], and the ageing effects analysed [112, 116, 117].

ADVISOR supplies two supercapacitor models, both of which use a variable resistor and variable capacitor in series. Such models are well suited for use in ADVISOR as they allow the voltage and current for the supercapacitor to be easily calculated based on the power demand information, and power demand is the variable which ADVISOR uses to connect the different vehicle components.

Batteries may be modelled as an ideal voltage source and a resistor in series for the simplest model. A commonly used model adds an RC-block to the voltage source and resistor – this is known as a Thevenin model or Randle's cell, and it may be used with constant values for the circuit elements, or with values that vary by SOC [128, 129]. The batteries may also be modelled using a more complex physical model [130] or a mathematical model [132]. As battery performance degrades significantly over time, battery models have been created to track state of health, based on the conditions experienced by the battery including current magnitude and ambient temperature [128, 135, 136, 138].

There are four battery models in ADVISOR, three of which were provided with default values suitable for lead acid batteries. These include a model using a variable voltage source and variable resistor in series, a model based on calculations of the chemical reactions in the battery, and a neural network model. As with the supercapacitor models, a battery model based on a voltage source and resistor

represents the most easily implemented in ADVISOR due to the ability to calculate voltage and current without the need for recursive mathematics. However, the 'Rint' model has a high peak error of 12% [127], while the more complex 'RC' model (which was not tested for lead-acid batteries by ADVISOR) also has a fairly high peak error of 4%. The other two battery models are not suitable for use in the Cobra, as the fundamental lead-acid battery model is created for a specific battery from Optima, while the neural net model requires extensive scenario training.

Therefore, if the Cobra batteries are to be modelled in a default ADVISOR format, they must either undergo extensive and time-consuming tests, or be used in a simpler model which has high peak errors. The third option is to develop a simple yet more accurate model, which is the option pursued by the author of this thesis. The following section describes the battery-powered Cobra and the development of its model.

3 The Battery Cobra

The vehicle used in this research is an AC Cobra kit car, fitted with an electric drive motor and a pack of lead acid batteries. The motor is a water-cooled AC induction motor from MES-DEA and has a nominal power output of 9kW [141], and a peak power output of 30kW [142]. It accepts a voltage of 0-400V and when acting as a generator it can output a current of up to $110A_{RMS}$ [142]. The battery pack consists of six 12V, 70Ah Hawker Genesis lead acid batteries connected in series [40]. As a low power and low energy vehicle, it is suitable for urban commuting but not for extended journeys or motorway travel. It is a low cost vehicle, and therefore the added supercapacitor pack will need to be small and relatively inexpensive.

3.1 The Cobra Data Logger

The Cobra was tested with a data logger recording battery voltage, battery current and vehicle speed, and pictured in Figure 3.1. The data was collected at 10Hz. Since ADVISOR uses one second increments, the data was then averaged in sets of ten to create the power and speed data to be used in the model. The Cobra batteries were not tested under temperature control conditions, and so temperature effects were not included in the modelling.

Figure 3.1: The Cobra data logger (reconfigured to measure a single 12V battery, rather than the full 72V pack, hence the warning sticker).

3.1.1 Voltage and Current

The voltage and current transducers used the same circuit board (the 'VT/CT' board) in the data logger. Both transducers were manufactured by LEM components, part number LV 25-P for the voltage and number LA 125-P for the current. Both transducers require an input voltage of ±12V, however the auxiliary battery outputs +12V. Therefore, a DC/DC converter was used to interface between the auxiliary battery and the transducers, specifically type TEL 3-1222(NP) from Traco Power. The voltage and current transducers were purchased by a fourth year student at Strathclyde, Gordon Noble, who also designed the circuit in which they operated. The transducers were later retested and some elements resized by the author of this thesis. The final form of the circuit as used in the Cobra is shown in Figure 3.2 – in this figure, connections to the DC/DC converter are labelled 'D', those to the voltage transducer are labelled 'V' and pins out are labelled 'P'. A photo of the circuit board is shown in Figure 3.3.

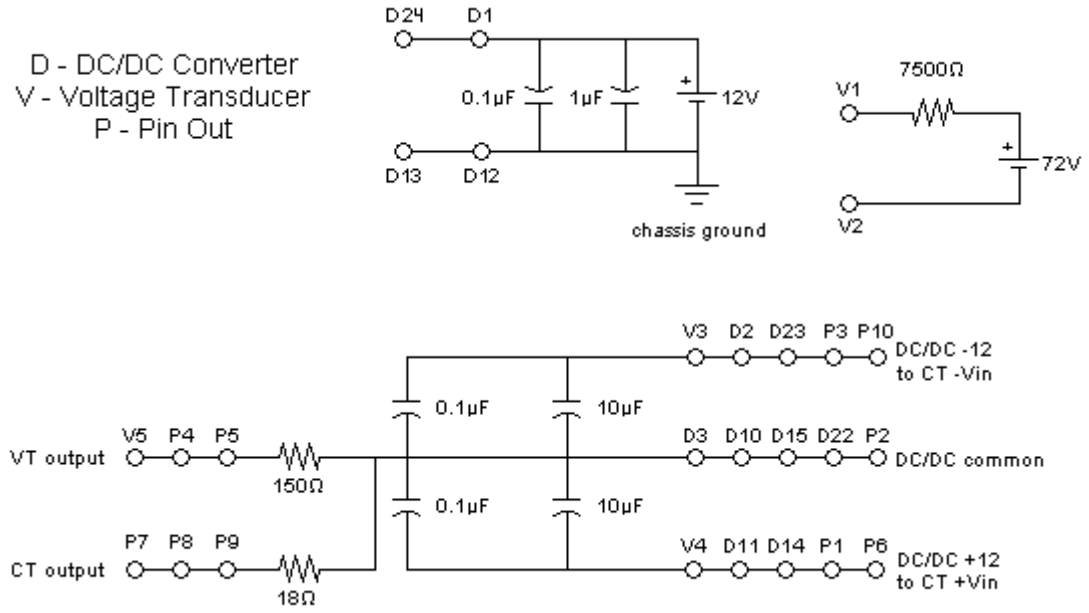

Figure 3.2: Circuit diagram for the voltage and current transducer circuit board.

This circuit board was also used for measuring the voltage of the individual Cobra batteries during discharge tests. This required recalibrating the voltage transducer by removing the 7.5kΩ resistor and replacing it with a 1.2kΩ resistor. A warning notice was placed on the data logger as a reminder of this change.

Figure 3.3: The VT/CT board. The 150Ω resistor is obscured by the blue voltage transducer.

3.1.2 Speed

Speed information is provided by the Cobra motor controller in the form of two square waves, each representing one phase of the Cobra motor. A frequency-to-voltage (FTV) circuit designed by Mr Bob Baird was used to create a voltage output from this signal. The Cobra motor speed is proportional to the vehicle speed, and this relationship was determined by comparing the voltage output of the FTV circuit with the rotational speed of the Cobra's rear wheels as measured using a handheld tachometer. The wheels have a circumference of 2.15m, thus 2.15**rps* gives the driving speed in meters per second, where 1m/s = 2.24mph.

The speed sensor was compared to the speedometer on the Cobra dashboard to confirm the calculations. A picture of the FTV board is shown in Figure 3.4.

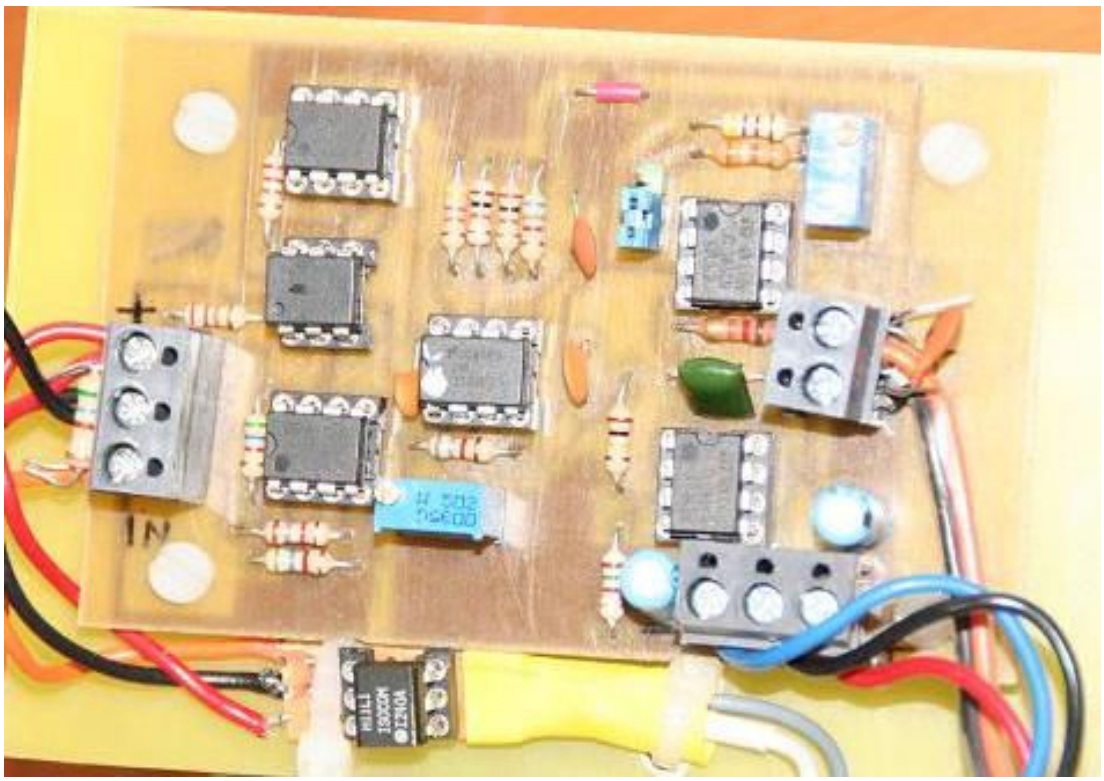

Figure 3.4: The FTV speed sensor board.

3.1.3 Routing Board

The data logger routing board managed the power flow in the data logger. A power switch was used to connect a 12V power source (usually the auxiliary battery) to the DC/DC converter and thence to the transducers. A second switch triggered a relay which in turn connected the traction battery pack to the 7.5kΩ measurement resistor. Each switch had an associated LED to indicate if it was on or off, and both the power circuit and traction battery circuit were fused, with ratings of 500mA and 100mA respectively. A picture of the routing board is shown in Figure 3.5.

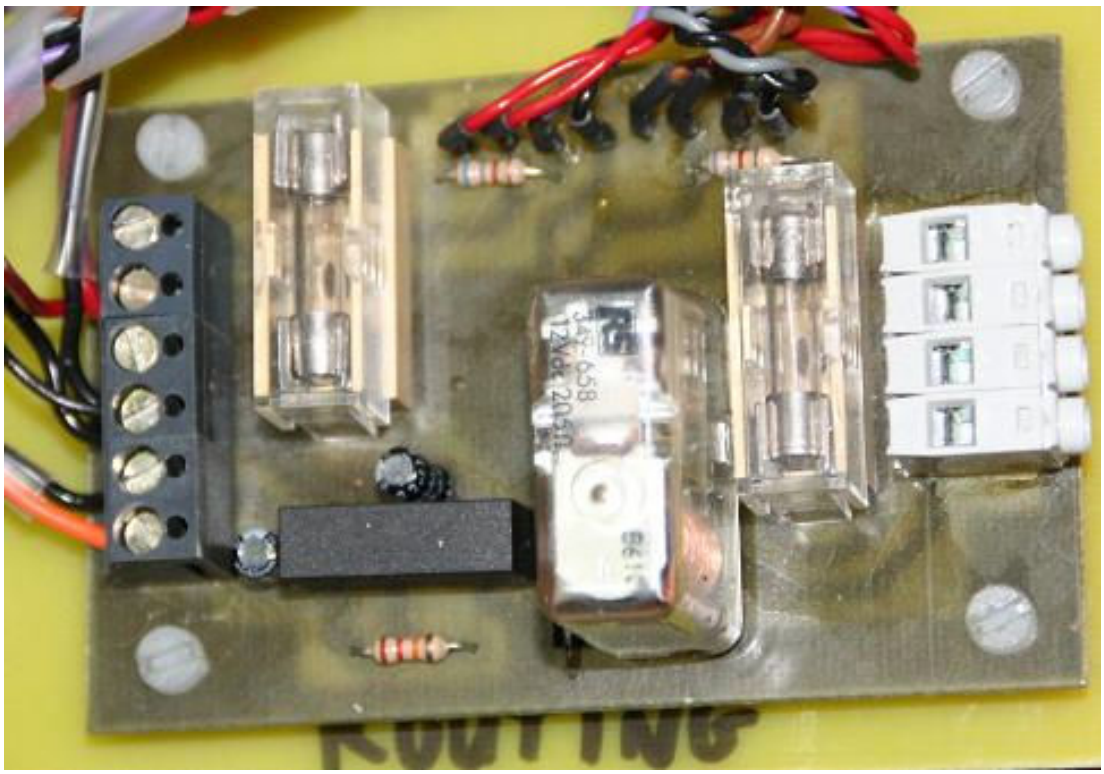

Figure 3.5: The data logger routing board.

3.1.4 Compact Reconfigurable Input/Output Device (cRIO)

The voltage outputs of the various transducers were read by a Compact Reconfigurable Input/Ouput device, or cRIO, from National Instrumentsٍ. The cRIO consists of a Real Time (RT) control unit (part #9014) and a chassis (#9104) which contains a Field Programmable Gate Array (FPGA) with 3 million gates. A wide range of modules are available to be plugged in to the FPGA chassis, in this case an Analogue Input module (#9205). Other modules are available for future development and control of the vehicle, but they were not used in this research. The cRIO is shown in Figure 3.6.

An FPGA is an array of programmable logic gates. The array offers true parallel programming, with operation speeds of nanoseconds. This makes it a very fast and precise control unit, albeit with limited memory. Meanwhile the Real Time controller operates in microseconds and also features very accurate timing. The RT unit may also be interfaced with a laptop; laptops do not offer accurate timing as they must maintain multiple processes with no parallel computing capability (or limited parallel computing if the laptop has a multi-core processor). The laptop must switch

rapidly between programs including queries to the keyboard and mouse, which prevents accurate time keeping if the time frame is in the order of milliseconds or faster. However, laptops offer a convenient graphical interface to monitor the operation of the cRIO.

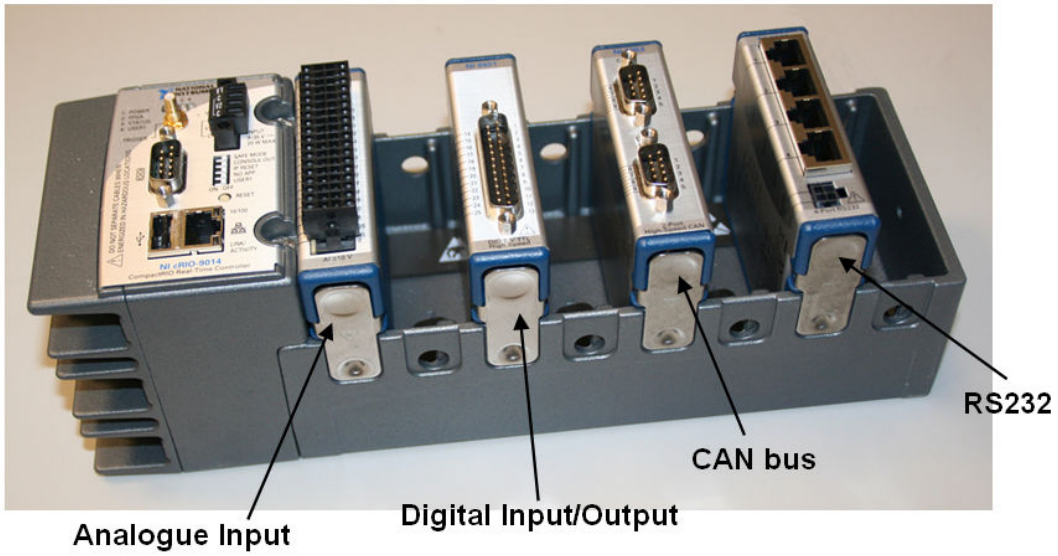

Figure 3.6: The cRIO

The cRIO was programmed with LabView 8.6. The LabView program consisted of three elements:

1) An FPGA program to read the data from the Analogue Input Module
2) An RT program to calibrate the data and save it to a memory stick
3) An optional laptop program to graph the data as it was collected.

The FPGA program read the data from the Analogue Input module at a rate of 10Hz. This data was stored in a FIFO ('first in, first out') structure which could then be read by the RT controller. Separating the data collection program from the data manipulation program ensured that data collection would run at the precise speed requested. The FPGA block diagram is shown in Figure 3.7.

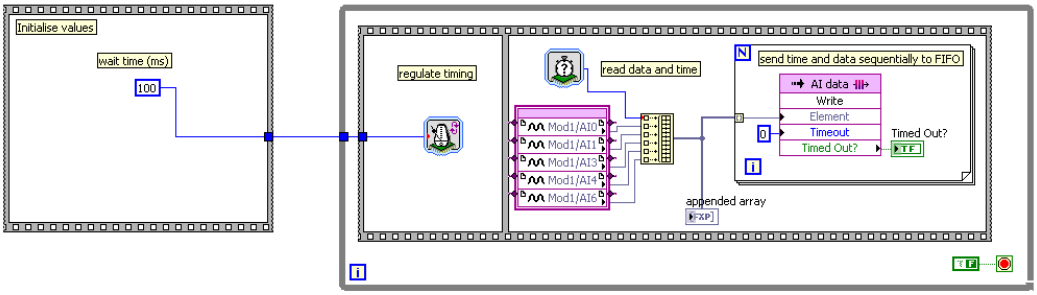

Figure 3.7: The FPGA data acquisition program, where data is read from the Analogue Input module.

The RT program read the data that had been placed in the FIFO structure by the FPGA program, calibrated the current and voltage data by multiplying it by an appropriate factor, and saved it as a CSV file to a memory stick. The RT program was also responsible for starting and stopping the FPGA program. This was accomplished by using a 'state machine'. The program began in the 'Start' state (shown in Figure 3.8), checking the user switch to determine if it was on or off.

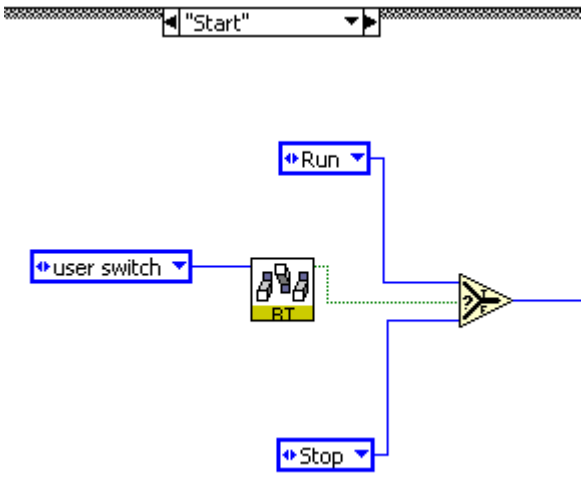

Figure 3.8: The Start state for the RT program.

If the user switch was off, the program would shift to the 'Stop' state, and if it was on, it would shift to the 'Run' state. The 'Stop' state ended the program, while the 'Run' state initialised the CSV file, started the FPGA program, and manipulated the data. It also monitored the user switch – when this was turned off, or if an error occurred, the FPGA program would be halted and the CSV file closed, then the

program would shift to the 'Stop' state. Segments of the 'Run' state are shown in Figures 3.9 and 3.10.

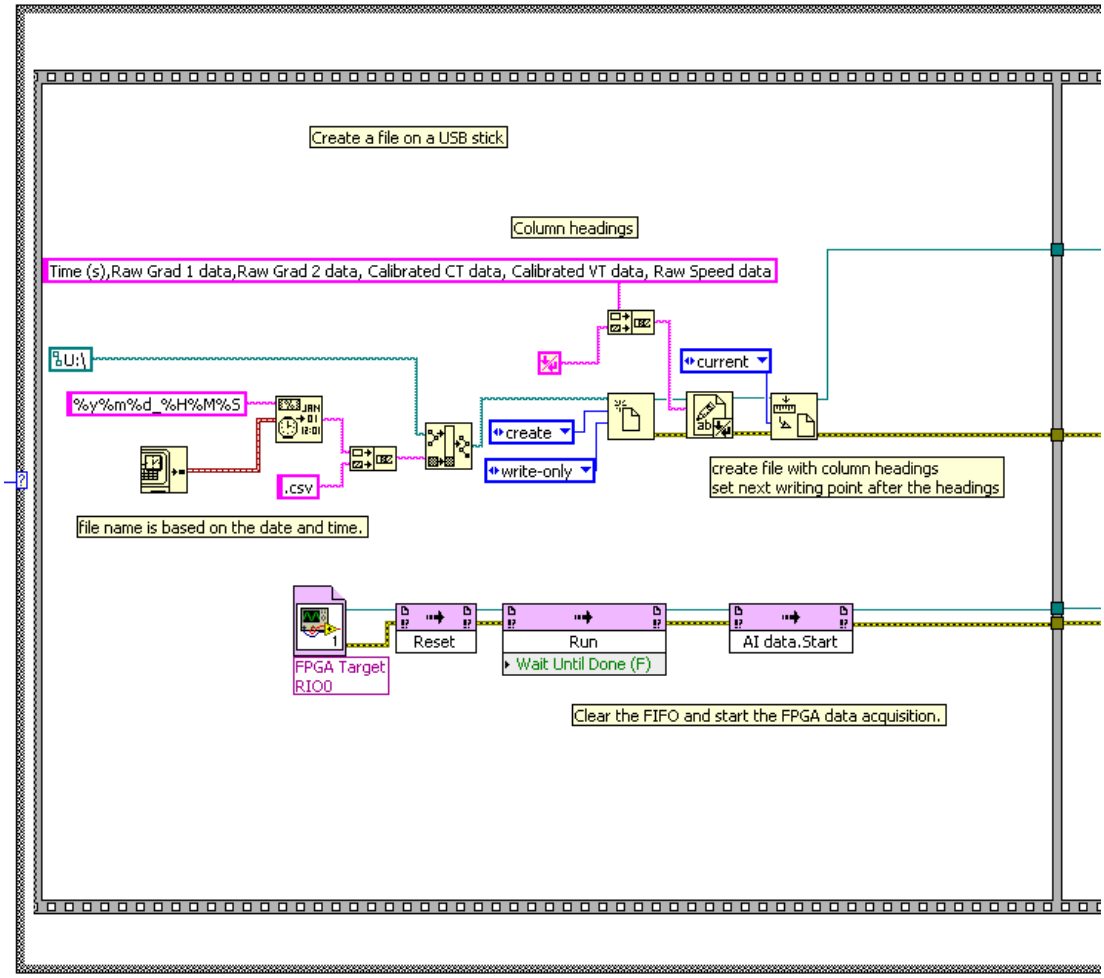

Figure 3.9: The initialisation stage of the Run state in the RT program, where the CSV file is created and the FPGA program started.

Finally, the laptop program collected the data from the RT unit and displayed it in a series of graphs. This allowed the data collection to be monitored while the Cobra was on blocks, however the laptop was not used while the Cobra was on the road to prevent damage or theft. The laptop program block diagram is shown in Figure 3.11, and the front panel is shown in Figure 3.12.

Note that neither the RT program nor the FPGA program have graphical interfaces on the front panel, as such interfaces can interfere with the timing of the program

operation. The laptop program exists purely to provide a graphical interface if this is required.

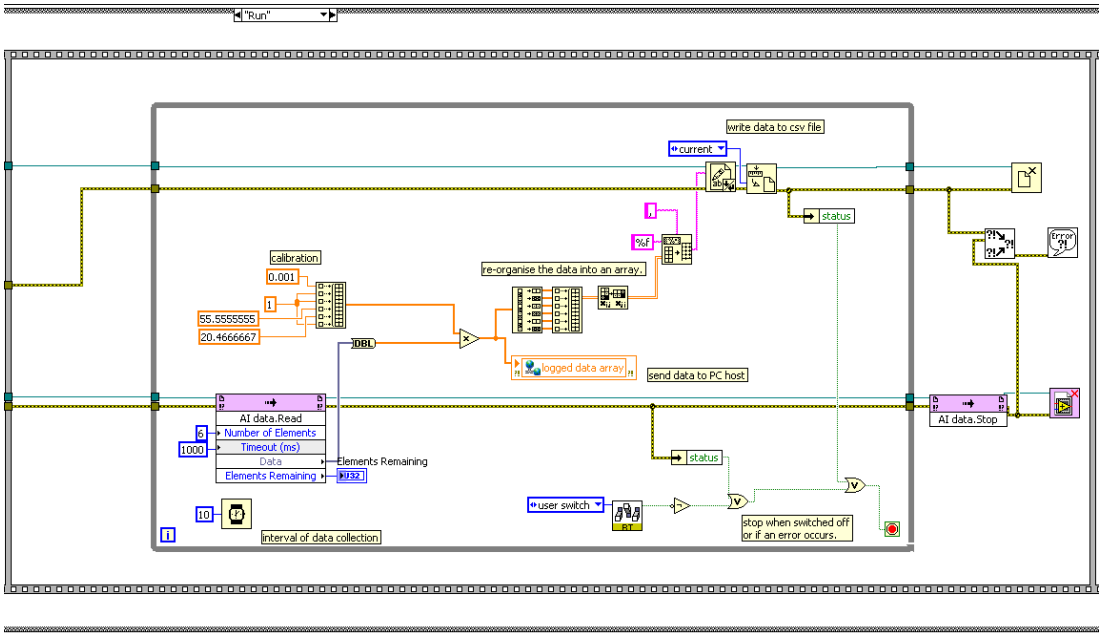

Figure 3.10: The main body of the Run state in the RT program, where the data is collected, calibrated and saved to file.

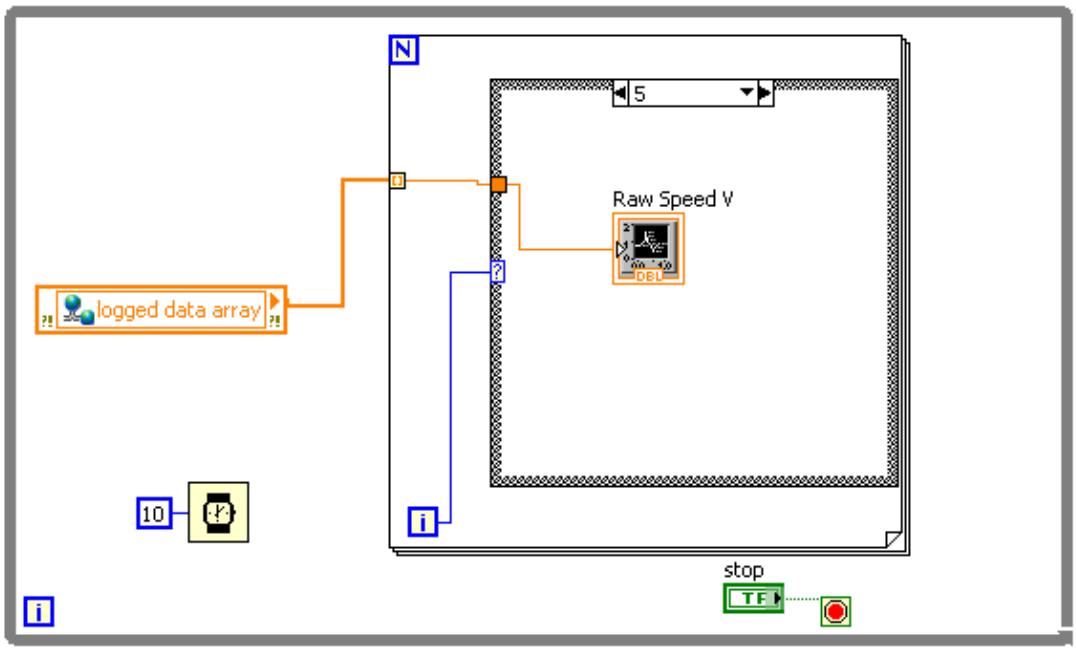

Figure 3.11: The laptop program reads the calibrated data from the array created in the RT program.

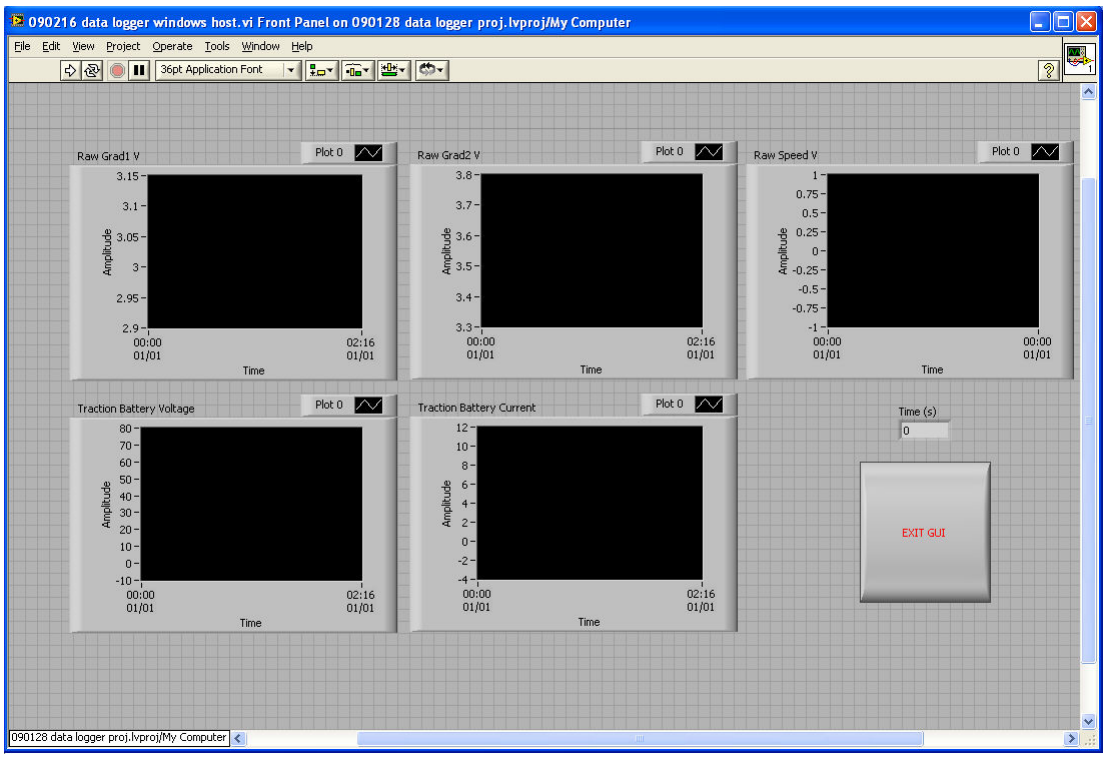

Figure 3.12: The front panel of the laptop program. All the data is plotted on its own graph, with the units determined automatically by the program.

The cRIO was located in a secure box under the bonnet of the Cobra, to prevent ingress of water.

3.2 Modelling the Cobra Battery Pack

3.2.1 Theory of Randle's Cell Model

In order to investigate control of a battery/supercapacitor hybrid, an initial model of the Cobra batteries was created by the author within the ADVISOR environment. The model uses traction and accessory power demand information as inputs to the battery model; this information was created from a range of drive cycles taken from within ADVISOR or generated by the author while driving the Cobra around Glasgow. The power demand information forms a request from the modelled battery pack, which then calculates the current needed to supply the power. If the batteries cannot supply the requested power while remaining within their voltage parameters, they will instead supply the maximum power possible, and the discrepancy between the requested and supplied power is noted.

The 'Rint' model available as standard from ADVISOR was used as a starting point, as it is a simple model already tested and validated on Hawker Genesis batteries at NREL [127]. The Rint model uses a voltage source and resistor in series, with both values varying with respect to SOC. The model starts with a requested power value, P (W), which is related to voltage and current as:

$$P = V_{meas}I, \tag{3-1}$$

where V_{meas} (V) is the voltage measured at the terminals and I (A) is the current. The measured voltage is the open circuit voltage V_{OC} (V) minus the voltage drop caused by the internal resistance R (Ω) of the battery:

$$V_{meas} = V_{OC} - IR. \tag{3-2}$$

V_{OC} is determined by the state of charge of the battery, which in turn can be tracked by counting the Ah extracted from the battery. Thus, power can be defined in terms of current as:

$$P = (V_{OC}\text{-}IR)I \tag{3-3}$$

This can be rewritten to give a quadratic equation:

$$P = V_{OC}I\text{-}I^2R \tag{3-4}$$

$$I^2R - V_{OC}I + P = 0 \tag{3-5}$$

Solving this quadratic equation gives one value for the current as:

$$I = \frac{V_{OC} - \sqrt{V_{OC}^{\ 2} - 4RP}}{2R}. \tag{3-6}$$

The alternative solution is:

$$I = \frac{V_{OC} + \sqrt{V_{OC}^{\ 2} - 4RP}}{2R} \tag{3-7}$$

which is neglected; it results in much higher battery currents than those from Equation 3-6, which would present the lower and therefore more easily achievable steady-state solution. This must always be the case, as V_{OC} and the square root term will always have positive values. Note also that if the power has a value such that:

$$P > \frac{V_{OC}^{\ 2}}{4R}, \tag{3-8}$$

then the solution is imaginary and the power cannot be supplied by the batteries. Once the current is known, the measured voltage of the batteries can be determined using Equation 3-2.

This approach does not take into account the dynamic response of the battery, which is influenced by the capacitive effects of the battery plates. Correctly simulating this behaviour is a particular strength of the Randle's cell model, described in section 2.7.2 and shown in Figure 2.22. The figure is repeated here for convenience, as Figure 3.13.

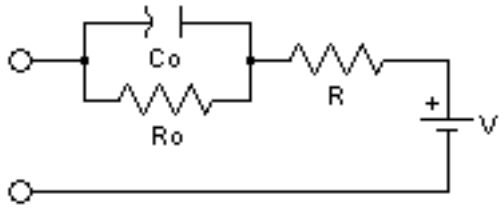

Figure 3.13: The Randle's cell battery model.

The parallel RC-branch, shown in Figure 3.13 as R_o and C_o, is used to model this capacitive behaviour. The voltages across the parallel resistor R_o and capacitor C_o are:

$$V_{Ro} = i_{Ro} R_o \tag{3-9}$$

$$V_{Co} = \frac{1}{C_o} \int i_{Co} dt + V_{initial} \tag{3-10}$$

V_{Ro} and V_{Co} (V) are the respective voltages across the two elements, i_{Ro} and i_{Co} (A) are the respective currents, $V_{initial}$ (V) is the voltage across the capacitor C_o at the start of whatever time period is under consideration, and t (s) is time. R_o (Ω) and C_o (F) are the defining quantities for the resistor and capacitor shown in Figure 3.13. As the elements are in parallel, they must have equal voltages, therefore equating 3-9 and 3-10 and taking the derivative of both sides, gives:

$$V_{Ro} = i_{Ro}R_o = V_{Co} = \frac{1}{C_o}\int i_{Co}dt + V_{initial} \tag{3-11}$$

$$R_o \frac{di_{Ro}}{dt} = \frac{i_{Co}}{C_o} + 0 \tag{3-12}$$

$$i_{Co} = R_o C_o \frac{di_{Ro}}{dt} \tag{3-13}$$

The sum of the currents in the capacitor and resistor must be equal to the current *i(t)* in the battery.

$$R_o C_o \frac{di_{Ro}}{dt} + i_{Ro} = i(t) \tag{3-14}$$

If *i(t)* is a constant, *I*, then this differential equation can be solved with an exponent:

$$i_{Ro}(t) = I + Ke^{-t/R_o C_o} \tag{3-15}$$

where *K* is a constant. The capacitor will start with a certain voltage $V_{initial}$, which is equal to $V_{Ro}(0)$ and $V_{Co}(0)$. Therefore:

$$V_{initial} = i_{Ro}(0)R_o \tag{3-16}$$

Solving this gives the value for *K*:

$$i_{Ro}(0) = V_{initial}/R_o = I + K \tag{3-17}$$

$$K = V_{initial} / R_o - I \tag{3-18}$$

Thus the current on the resistor R_o for a constant current discharge is:

$$i_{Ro}(t) = I + (V_{initial} / R_o - I) e^{-t / R_o C_o} \tag{3-19}$$

If the battery is left to rest for some time after discharge, then the voltage on C_o, $V_{initial}$, will drop 0. The form of this voltage decay can also be calculated from equation 3-19 as the battery current I is 0:

$$i_{Ro\text{Resting}}(t) = \frac{V_{initial}}{R_o} e^{-t / R_o C_o} \tag{3-20}$$

and from equation 3-11, the voltage on C_o is described by the equation:

$$V_{Co\text{Resting}} = V_{initial} e^{-t / R_o C_o} \tag{3-21}$$

The quantity $R_o C_o$ is known as the time constant, and is typically represented by the letter τ. When the time t equals τ, then the voltage V_{Co} will have decreased to approximately 36.8% of its initial value. When t is equal to 5τ, then the capacitor will effectively be completely discharged, having dropped to less than 0.7% of $V_{initial}$. Therefore, if the battery is discharged from a fully rested state such that $V_{initial} = 0$, the current on the resistor R_o during the discharge becomes:

$$i_{Ro}(t) = I(1 - e^{-t / R_o C_o}) \tag{3-22}$$

while the battery voltage is:

$$V_{meas}(t) = V_{OC} - IR - IR_o(1 - e^{-t / R_o C_o}) \tag{3-23}$$

3.2.2 Applicability of Randle's Cell Model

To determine if the parallel branch R_o and C_o has a significant impact on the Cobra batteries, the batteries were discharged individually across a bank of resistors. The voltage and current information were recorded using the Cobra data logger, with the

voltage sensor recalibrated to account for the fact that single batteries were being measured instead of a pack of six. The details of the data logger are given in Section 3.1. The bank of resistors included three resistors of 3.1Ω, one resistor of 1Ω, and one resistor of 0.5Ω, each in parallel and individually switched. This meant that the discharge resistance could be varied depending on the setting of the switches. A diagram of the experimental set-up and a photo of the resistor bank are shown in Figure 3.14. Sample results are shown in Figure 3.15.

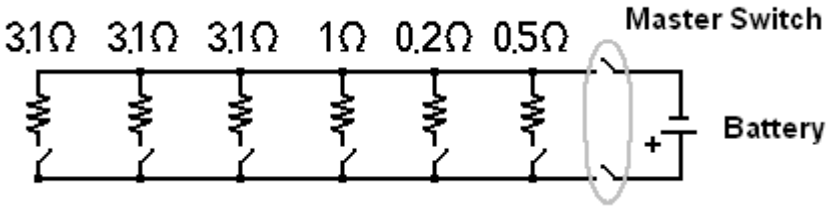

(a)

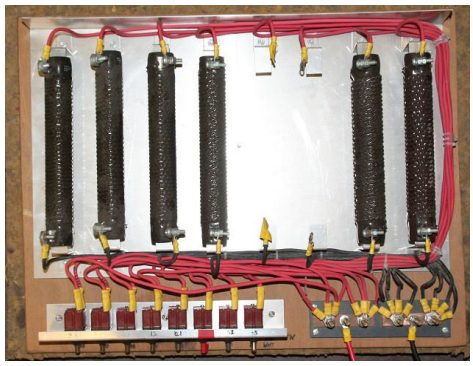

(b)

Figure 3.14: a) A diagram of the experimental set-up for the battery discharge tests. b) A photo of the resistor bank. The 0.2Ω resistor was not used in the tests.

From equation 3-23, it can be seen that at time $t = 0$, the IR_o term goes to zero and the initial voltage drop on the batteries is due solely to the resistance R. The subsequent decay of the battery was fit using curve fitting software KaleidaGraph to find R_o and C_o using equation 3-23 – a sample fit is shown in Figure 3.15. The current was approximated to be a constant current, using the average value for the first 100 seconds of the discharge. The actual current deviated from the average by up to 3% in the first 10 seconds of the discharge, and by less than 1% thereafter. The value for R was found using the initial voltage drop from the discharge together with the initial measured current values. R was found to be similar for each battery, with a typical value of 0.011Ω. It did not vary substantially with SOC to below 30%. SOC effects are described in greater detail in Section 3.2.3.

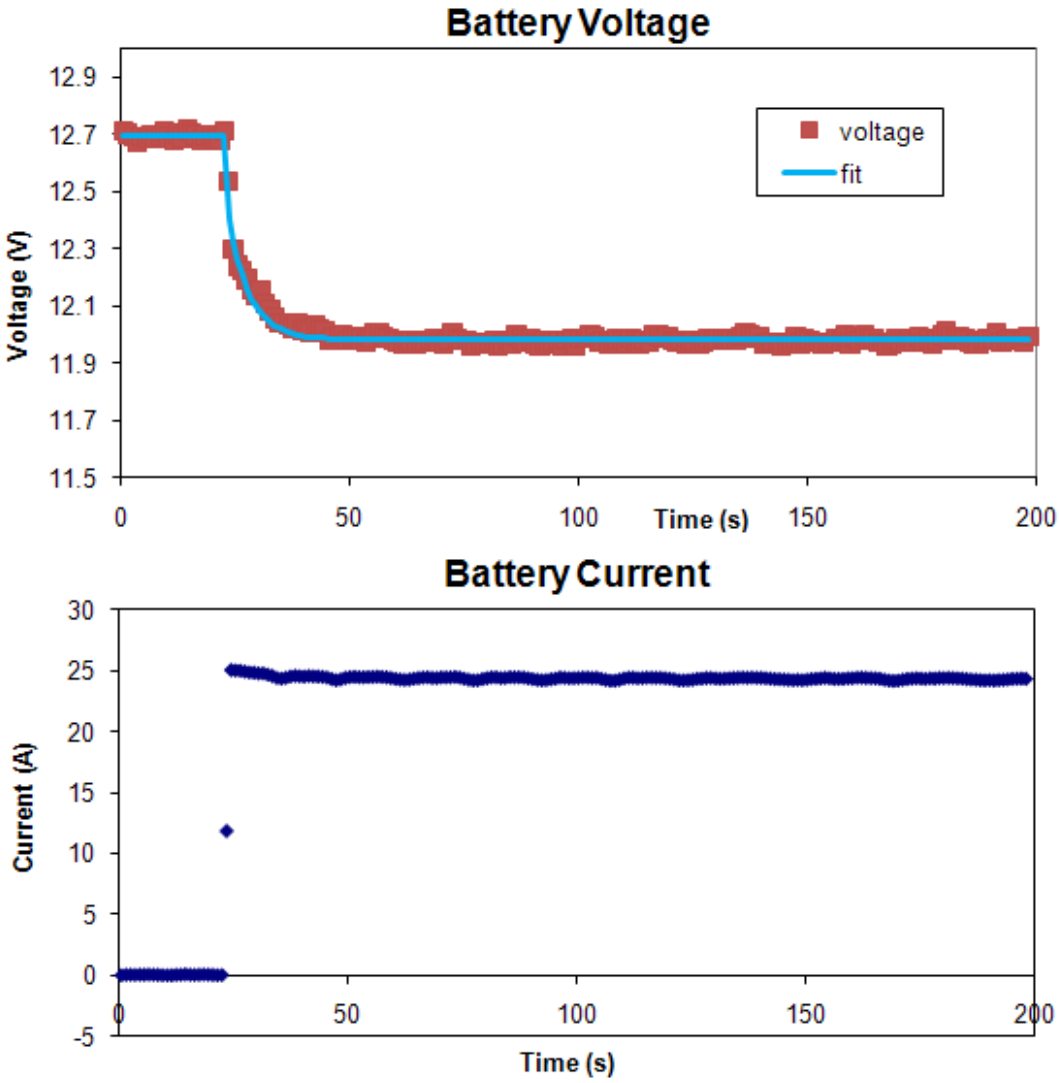

Figure 3.15: Voltage and Current for a single Cobra battery discharged across a resistor bank, with overall resistance of 0.51Ω. The voltage has been fit with Equation 3-23.

Each of the six batteries was tested individually at a range of currents and SOCs. No battery was found to be significantly underperforming or outperforming the pack, and as the battery pack is modelled in ADVISOR as a unit, it was not considered necessary to identify minor differences in the individual battery parameters. The battery test results were combined in order to identify the key parameters which would have a significant impact on the overall pack performance and thus would require additional study.

Test results showed that the R_o and C_o terms were significant, and that R_o varied substantially based on the magnitude of the discharge current. This is the expected behaviour of any battery, and is due to the charge transfer resistance of the electrochemical reaction; the rate at which electrons take part in the reaction (the charge transfer) is proportional to the current and this appears as a higher resistance at lower currents [143]. The fitted values for R_o and C_o are shown in Figure 3.16. Note that at low currents, R_o can be more than four times the value of R.

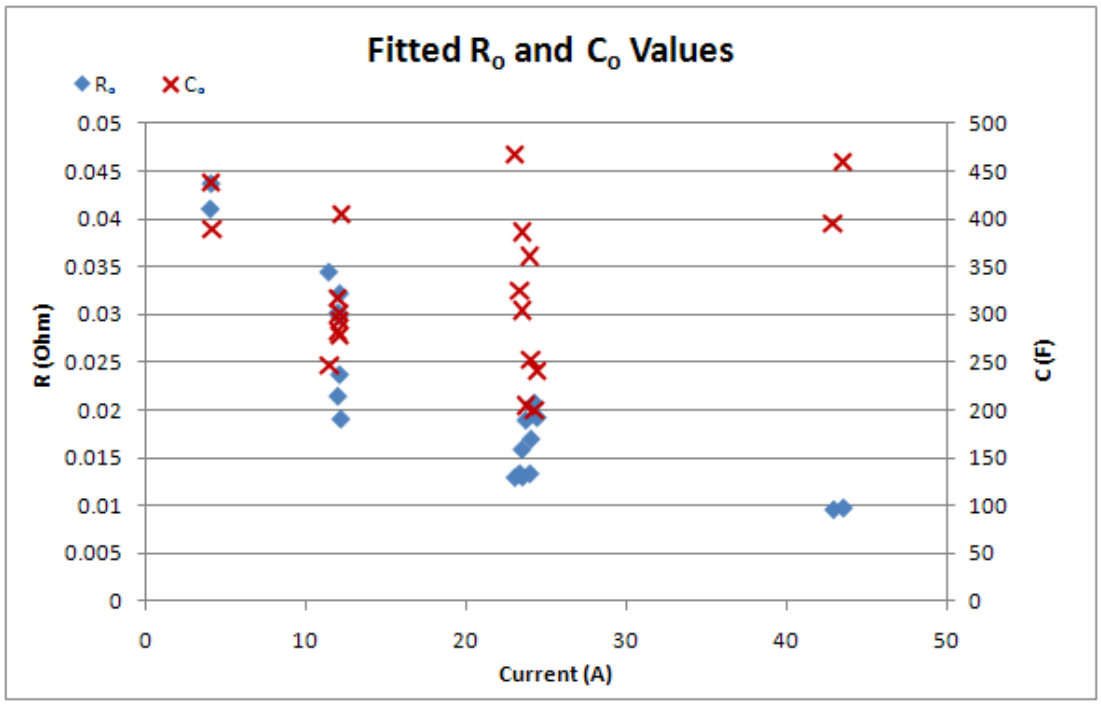

Figure 3.16: Fitted values of Ro and Co for individual Cobra batteries being discharged across a bank of resistors.

The fitted values for C_o varied widely with no obvious trends: this is due to the low impact on the value of V_{meas} due to variations in C_o, and hence the difficulty in creating an accurate fit of this variable. Considering instead the time constant τ, as shown in Figure 3.17, the relationship of the exponential term to the current magnitude becomes apparent. This shows that the capacitive effects for the Cobra batteries should not be ignored if good results are to be achieved. On the other hand, recall that the current value is not known in advance for any ADVISOR-based model, but must be determined based on the power demand information. To interface with the ADVISOR-based model, a simple yet accurate battery model was

required. The remainder of this section describes the development of the author's Cobra battery model.

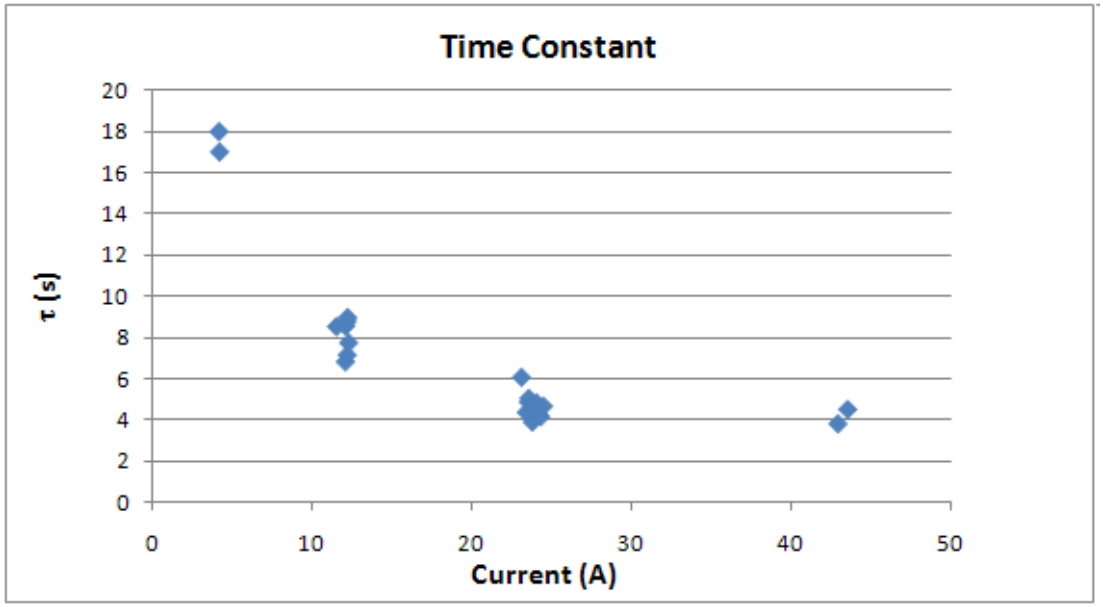

Figure 3.17: Fitted values for the time constant τ for individual Cobra batteries being discharged across a bank of resistors.

3.2.3 State of Charge

The Cobra battery pack was tested to determine the relationship of voltage to SOC. The pack was tested *in situ* with the Cobra motor providing the load for discharge tests. The rear section of the Cobra was jacked up and placed on blocks for this test, allowing the rear wheels to spin freely, so a small discharge current could be applied over a long period of time by means of the motor controller. Voltage and current data were recorded at 10Hz using the data logger, then averaged in blocks of ten to produce 1Hz data. The resulting current data fluctuated with a typical standard deviation of 0.34A for each discharge, and the average current of each individual discharge varied from 4.86A to 8.22A. The average current over all of the discharge tests was 6.37A. Sample data from the discharge tests is shown in Figure 3.18.

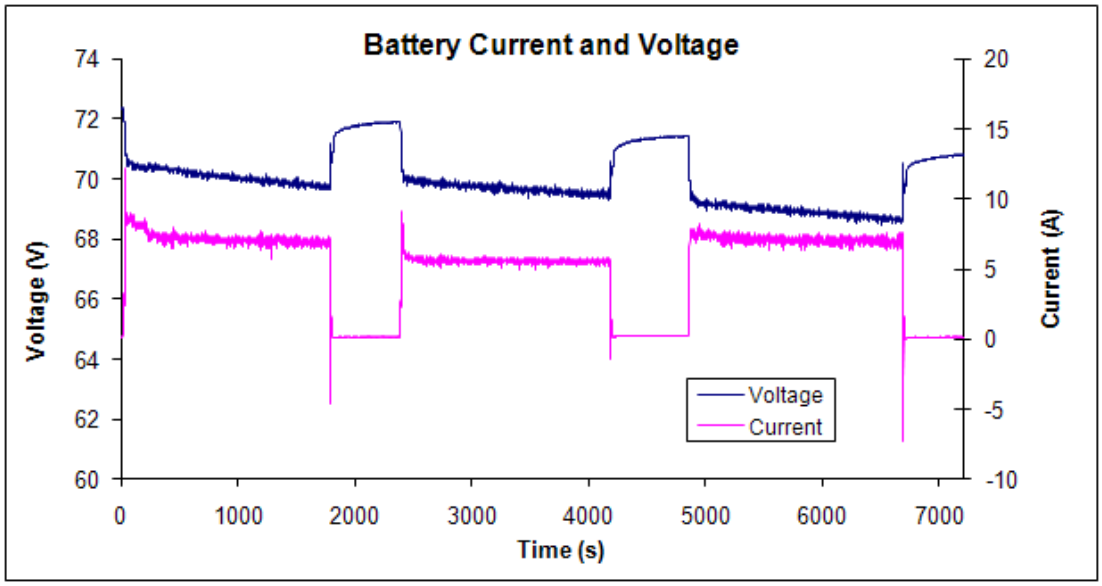

Figure 3.18: Sample voltage and current data from the Cobra battery pack discharge tests performed with the Cobra motor acting as a load.

The SOC was determined using Ah counting, and a commercial battery charger from EnerSys-Hawker was subsequently used to recharge the batteries. The battery charger is a Lifeplus TC3 model configured to charge battery packs of 60V or 72V nominal voltage [144], and the peak charging current has been measured as 55A. A count of the Ah replaced during charging gave the value for the Coulombic efficiency of the batteries, using:

$$\eta_{coul} = Ah_{out}/Ah_{in} \qquad (3\text{-}24)$$

where η_{coul} is the Coulombic efficiency, Ah_{out} is the count of the Amp-hours removed from the battery in discharging, and Ah_{in} is the count of the Amp-hours delivered to the batteries during charging. The pack's Coulombic efficiency was measured as 91%; Coulombic efficiency refers to the batteries' internal charging losses due to some energy producing water vapour and corrosion instead of the desired reaction [145].

The open circuit voltage decreases linearly with SOC down to below 20% SOC, as shown in Figure 3.19. The open circuit voltage V_{oc} was matched to SOC with a line found using the least squares method available in Microsoft Excel. This gives the equation:

$$V_{OC} = 10SOC + 67.36 \quad (3\text{-}25)$$

If the Cobra batteries are partially discharged, the SOC can be estimated from the measured voltage using this equation.

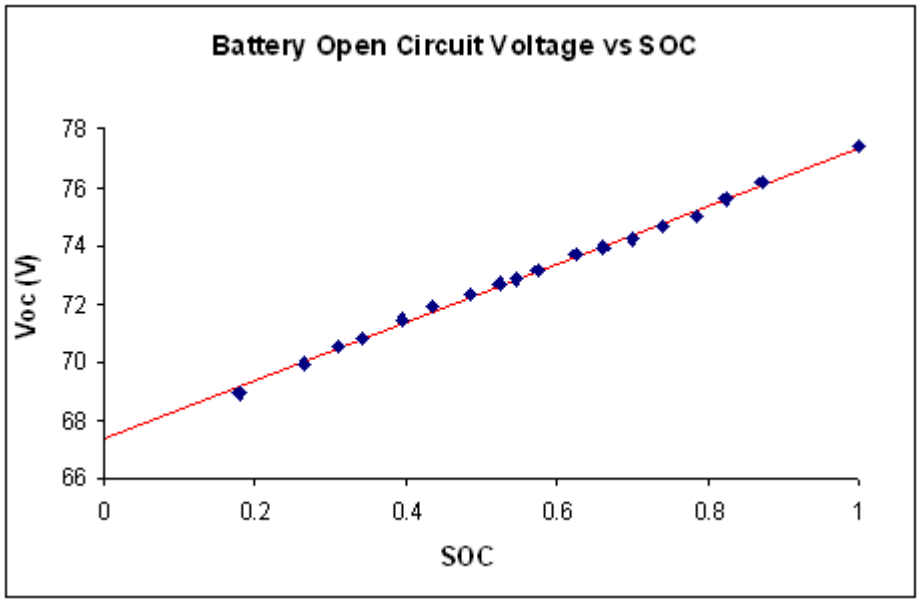

Figure 3.19: The Cobra battery open circuit voltage with respect to state of charge. The red line shows the 'least squares' fit to the data described in Equation 3-25.

This voltage decrease is more rapid than for the default battery model provided in ADVISOR. This is probably because of ageing effects in the Cobra batteries, which were bought in 2002 and have been infrequently cycled. A comparison of the ADVISOR battery voltage and that of the Cobra batteries is shown in Figure 3.20. The ADVISOR batteries described by the figure, like the Cobra batteries, are Hawker Genesis gel-type batteries, but with a capacity of 26Ah, while the Cobra batteries have a capacity of 70Ah.

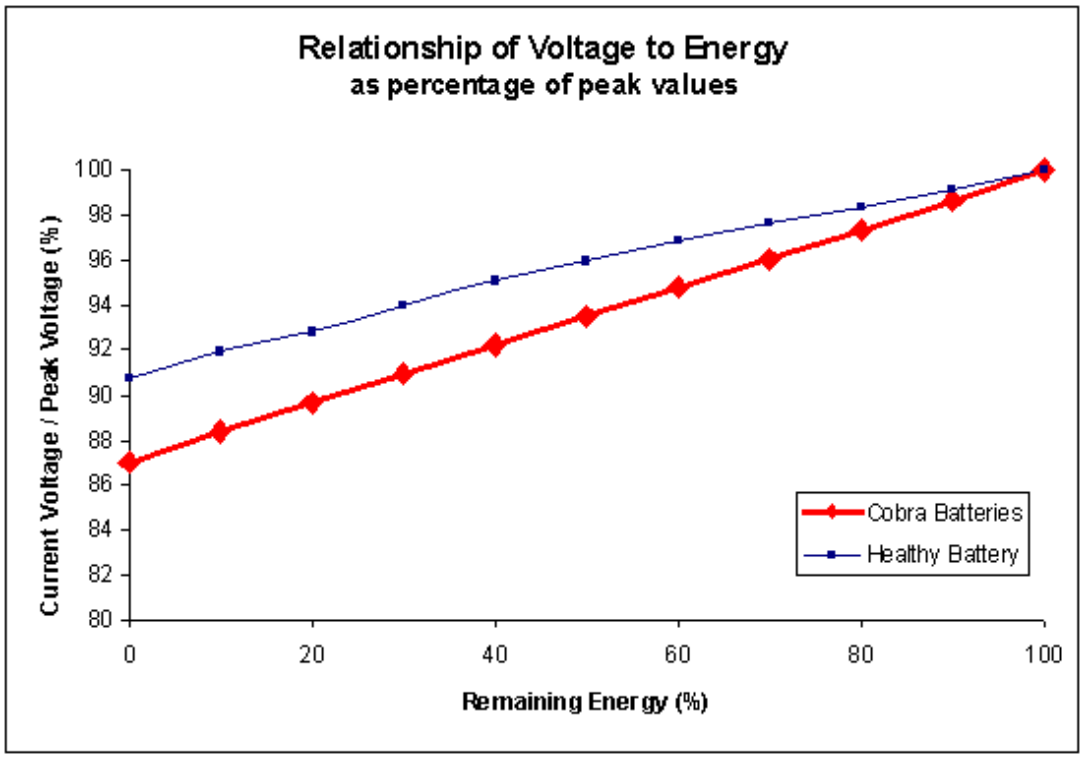

Figure 3.20: The relationship of voltage to energy for healthy lead acid batteries and for the seven year old Cobra batteries. The data for the healthy batteries is from ADVISOR. Data for the Cobra is extrapolated from Equation 3-25.

As the Cobra batteries were not tested when purchased, it is not possible to compare their original performance with their current performance. Had the batteries been tested when purchased, the loss of performance in the Cobra batteries would be categorised as a loss of capacity – i.e. a fixed reduction in voltage corresponds to a fixed decrease in capacity, and a shorter discharge would be needed to accomplish this reduction. This is the standard method of tracking ageing effects in batteries, but is not possible here due to the lack of data for the batteries when new. Loss of capacity is the natural result of most ageing processes discussed in section 2.7.3 – sludging and corrosion reduce the amount of available active material on the positive plates, while sulphation renders parts of the negative plates inactive.

3.2.4 Low State of Charge

During the discharge tests, the behaviour of the battery pack was fairly consistent down to about 25% SOC, at which point the battery voltage began to drop increasingly rapidly. The collapse of the voltage is illustrated in Figure 3.21, together with the states of charge at each rest period, and the open circuit voltages

predicted for each SOC using equation 3-25. At 31.3% and 26.5% SOC, the battery pack reaches the predicted voltage. During the discharge to 21.8%, the voltage begins to decline much more rapidly. During the rest period at 21.8%, the voltage does not recover as expected – hence this data point was not used in calculating equation 3-25. Finally, while discharging to 17.8% SOC the voltage collapses dramatically before stabilising somewhat. At this point the batteries were left to sit overnight, and as described in Section 3.2.3, the voltage then recovered to fit the same voltage pattern as that of the higher SOCs.

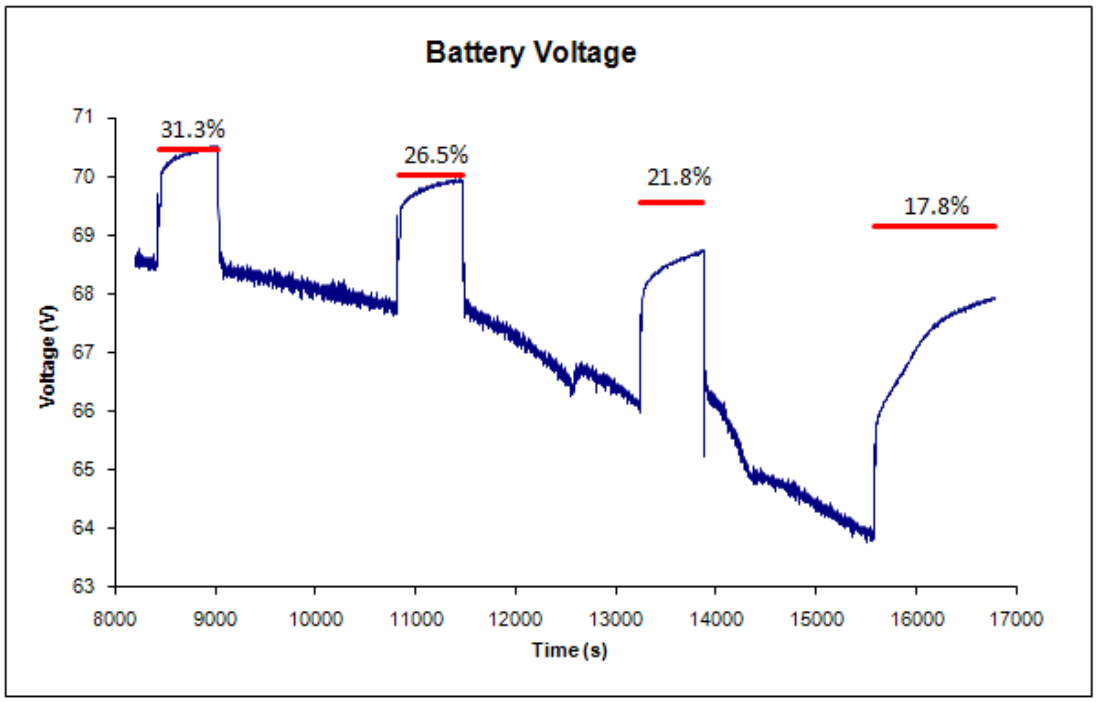

Figure 3.21: The voltage of the Cobra batteries during a discharge from 31.3% to 17.8% SOC. The voltage collapse at approximately 25% SOC indicates likely failure of the Cobra if driven beyond this point.

This data indicates that the Cobra is likely to fail if driven below 25% SOC, creating a hazard for the driver and for traffic in general. The battery model was therefore not developed for this region.

3.2.5 The Voltage Drop

Thanks to the varying resistance, described as R_o in the Randle's cell model shown in Figures 2.22 and 3.13, the resistance of the batteries varies substantially with current magnitude. For example, consider a sample test of the battery pack, performed while

the Cobra was on blocks to allow the wheels to spin freely. The current and voltage of the batteries during these tests, recorded at a rate of 1Hz, are shown in Figure 3.22. This data was not recorded with the Cobra data logger, but with a voltage probe from Testec (TT-SI 9002) with an attenuation of 1:20 and an accuracy of 2% [146] and an AC/DC current clamp from Tenma (72-6174) with an attenuation of 1:100 and an accuracy of 2% + 2A [147]; the data was recorded by a Tektronix oscilloscope (TDS 2024) [148].

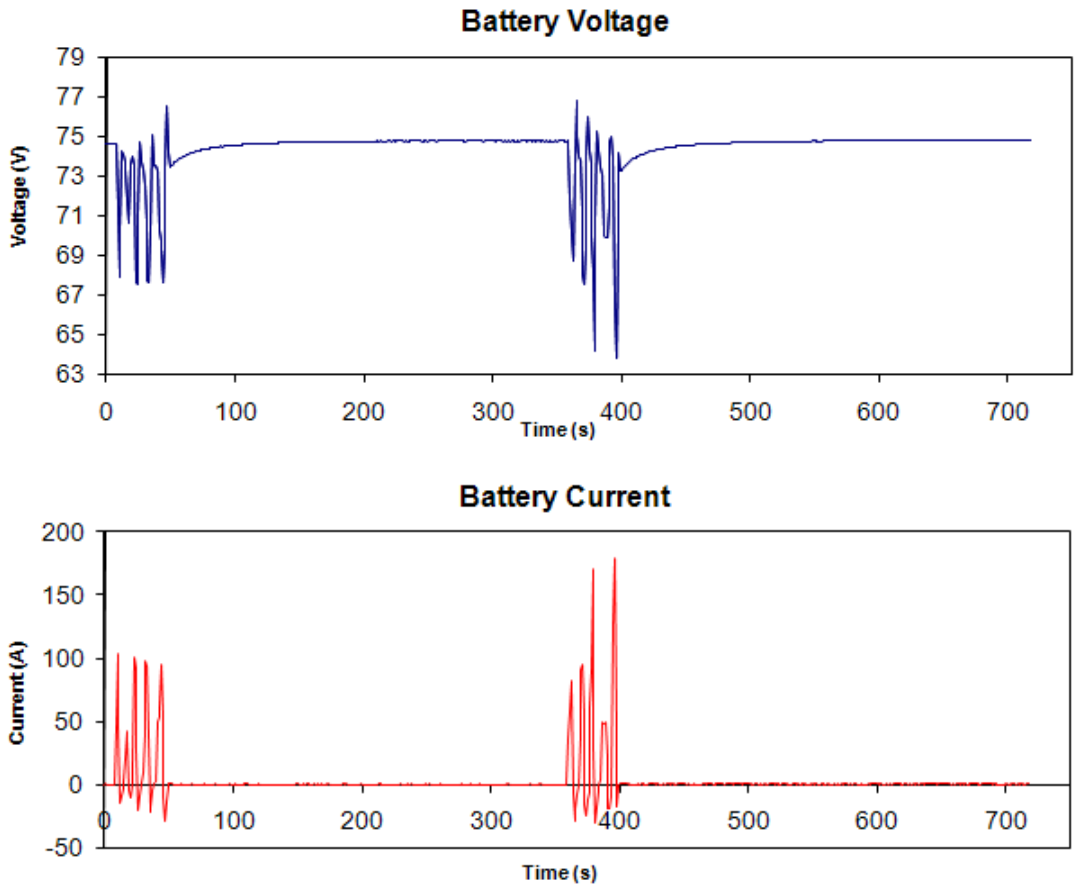

Figure 3.22: Current and voltage for the Cobra batteries during a test performed with the Cobra on blocks.

The open circuit voltage for the batteries was measured as 74.77V at the end of each test. The test removed a total of 0.61Ah from the batteries, which represents less than 1% of the total battery charge and was not sufficient to change the open circuit voltage by a measurable quantity. The apparent resistance of the batteries at each one second time step was calculated using the equation:

$$V_{OC} - IR_{app} = V_{meas} \quad (3\text{-}26)$$

where I is the current (A), R_{app} is the apparent resistance (Ω) and V_{meas} (V) is the measured voltage. The apparent resistance during this test, as calculated using equation 3-26 for each recorded data point, is shown in Figure 3.23.

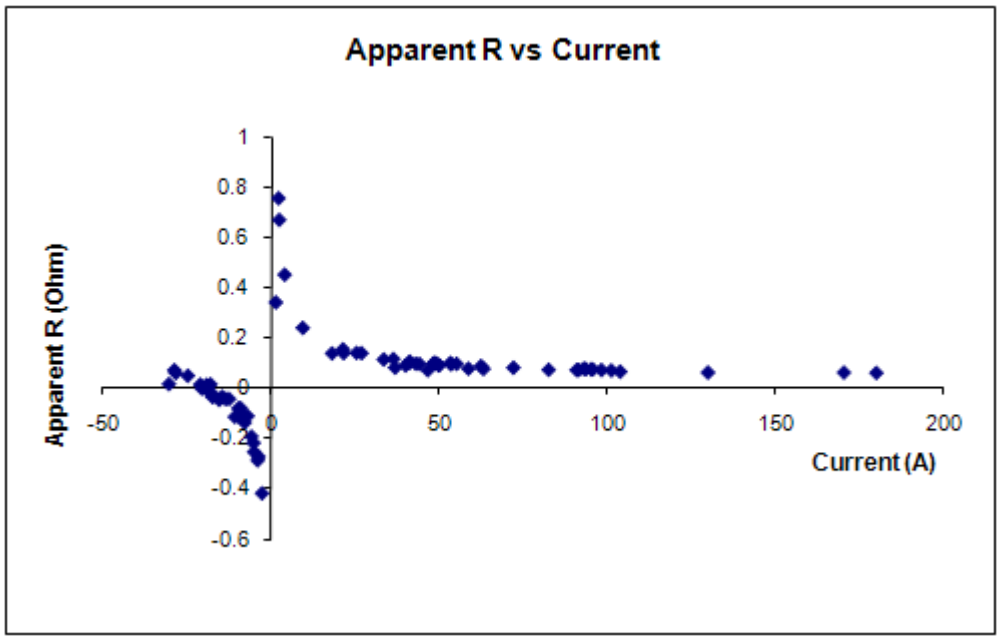

Figure 3.23: The apparent resistance of the Cobra batteries for different currents. Charging currents are negative on this graph, and discharging currents are positive.

For an ideal battery, the apparent resistance should be a constant with respect to current. However, for the real battery the apparent resistance looks more like an exponential function with respect to current, as increasingly small currents do not correspond to increasingly small differences in V_{OC} and V_{meas}. In theory the resistance might be modelled using a current-dependent equation, however in practice using such an equation in a power-based model like ADVISOR creates problems of recursion, and as discussed in Section 3.2 this is something to be avoided if a simple model is to be created.

A more suitable equation for an ADVISOR-based model should focus on the voltage, as in ADVISOR the battery voltage and power demand are used to find the battery current. The capacitance effects in the battery, as modelled by the Randle's Cell, create a delay in the voltage recovery in the battery. The author asserts that if the

battery is not left in open circuit then voltage recovery does not occur, and the capacitance effects resemble a voltage *suppression*. This forms the basis for the author's battery model, which approximates the voltage suppression as a constant voltage drop. This drop would be more significant at lower currents, accounting for the apparent increase in resistance. Furthermore, if a charging current is briefly applied the voltage drop is still evident, and this would create the apparent negative resistance. By this approximation, the measured battery voltage V_{meas} actually follows the equation:

$$V_{OC} - V_{drop} - IR = V_{meas} \tag{3-27}$$

where V_{drop} is the constant voltage drop. This can be rearranged to give

$$V_{OC} - V_{meas} = V_{drop} + IR \tag{3-28}$$

which in turn can be fit with a line to find the voltage drop and resistance. Figure 3.24 plots V_{OC} -V_{meas} vs. current for the same data set as that shown in Figure 3.23. Figure 3.24 also shows a line of best fit, created in Excel using the least squares method. The positive value of the y-intercept for this fit indicates the presence of a constant voltage drop. An alternative fit, also created in Excel, is shown with the y-intercept value forced to 0 to represent no voltage drop effect.

Using similar tests at a range of different states of charge, the typical voltage drop has been found to be 1.5V, with an internal resistance of 0.06Ω for the pack. These values are suitable for SOC greater than 25%. The internal resistance translates to 0.01Ω for each battery – slightly less than the value of 0.011Ω found with the discharge tests of the individual batteries described in Section 3.2.

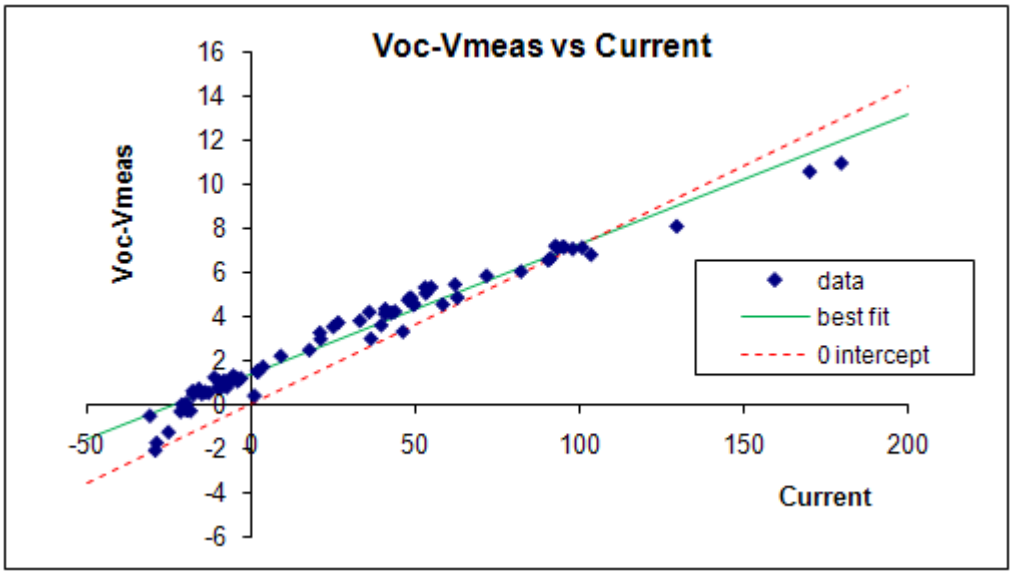

Figure 3.24: The relationship of V_{oc}-V_{meas} vs. current for the Cobra batteries in the same test as that shown in Figure 3.23. An alternate fit with the y-intercept forced to 0 is also shown – this shows the model with the voltage drop not included.

When the batteries receive an extended charge from the EnerSys charger the voltage behaviour is reversed, with a constant voltage rise added to the voltage rise caused by the internal resistance. The constant voltage rise is indicated by a negative y-intercept value for the best fit, as can be seen in Figure 3.25.

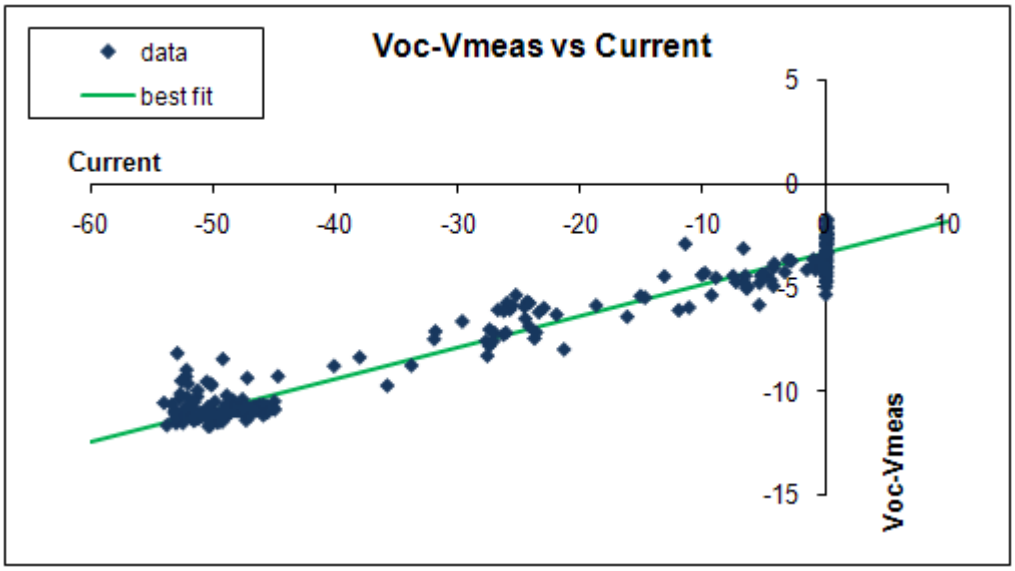

Figure 3.25: The relationship of V_{oc}-V_{meas} vs. current for the Cobra batteries during a recharge

However, during a drive, the short charges experienced by the batteries are not enough to instigate this behaviour. Note that in Figure 3.24, the charging currents, i.e. the negative currents, follow the same line with respect to V_{OC} -V_{meas} as do the discharging currents. The model therefore does not include any sort of voltage rise behaviour for the drive cycles, as this would greatly overestimate the battery voltage during regenerative braking.

The power losses in the batteries, using the original Rint model from ADVISOR, are calculated using the equation:

$$P_{loss} = I^2R \tag{3-29}$$

P_{loss} (W) is the power lost at each time step, and this is used to calculate the total energy lost and hence the efficiency of the batteries. For the new Cobra model, the 1.5V voltage drop is applied directly without being associated with a specific resistance. However, there is a resistance involved – the current-dependent R_o term, which carries a current i_{Ro} as described in Section 3.2. For this model, the losses associated with the 1.5V voltage drop term are estimated using the equation

$$P_{droploss} = 1.5I \tag{3-30}$$

This term is added to the losses calculated using equation 3-29 to find the total power losses in the batteries for each simulation time step.

3.2.6 Voltage Recovery

After a battery has been subjected to a current, it takes some time for the voltage to return to the open circuit value, due to the capacitance effects occurring between the plates of the battery. For the author's battery model, the capacitance effects were approximated during discharge of the batteries as a constant voltage suppression. When the batteries were at rest and during the brief charging periods experienced during drive cycles, the capacitance effects were modelled with equation 3-21, using values found in tests of the Cobra batteries.

The voltage recovery of the Cobra batteries was assessed during the discharge tests described in section 3.2.3. After each discharge the battery was left to rest, allowing measurements of both the open circuit voltage and the voltage recovery behaviour. For the values shown in Figure 3.19, ten minutes rest was sufficient for voltage recovery for all but the last data point (with one data point unused because insufficient time was left for recovery – see Section 3.2.4). This was confirmed at SOCs of 66.2% and 48.5% by leaving the batteries overnight; additional voltage recovery for the pack was only 0.01V in the first case, and 0.06V in the second. The final data point, with an SOC of 17.8%, is taken from the voltage measurement on the following day. Overnight voltage recovery for this point was 0.98V.

The data from each voltage recovery event was modelled as an exponential equation, using the fitting function in the Kaleidagraph software. The voltage on C_o was assumed to be consistent for each test, as the tests involved similar currents (4.86A to 8.22A, with an average value of 6.37A, as stated in Section 3.2.3) and at steady state, prior to disconnection of the load, $V_{initial}$ is equal to iR_o and R_o is essentially constant for a given value of i. Because the model uses a constant value of 1.5V for the voltage drop, it was assumed that the recovery would begin from a value of 1.5V below open circuit voltage. The time constant τ was therefore the only variable that was found using the fit. Average results for the fit were then used to created a voltage recovery equation:

$$V_{meas} = V_{OC} - 1.5e^{-0.02t} \qquad (3\text{-}31)$$

where t is the time in seconds since a power with magnitude greater than 100W was applied. The limit of 100W was chosen based on the accessory load of the Cobra, which was typically about 17W when the inverter fan was not running, and typically about 140W when the inverter fan was operational. The effect of the fan on the battery voltage behaviour was noticeable in testing – when the Cobra was stationary during a drive cycle, the battery voltage was found to remain in a suppressed state when accessory power was high (e.g. the fan was operational), and to show recovery behaviour when the accessory power was low. This behaviour is demonstrated in the following section.

3.3 Model Verification

The Cobra battery model combines accuracy with simplicity. By calculating the voltage effects mathematically instead of with an equivalent circuit, the model slots neatly into the existing structure of ADVISOR without the need for complex calculations. The parameters are easy to obtain with a few tests. Specifically:

1) The relationship of voltage and SOC is determined through discharge tests, using Ah-counting to determine SOC. Sufficient time must be left for voltage recovery to accurately determine the resulting characteristic.
2) The relationship of current and voltage is modelled using a combination of a constant resistance and constant voltage drop. This linear fit was obtained by testing the Cobra at several speed ranges of the motor, to create a range of currents and voltages.
3) The voltage recovery of the batteries is approximated using a single exponential equation, found from the voltage recovery of the batteries during the discharge tests.

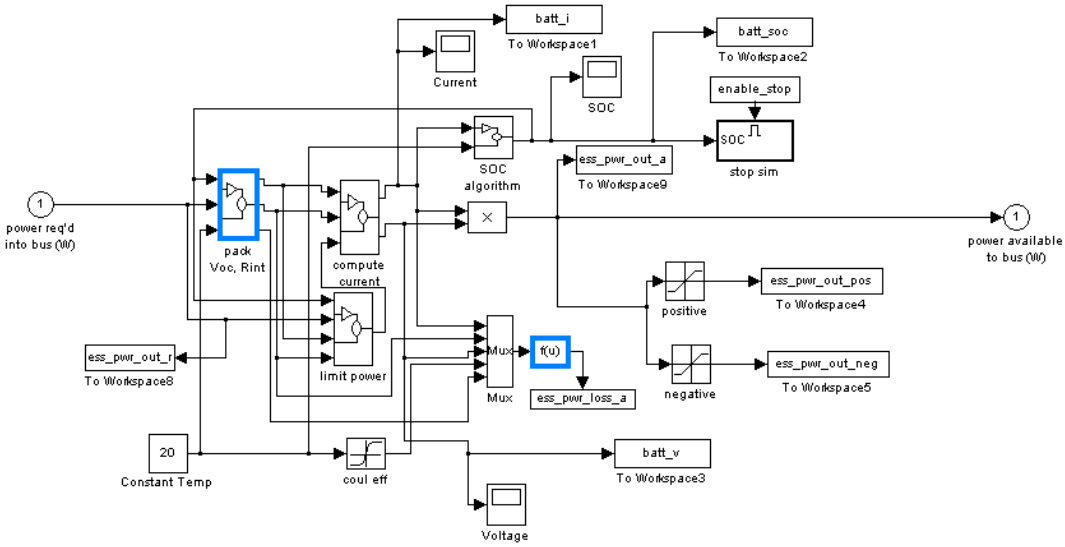

Figure 3.26: The basic structure of the author's battery model in Matlab/Simulink, which is based on the Rint model in ADVISOR. Blocks altered by the author have been highlighted.

The model is implemented in Matlab/Simulink, using time steps of one second and the discrete, fixed-step solver. This enables it to be used in ADVISOR and in the ADVISOR-based hybrid model developed by the author. The overall

Matlab/Simulink battery model is shown in Figure 3.26, with the blocks modified by the author highlighted in blue. Specifically, the calculation of Voc has been modified to include the voltage drop and voltage recovery effects, and the power losses block has been updated to include losses associated with the voltage drop term, using Equation 3-30.

A simplified flow chart of the model is shown in Figure 3.27. As shown in the flow chart, the requested power is used to determine the open circuit voltage of the battery. The values of V_{oc}, R_{int} and SOC are then used to limit the power if necessary to keep the battery and motor/controller voltages within prescribed limits, and to ensure that the battery is not charged above 99.9% or discharged below 0.1% SOC. The current and the measured voltage for the battery are then calculated, giving the power delivered by the battery. The SOC of the battery is updated, and the losses are calculated. If the SOC falls below 0.1%, the simulation is halted – this is the boundary condition from the ADVISOR battery model. The Cobra battery model was not developed below 25% SOC, however this condition was never reached in simulations.

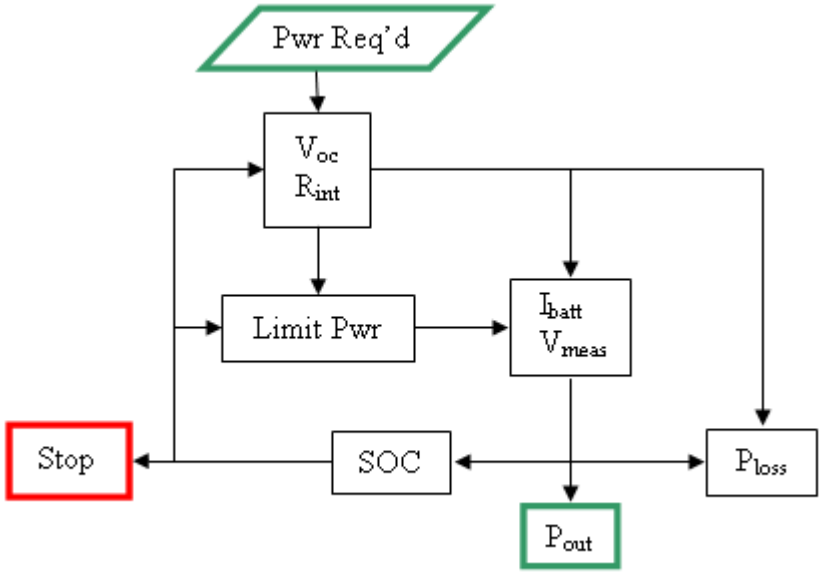

Figure 3.27: The author's battery model represented as a flow chart.

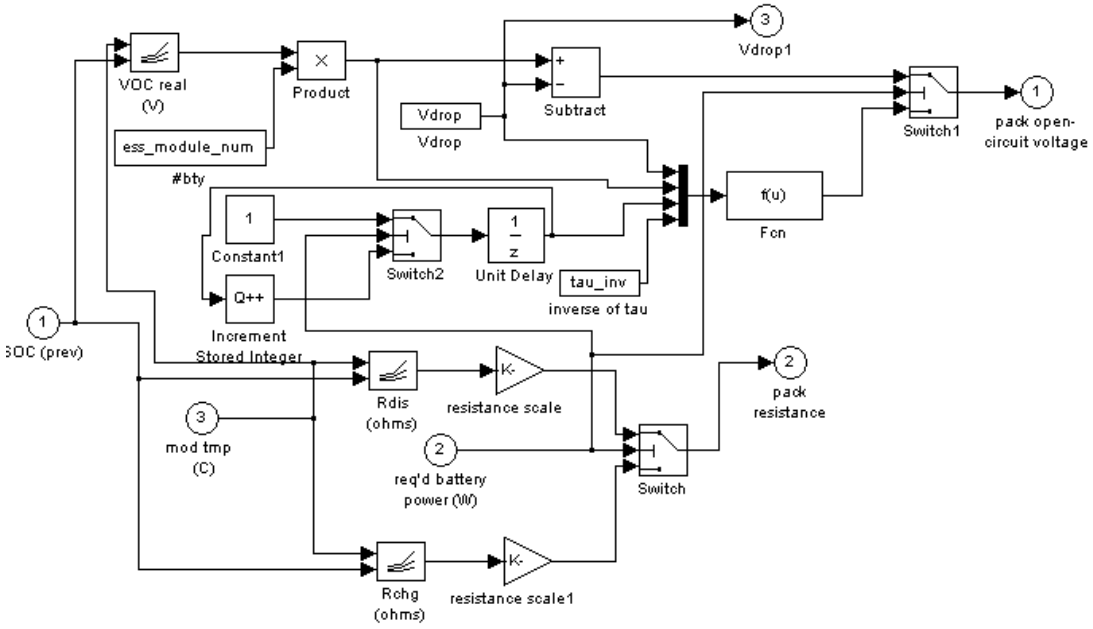

Figure 3.28: Inside the "pack Voc, Rint" block in the author's supercapacitor battery model. This block implements the V_{drop} effect and the voltage recovery of the batteries.

In the "pack Voc, Rint" block, shown in more detail in Figure 3.28, the SOC is used to find the actual open circuit voltage for the battery. The voltage is then modified by subtracting the voltage drop for any power demand larger than 100W. The voltage drop for a pack of *N* batteries is modelled as:

$$V_{drop} = 1.5N/6 \qquad (3\text{-}32)$$

thus for the standard Cobra pack of six batteries, the voltage drop is 1.5V. If the power demand is less than 100W, the voltage recovery equation 3-31 is used to modify the battery voltage as it returns to the actual open circuit value. Again, to allow different numbers of batteries to be modelled, the equation is modified to give:

$$V_{meas} = V_{OC} - \frac{1.5N}{6} e^{-0.02t} \qquad (3\text{-}33)$$

The model also gives the option of modifying the open circuit voltage and pack resistance by temperature; this option is available in the original ADVISOR model, but temperature effects were not found to be necessary for the Cobra model. This is

evidenced by the fact that error levels during drive cycles remained consistent throughout each cycle, demonstrating that the battery performance was not changing.

The functions and variables depicted in Figure 3.28 are therefore as follows:

- VOC real (V) → Battery voltage indexed by SOC, based on Equation 3-25, with the option to be indexed by temperature.
- ess_module_num → the number of batteries, *N*.
- Vdrop → the voltage drop 1.5*N*/6, shown in Equation 3-32.
- tau_inv → the inverse of the voltage recovery time constant, $0.02s^{-1}$
- Fcn → the voltage recovery function shown in Equation 3-33.
- Rdis/Rchg → The internal resistance of the batteries – 0.01Ω per battery (becoming 0.06Ω for a pack of 6). The model leaves the option for these values to be indexed by SOC and/or by temperature.

The author's battery model provides a simple approximation to the effects caused by the capacitance of the battery plates. A more detailed model may be possible using a Randle's cell model with variable components, including a substantial current-based variation, however the development of such a model was determined to be unnecessary for simulating the Cobra. The simple model developed instead has proved to provide a good correlation to the actual battery performance, offering significant improvement to the models provided in ADVISOR. The peak error for the new Cobra model is just 3.1% - less than a third of the error reported for the Rint model by the ADVISOR creators, and also smaller than the 4% peak error reported for the RC model [127]. This section describes the verification process for the Cobra battery model.

3.3.1 Drive Cycles

Test results for several drive cycles for the Cobra were obtained by recording several drives around Glasgow. Two routes were used. For short data collection the car was driven around the nearby George Square, a distance of approximately 0.7 miles. A longer cycle was obtained by driving the Cobra approximately 2.7 miles, parking it for 10 minutes on Lomond Street and then returning. This longer cycle imitates a

short city commute – the 10 minutes wait is sufficient for full voltage recovery. Both routes are shown in Figure 3.29. Speed and power requirements for sample trips are shown in Figures 3.30 and 3.31 respectively.

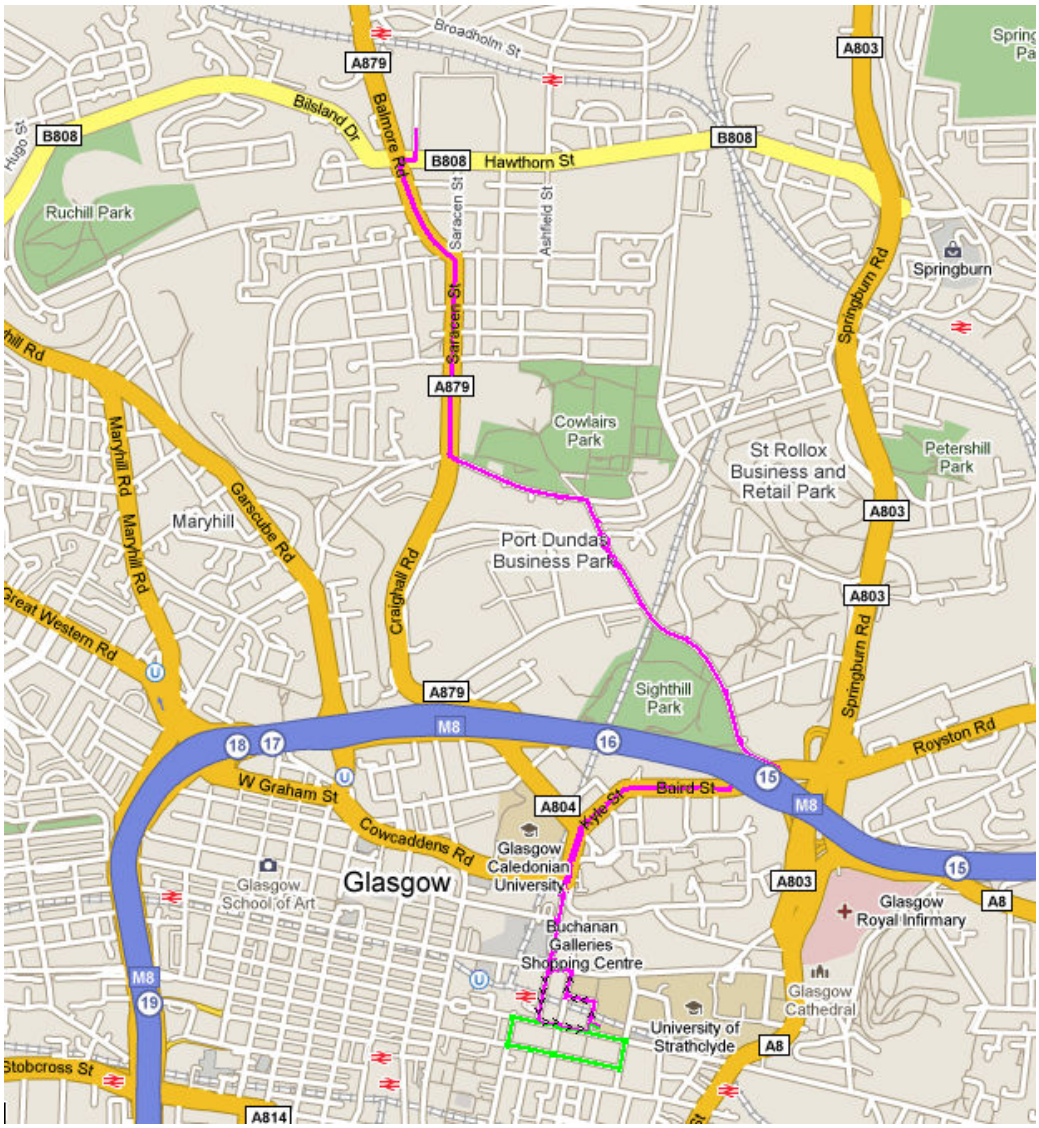

Figure 3.29: A map of Glasgow (©2009 Google – Map data ©2009 Tele Atlas). The pink line shows the long drive cycle which represents a city commute – the Cobra is driven to the end of the route, left for 10 minutes and then driven back, for a round-trip distance of 5.4 miles. The green line shows the short drive cycle, which allows a quick test of the Cobra and is suitable for tests at a range of states of charge.

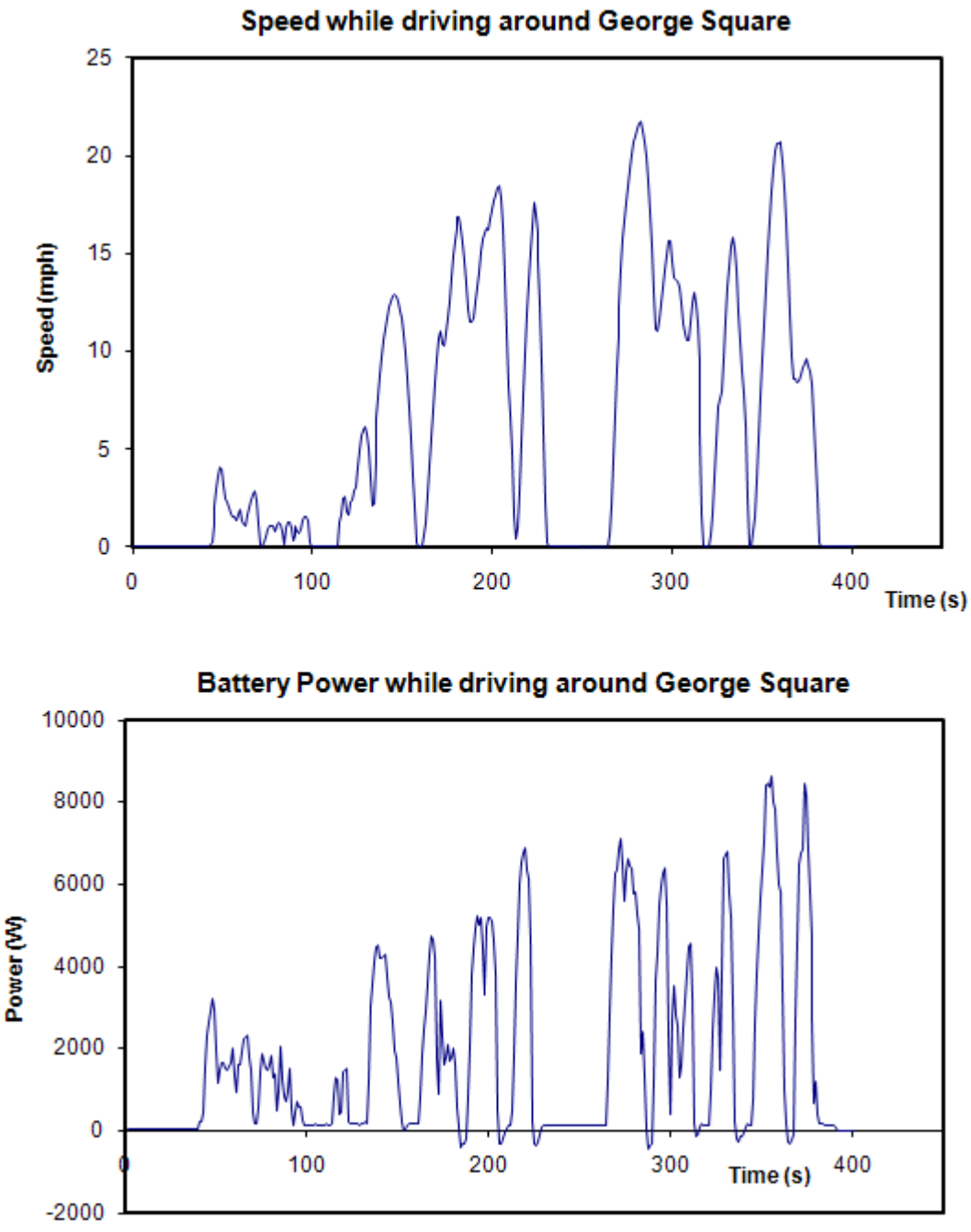

Figure 3.30: Speed and power for a trip around George Square.

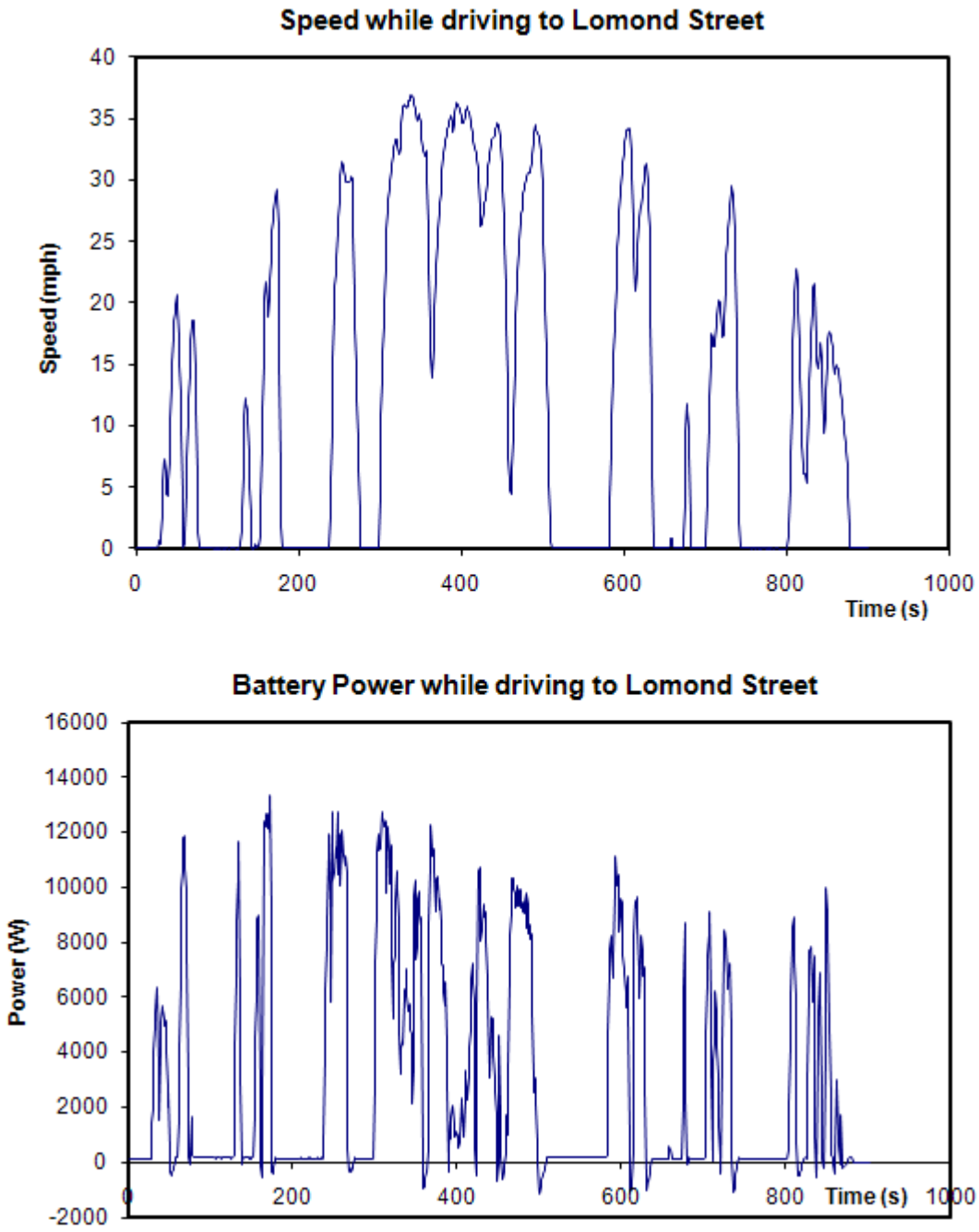

Figure 3.31: Speed and power for a trip to Lomond Street.

The Cobra model has been compared to the basic ADVISOR Rint model using these drive cycles. (No direct comparison is made to the ADVISOR RC model as the relevant parameters were not known for the Cobra batteries or for similar lead-acid batteries.) Example results are shown in Figures 3.32 and 3.33; in this test, performed on July 27, 2009, the Cobra was driven to Lomond Street and back. The

power information was used in the ADVISOR Rint model and in the new Cobra model. Figure 3.32 shows the battery voltage during this trip, along with the voltages predicted by the two models. The new model correctly shows the significant voltage drop for low currents and the slow process of voltage recovery. It also indicates the final voltage and SOC of the battery with an error of less than 1%. The new model performed better when Peukert adjustments (discussed in Section 2.2.2) were not included in SOC calculations, and these are not included in the model shown below.

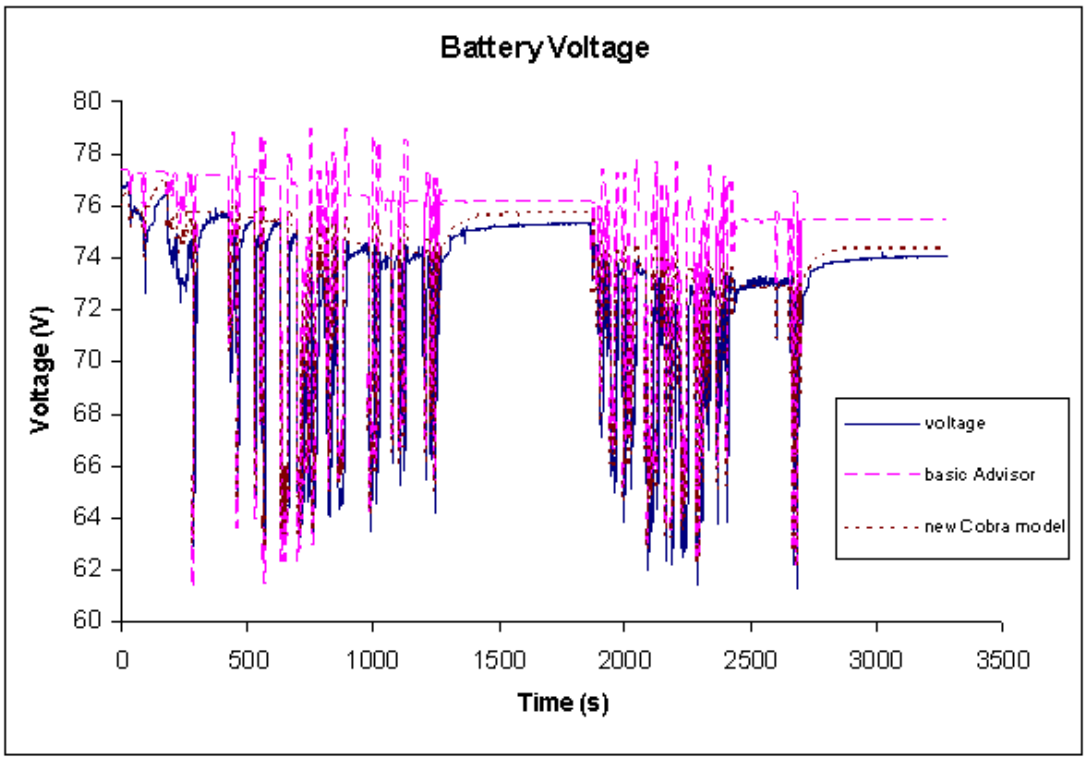

Figure 3.32: The actual battery voltage for a trip to Lomond Street and back, together with battery voltages predicted for the trip using the original Rint ADVISOR model and the newly developed Cobra model. Close-up sections of this data are shown in Figures 3.34 and 3.35.

Figure 3.33 shows the error in the basic Rint ADVISOR model and in the new Cobra model. For this cycle the Cobra model has errors of up to 3.1%, a significant improvement on the ADVISOR model which has errors of up to 6.3%. Note that the current and voltage errors mirror each other. This occurs because the model uses the power information from the cycle – the model voltage and current, multiplied together, will be equal to the actual power. Future examples will show only the

battery voltage for ease of comparison – in each case an error in voltage will match a similar error in current.

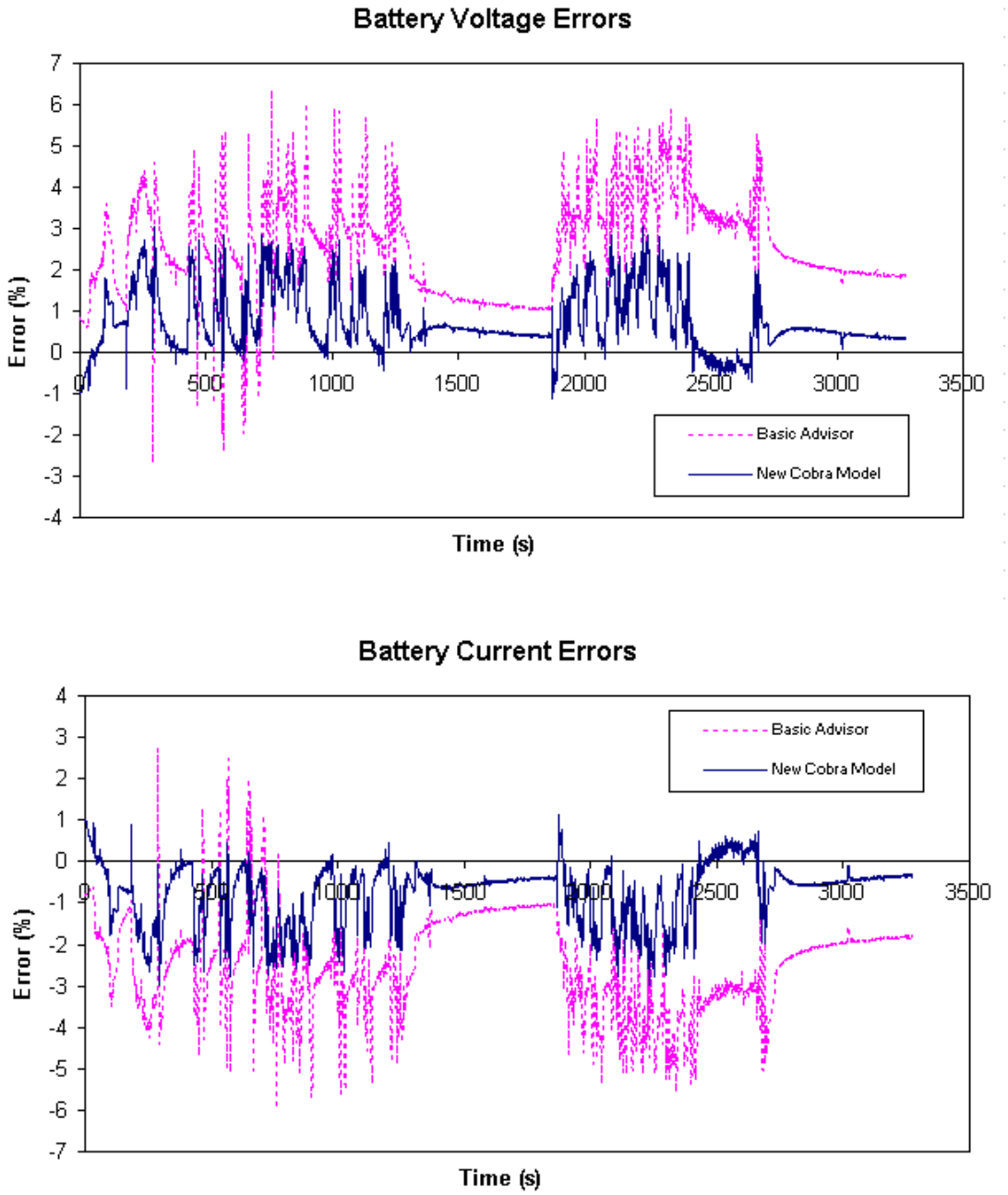

Figure 3.33: The errors for the basic Rint ADVISOR model and the new Cobra model for the battery voltage and current in the drive cycle shown in Figure 3.32.

Two other drive cycles were tested: the first was taken on July 22, 2009 and featured two trips around George Square over 1636s, while the second was taken on August 4, 2009 and involved a trip to Lomond Street and back, followed by two trips around

George Square, for a total time of 5318s. The other drive cycles tested showed similar errors for the new model, with the peak errors of 2.3% to 3.1% respectively for battery voltage. The average magnitude of the error for the three drive cycles ranged from 0.5%-0.7%. At the end of each cycle the error in modelled and measured SOC as calculated using Equation 3-25 was always less than 1%. The new model always outperformed the standard ADVISOR Rint model.

3.3.2 Verification of Voltage Drop Term

The benefit to the model of the constant V_{drop} term is apparent with a closer study of the drive cycle shown in Figure 3.32. Figure 3.34 shows the battery voltage for a subset of Figure 3.32, from a time of 2400 seconds to 2700 seconds. The battery voltage is modelled with the new Cobra model with and without the inclusion of the constant V_{drop}. The chosen time frame includes an extended stop at a busy intersection. During this time, there was a power drain of about 140W as the traction batteries maintained the auxiliary battery voltage, while in turn the auxiliary battery powered the motor inverter's cooling fan as well as the various dashboard lights and meters. The V_{drop} term is needed to correctly show the decrease in voltage, which is in excess of what would be expected from internal resistance alone. Note that the battery voltage remains suppressed and shows minimal recovery behaviour during this stop, which lasted for more than three minutes.

Another subset of Figure 3.32 is shown in Figure 3.35. This figure shows a section that includes high currents – the peak current is 182.5A. The voltage drop model offers a superior fit to the model without the V_{drop} term.

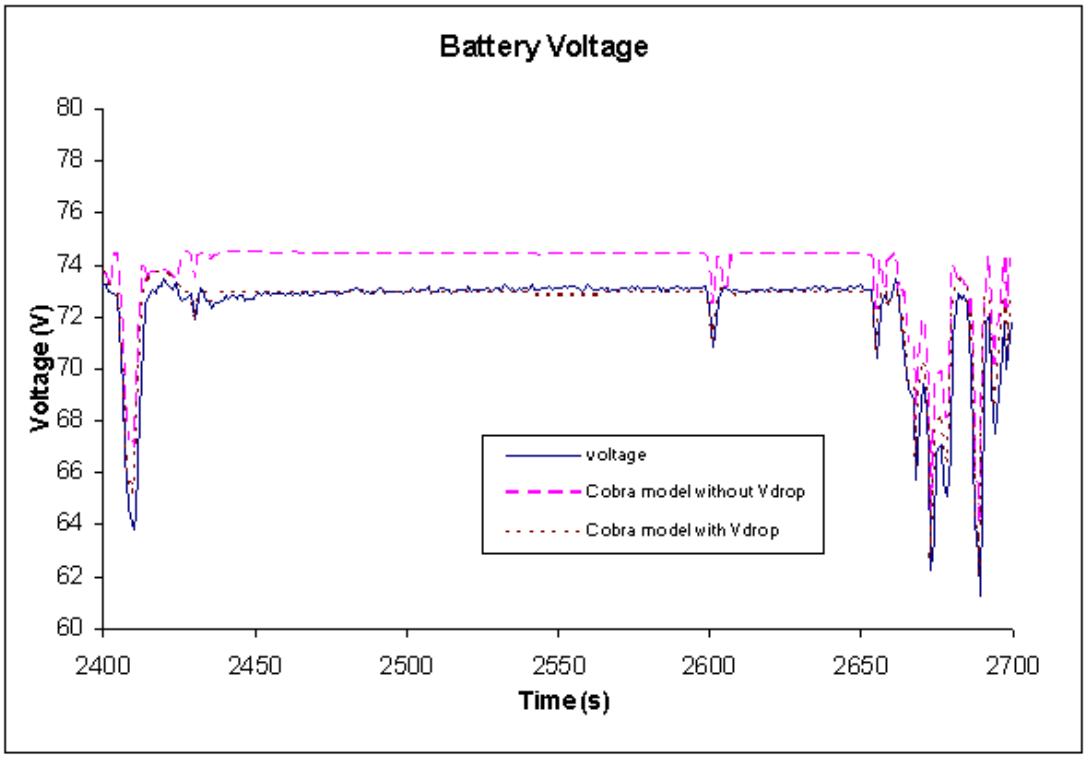

Figure 3.34: The Cobra model with and without the Vdrop term, compared to the actual voltage of the Cobra batteries for a subset of Figure 3.32.

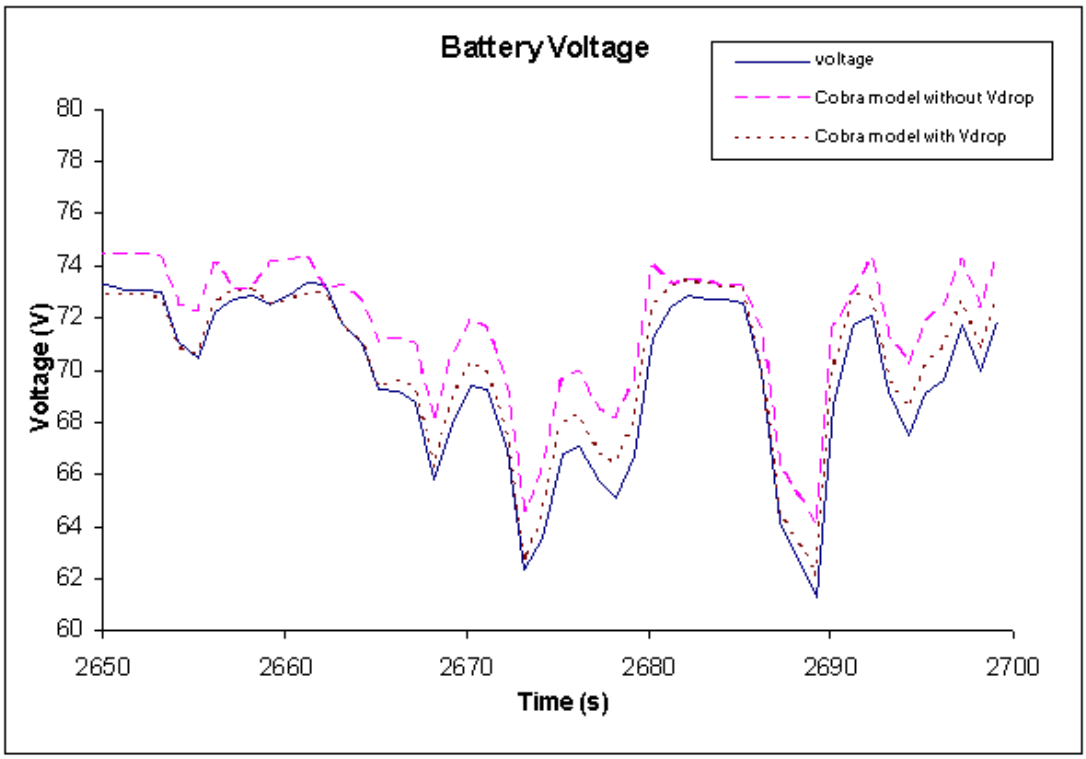

Figure 3.35: The Cobra model with and without the Vdrop term, compared to the actual voltage of the Cobra batteries for a subset of Figure 3.32.

The accuracy of the new model could not be achieved by neglecting the Vdrop term and simply using a larger value for the internal resistance. Consider Figure 3.36, which compares the complete Cobra model with a new model featuring no voltage drop and with the internal resistance increased from 0.06Ω to 0.07Ω for the pack. The figure displays the same data sets as Figures 3.34 and 3.35, with an extended stop in heavy traffic included in the upper plot and a short section of driving with high currents shown in the lower plot. Now that the internal resistance is higher, the model without a V_{drop} term performs well at high currents – equal to the performance of the complete model. But the V_{drop} term is essential to correctly display the voltage of the batteries while the car is idling. This is because of the increased charge transfer resistance, for which a constant internal resistance value cannot account.

Some further examples are shown in Figure 3.37. These plots show sections of other drive cycles – in the first case a trip around George Square taken on July 22, 2009 and the second case from a drive back from Lomond Street, August 4, 2009. Both plots show periods of driving interspersed with short stops in traffic. In each case the model without a V_{drop} term performs poorly during periods of low discharge current, even if it performs well during high currents. The model without a V_{drop} term also performs poorly during periods of regenerative braking, which are visible in the plots as small spikes in voltage just before periods of idling. Meanwhile the Cobra model, including the V_{drop} term, performs well at all currents, including the small charging currents generated by the Cobra and during periods spent idling in traffic.

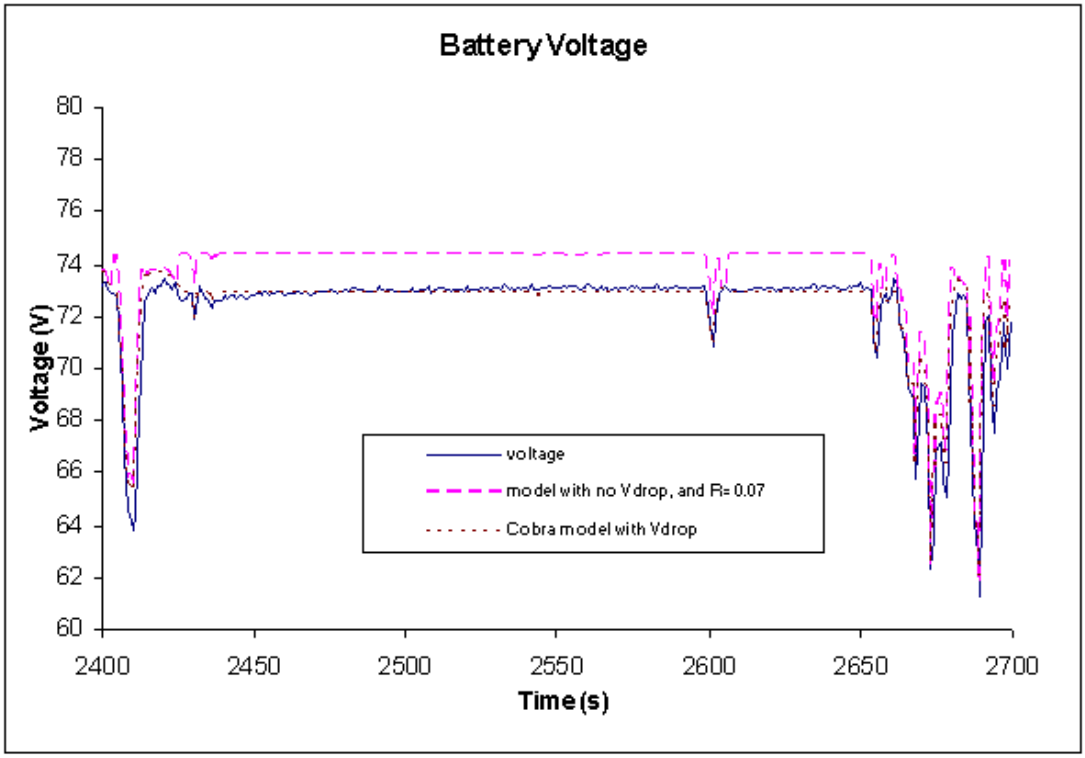

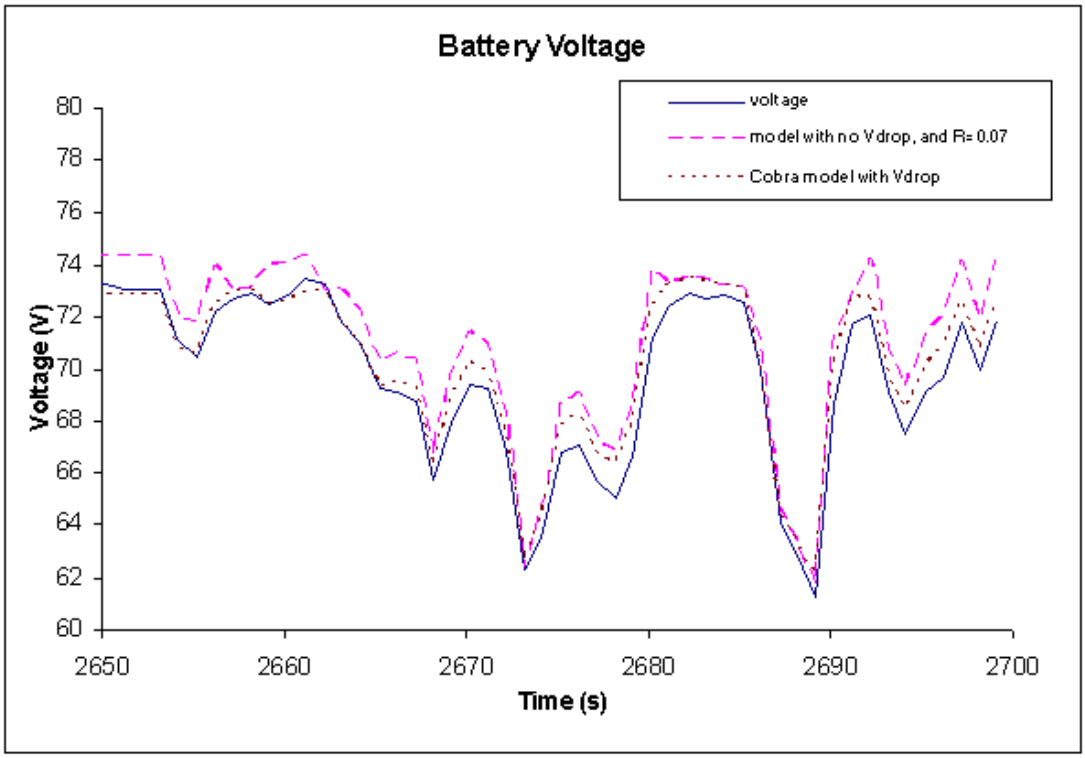

Figure 3.36: The complete Cobra model compared to a model with no Vdrop term, and with the internal resistance of the battery pack increased to 0.07Ω.

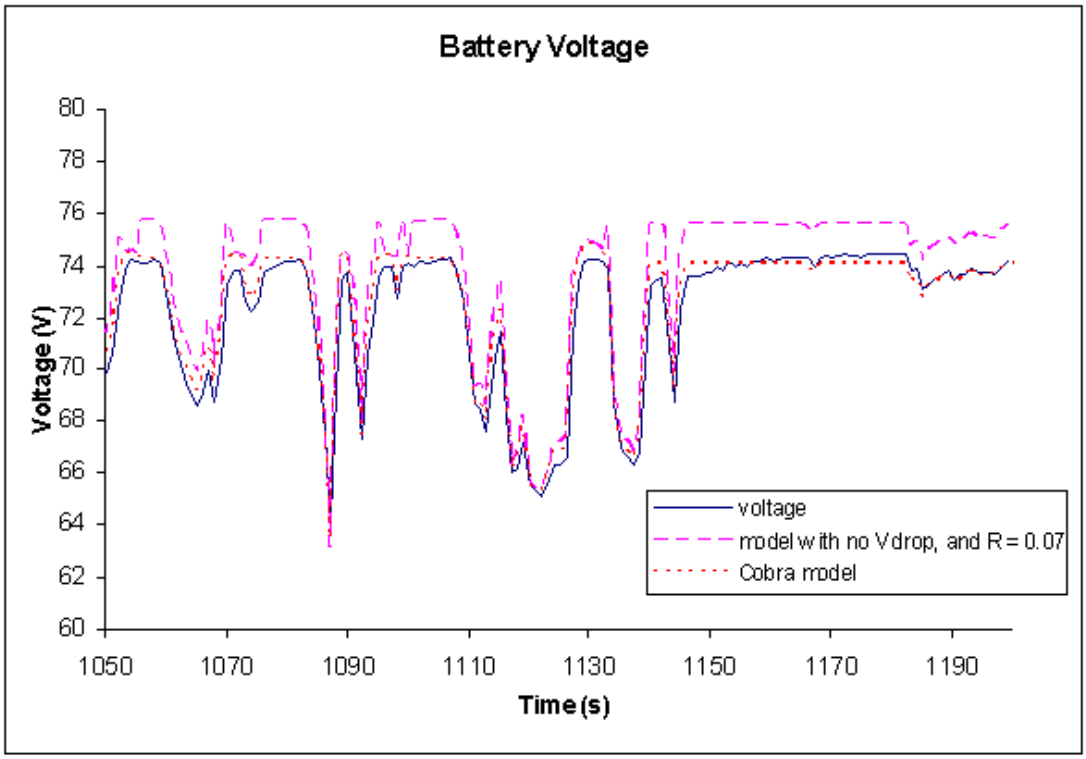

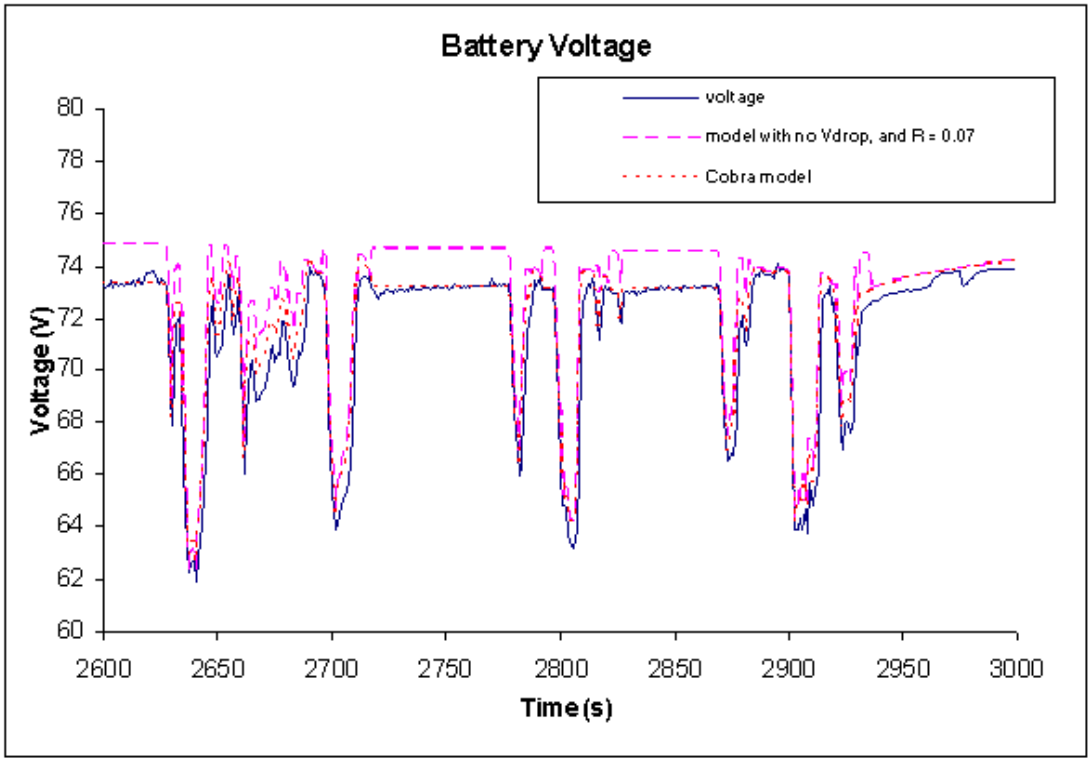

Figure 3.37: Further examples of the complete Cobra model compared to a model with no Vdrop term, and with the internal resistance of the battery pack increased to 0.07Ω.

3.3.3 Verification of Voltage Recovery Model

As described in Sections 3.2.5 and 3.3.2, the battery model features a constant voltage drop of 1.5V during both charge and discharge operation. However, when the battery is at rest, the voltage recovers to the open circuit value that corresponds to its current state of charge. In order to ensure that the voltage drop is applied while still permitting the voltage to reach open circuit value, the battery model includes a voltage recovery term as shown in Equation 3-33.

The voltage recovery of the batteries depends on the magnitude and duration of the current to which the batteries were subjected. For this model the voltage recovery was modelled with a fixed equation irrespective of the preceding currents, yet the results are very accurate. Some examples are shown in Figure 3.38, comparing the Cobra model with and without a voltage recovery component to the actual voltage. These examples show data taken on July 22 and on August 4, respectively. For each drive cycle tested, the models follow the general shape of the actual recovery, with a displacement in each recovery event of less than 1% from the measured voltage. Additionally, the voltage recovery term ensures that the voltage drop will be correctly applied during charging events and short periods (of a few seconds) when the power output of the batteries is less than 100W.

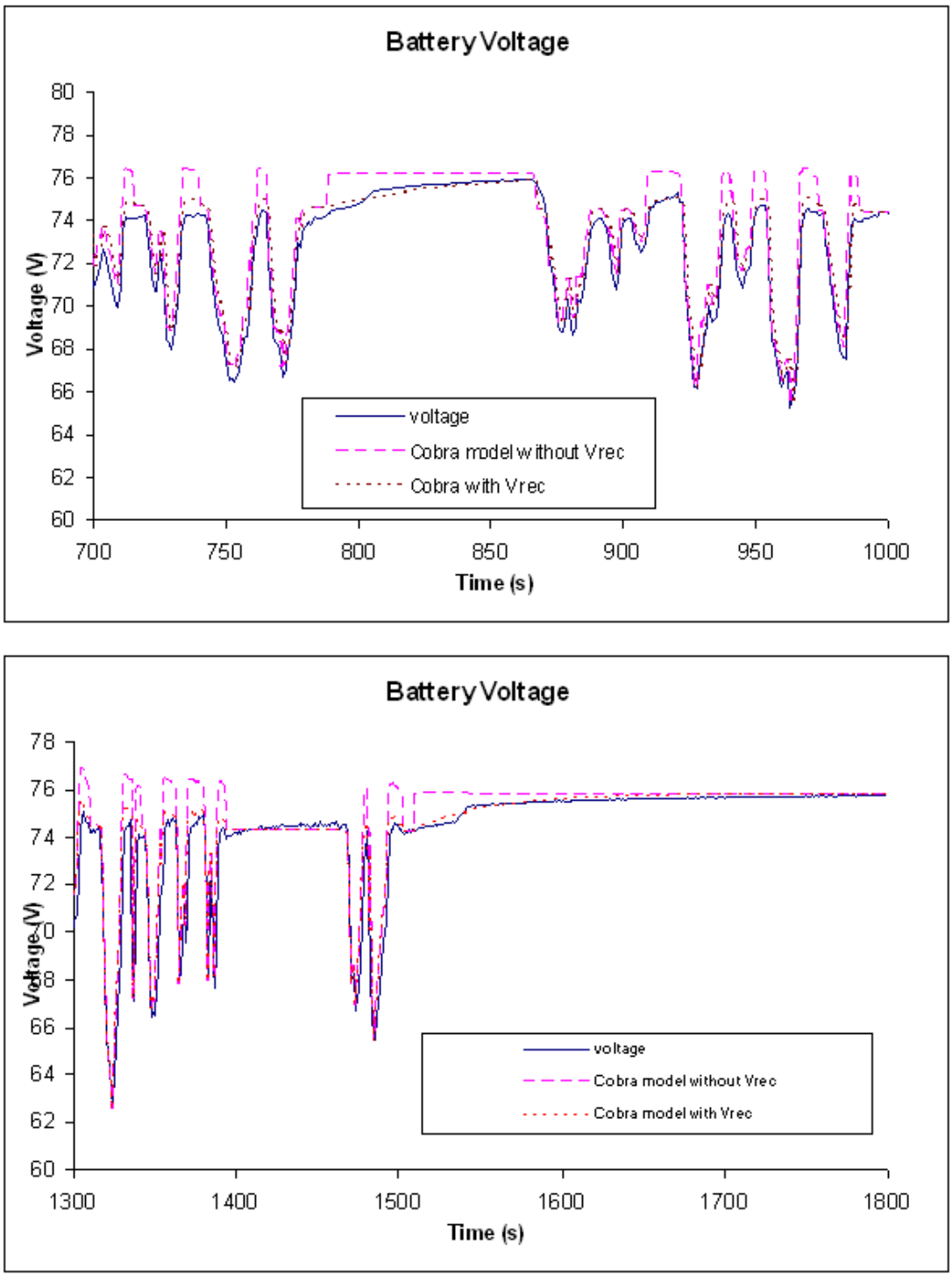

Figure 3.38: Two drive cycle sections showing the actual battery pack voltage and with voltages as modelled with the new Cobra model, with and without a voltage recovery component. The upper plot shows data from July 22, and the lower plot shows data from August 4.

3.4 Regenerative Braking

To recover 100% of the available kinetic energy from a regenerative braking event, one must have active brake management on all four wheels in order to avoid the risk of going into a skid [149]. The Cobra does not have this feature, and thus regenerative braking is restricted to a few hundred Watts from the rear wheels, with the remainder of the braking supplied by friction brakes. However, one important feature of supercapacitors is their ability to accept high regenerated power. In order to fully assess their impact in a battery/supercapacitor hybrid, it is important to determine the amount of regenerated energy which would be available if the friction brakes were not used. This information was extracted from a study of the Cobra motor performance during driving tests.

To assess the relationship of power, speed and acceleration for the Cobra, a section of the George Square trips which is fairly flat was used. The entire trip involved a steep hill with a 9.2% grade at the beginning and end of the trip (specifically John Street which leads to the Royal College Building cartway and the Cobra garage) which was left out of the initial assessment so that a direct relationship between road speed and motor power demand could be analysed. Example drive data is shown in Figures 3.39 and 3.40. The George Square trip involves 5 sets of traffic lights – differences in the traffic patterns and states of the traffic lights are responsible for the power, speed and time differences between trips 1 and 2.

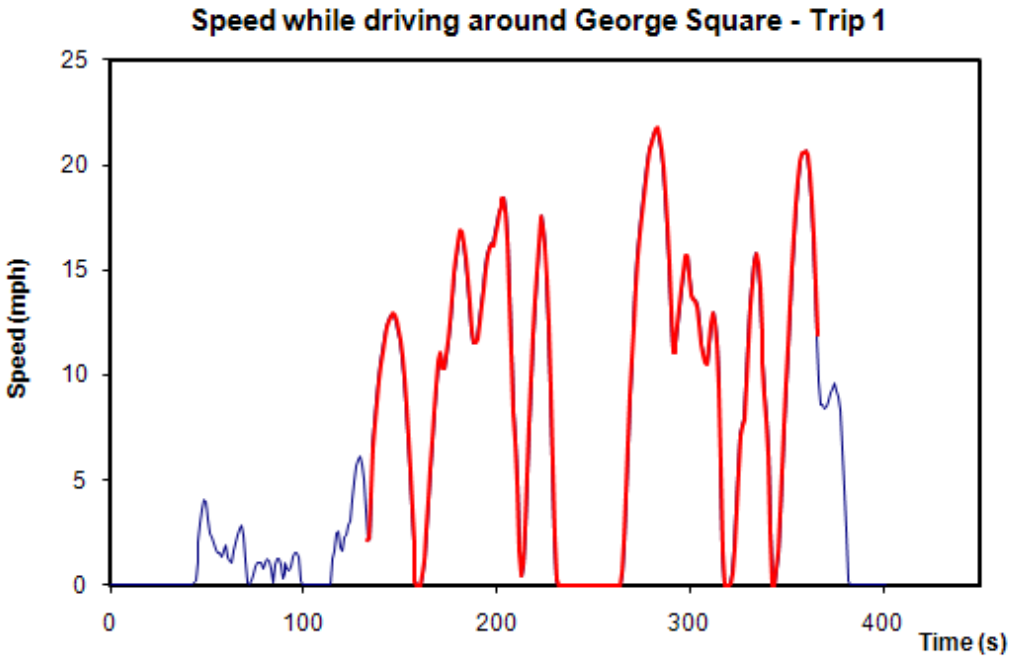

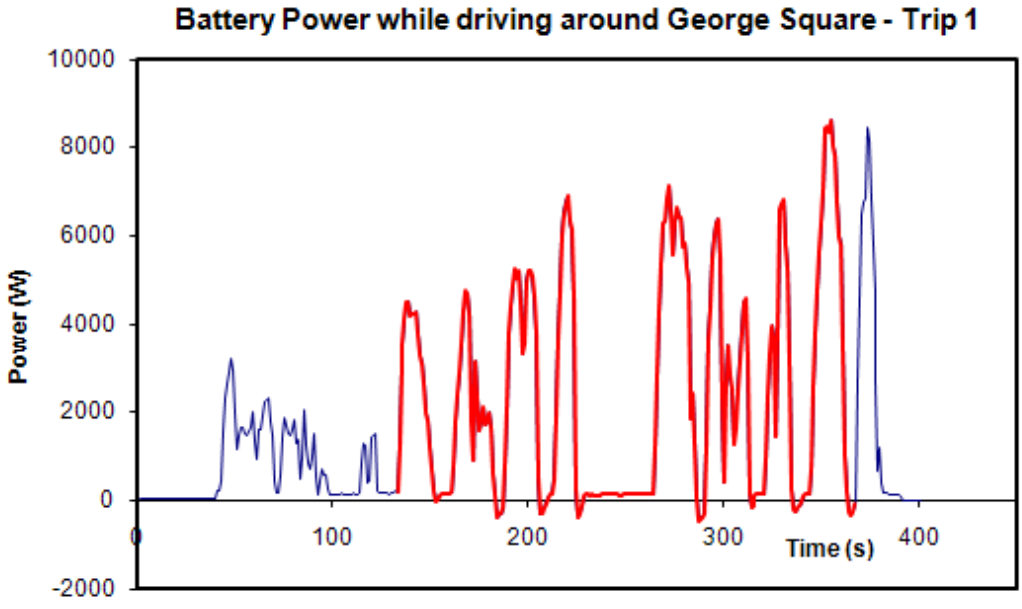

Figure 3.39: A trip around George Square, performed on July 22, 2009. The section highlighted in red shows the flat part of the trip, subsequently used for assessing the relationship of speed, acceleration and power in the Cobra.

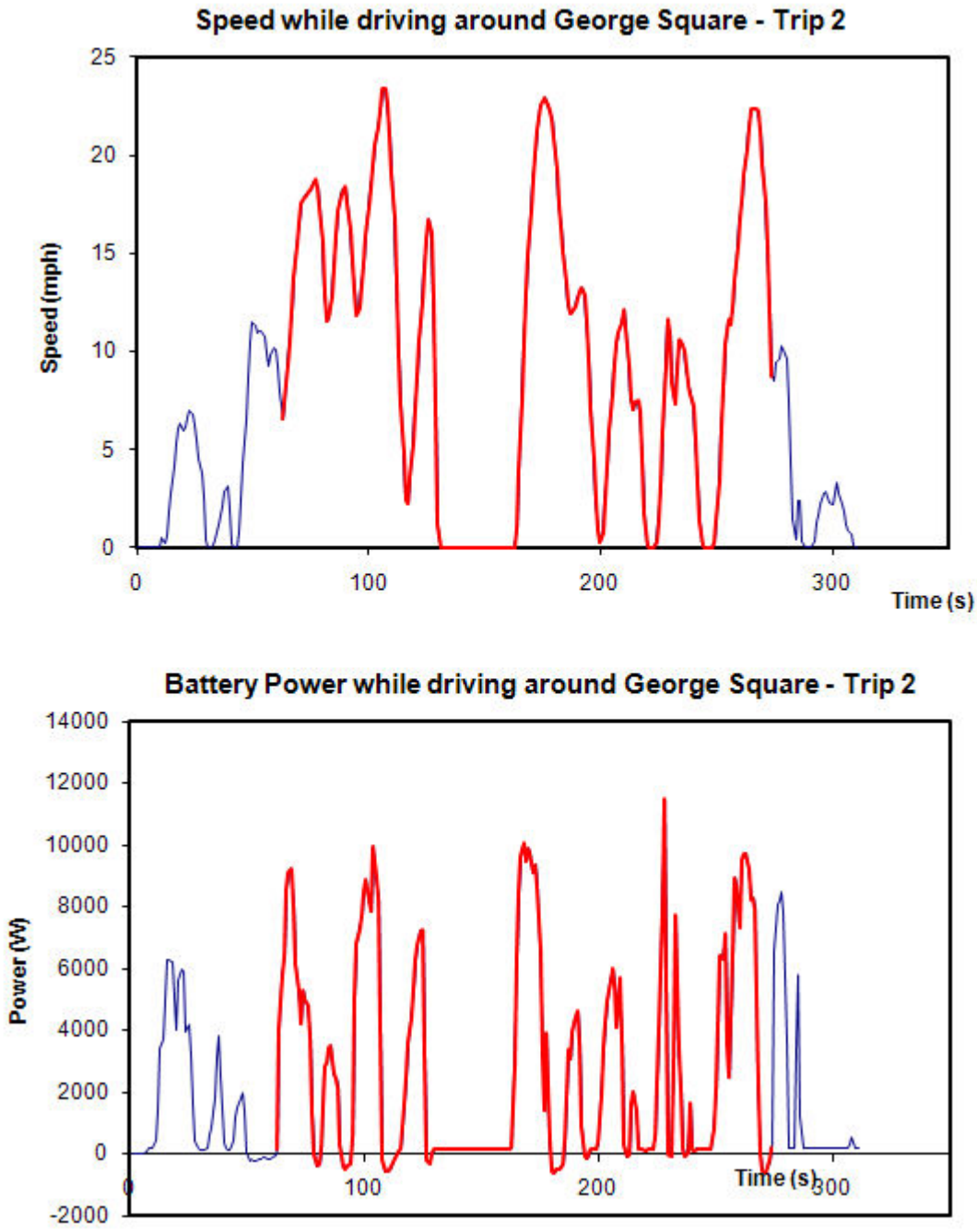

Figure 3.40: The second trip around George Square performed on July 22, 2009. The section highlighted in red shows the flat part of the trip, subsequently used for assessing the relationship of speed, acceleration and power in the Cobra.

The power drawn from the batteries, the speed of the vehicle and the acceleration are all related, and the relationship between these variables was taken from Figures 3.39 and 3.40, respectively, is shown in Figure 3.41. The speed and power data was used as recorded by the Cobra data logger, while the acceleration data was calculated from the speed assuming a linear change in speed from data point n-1 to n, such that:

$$a_n = 0.44704 * \frac{s_n - s_{n-1}}{t_n - t_{n-1}} \quad (3\text{-}34)$$

where a_n is the acceleration (m/s^2), s_n is the speed (mph) and t_n is the time (s) for data point n.

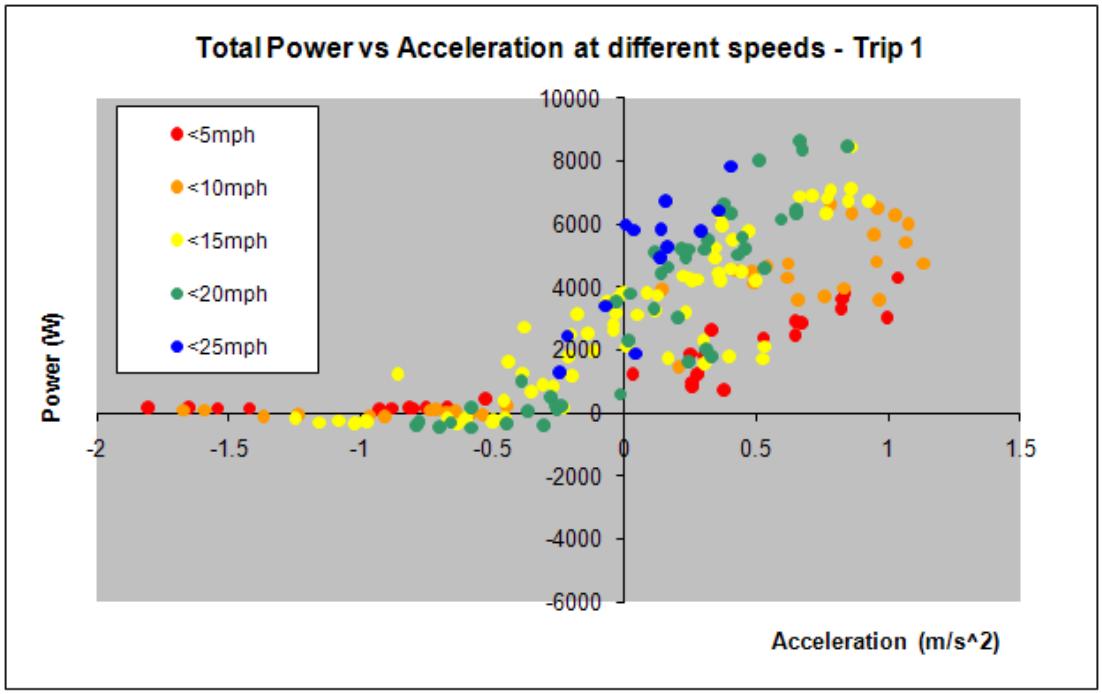

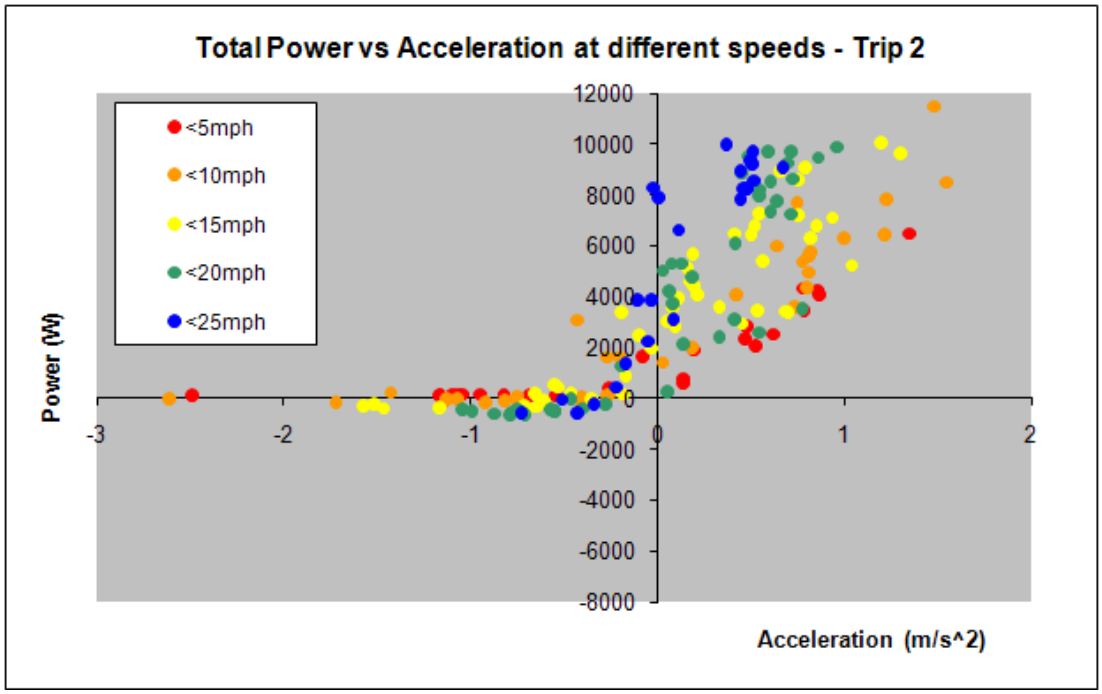

Figure 3.41: The relationship between power and acceleration for different speed ranges during the Cobra's trips around George Square.

The data was organised into segments of 5mph for analysis, i.e. all data points of speed $0 < s < 5$mph, $5 \leq s < 10$mph, etc. This was chosen so that sufficient data points would be found in any given segment to be analysed meaningfully; there were 1-7 useful data points within each 1mph segment, and 20-30 useful data points within each 5mph segment. A data point was considered useful if it had a power demand higher than 140W – 140W is the typical power draw of the Cobra accessories and any lower power demand is associated with regenerative braking, which in turn means that some power that could have been regenerated might instead have been lost in the Cobra's friction brakes and hence gone unrecorded by the data logger.

For any given speed, the relationship of positive power and acceleration is broadly linear, as shown in the first quadrant of Figure 3.41. However, as regeneration was limited by the Cobra motor controller, the relationship deteriorates for deceleration events (i.e. acceleration <0m/s^2) with a power value lower than 140W. These events could potentially deliver much more power back to the batteries, if only the friction brakes were not used.

One potential benefit from the supercapacitors is that they could enable more energy to be absorbed from regeneration events, so it is important to be able to estimate the full amount of power and regeneration time that could be available. Fortunately this can be extrapolated from the behaviour of the vehicle during positive acceleration.

Consider a simulated motor, courtesy of ADVISOR. The ADVISOR simulation was performed using the default EV architecture with rear wheel drive, featuring small vehicle body (VEH_SMCAR.mat), lead-acid battery pack (ESS_PB25.mat), 1-speed transmission (TX_1SPD.mat), and standard power train control (PTC_EV). Additionally, the simulation used the small car wheel model, altered to feature 100% regenerative braking at all speeds, while the accessories model was altered to feature a constant 140W accessory power demand. The mass of the vehicle was specified to be 855.5kg – the weight of the Cobra plus a 70kg occupant. Finally, the motor itself

was chosen to be a 75kW AC motor, limited to 80% peak efficiency. This motor does not match the Cobra motor, but nevertheless gave a reasonable approximation of the Cobra power demand: the total positive energy demanded for the simulation differed by 5.6% from the actual positive energy for trip 1, and by 9.1% from the actual positive energy for trip 2. Furthermore, the peak power demand for the simulation had an error of 1.4% for trip 1 and 4.3% for trip 2. As the simulation was performed to create an analogous situation to that of the Cobra motor, rather than to be used in a Cobra model, this level of error was judged to be low enough to create a meaningful analogy.

The relationship of speed, acceleration and power for the simulated motor modelled using the first of the two George Square trips is shown in Figure 3.42. For the modelled motor, if the speed and acceleration demands of the vehicle are the same, then the motor power demand will always be the same. Here each 5 mph block of speeds has been put in a group. Within each group the relationship of power and acceleration was defined using a line of best fit within Excel. Note that the linear behaviour continues into the region of negative power and acceleration, indicating that the regenerated power broadly follows the same relationship as the traction power. It is also worth noting that the power demand is not 0W when there is no acceleration, and that this power demand is higher at higher speeds. This power is used to overcome the rolling resistance and aerodynamic drag on the vehicle, both of which are functions of the vehicle speed [62]. Hence, at high speeds a small deceleration is associated with a positive power demand and is not a regenerative event.

Unfortunately it was not possible to model the Cobra motor directly, as an electrical failure of this motor occurred on August 10, 2009 and prevented the determination of the relevant parameters.

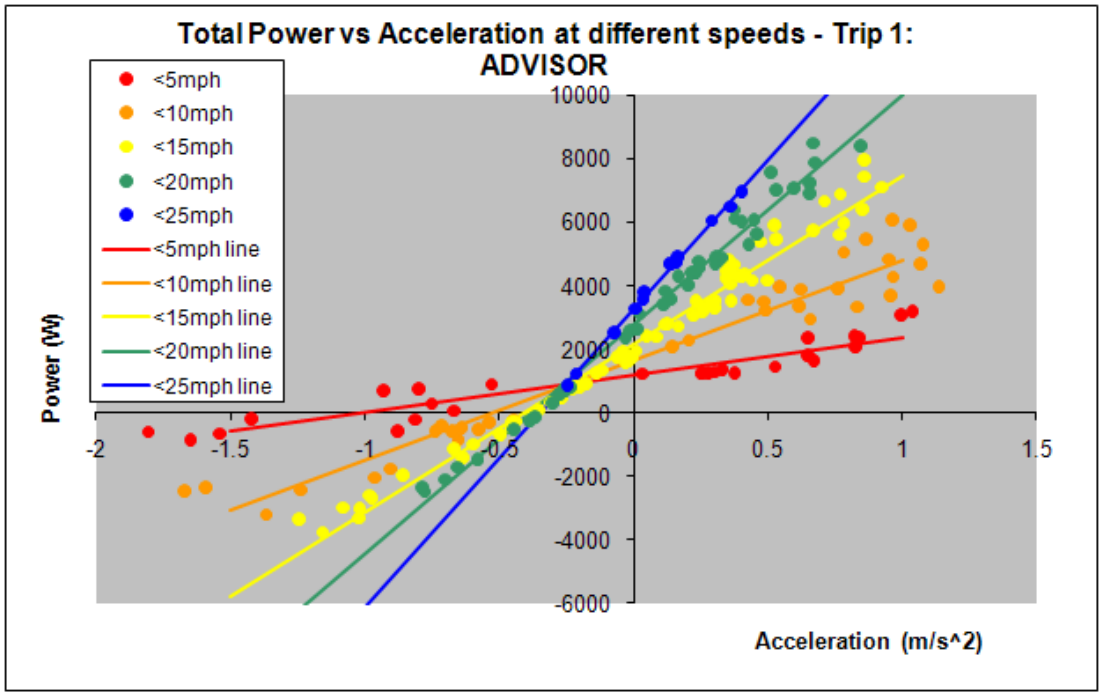

Figure 3.42: A model of a motor in ADVISOR, were it to make the first of the trips around George Square.

Each of the lines relating power to acceleration is described with a slope and an intercept, and these values themselves progress in a linear fashion for different speeds. The characteristics of these lines, taken from the ADVISOR model data for the two trips described above, are displayed in Figure 3.43.

The simulated data from ADVISOR demonstrates the concept that negative (i.e. regenerated) power should follow the same behaviour pattern as positive power so long as the friction brakes are not used. It also demonstrates that if the speed and acceleration are known for a vehicle, the required power in or out of the vehicle can be determined as long as the ground is flat. This means that the available regeneration power for the Cobra can be determined from the power data taken during periods of net power output – when the car is accelerating, maintaining constant speed, or decelerating slightly (before regeneration is enabled).

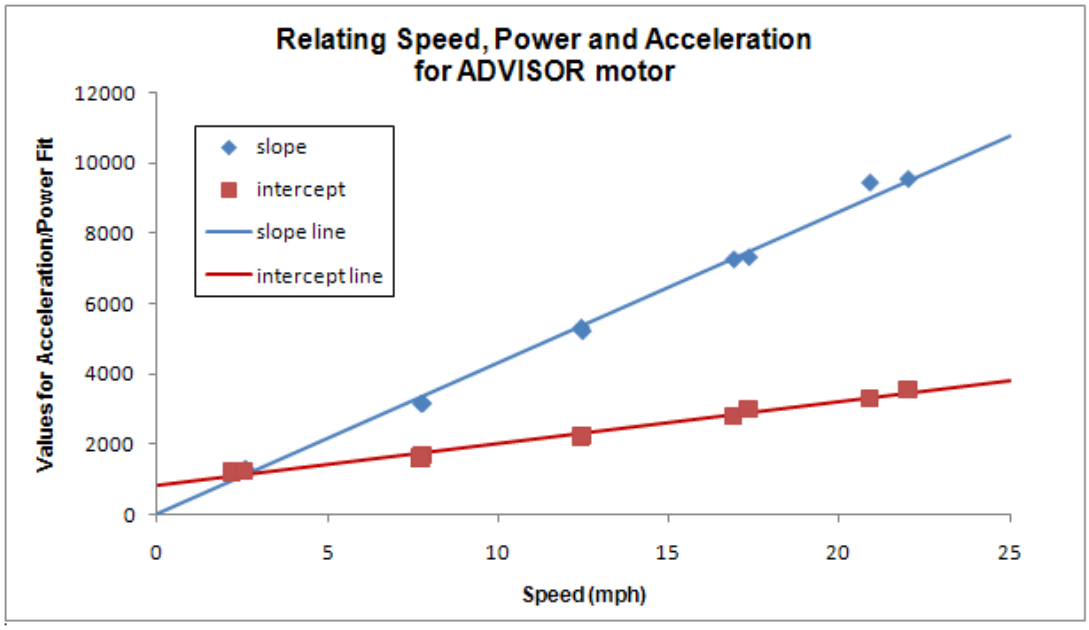

Figure 3.43: Relating speed, power and acceleration for the motor modelled in ADVISOR for the George Square trips.

To this end, the power, speed and acceleration data for the Cobra during the two trips was re-assessed. As with the ADVISOR simulation, the Cobra data was grouped by speed into 5mph blocks, and then fitted using a linear regression to find the relationship of power and acceleration for all values with a power demand greater than 140W. Then the slopes and intercepts for those lines were in turn associated with a speed value – the average speed for each block. The relationships of slope to speed and intercept to speed were again estimated with a linear fit, as shown in Figure 3.44. The resulting equations are:

$$P = Ma + B \quad (3\text{-}35)$$

$$M = 361s + 630 \quad (3\text{-}36)$$

$$B = 113s + 1541 \quad (3\text{-}37)$$

P (W) is the power, a (m/s^2) is the acceleration, M (Ws^2/m) and B (W) are the coefficients for the line relating the two, and s (mph) is the speed.

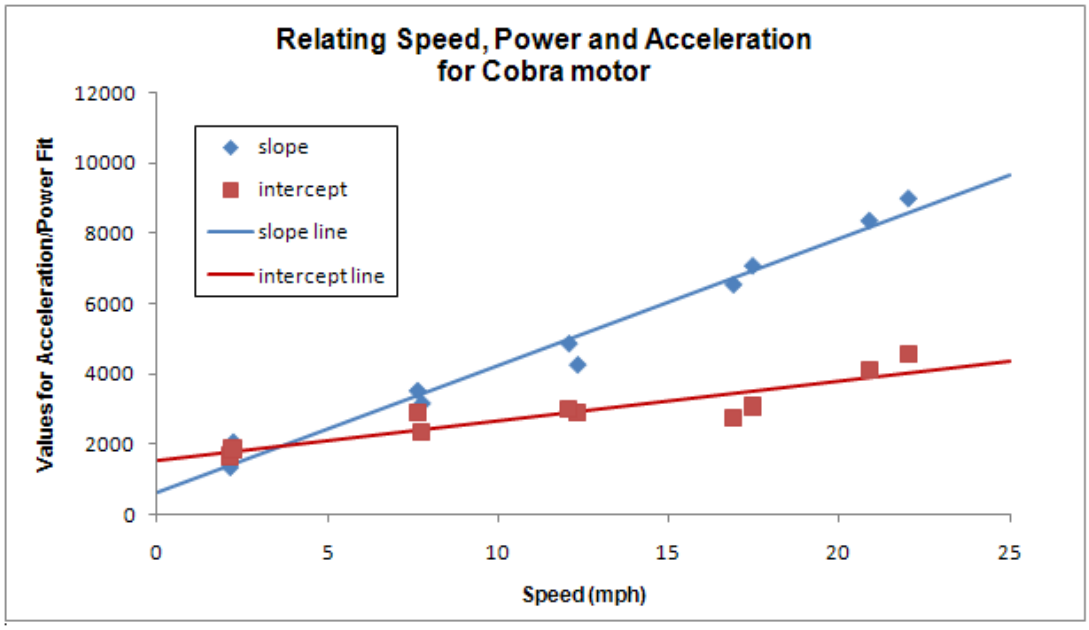

Figure 3.44: Relating speed, power and acceleration for the Cobra on the July 22 George Square trips.

Two additional trips around George Square were recorded and the data subsequently assessed, these having been performed on August 4, 2009. They showed a somewhat different profile, as shown in Figure 3.45. This led to alternate equations to 3-36 and 3-37:

$$M = 419s + 1610 \qquad (3\text{-}38)$$

$$B = 80s + 1309 \qquad (3\text{-}39)$$

These two fits were used to create alternate regenerative braking profiles for the Cobra, which are presented in Section 3.5. In addition, a third profile was created which used 50% of the regenerative braking available using the July 22 trip fits. This gave four regeneration profiles in total: Low Regen, from the original data, Medium Regen, from the 50% data, High Regen, from the July 22 fits, and Super Regen, from the August 4 fits. This allowed the availability of regenerative braking energy to be considered as a factor in determining the usefulness of supercapacitors in a battery electric vehicle. The different regeneration profiles and drive cycles are described in the following section.

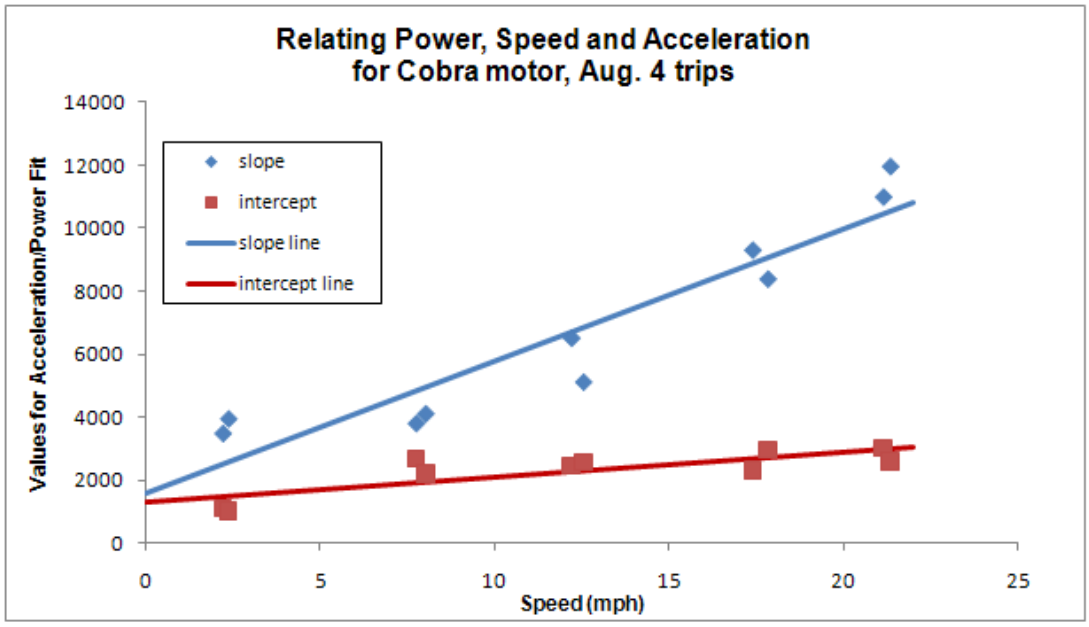

Figure 3.45: Relating speed, power and acceleration for the Cobra on the August 4 George Square trips.

3.5 Drive Cycles

Two speed profiles were used as the basis to create seven drive cycles for the optimisation strategy testing. First, a drive cycle was created using driving data collected from the Cobra during the four trips around George Square, driven on July 22 and August 4. The portions of the cycles driven on John Street were left out to avoid the complication of the 9.2% gradient on that street. The complete cycle was created by joining the cycles one after the other – the resulting speed profile is shown in Figure 3.46, with dashed vertical lines indicating where the cycles were joined. The composite power profile was likewise created by joining the cycles sequentially, with the power values at the connection points averaged to create a smooth connection.

The cycle was enhanced by employing the four different regeneration profiles as described in Section 3.4. The Low Regeneration profile used the original power information for both acceleration and deceleration. The other profiles used the original power information only for accelerations. For decelerations, a different regeneration power was used: the Super Regeneration profile was created using equations 3-38 and 3-39, the High Regeneration profile used equations 3-36 and 3-37

to determine the regeneration power, and finally the Medium Regeneration profile used ½ the High profile's regeneration power.

In each case it is assumed that the actual deceleration of the vehicle is the same, but the percentage of kinetic energy that is regenerated vs. the percentage that is dissipated by the friction brakes changes depending on the regeneration profile. This value ranges from 9% of kinetic energy captured for the Low Regeneration profile to 70% for the Super profile – a typical value for an electric vehicle is 30% of kinetic energy [149], however for urban vehicles the percentage may be more than 87% [150]. This is because the lower speeds of an urban vehicle result both in lower friction losses and in smaller braking power requirements, and it should be possible to fully capture up to 19kW of regenerated power [150]. The Super Regeneration profile would therefore be theoretically possible for the Cobra. However, to ensure user comfort and avoid the risk of skidding, it would also require active braking management on both axles [149, 150], while the Cobra currently offers control of the rear axle only. The Super Regeneration profile should therefore be seen as a theoretical possibility, to ensure completeness of the analysis of regenerative braking effects, rather than as a practical profile for the Cobra. The different power profiles for the George Square cycle are shown in Figure 3.47.

A second set of cycles was developed from the ECE-15 test cycle. This is a standard test cycle used throughout Europe for passenger vehicle of all kinds. Using this cycle for the Cobra model allows it to be viewed and discussed in a broader context of vehicle testing. This set of cycles was formed from four repeated instances of the ECE-15 cycle. As with the George Square cycle, equations 3-38 and 3-39 were used to produce the Super Regeneration cycle and equations 3-36 and 3-37 were used to produce the High Regeneration cycle. However, unlike the George Square cycle these equations were used to find the positive (discharging) power values as well, as the Cobra was never actually driven on the ECE-15 cycle. Thus there are some discrepancies in discharging power values between Super and High Regeneration profiles. Finally, the Medium Regeneration profile was derived from the High profile by dividing all charging power values by two. A Low Regeneration option

was not produced for this cycle; as described above the Low profile gives the real-life regeneration profile of the Cobra in the George Square cycles, and this information is not available for the ECE-15 cycles. The speed and power information for the different ECE-15 profiles are shown in Figure 3.48.

Details of all seven drive cycles are shown in Table 3.1. The percentage of kinetic energy captured for each cycle is found from the average of the kinetic energy captured for each braking event for that cycle. For each braking event, this value was calculated using the total energy captured over the course of the event, divided by the total change in kinetic energy. Thus, if a braking event began at time t_1 and ended at time t_n, then:

$$KE_{\%captured} = 100\% * \frac{140 * (t_1 - t_n) - \sum_{t_1}^{t_n} P(t)}{\frac{1}{2} m(v(t_1)^2 - v(t_n)^2)} \qquad (3\text{-}40)$$

where $P(t)$ (W) is the power at time t, m (kg) is the mass of the vehicle, and $v(t)$ (m/s) is the speed at time t. The value '140' represents the power drawn by the accessories; thus if a regenerative power of -100W is measured at the batteries, it is assumed that the actual captured power is -240W, with 140W being sent to the auxiliary battery and thence to the electrical accessories.

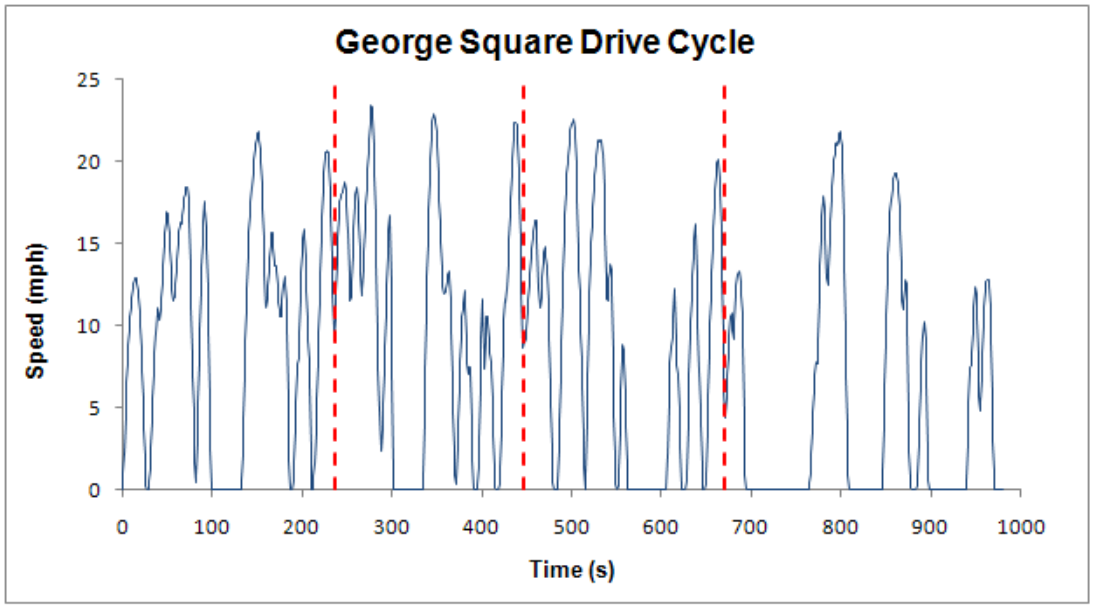

Figure 3.46: Speed of the George Square test cycle. It was developed by joining four individual trips around the square, with the joins indicated by dashed vertical lines.

Table 3.1: Properties of the drive cycles used for simulating the Cobra.

CYCLE	**ECE-15**			**George Square**			
Regeneration	Med	High	Super	Low	Med	High	Super
Time (s)	783			981			
Distance (km)	3.976			3.482			
Peak Power (kW)	11.3	11.3	11.5	11.5			
Peak Regen. (kW)	-1.25	-2.5	-5.1	-0.8	-2.85	-5.7	-9.7
Total E out (kWh)	0.57	0.57	0.52	0.61			
Total E in (kWh)	0.015	0.03	0.1	0.01	0.03	0.06	0.13
E in/E out (%)	2.55%	5.1%	18.5%	1.67%	5.07%	9.52%	21.47%
KE captured (%)	14%	24%	76%	9%	18%	30%	70%

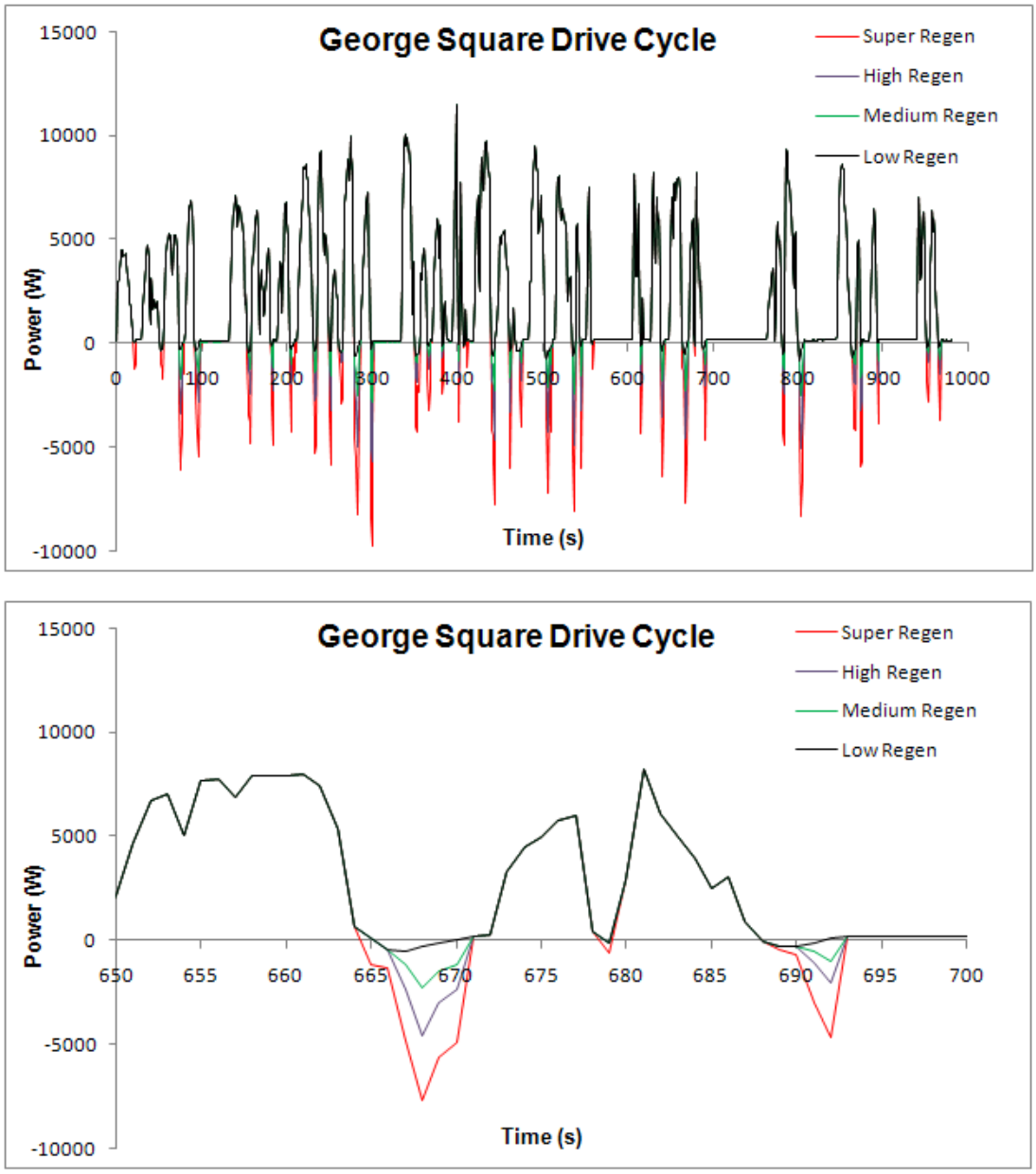

Figure 3.47: Power for the George Square cycle, with varying amounts of regenerative braking. The lower plot shows a detail of the upper plot to highlight the different regeneration schemes.

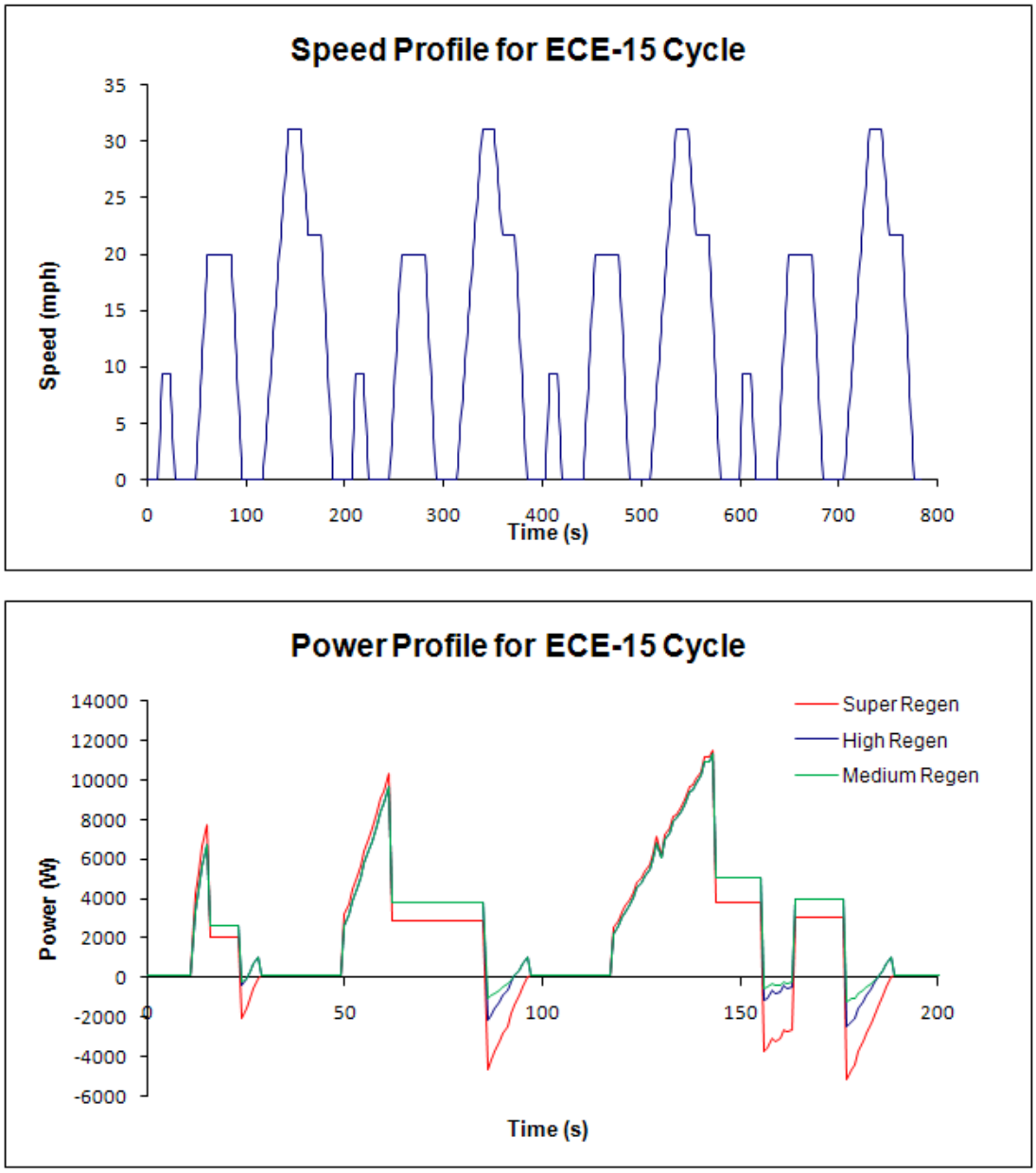

Figure 3.48: The ECE-15 test cycle repeated four times. The upper plot shows the speed while the lower plot shows the power for just one iteration of the cycle, demonstrating the different power schemes. Equations 3-36 to 3-39 were used to find the discharging power as well as the charging power, hence the discrepancies between the Super Regeneration and the High and Medium Regeneration profiles.

3.6 Chapter Summary

A model of the Cobra battery pack has been created using the ADVISOR Rint battery model as a starting point. Voltage and resistance data for the existing Cobra batteries was entered into the model, however this did not give a satisfactory fit between modelled data and test results. It was essential to create a model that could

be used within the ADVISOR framework that would accurately and repeatedly calculate voltage and current from power demand information. This was achieved with the inclusion of a modelled constant voltage drop during discharge and a delayed voltage recovery when the batteries are not being discharged. This novel battery model, developed by the author, combines simplicity with accuracy, and is suitable for use in ADVISOR. The peak error of this new model was 3.1% - less than a third of the 12% error recorded by ADVISOR's developers for the original Rint model, and also noticeably lower than the 4% error found by the developers for ADVISOR's RC model. Although this model was developed for the Cobra batteries, the charge transfer resistance and capacitive effects which it simulates are a common feature of batteries and the model should therefore be broadly applicable.

The model was verified using data recorded during driving tests in Glasgow. The Cobra was driven on a 5.4 mile route with a 10 minute pause halfway through, imitating a city commute. The Cobra was also driven on a short 0.7 mile route at a range of states of charge.

The Cobra offers limited regenerative braking, as it is a low budget car it does not offer the active braking control necessary to extract the full energy that might be available. To assess the amount of energy that could potentially be extracted, the relationship of the Cobra's power, speed and acceleration was assessed and a regeneration profile extrapolated. This led to the creation of four possible regeneration profiles: Low, Medium, High and Super Regeneration. These were subsequently used for testing the optimisation strategies.

The hybrid Cobra was developed using the battery-only Cobra as a starting point. The additional supercapacitor pack was sized and the control strategy determined using a hybrid battery/supercapacitor model developed by the author. The effect of the different regeneration profiles was also investigated. The development of that model and the sizing of the supercapacitor pack are discussed in the next chapter.

4 Design and Model of the Hybrid System

The first stage in designing a hybrid system is to specify an appropriate pack size and rating of supercapacitor. The ideal supercapacitor pack would be small, light, cheap, have both high energy and high power density, and very low internal resistance. Additionally, it should be resistant to damage, and should be fail safe should any damage occur. However, a practical supercapacitor pack must feature some compromises. For example, higher energy and power densities mean higher cost, and for commercially available supercapacitors the materials with the best performance also have a risk of producing toxic by-products [151].

This chapter discusses the current state of commercially available supercapacitors, and sizing considerations given the available technology. It then describes the supercapacitor model used to simulate the hybrid Cobra. The batteries and supercapacitors in this model are both controlled with half bridge converters, and the development and modelling of these converters is discussed. The chapter concludes with a description of the complete hybrid model and power flow control strategy.

4.1 Commercially Available Supercapacitors

Large-scale supercapacitors range in capacitance from a few hundred to several thousand Farads. Commercial data from five supercapacitor companies was assessed to determine what performance is available with current technology. These companies are Ness [152], Maxwell [42], batScap [153], Nippon Chemi-con [154] and Epcos* [155]. These capacitors range between 120F and 9000F and have operating voltages of 2.3V to 2.7V per cell.

In general a higher capacitance device will have a lower resistance and a higher cost per unit, while energy density remains roughly constant regardless of capacitance. Larger supercapacitors also tend to be a bit cheaper per unit energy. Figure 4.1 shows how capacitance relates to the DC equivalent series resistance (ESR) and

* Epcos ceased manufacture of supercapacitors in 2006.

energy density for supercapacitors from different companies. Figure 4.2 shows the cost per unit and cost vs. energy content of selected capacitors from three of the companies, using cost information from 2007 and 2008. In both figures, the energy and resistance information was taken from the product datasheets, and the energy density describes the nominal energy content of the supercapacitors at peak voltage.

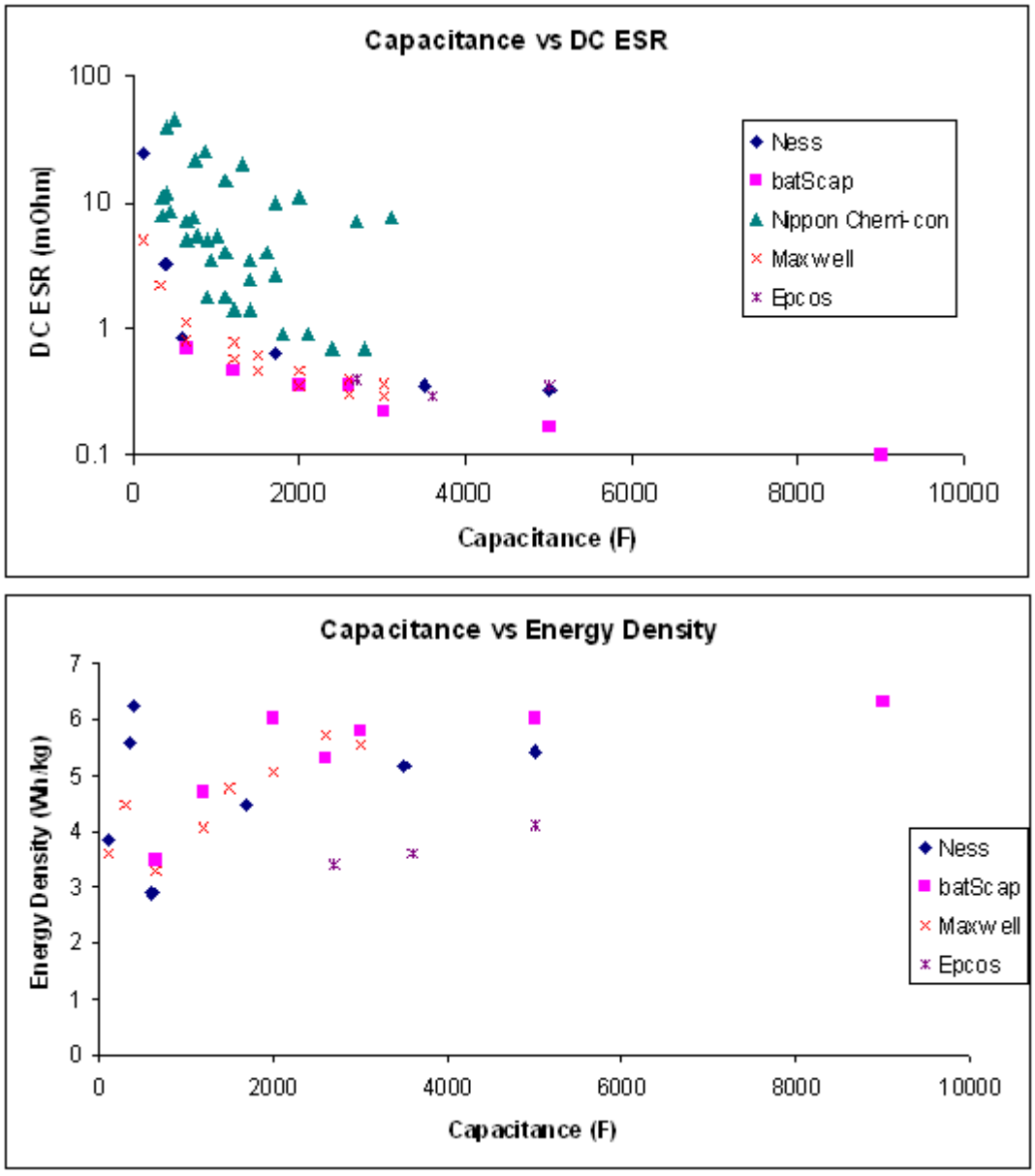

Figure 4.1: The upper plot shows the capacitance vs the DC equivalent series resistance (ESR) for several commercially available supercapacitors. The lower plot shows the capacitance vs the energy density for the same capacitors. Energy density information was not available for the Nippon Chemi-con capacitors.

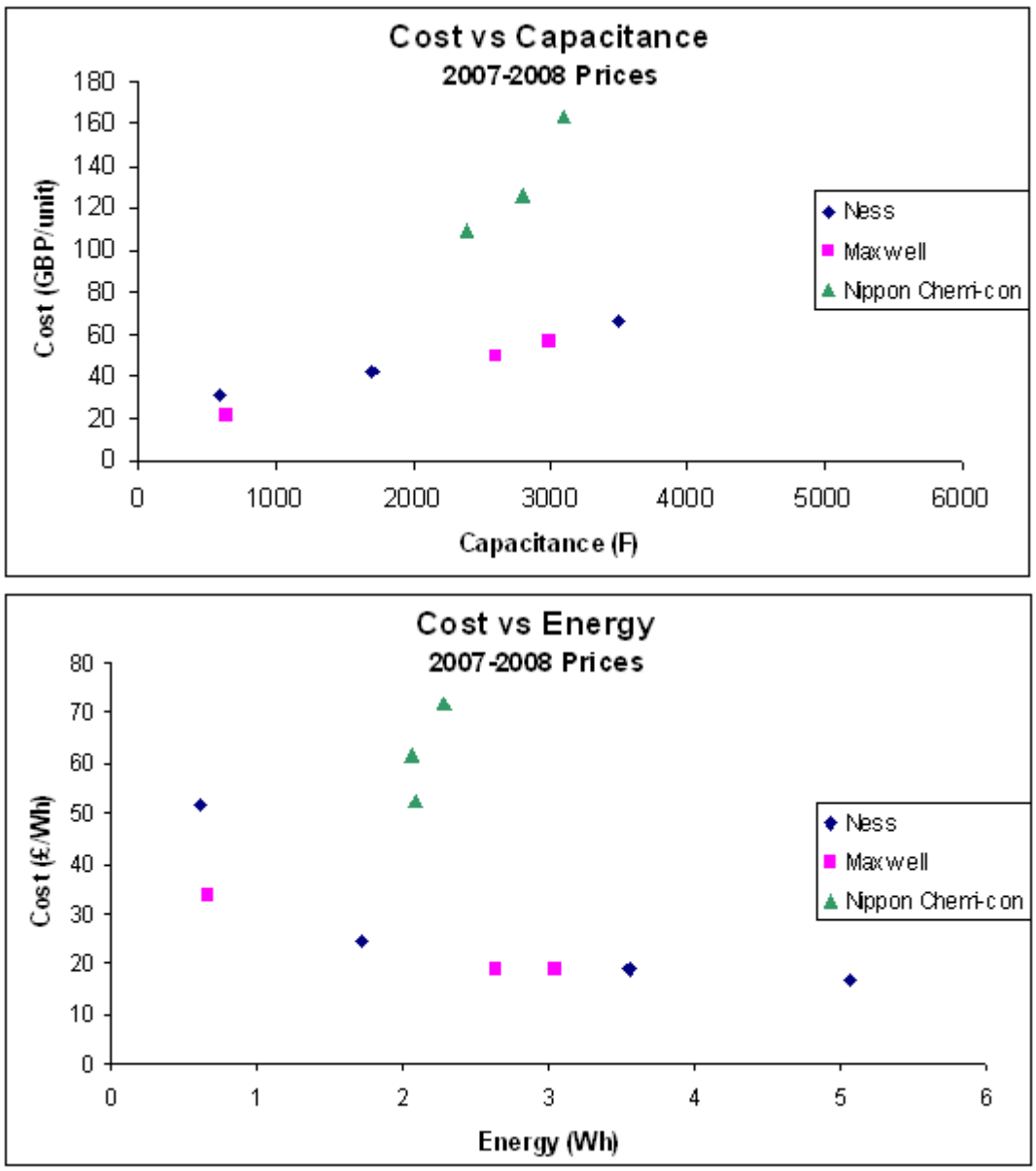

Figure 4.2: The cost for selected supercapacitors from Ness, Maxwell and Nippon Chemi-con, with price information from 2007 and 2008. The upper plot shows the cost per unit and the lower plot shows cost per Wh for the same capacitors.

As can be seen in Figure 4.2, Maxwell and Ness show a broadly linear relationship of cost and capacitance, but Nippon Chemi-con's supercapacitors are much more expensive. Furthermore, Figure 4.1 shows that the capacitors from Nippon Chemi-con have a much higher resistance than any of the other capacitors. The difference in both cost and resistance is down to the materials. Companies based in America or Europe use the toxic substance acetonitrile as a solvent. Acetonitrile has been banned in Japan because of its toxicity, and so Nippon Chemi-con uses propylene carbonate instead [151].

Some companies offer several options for a single capacitance. Nippon Chemi-con offers capacitors with different operating voltages and resistances. Maxwell offers capacitors with different resistance, although all have a peak voltage of 2.7V. A lower voltage or higher resistance means a lower price. Choosing an appropriate supercapacitor pack for use in a vehicle means trading off between a number of factors including cost, resistance, voltage and size.

4.2 Sizing a Supercapacitor Pack

Sizing a supercapacitor pack means determining the amount of energy it will need to store, the operating voltage, and the number and layout of individual capacitors needed to provide this energy and voltage. This is partially determined by the characteristics of the battery-powered vehicle to which the capacitors are to be added. If the vehicle has a pre-determined battery pack and motor, as the Cobra does, then this will apply certain constraints to the supercapacitor pack sizing. For example, the operating voltage of the pack will need to be suitable for interfacing with the batteries and motor, and the supercapacitor pack will need to physically fit into the vehicle. The intended purpose of the vehicle is also important; since the Cobra is a low-budget vehicle the supercapacitor pack and electronics will also need to be low-budget. Finally, the ideal pack size depends on what purpose the pack is to serve. This section will consider the pack sizing implications for two options:

- to increase the vehicle efficiency
- to extend the life of the batteries by minimising their peak currents.

Each of these options requires different considerations for selecting a pack size. These options have been chosen out of the list of four options given in Section 1.3 as being most suitable for the Cobra; the option to improve vehicle acceleration performance was not investigated as the Cobra power is limited by the motor, rather than by the batteries. The option to replace some batteries with supercapacitors was also not investigated, as this would excessively limit the range.

It is crucial to include the effects of the power electronics in any calculation of optimal pack sizing. Power electronics are essential for the integration of supercapacitors with batteries in an electric vehicle, as discussed in section 2.4. It is easy to assess the supercapacitors as an ideal element providing and sinking a certain amount of power, but the electronics required to achieve this introduce certain practical limitations. These must be considered if a physically useful result is to be found.

4.2.1 Pack Voltage

The cost per unit energy for the acetonitrile-based supercapacitors decreases as the unit capacitance increases, as shown in Figure 4.2. It is therefore cheaper to buy a small number of large capacitors than to buy a large number of smaller capacitors. However, this introduces a problem – extracting the power from the capacitors.

Consider a supercapacitor pack which might be purchased for use in the Cobra. Assume the pack will need to contain 17Wh; this could be accomplished with 30 capacitors with a capacitance of 650F, or with just 8 capacitors with a capacitance of 2600F. In 2007, high-power 650F supercapacitors from Maxwell cost £22.01, while high-power 2600F supercapacitors from the same company cost £49.50 each. In this scenario, the pack consisting of 650F capacitors would cost £660.30 while the pack with 2600F capacitors would cost just £396.00. The difference in cost is stark, and that is even without considering the fact that the eight 2600F capacitors would need far less in the way of charge-balancing electronics to connect them.

Now consider the power output of each pack. The power provided by a pack of supercapacitors is given by

$$P = (V_{OC} - IR)I, \tag{4-1}$$

where V_{OC} is the open circuit voltage of the unit, I is the current, R is the internal resistance and P is the provided power. Driving tests with the Cobra have found a peak power of 12kW and a typical average power of 2.5kW. The 650F supercapacitor pack has an operating voltage of 75V, and a nominal resistance of

24mΩ. If the supercapacitors are to supply a power of 9.5kW (the Cobra peak power minus the average power) when fully charged, this pack will need to supply a current of 132A. The 2600F supercapacitor pack, on the other hand, has an operating voltage of just 20V and a nominal resistance of 2.48mΩ. This pack must provide a current of 507A to provide the same power. This is possible for the supercapacitors, but would require very robust, heavy and expensive power electronics to deliver this power to the motor.

It is important that the supercapacitor pack voltage is high enough to supply the required power at reasonable currents. What is considered reasonable will depend on the budget and intended market for the vehicle – for the Cobra supercapacitor pack, the peak current has been defined as 250A, as this is the peak current possible in the battery-only Cobra. For cost reasons, the supercapacitor pack voltage should not be any higher than what is necessary; supercapacitor voltage is limited to 2.7V per unit, so a higher voltage means more units, and hence a higher cost as described above. In this case, the Cobra is an existing battery-powered vehicle to which supercapacitors will be added, and the supercapacitor pack should be sized to fit. The supercapacitor pack will be assumed to have a similar nominal voltage to the batteries – thirty supercapacitors in series will have a nominal voltage of 75V, as the battery pack, with a nominal voltage of 72V, has a typical terminal voltage of ~75V. The energy needs of the different proposed optimisations will then dictate the capacitance of the individual supercapacitors in the pack.

4.2.2 Sizing Considerations for Maximising Efficiency

The batteries are the ultimate source of almost all the energy in the vehicle. The supercapacitors may also be charged while the vehicle is plugged in, but they will contain only a fraction of the total vehicle energy. For example, a pack of thirty 5000F supercapacitors charged to 75V contains 0.13kWh, while thirty 600F supercapacitors contain 0.016 kWh. The Cobra batteries contain 5.04 kWh, so a single pack of supercapacitors for the Cobra would contain between 0.3% and 2.5% of the vehicle's total energy. Apart from this small contribution, any energy that comes from the supercapacitors will have come to the supercapacitors during a drive cycle, either from the batteries or from regenerative braking.

The benefits of sending regenerated energy to the supercapacitors have already been discussed in Section 2.2.2. The supercapacitors can receive a much higher charging current without being damaged than can the batteries, allowing more energy to be recaptured and increasing overall efficiency. For example, the Cobra battery charging currents are limited to 55A, but the supercapacitors can receive the full 110A which the motor can generate. The supercapacitor pack should therefore be large enough to capture all of the regenerated energy from a braking event.

What pack size is therefore needed for the Cobra, if the goal is to capture all of the regenerated braking energy? The energy contained in a moving vehicle is given by the equation

$$E = \tfrac{1}{2} m v^2, \qquad (4\text{-}2)$$

where E (J) is the energy, m (kg) is the mass of the vehicle and v (m/s) is the velocity. This is the upper limit to the energy that can be captured via regenerative braking.

The battery-only Cobra weighs 785.5kg and has a top speed of 40mph, or 17.88m/s. Assuming a 70kg driver, this means the maximum kinetic energy of the vehicle is 38Wh. (For further comment on vehicle mass, see Section 4.5.2.) Some of this energy will be lost in the motor/generator and in the power electronics connecting the motor to the supercapacitor.

According to [149], typically up to 30% of the kinetic energy of a vehicle can be retrieved in regenerative braking, thus the supercapacitors will receive at most 11.4Wh. This is the energy that must be available in the supercapacitor pack. In the Cobra, as in a number of other cars which use supercapacitors [19, 49, 59, 69], the capacitors are not discharged below 50% of their peak voltage, making 75% of their total energy available (from Equation 2-5). The ideal pack must therefore have a total energy content of 15.2Wh. If the pack consists of thirty supercapacitors with a peak voltage of 2.5V each, then each capacitor should have a capacitance of 584F. This value will go up or down depending on the actual regeneration profile of the

vehicle – more energy could be available with active braking management on each wheel, while some vehicles will use a regeneration scheme that recoups less energy. The battery-only Cobra typically recoups only 9% of the kinetic energy, and thus would receive at most 3.4Wh. For a pack of thirty supercapacitors, the individual capacitors would need to be only 131F to capture all the available regenerated energy. On the other hand, with full traction control an urban vehicle like the Cobra could capture more than 87% of the vehicle's kinetic energy [150], and the supercapacitors in the pack would need 1270F to capture this energy.

Complicating this is the fact that lower capacitance is associated with higher resistance in supercapacitors. This means that simply sizing the supercapacitor pack to capture braking energy is not likely to present the optimal solution for maximising efficiency. A 600F supercapacitor from Ness has a DC equivalent series resistance of 0.83mΩ, while a 5000F capacitor has a DC ESR of 0.33mΩ - less than half the value of the smaller capacitors. This means the 5000F supercapacitor pack would have a lower resistance, improving efficiency. Additionally, a larger supercapacitor pack would contain more energy, and therefore would increase the range of the vehicle slightly purely by virtue of having more energy available.

In addition to receiving regenerative energy, the supercapacitors may be recharged from the batteries. If the supercapacitors are charged from the batteries, they may be able to provide more high power peaks; this offers an efficiency benefit as the supercapacitors have a lower internal resistance than the batteries and hence lower losses. For example, the Cobra battery pack has an internal resistance of 60mΩ, not counting the voltage drop effect described in Section 3.2.5. This is two orders of magnitude higher than the resistance of the supercapacitor packs described in the previous paragraph. However, when the batteries charge the supercapacitors, this can have a negative effect on the vehicle efficiency. This energy must travel from the batteries to the supercapacitors, suffering internal losses in both devices and also in the intervening power electronics. It must then travel from the supercapacitors to the motor, with further losses in the devices and in the power electronics. The

optimal charging rate was examined using the control strategy described in Section 4.5.1.

4.2.3 Sizing Considerations for Constant Battery Power

The minimum battery current can be achieved by having the battery supply a constant power equal to the average power needed for the drive cycle, and to have the supercapacitors supplying all the excess power and also absorbing power from the battery whenever the vehicle demand is less than the average. This is the strategy described as ideal by Barrade and Rufer in [70]. The obvious problem with this strategy is that every cycle will have a different average power and energy requirement, and it is impossible to know in advance exactly when the supercapacitors will be needed to provide or sink power.

Consider a drive cycle in which the batteries supply a certain total energy E_{tot} at a constant power. Whenever the vehicle requires power above average, the excess must be supplied from the supercapacitors; E_{excess} is defined to be the total energy supplied from the supercapacitors to the motor in this fashion. Whenever the vehicle requires power below average, the battery will supply the required power to the motor, and the remainder of its constant output must go to the supercapacitors. The total energy delivered to the supercapacitors from the batteries is defined as $E_{shortfall}$. This also includes the full value of the battery output power whenever the vehicle is braking. Finally, all of the regenerated energy from braking, $E_{regen,}$ is sent to the supercapacitors. This classification of the energy in the system is illustrated in Figure 4.3.

In order to discuss the losses in the energy storage system, the following efficiencies are defined: supercapacitor pack efficiency η_s, battery pack efficiency η_b, efficiency of power electronics between batteries and motor η_{btm}, between supercapacitors and motor η_{stm}, and between batteries and supercapacitors η_{bts},. Hence the total losses in the energy storage system can be expressed as:

$$\begin{aligned} E_{lost} = {} & E_{excess}(1-\eta_s)(1-\eta_{stm}) + E_{shortfall}(1-\eta_b)(1-\eta_{bts})(1-\eta_s) + \\ & E_{regen}(1-\eta_s)(1-\eta_{stm}) + (E_{tot} - E_{shortfall})(1-\eta_b)(1-\eta_{btm}) \end{aligned} \tag{4-3}$$

The losses in the motor and in later stages of the vehicle are not considered here because they would be the same no matter what energy storage system was used, assuming the drive cycle is driven in the same manner. The energy flow and efficiencies are illustrated in Figure 4.4.

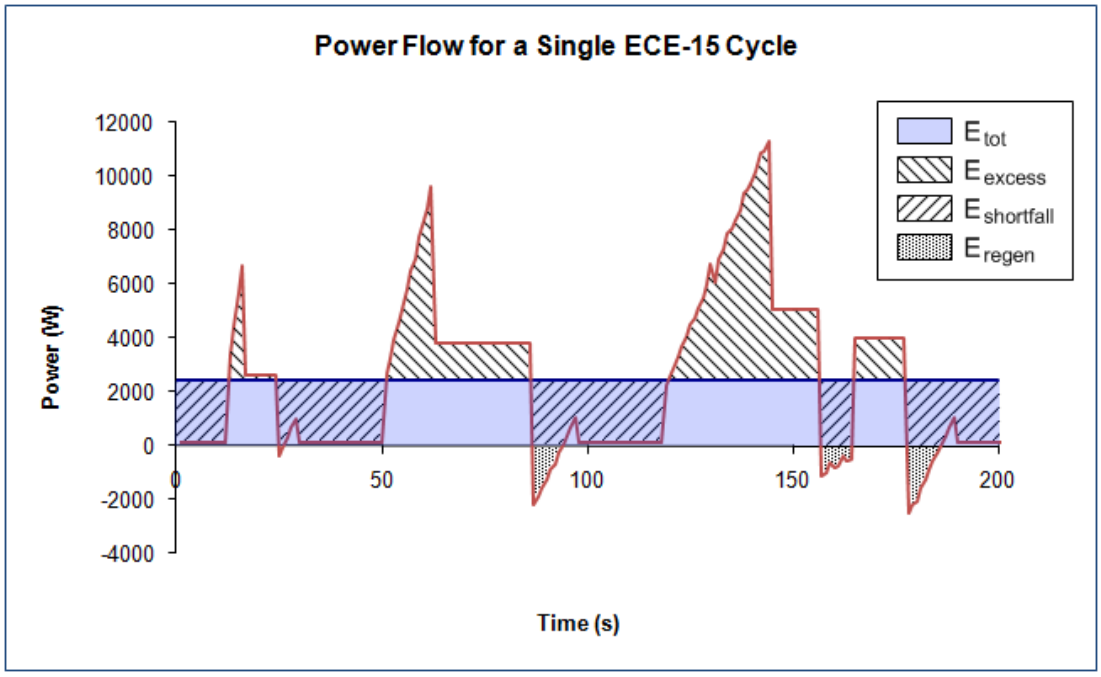

Figure 4.3: Example of the energy categorisation for a single ECE-15 cycle. The red line shows the power for the cycle and the blue line shows the average power. The area under the blue line is therefore the total energy E_{tot}. E_{excess}, $E_{shortfall}$ and E_{regen} are also indicated with their respective areas.

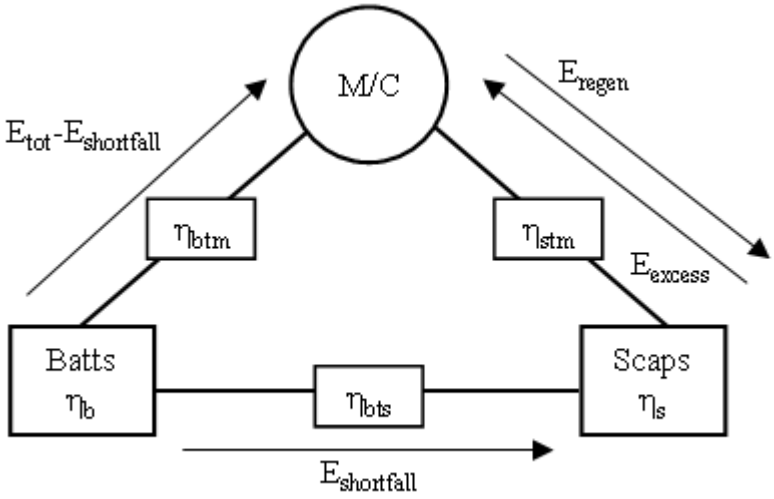

Figure 4.4: A diagram of the energy flow and efficiency losses in a battery/supercapacitor hybrid vehicle.

Consider a simplified scenario in which the efficiencies have fixed values. In this case η_s is 98% (as per [21]), η_b is 82.5% [22], and the power electronics have an efficiency of 98%. This is a typical value for the efficiency of the power electronics, described in detail in Section 4.4, across a power range of 2-3kW. The drive cycle in this example is the ECE-15 cycle from Advisor, a standard cycle used in Europe to test a wide variety of vehicles. The cycle details are shown in Figure 2.1. This power information was calculated using equations 3-35, 3-36 and 3-37, and represents the power requested from the energy storage for given speeds and accelerations, based on measurements of the Cobra batteries during actual drive cycles. Thus the power and energy described here includes the losses due to friction, air resistance, and motor efficiency.

For a small car with similar details to the Cobra, the ECE-15 cycle requires a total of 484kJ of energy, delivered at an average power of 2410W over 200s. A total energy of 492kJ is delivered at powers above the average (E_{excess}) and 18kJ is delivered at powers below the average ($E_{shortfall}$), with a further 26kJ available from regenerative braking (E_{regen}), assuming the friction brakes are not used (484 = 492 + 18 – 26). Using equation 4-3, the amount of energy lost is 1.8kJ. The vehicle travels 0.99km in the course of the cycle, so the yield is calculated as 7.36km/kWh. The average power output of the batteries, accounting for the losses, becomes 2431kW, and the output current to provide this power is 33A when the batteries are fully charged, rising to 36A when the batteries are at 30% SOC.

To achieve this performance, a sufficiently large supercapacitor pack is needed to handle all the fluctuations in power. The supercapacitor pack sizing is accomplished by following the process defined by Barrade [70]. The cumulative energy needs of the cycle, as a function of time, are compared to the energy output that results from a constant power, as shown in Figure 4.5. The difference between these two curves is the power fluctuation that must be provided from and to the supercapacitors – shown in green in Figure 4.5. The energy rating of the supercapacitors must therefore be equal to the difference between the maximum value and the minimum value of the fluctuations shown in the green curve. In this case, the difference is 146kJ.

Assuming the supercapacitors can provide 75% of their energy content and given a pack of thirty series-connected supercapacitors, then from Equation 2-5:

$$(146000\text{J})*4/3=1/2*30*(2.5\text{V})^2*C \qquad (4\text{-}4)$$

The supercapacitors in the pack would need a total of 195kJ and an individual capacitance of 2076F to meet the energy demand.

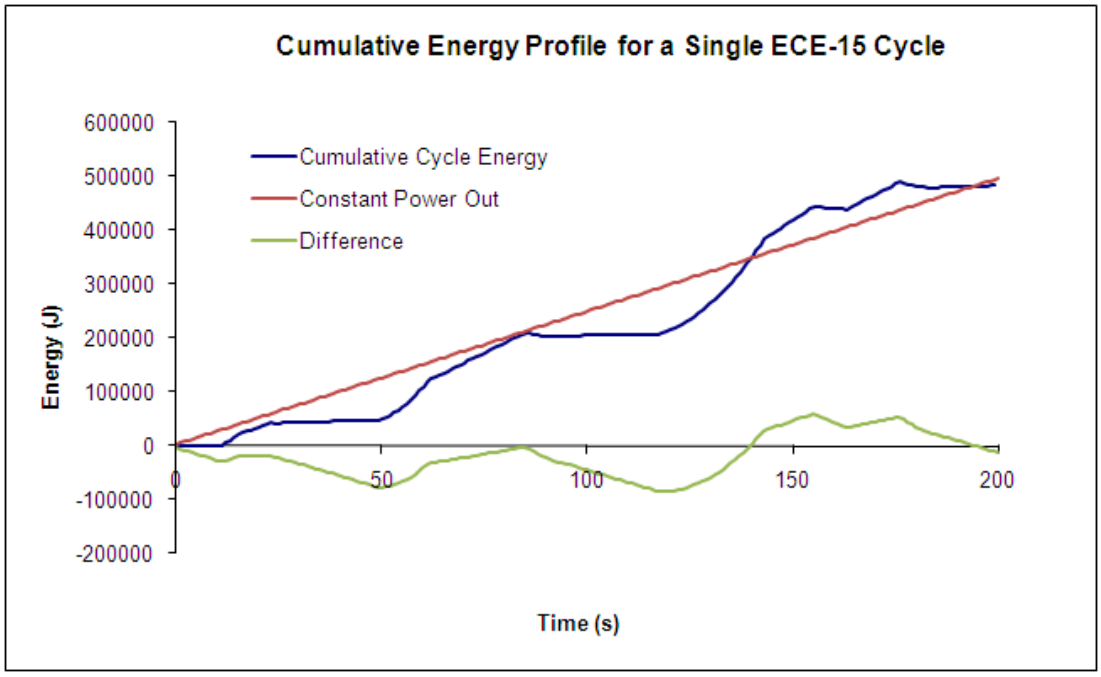

Figure 4.5: Cumulative energy of a single ECE-15 cycle, along with the equivalent constant power out, ideally supplied by the batteries, and the difference between the two, ideally supplied by the supercapacitors.

The supercapacitor must start at some SOC lower than 100%, because it starts out by sinking power from the battery. This is indicated by the negative value of the green line in Figure 4.5. The supercapacitor then supplies power until it reaches its original SOC at a time of 84s, then sinks power again until it has received 76kJ – this is the minimum point on the green line in, and occurs at 118s. After this point the supercapacitor delivers power until it has again returned to its starting SOC, then delivers further power until it has supplied 70kJ more than its starting SOC – this is the maximum point on the green line. Additionally, one quarter of the total energy, 49kJ cannot be accessed.

Using this information, the starting SOC of the supercapacitor can be calculated:

(70kJ+49kJ)/195kJ = 1-76kJ/195kJ = 0.61 (4-5)

This highlights the impracticality of this method of control – how could the required starting SOC be known in advance? This analysis remains useful as a comparison of the different pack sizes that would be needed to achieve the maximum benefit for an efficiency-maximising strategy vs. a battery current-minimising strategy. It also provides a lower limit for the peak battery current value, in this case 33-36A as described above.

4.2.4 Cost

Ultimately, the chosen supercapacitor pack must be cost-effective. For a low-cost vehicle like the Cobra, this is a significant limiting factor. The Cobra batteries cost £154.14 each in 2007, giving a total pack cost of £924.84. This cost must be kept in mind when considering the cost benefit of a hybridisation strategy.

If the supercapacitors are to be added as a means of extending the battery life, then the cost analysis is fairly straightforward. First, the expected lifetime of the batteries in normal use, without the addition of supercapacitors, must be determined through testing. For example, if the batteries will typically last for 3 years when used without the supercapacitors, and if the vehicle itself is used for 9 years, then the batteries must be replaced twice in the vehicle lifetime. Next, the typical life extension provided by the supercapacitors must be determined. If the supercapacitors increase the battery lifetime by 50%, to 4.5 years, then this will be a worthwhile strategy only if the supercapacitors and the associated electronics cost less than a replacement battery pack. In this scenario the batteries will be replaced once in the life of the vehicle, not twice, making up for the additional costs associated with installing a pack of supercapacitors. If the supercapacitors can extend the battery life by 200%, to 9 years, then they and the electronics could cost up to £1850 and remain a worthwhile investment. If the batteries have remaining life when the vehicle is scrapped, then they may retain some resale value – in [156] this value is calculated as 70% of the original battery cost, multiplied by the percentage of life remaining.

Assessing the benefit of hybridisation in a scheme to increase range or to improve acceleration is more complex. One approach is to consider the benefit that would be achieved by adding an additional battery to the pack. One extra battery for the Cobra would cost £154.14, and the battery Cobra model can be altered to account for an extra battery in the string, showing the benefit to range and performance. The currents in each battery would also be reduced, so there could be life extension benefits as well. Of course, adding a battery would also increase the voltage of the system. The Cobra motor can accept a voltage up to 400V, so this would be possible. Thus, the addition of one or more additional batteries is considered in this study as an alternative to adding supercapacitors, and provides a check that the supercapacitors have a worthwhile effect.

4.2.5 Pack Sizing Summary

Following the pack sizing methods described in Sections 4.2.2 and 4.2.3, suggested supercapacitor pack sizes for each cycle is shown in Table 4.1. In each case it is assumed that the pack consists of thirty supercapacitors in series, to meet the voltage needs of the vehicle.

The first sizing method indicates the supercapacitor pack size that is needed to capture all of the regenerative braking energy. This is the minimum pack size that is needed for an efficiency-maximising strategy, and the amount of regenerative energy that is available in the cycle makes a substantial difference to the pack size. However, the methodology does not account for the increased internal resistance of the smaller supercapacitors, nor can it optimise the charging power from the batteries. These elements must be determined through simulations, as described in the remainder of this chapter.

The second sizing method indicates the supercapacitor pack size that is needed to permit the batteries to deliver a constant power throughout the cycle, assuming perfect control of the cycle. Interestingly, the amount of regenerative braking in the cycle does not make a substantial impact to the optimal size of the supercapacitors. The major flaw in this method is that no drive cycle can be known in advance, and so

perfect control is impossible. Again, the simulations described in this chapter are used to find an effective pack size given a rule-based control strategy.

The final aspect to the sizing of the supercapacitor pack is cost. For each suggested pack, the cost of the smallest suitable, commercially-available supercapacitors is given. Only those supercapacitors which were used in the hybrid system simulations are considered; a full list is given in Table 4.3. Costs in this table are given for 650F, 1700F, 2600F and 5000F supercapacitors – smaller capacitances were not considered as such supercapacitors have DC resistance values in excess of 1mΩ.

Table 4.1: Theoretical pack sizes for supercapacitor packs given different cycles and strategies. Sizing for optimal efficiency follows the method discussed in Section 4.2.2, while sizing for minimised peak battery currents follows the method detailed in Section 4.2.3.

Cycle	Regen.	Sized for efficiency	Cost of pack	Sized for battery current minimisation	Cost of pack
ECE-15	Medium	268F	£660.3	2051F	£1485
	High	462F	£660.3	2016F	£1485
	Super	1475F	£1275	2211F	£1485
George Square	Low	175F	£660.3	4691F	£2580
	Medium	356F	£660.3	4619F	£2580
	High	581F	£660.3	4486F	£2580
	Super	1371F	£1275	4017F	£2580

4.3 Modelling the Cobra Supercapacitor Pack

The electrical simulation model for supercapacitors in an electric vehicle must be suitable for a rapidly changing and irregular power profile, including both charging and discharging. The Cobra model is based on ADVISOR, so the supercapacitor model also needs to operate within this framework. The ADVISOR simulations use electrical power as the input and output variable for each component, and any model used with this program must take this form. A number of variables must be tracked – of particular interest for this research are the current, voltage and power losses.

These will vary in time increments of one second as this is the simulation time step used by ADVISOR.

The supercapacitors were tested with a 1470E potentiostat from Solartron, which has a peak current of 4A and a peak voltage of 30V. The test current is therefore significantly lower than the currents the capacitors would experience in a vehicle, which in the hybrid Cobra would be up to 250A. The literature indicates that supercapacitor characteristics are not affected by the current magnitude [107]. To confirm this, four 10F supercapacitors were tested with a range of currents. These supercapacitors contain an organic electrolyte and carbon electrodes, like the 650F supercapacitors. Unlike the 650F supercapacitors, the 10F ones have a peak voltage of 2.3V – no 10F supercapacitor was available with a 2.7V peak voltage. The 10F supercapacitors were cycled 15 times between 0V and 2.3V at currents ranging from 0.05A to 3.85A. The nominal charging time for a supercapacitor can be calculated using equation 3-10, which for a constant current becomes:

$$\Delta V = \frac{1}{C}(I\Delta t) \tag{4-6}$$

$$C = I\frac{\Delta t}{\Delta V} \tag{4-7}$$

where C is the capacitance, I is the constant current, ΔV is the change in voltage and Δt is the time for which the current is applied. If two different supercapacitors experience two different currents such that ΔV and Δt are the same for both, then:

$$\frac{C_1}{C_2} = \frac{I_1}{I_2} \tag{4-8}$$

Therefore, the nominal charging time for a 10F supercapacitor experience a current I is the same as for a 650F supercapacitor experiencing a current of $65I$, and the current range of 0.05A to 3.85A for the 10F capacitors is equivalent in terms of charging time to currents of 3.25A to 250.25A, respectively.

As shown in Figure 4.6, the overall capacitance of the 10F supercapacitors during repeated cycles, using the potentiostat at different currents showed an average decrease of 7% as the current increased from 0.05A to 3.85A. This suggests that the calculated capacitance of the 650F capacitors may be slightly overstated, but the margin of error will be small. The energy efficiency of the 10F supercapacitors was found to be ≥99% at all currents for three of the supercapacitors, while the fourth had an efficiency of 97%. This confirms that the energy efficiency of the supercapacitors is not dependent on current for the current ranges investigated.

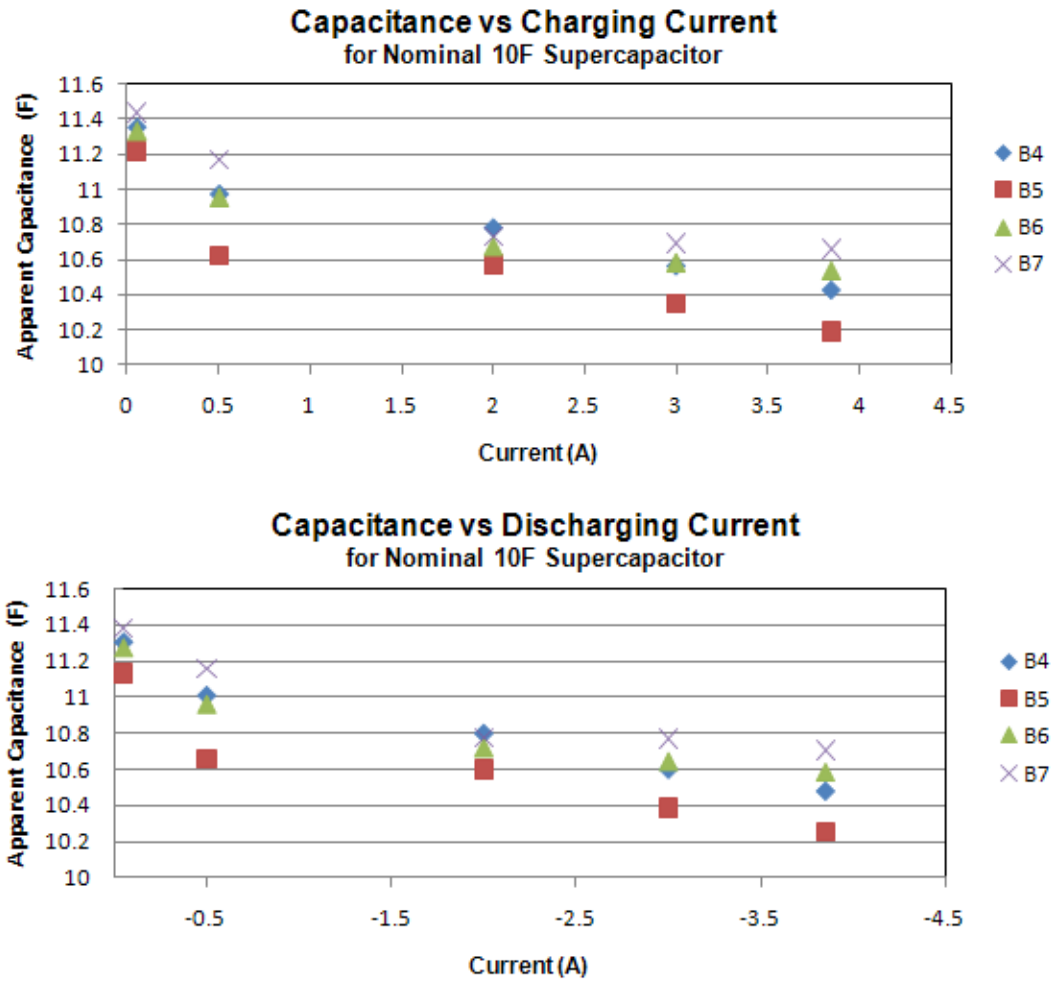

Figure 4.6: The overall capacitance of a nominal 10F supercapacitor after several cycles at various currents.

4.3.1 Test Results

Tests performed on the commercial Maxwell supercapacitors have confirmed the relationship of voltage to capacitance, which was described in section 2.6.1. These tests also indicated the effects of the deep pore structure on the capacitor's behaviour. Three types of test were performed. First, the supercapacitors were cycled between 0V to the peak voltage of 2.7V with a constant current of 3.8A to demonstrate their behaviour throughout their full voltage range. These cycles were repeated fifteen consecutive times in order to allow the cycling regime to penetrate to the deep pore structures, as illustrated in Figure 2.15. Fifteen cycles was sufficient to ensure that the calculated capacitance was stable, varying by less than 0.5% over the last five cycles for each capacitor. Next, the capacitors were cycled between 1.25V and 2.5V as this is more representative of the voltage range that would typically be encountered in use in the Cobra. The minimum voltage is chosen to allow three quarters of their stored energy to be extracted, while limiting high currents and poor efficiency in the power electronics which would occur with a much lower pack voltage. The maximum voltage is reduced slightly, on the advice of Maxwell, to reduce the risk of overcharge when used with regenerative braking. These cycles were also performed fifteen times consecutively. The final test involved subjecting the capacitors to a variable current intended to imitate the currents they might encounter while in use. This test was derived from models of the capacitors in the ECE drive cycle, which is shown in Figure 2.1.

It should be noted at this point that some of the 650F supercapacitors were purchased in early 2007, and several more were purchased in early 2009. Although the two sets of capacitors have the same nominal capacitance and are from the same product series, the newer set have a significantly improved performance, with an effective capacitance 10% higher than the older capacitors. The newer set also have a significantly increased cost of £38.54 per unit, while the older set cost £22.01 per unit. It is not known what part of the cost increase is due to different manufacturing techniques, and what part is due to the global economic upheaval that began in 2008. The modelling efforts focus on the newer supercapacitors, but the older ones are mentioned to provide an illustration of the rapid advancements that are being made in

the supercapacitor industry, and the difficulty of fully anticipating the performance of a commercial supercapacitor based on the nominal qualities alone.

When a single, newer 650F capacitor is repeatedly cycled from 0V to 2.7V with a DC current of 3.8A, its apparent overall capacitance by the end of the cycles is found to be within 1.5% of its nominal capacitance – in other words, the amount of energy put into the capacitor is equivalent to the energy needed to charge an ideal 650F capacitor to the same voltage. But the apparent capacitance at each step of the charging process is highly variable.

As an illustration, consider the test results of a specific capacitor, designated E30, being charged from 0V to 2.7V with a constant DC current of 3.8A. A single charge after repeated cycling at this current took place over a period of 454 seconds. An examination of this charging event reveals the varying nature of the capacitance with respect to voltage. Equation 4-7 can be used to find the apparent capacitance of this capacitor as 645.1F, very close to the nominal value:

$$C = I\frac{\Delta t}{\Delta V} = 3.8\frac{454}{2.7} = 645.1\,\text{F} \qquad (4\text{-}9)$$

However, when the above calculation is performed at one second intervals, a very different picture emerges. Rather than a constant capacitance, it shows a capacitance that varies from 482F at the beginning of the charge to as much as 815F towards the end. The relationship of capacitance to potential is roughly linear, and is due to the interfacial tension between the electrodes and electrolyte, as discussed in Section 2.6.1.

Consider now the discharging event which immediately preceded this charging event. The capacitor discharge current was also 3.8A. This discharge from 2.7V to 0V took 452.4 seconds, indicating an overall capacitance of 642.7F – slightly lower than the value found for the charge. The lower apparent capacitance on discharge allows a calculation of the supercapacitor's energy efficiency: from equation 2-5, energy content is proportional to capacitance. So:

$$\frac{E_{out}}{E_{in}} = \frac{C_{discharge}}{C_{charge}} = \frac{642.7}{645.1} = 0.996 \qquad (4\text{-}10)$$

The discharge capacitance also varies with respect to voltage, but with a slightly different profile than the charging capacitance. Figure 4.7 illustrates the relationship of capacitance vs. voltage for the supercapacitor during a charge and a discharge. The small oscillations in capacitance values at higher potentials are caused by inaccuracies in the equipment.

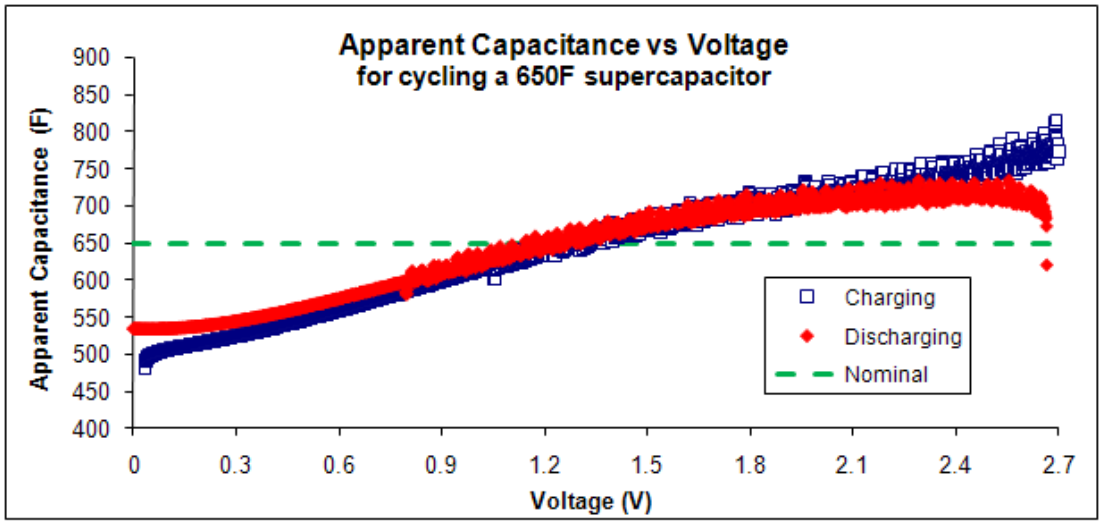

Figure 4.7: Capacitance vs. Potential calculated at one second intervals when cycling a single 650F capacitor.

Compare these results with the apparent capacitance found at the start of the cycling. The very first charge in this series brought the capacitor from 0.15V to 2.7V in 453.2 seconds. (This was the first test performed on this capacitor at Strathclyde, so the small residual charge is a remnant from the factory.) The capacitance calculated from this charging event is 674.7F – almost 5% higher than the capacitance found after several cycles. This much higher measured capacitance is due to charge 'disappearing' into the deep pore structure of the capacitor. This energy is not gone – after the capacitor is discharged to 0V and left in open circuit, the ions move back out of the pores and cause the measured voltage to rise again, as discussed in section 2.6.1. Nevertheless, the subsequent discharge showed an apparent capacitance of 642.8F. This means that this charge/discharge cycle had an apparent energy efficiency of 95.3%.

The supercapacitors were also cycled between 1.25V and 2.5V, to examine their behaviour over the range which they would typically experience while in use in a vehicle. For supercapacitor E30, these half-cycle tests found an overall capacitance of 686.3F while charging and 685.5F while discharging. The higher overall capacitance is down to the higher voltages used and the higher interfacial tension that this creates. Note, though, that the relationship of capacitance to voltage did not quite agree with the values found during the full cycles; this discrepancy is shown in Figure 4.8. Capacitance values for this figure are calculated at 1-second intervals, however only selected data points are shown for clarity.

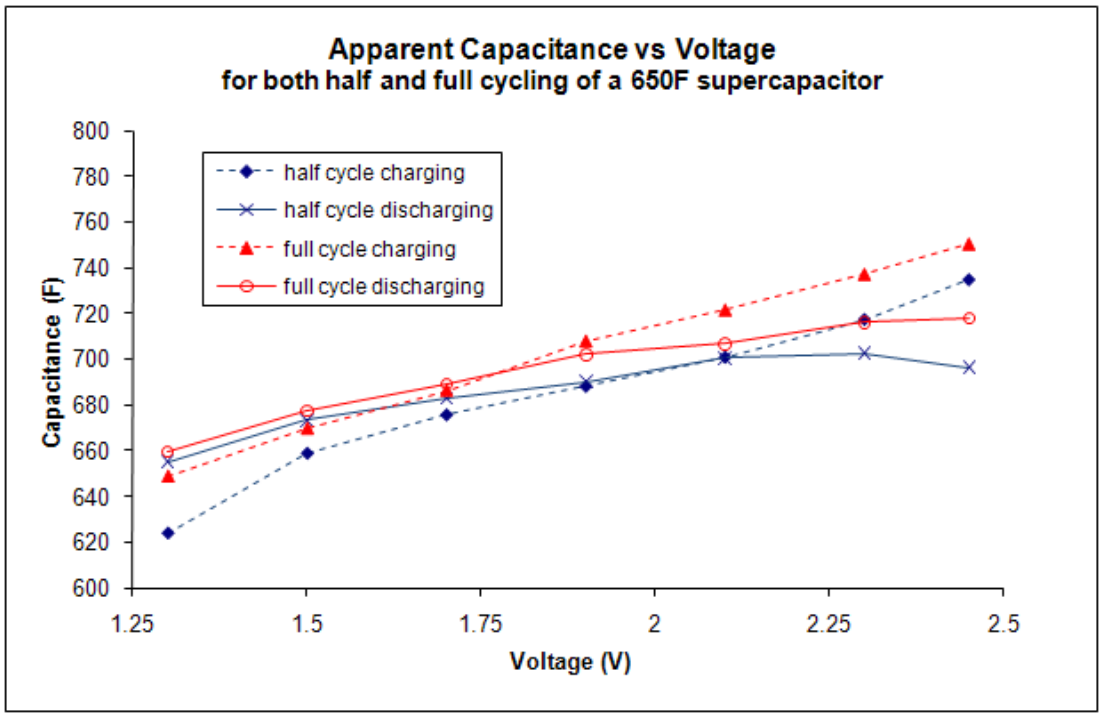

Figure 4.8: Apparent capacitance vs Potential when cycling a single 650F capacitor between 0 and 2.7V (full cycle) and between 1.25 and 2.5V (half cycle).

These tests illustrate the difficulty in creating an accurate model of a supercapacitor. The history of the capacitor makes a noticeable difference to its behaviour – a supercapacitor which has been resting in a discharged state will seem to have a higher capacitance when charged than will a supercapacitor that is undergoing repeated cycles. Furthermore, a capacitor which is cycling over its full voltage range shows different effective capacitance at each voltage than a capacitor cycling over a

part of its range. These variations can lead to a very complex model – but more complexity generally implies a longer processing time for the simulation, and a longer testing time for acquiring parameters. If several sizes of supercapacitors are to be simulated for comparison, then each size would need to be purchased and characterised, increasing costs. Thus the simulations should use the simplest possible model for the supercapacitor which still gives an appropriately accurate result. The battery model, described in Section 3.2, has an error of 3%. Ideally, the supercapacitor model will be no less accurate. To assess this, a drive cycle-like current profile was applied to the capacitors and simulated across a range of supercapacitor models.

4.3.2 Selecting a Model

The test cycle was based on the ECE drive cycle shown in Figure 2.1. This was used to create a current profile for a supercapacitor pack assisting the batteries during this cycle. This profile includes periods of discharging power, when the supercapacitors assist with vehicle acceleration, and periods of recharging when the supercapacitors are either capturing energy from regenerative braking or being recharged by the batteries.

The currents were scaled down by a factor of 60 due to the limitations of the test equipment, and the time was extended by a factor of 2 so that the total energy moving in and out of a single supercapacitor would remain approximately the same as for that supercapacitor as part of a pack of 30 in the actual drive cycle. Time periods in open circuit were not extended for the test cycle. Each capacitor was charged to 2.5V and then left in open circuit for ten minutes before the cycle was applied. This was to broadly imitate the experience of supercapacitors in an electric vehicle, plugged into a charging unit until a few minutes before the vehicle is driven. The voltage of the tested capacitors varied throughout the test from about 1.5V to about 2.5V (with minor variations depending on the individual capacitor chosen) thus experiencing most of its useful range. The current and voltage profile of a sample capacitor are shown in Figure 4.11. The current and voltage were multiplied at one second intervals to create a power profile suitable for use in an ADVISOR-based model for each capacitor.

ADVISOR calculates supercapacitor state of charge as a fraction of peak voltage, not as a fraction of energy. For clarity, this value will be referred to as SOC_V in this thesis, as elsewhere the supercapacitor SOC is treated as a fraction of total energy content, as is the battery SOC. The basic ADVISOR model uses the initial SOC_V of a supercapacitor to find the open circuit voltage, and then uses that, together with the resistance and the requested power, to determine the device current and measured voltage. The current and capacitance are then used to find the new SOC_V for the next step. These steps are performed in a similar fashion to those in the battery model, as:

$$P = V_{meas} I \tag{4-11}$$

and

$$V_{meas} = V_{OC} - IR \tag{4-12}$$

where P (W) is the power, V_{meas} (V) is the voltage measured at the terminals, I (A) is the current, V_{OC} (V) is the open circuit voltage and R (Ω) is the internal resistance. Thus, power can be defined in terms of current as:

$$P = (V_{OC} - IR)I \tag{4-13}$$

For a given power demand, open circuit voltage and resistance, the current can be found using:

$$I = \frac{V_{OC} - \sqrt{V_{OC}^{\,2} - 4RP}}{2R} \tag{4-14}$$

As in the battery model, the alternate solution:

$$I = \frac{V_{OC} + \sqrt{V_{OC}^{\,2} - 4RP}}{2R} \tag{4-15}$$

is neglected because of the higher currents resulting from it. The new supercapacitor SOC_V is found using:

$$V_{OC(n+1)} = V_{OC(n)} - I\frac{\Delta t}{C} \tag{4-16}$$

$$SOC_V = \frac{V_{OC(n+1)} - V_{0\%}}{V_{100\%} - V_{0\%}} \tag{4-17}$$

where Δt is the time step of the simulation, n indicates the time step in question, C is the capacitance, and $V_{0\%}$ and $V_{100\%}$ are the supercapacitor voltages at 0% and 100% SOC, respectively.

If the requested power causes the supercapacitor voltage to exceed set boundaries, then the supercapacitor will supply or sink whatever power it can handle while remaining within the boundaries, and the discrepancy between requested and actual power is noted. This model does not include or account for temperature effects.

The supercapacitor pack model is implemented in Matlab/Simulink, using a discrete, fixed-step solver with a time step of one second. As with the battery model, this enables it to be used in ADVISOR and the author's ADVISOR-based hybrid energy storage system model. The author's modified Matlab/Simulink model is shown in Figure 4.9, with a simplified flow chart representing the model shown in Figure 4.10.

The model has been modified by the author to include varying capacitance values. Four variations of this model were tested. These were:

1) a model using the nominal capacitance of 650F
2) a model with a capacitance varying with voltage, as derived with full cycle tests (the data shown in Figure 4.7)
3) a model using the overall capacitance found in the half cycle tests – in this case, 686F for charging and 685F for discharging
4) a model with a capacitance varying with voltage, as derived with half cycle tests (the half cycle data shown in Figure 4.8).

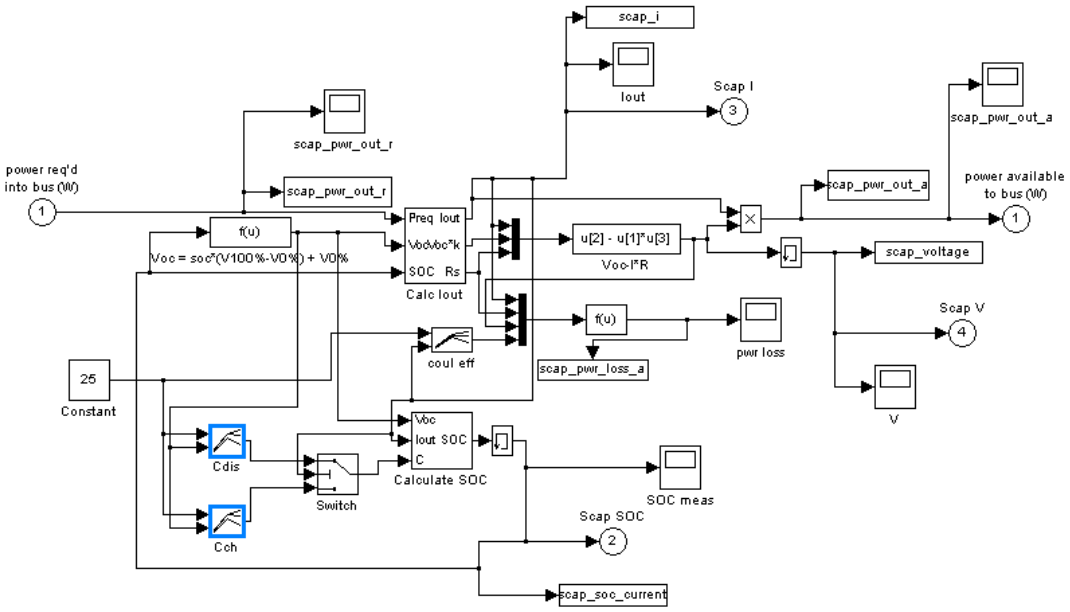

Figure 4.9: The supercapacitor model implemented in Matlab/Simulink. The highlighted blocks indicate alterations made by the author to the basic ADVISOR model.

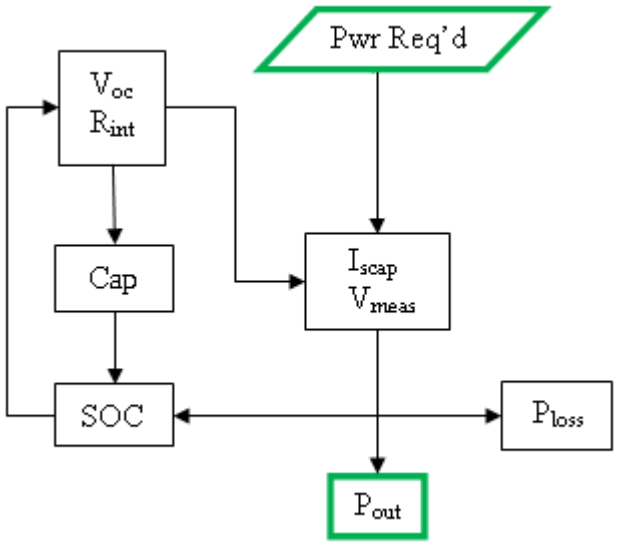

Figure 4.10: A flow chart representing the supercapacitor model.

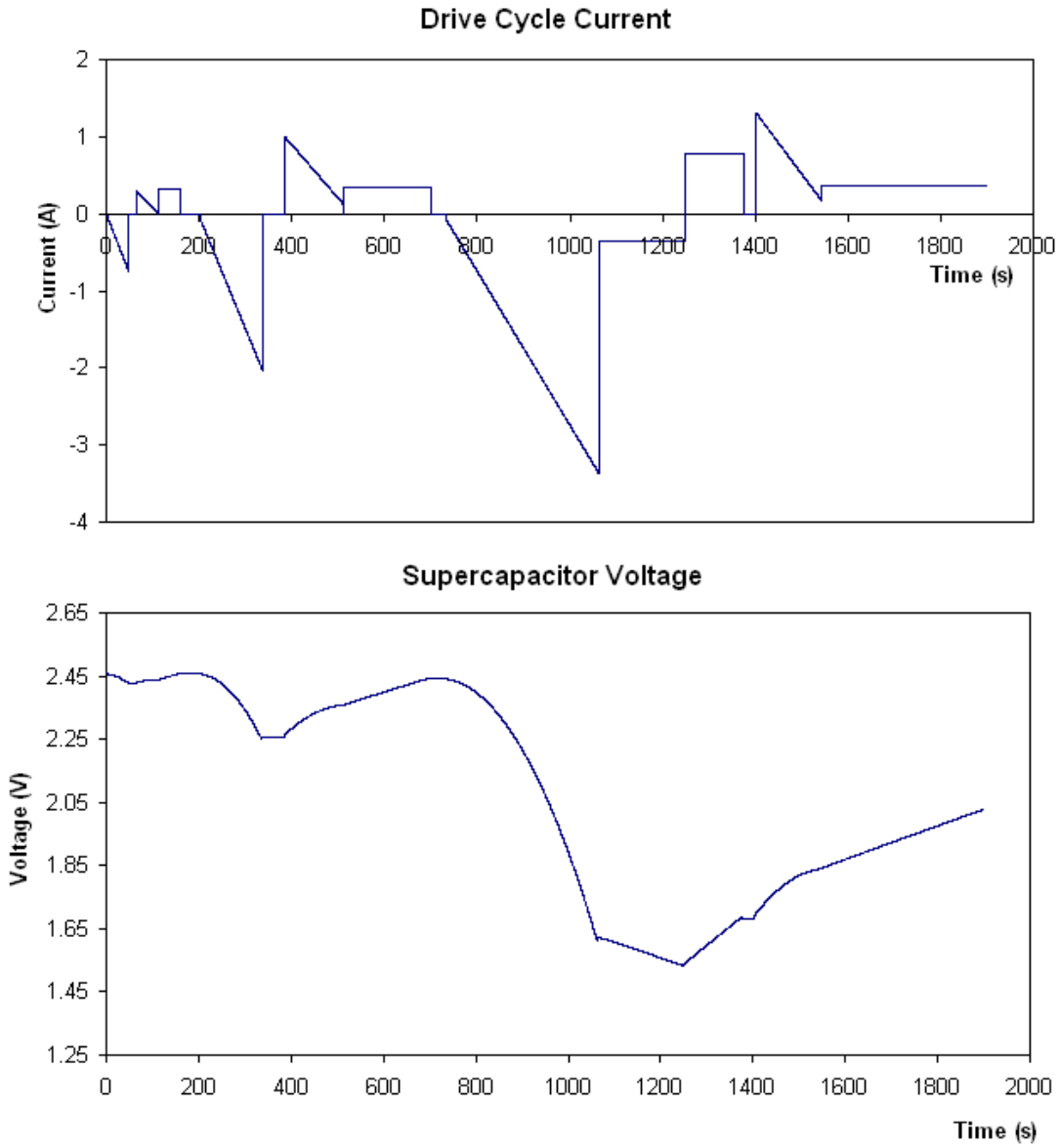

Figure 4.11: The upper plot shows the current profile used to replicate the energy flow that a supercapacitor could experience as part of a battery/supercapacitor vehicle during the ECE cycle. The lower plot shows the voltage of a 650F supercapacitor (E28) subjected to this current. Negative currents indicate discharging, and positive currents indicate charging.

The drive cycle tests were performed with the 1470E potentiostat from Solartron, as described at the beginning of Section 4.3. Each model used a constant resistance based on the potentiostat channel which was used to perform the tests. The test equipment was in use by several researchers, thus the channel chosen was based on availability. Four channels were used at different times, with the average resistance of the cables plus the supercapacitor ranging from 1.4mΩ for channel 3 to 3.3mΩ for channel 1. The resistance was sensitive to cable position: in cases where an

individual supercapacitor was disconnected from the equipment and later reconnected to the same channel for another test, the measured resistance varied by up to 2mΩ. This is much higher than the nominal supercapacitor resistance of 0.8mΩ, therefore the supercapacitor resistance in the final Cobra model was taken as the nominal resistance in all cases.

For supercapacitor E28, used as the example here, each model used a constant resistance of 2.7mΩ for discharging, the average supercapacitor plus cable resistance for channel 6. This was chosen so that the model would conform to the test data, which included the cables in the voltage measurements. E28 was measured by the potentiostat to be at a voltage of 2.456V at the start of the test, giving an SOC_V of 0.9824 from Equation 4-17. The modelled capacitor therefore had an initial SOC_V value of 0.9824 to ensure the starting voltage of the simulation matched the starting voltage of the test. Other individual supercapacitors analysed in this fashion had different values for resistance and starting SOC, appropriate to their starting voltage and test channel used.

The results of these simulations are shown in Figure 4.12. The poorest performing model used the nominal voltage, 650F. This model gave a peak error of 4.6%. The next most inaccurate model used a varying capacitance based on the full cycle tests, resulting in a peak error of 3%. The two half-cycle models performed well, with the constant 685F capacitance model having a peak error of 1.1%, outperforming the varying capacitance model which had a peak error of 2.2%.

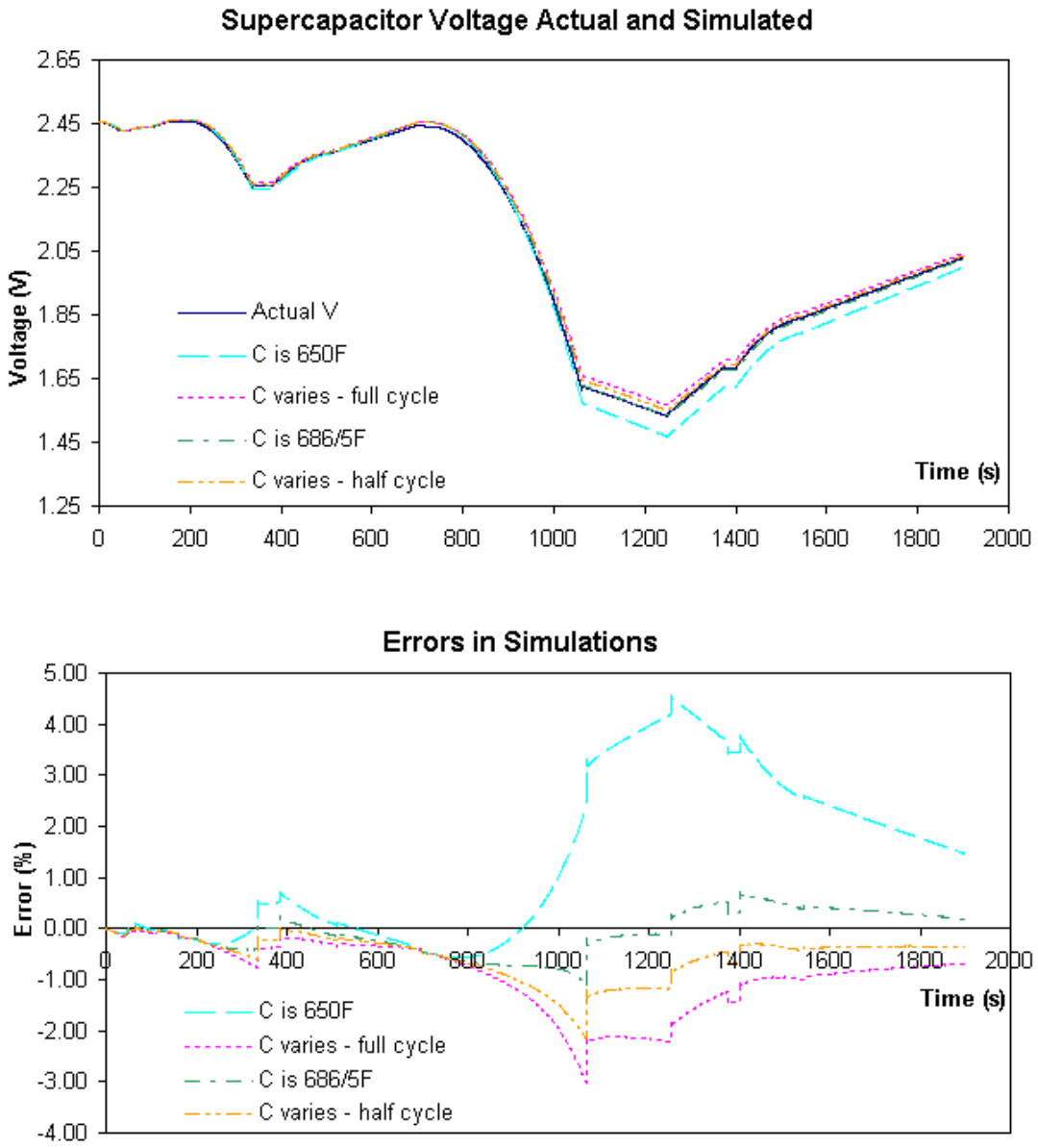

Figure 4.12: The voltage of a 650F supercapacitor (E28) in a drive cycle, and the simulated voltage of the supercapacitor using a variety of models. The lower plot shows the percentage error between the simulated voltage and the actual voltage.

It is worth considering why the model with a varying capacitance gives less accurate results than the model with a constant capacitance. It is clear that supercapacitors really do have a capacitance variation, but the exact nature of this variation depends on both the history of the capacitor and on the chosen cycling profile. Consider Figures 4.7 and 4.8, which show the apparent capacitance of a supercapacitor with respect to voltage during full and half cycle tests. When the supercapacitor first starts discharging, the apparent capacitance is depressed, although it soon rises to match the apparent capacitance when charging. This is due to the pore effects, as

described in Section 2.6.1, which cause the voltage of a freshly charged supercapacitor to drop as the charge is moved into the deep pore structures. If a discharge current is applied, then both effects will be lowering the voltage, creating a lower apparent capacitance.

The full cycle tests have a peak value of 2.7V, so the discharging capacitance around 2.7V is lower than the overall trend would indicate. Similarly, the half cycle tests have a peak value of 2.5V, so the apparent dip in charging capacitance for these tests occurs around 2.5V. A similar, though less dramatic, dip in the capacitance with respect to the overall trend can be seen when the capacitor first starts charging. This is again due to the pore effects, in which charge is moving out of the deep pore structures causing the measured voltage to rise. In both sets of tests this effect occurs at the minimum charging value for the cycle, which is 0V for the full cycle tests, but 1.25V for the half cycle tests. The 'drive cycle' current profile for the supercapacitors features a number of short periods in open circuit, when the supercapacitors are not being used. A charge starting after a period in open circuit will not have the same capacitance to voltage relationship as will a charge that is ongoing, and the same is true for discharges. The model with a varying voltage can never be truly accurate, without the inclusion of these pore effects.

Fortunately, the simple, constant capacitance model gives very good results. This means that the vehicle model need not be over-complicated. Although the nominal capacitance does not give the best results, it still had an error of less than 5% for each tested supercapacitor. This means that if several commercial supercapacitors are to be modelled, one can expect to make a valid comparison of their performance using only the nominal characteristics. It would be better if the capacitance in the upper regions of the capacitor voltage range could be predicted from the nominal capacitance, but unfortunately this is not the case. For the 650F Maxwell capacitors, there is a significant difference between the 2007 series and the 2009 series, although they are officially the same type of capacitor. The average half-cycle capacitance for the set of 2007 capacitors was 624F, while the average for the set of 2009 capacitors was 689F – a difference of 10%.

The supercapacitor pack model is formed from a number of individual supercapacitors in series. When assembled in a vehicle, the individual supercapacitors would be protected from overcharge by an integration kit available from Maxwell. The kit connects the supercapacitors in series with aluminium bus bars, with the addition of active voltage management of adjacent supercapacitors as illustrated in Figure 4.13. The physical construction of the active voltage management bars is proprietary information owned by Maxwell, however it should be noted that they do not interfere with normal charging and discharging of the supercapacitors. Instead, they trigger a discharge of a supercapacitor if its voltage exceeds 2.7V. The active voltage management bars create a maximum leakage current of 50µA at 25°C, rising to 100µA at 50°C. For a pack of thirty supercapacitors the maximum total leakage current would be 1.5mA – well below the margin of error for the data logging equipment (as described in Section 3.1). It is therefore not necessary to add additional resistance due to the charge-balancing electronics.

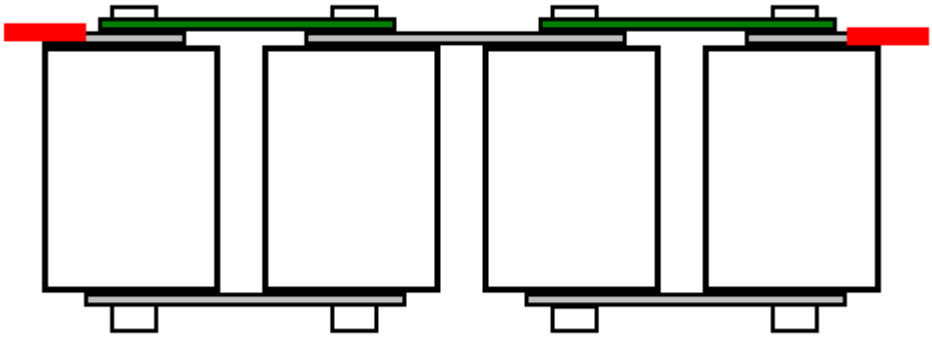

Figure 4.13: A pack of four supercapacitors with aluminium bus bars shown in grey, voltage management bars shown in green, and cables leading away from the pack in red.

4.4 Modelling the Power Electronics

A number of power electronic architectures were described in section 2.4. Of these options, half bridge converters were recommended for use in electric vehicles, due to their efficiency and simplicity, and the fact that they require lower current ratings than other architectures to achieve the same power output [78]. A

battery/supercapacitor vehicle can use either one or two half-bridge converters. If one converter is used, then either the batteries or the supercapacitors will act as the effective DC bus to the motor controller; either option brings its own difficulties. When the battery is used as the bus, it will be subjected to higher and more frequent currents, making it very difficult to optimise the system for increased battery life. When the supercapacitors are used as the bus then they must be kept at a high voltage suitable for supplying power to the motor controller. This means that much of the energy stored in the capacitors will ultimately be inaccessible.

This hybridisation scheme avoids these problems by using two half-bridge converters instead of one. This allows a high degree of control of power flow by making it possible to specify the exact power to come from each individual energy storage system. However, using two converters introduces a new problem: reduced efficiency. Two converters will necessarily result in a greater loss of energy than would occur in a single converter, plus a higher cost and complexity of control. A diagram of the hybrid Cobra's power electronics can be seen in Figure 4.14, with the existing Cobra drivetrain shown for comparison.

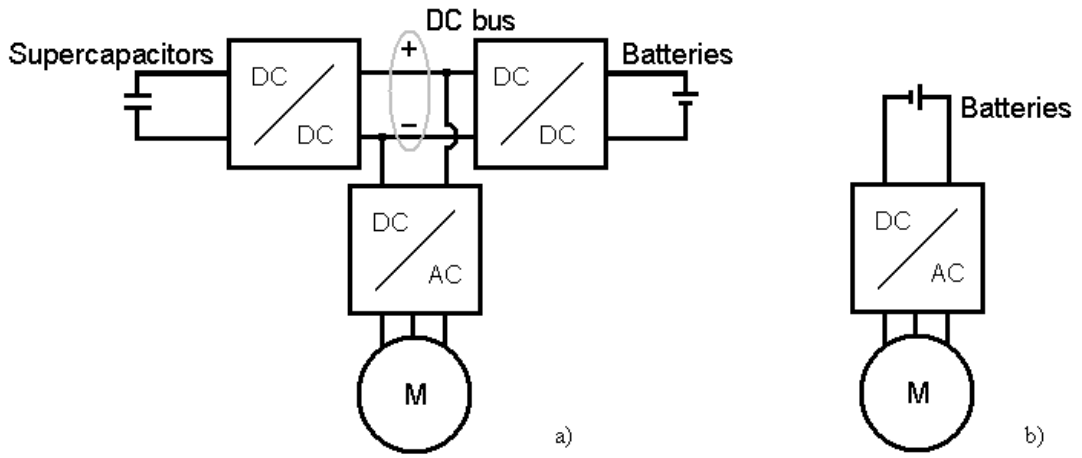

Figure 4.14 a) A schematic of the hybrid Cobra drive train. b) The original Cobra drivetrain.

Two models of the half bridge converters, including the switching behaviour, have been created in Matlab/Simulink – one with a resistive load to model output power, shown in Figure 4.15, and one with a controlled current source to model regenerative braking, shown in Figure 4.16. Each model features battery and supercapacitor

subsystems. The battery subsystem is shown in Figure 4.17 – the supercapacitor version is identically formed but with different values. The model uses a time step size of 10^{-7}s and a discrete, fixed-step solver. This model has been used to size the converter components, based on elements that are commercially available, and to allow a study of the switching control required. It is not used in the full hybrid model, as the high speed switching makes very high demands of the Matlab/Simulink software, which runs out of memory if the converter is modelled for 1 second or longer. Therefore the power electronic converter models have also been used to create efficiency maps for different power demands and SOCs for both the batteries and the supercapacitors. These efficiency maps are then used in the hybrid model to account for power electronics losses.

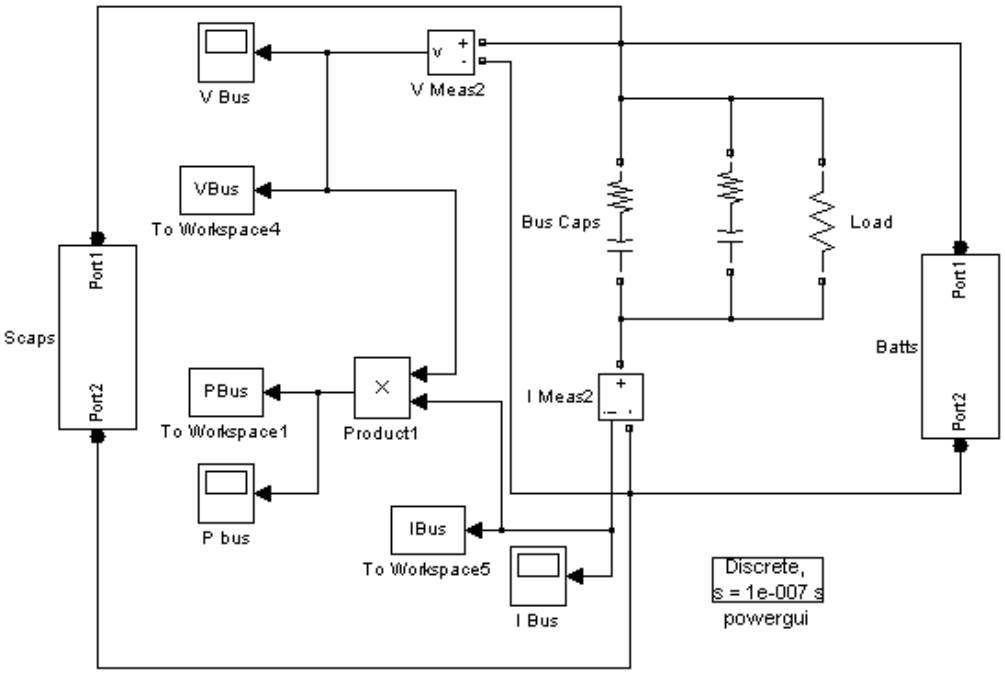

Figure 4.15: The Cobra bus with resistive load, modelled in Simulink. The converter switches are found in both the "Scaps" and "Batts" subsystem blocks.

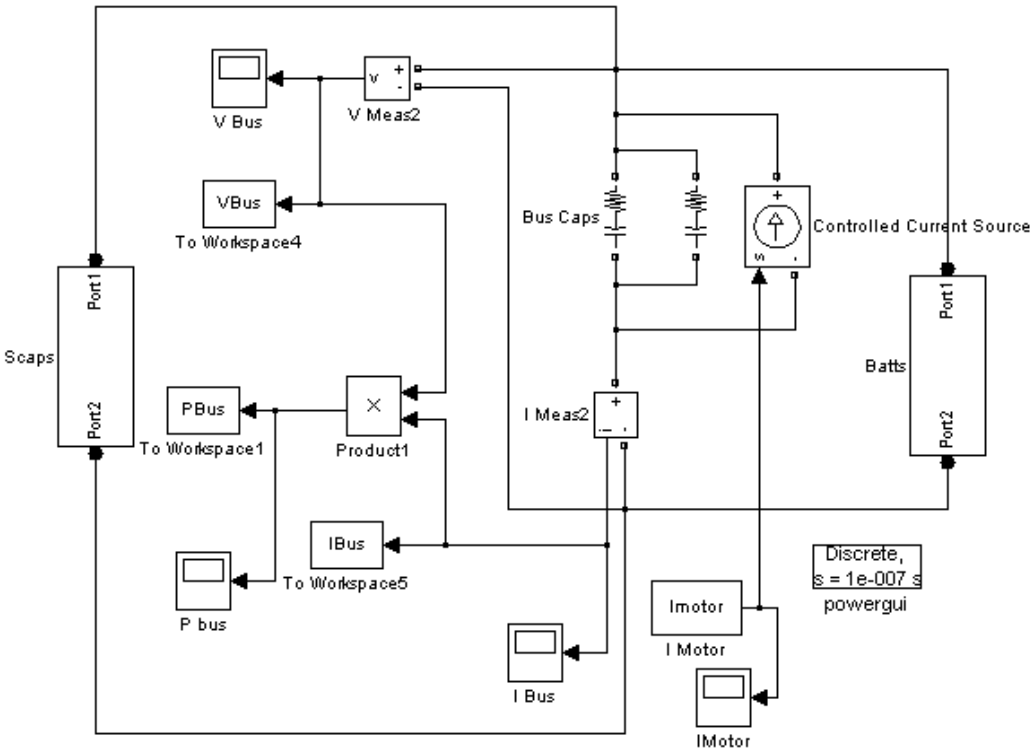

Figure 4.16: The Cobra bus with regenerative braking, modelled in Simulink. The converter switches are found in both the "Scaps" and "Batts" subsystem blocks.

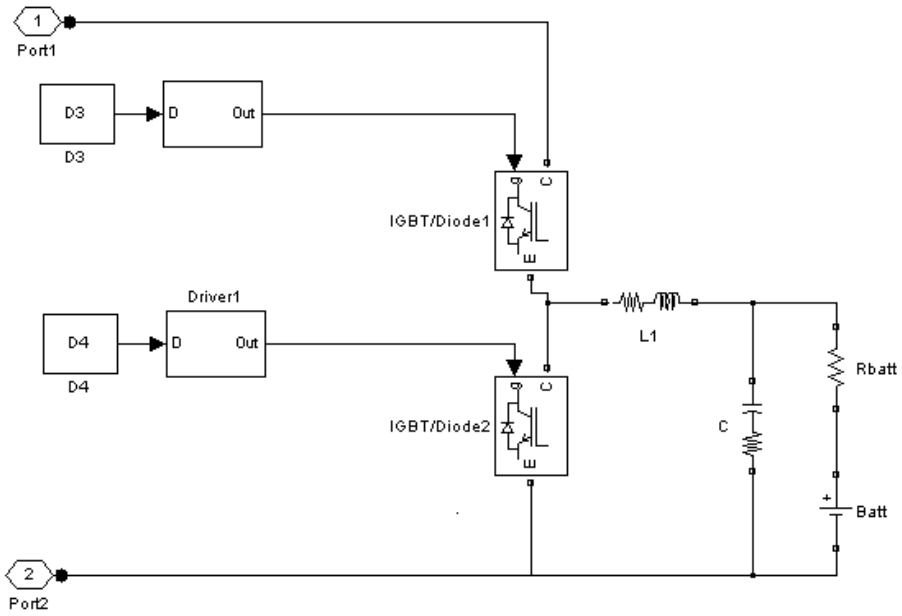

Figure 4.17: The half bridge converter on the battery side. The supercapacitor side is identically formed, with different values for the components. Ports 1 and 2 connect to the battery subsystem block ports in Figures 4.15 and 4.16. Measurement blocks have been removed for clarity.

As battery/supercapacitor hybridisation is a new field, there are no standards in place regarding the voltage and current ripples that should be permitted. Similar vehicles reported in the literature, as described in Section 2.3, have been used as a guideline. The vehicle in [62] used two half bridge converters, permitting a current ripple of up to 2A, which is 1% of the maximum current on the batteries, while for the supercapacitors the current ripple was limited to 1A, or 0.5% of the maximum current. The DC bus voltage ripple was controlled to be less than 2%. However, the vehicle in [51] limited the current ripple in the supercapacitors to 5A - 2.5% of the maximum. This vehicle used a single half bridge converter between the batteries and supercapacitors, and used the batteries as the DC bus.

For the Cobra model shown in Figure 4.14, the DC bus has a nominal voltage of 90V, a value chosen to take advantage of the regeneration power which could be possible with active braking management – up to 9.7kW for the Super Regeneration George Square cycle as described in Section 3.5. The Cobra motor can generate a current of no more than $110A_{RMS}$, so the chosen bus voltage allows the full power to be regenerated. It also ensures that the Cobra batteries may be charged without voltage becoming a limiting factor – bearing in mind that the battery pack has a voltage of 77.4 V when fully charged, and has a manufacturer-approved maximum voltage of 90V when charging [40]. The Cobra model DC bus is controlled to have no more than a 3% voltage ripple; ensuring a smaller voltage ripple would require additional bus capacitors and hence increased costs, as no electrolytic capacitors with sufficient voltage capability and capacitance higher than 15mF were found to be commercially available. Finally, the batteries and supercapacitors are limited to a current ripple of 2.5A - 1% of the maximum. This was chosen to match the battery current ripple tolerance of the vehicle in [62]. The electronics have been chosen to carry a current of up to 250A, as this is the peak current possible in the battery-only Cobra.

It is important to note that the converter could not be optimised for a specific supercapacitor pack, as several packs have been modelled using a variety of commercially available and theoretical types of supercapacitor. This allows a full,

model-based exploration of the possibilities of battery/supercapacitor hybridisation. For a production car with a determined supercapacitor pack, further optimisation of the power electronics would be possible. For this purpose, it is important to get a sense of what equipment would be required, its cost and efficiencies.

The components of the converters have been chosen to be inexpensive, as appropriate given the low cost of the Cobra itself. A number of appropriately priced, commercially available components were simulated using the models shown in Figures 4.15, 4.16 and 4.17, given a range of motor power demands (including regenerated power) and energy storage SOCs. The voltage and current ripples occurring at each power and SOC were determined via these simulations, and the components were sized to ensure that these values were within the specifications described above. Based on this work, appropriate components were selected, and these are described in Table 4.2.

Table 4.2: The DC/DC Converter Components

Item	Size	Weight	Cost
DC Bus Electrolytic Capacitor	2x15mF, 200V capacitors in parallel	1kg	£82 each* [157]
Battery Electrolytic Smoothing Capacitor	4700µF, 200V	0.48kg	£30.55 [158]
S-Cap Electrolytic Smoothing Capacitor	4700µF, 200V	0.48kg	£30.55 [158]
Switches	600V, 300A IGBTs	~0.15kg	£80.37 for two [159]
Battery Inductor	180µH, 300A air core inductor	~4.2kg	~£190 total [160]
Supercapacitor Inductor	300µH, 300A air core inductor	~3.5kg	

Unlike the other components, no suitable inductor of the required inductance and current/voltage rating can be found in mass production. The experimental battery/supercapacitor vehicles that have been built in the past have used bespoke inductors, created in-house [51, 56, 62]. For this model, an inductor similar to that in

* This capacitor is currently available only for mass orders. As the costs of the other items are given for small quantities, an equivalent small quantities cost was estimated based on the costs of similar capacitors from Farnell.

the Cranfield vehicle [62] has been used. Their inductor was created using 70 turns of flat enamelled copper wire with a cross-section of 16mm^2 around an air core, with a peak current capability of 300A, an inductance of 392μH, and a weight of 4.8kg. Inductance is proportional to the square of the number of turns [161], so to achieve 300μH with the same design, 60 turns of wire should be used, while 180μH would need 47 turns. Assuming the Cranfield inductor wire weighed 4kg (83% of the total weight), then the wire for the 300μH and 180μH inductors would weigh 3.4kg and 2.7kg respectively. This quantity of wire would cost about £190 in total from Planet Engineers [160]. So far the power electronics would cost £495.47 and weigh 9.81kg, not including the cables, heat sinks, fans and controller that would be needed to put it into operation.

This Matlab/Simulink power electronic model is not suitable for use in the full battery/supercapacitor hybrid model, as simulating the switching operation is too processor and memory-intensive to model for longer than a fraction of a second. For the full vehicle model the power electronics were therefore modelled using an efficiency map. This map gives the efficiency of the power electronics with respect to power flow and SOC for both batteries and supercapacitors, and was created using the same Simulink model used to size the power electronics components. The maps can be seen in Figure 4.18. Some power demands cannot be met, especially at lower states of charge, e.g. the supercapacitors cannot deliver a power ≥10kW if their SOC is below 60%, due to the high currents reducing the measured voltage of the energy storage system in question. This creates a physical limit to the power output, and these regions are left out of the efficiency maps. The half bridge converters have an efficiency that is typically >90% when the energy storage elements have a high SOC and the power output is low. The efficiency decreases as the power output increases and as the SOC of the elements decreases.

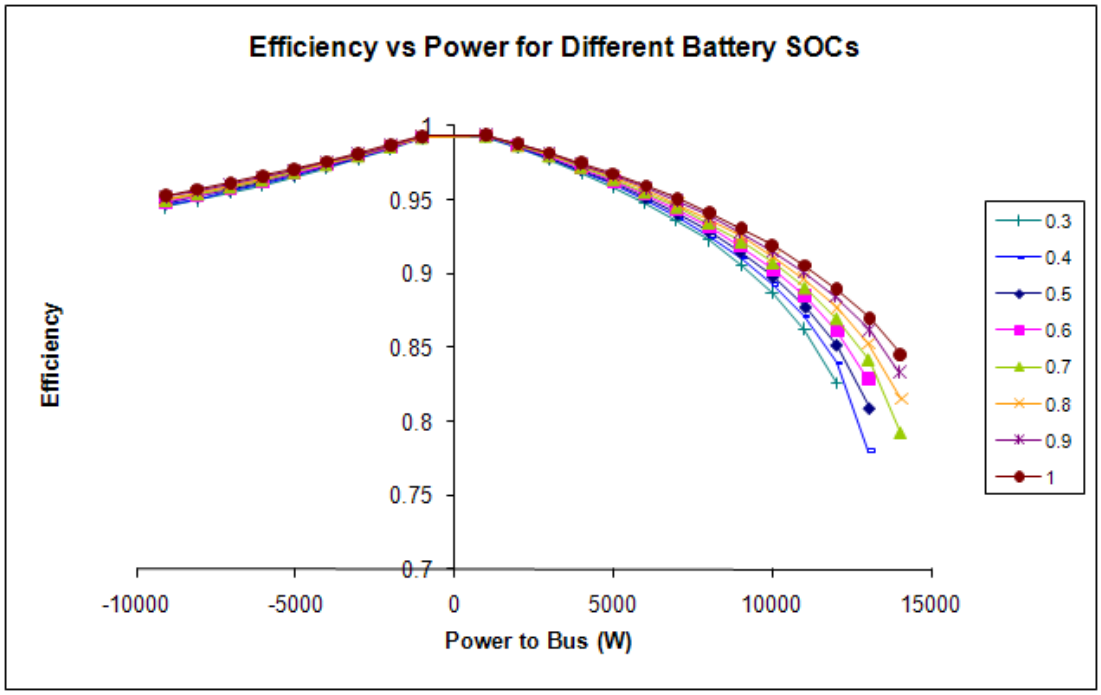

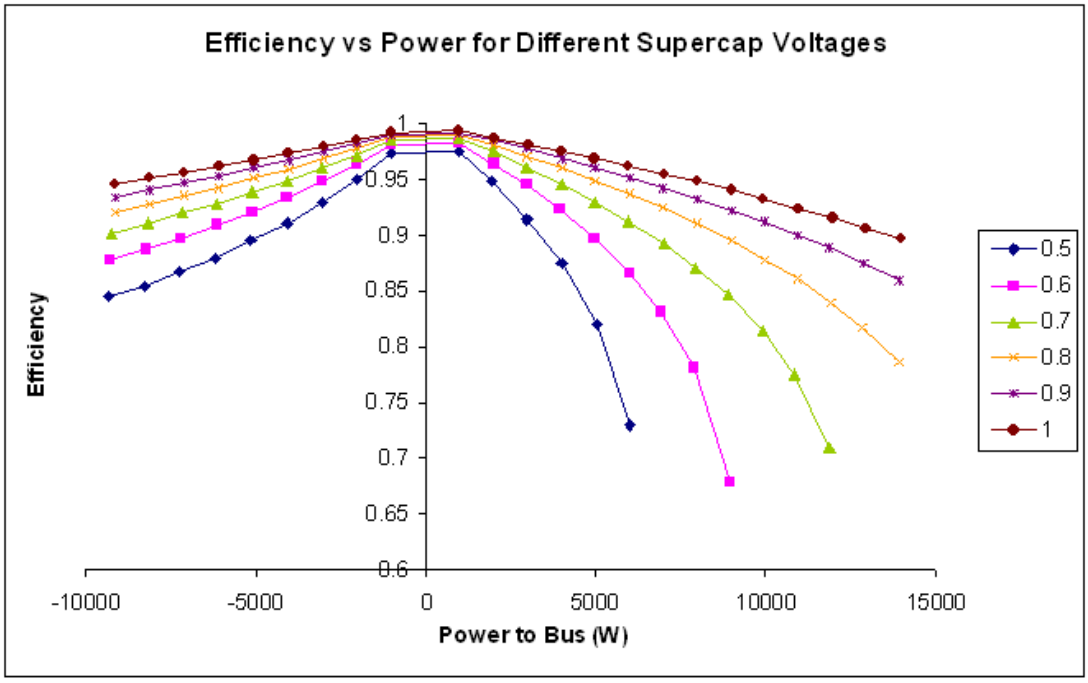

Figure 4.18 Half bridge converter efficiency maps used in the hybrid Cobra model. Negative power indicates that the converter is being used in 'boost' mode to charge the energy storage device, while a positive power is drawn from the energy storage to the motor in 'buck' mode. The supercapacitor pack is considered at different fractions of their peak voltage, as this is the method used by ADVISOR.

4.5 The Hybrid Energy Storage Model

The battery, supercapacitor and power electronics models were subsequently combined by the author to form the complete energy storage system model for the

battery/supercapacitor Cobra. This model was then used to test different control strategies, described in the next section.

The hybrid model is shown in Figure 4.19, and like its component models it is based in Matlab/Simulink, using the discrete fixed-step solver with a time step of 1 second. It uses the power and speed information for a given drive cycle, in one second increments, as the input data for simulation. In Figure 4.19, these are shown as the blocks 'PReq' and 'Speed', respectively. (In the full version of ADVISOR, power required would be calculated in previous blocks based on the vehicle mass, air resistance, wheel type, and motor efficiency, whereas this model uses the actual power recorded from the Cobra.) This information is delivered to the 'Power Routing' block which determines what part of the power demand will be met by the batteries and what part by the supercapacitors, based on the specific control strategy being studied. The Power Routing block also calculates the losses which occur in the power electronics.

The power request for the batteries is then sent to a 'Batteries' block, which contains the battery model described in Section 3.2 and shown in Figure 3.26. Likewise, the power request for the supercapacitors is sent to a 'Supercapacitors' block which contains the supercapacitor model described in Section 4.3 and shown in Figure 4.9. These then output their voltage, current, power and SOC information, the latter of which is returned to the Power Routing block to be used in directing the power flow for the next time step. The total power delivered by the supercapacitors and batteries is output at port Pout – this information is used in this model simply to compare actual power to requested power. If used inside ADVISOR, this information would be used to track power flow through the remainder of the vehicle.

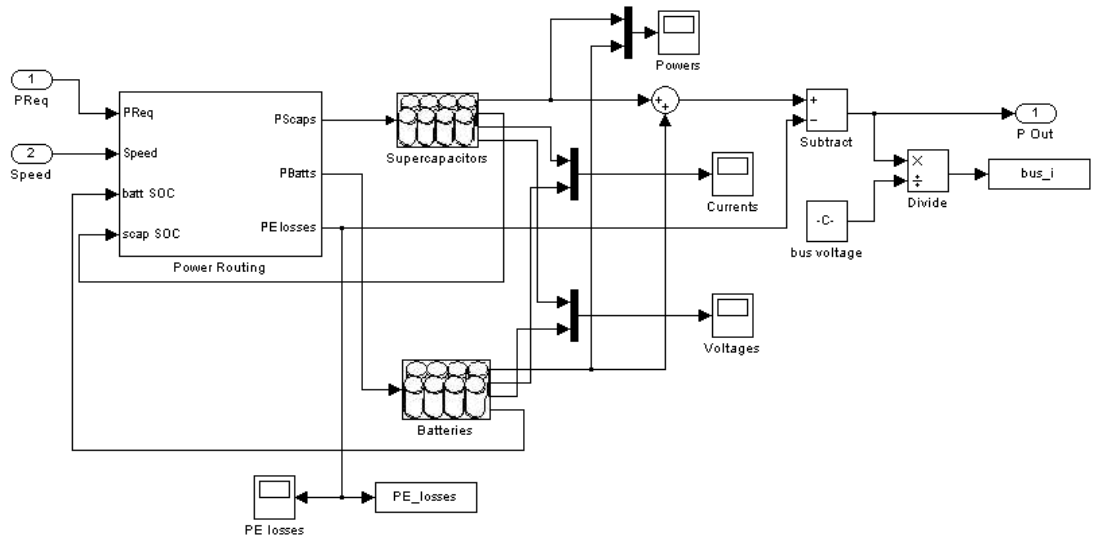

Figure 4.19: The hybrid battery/supercapacitor model in Simulink.

The battery and supercapacitor blocks each deliver their updated SOC status which is returned to the Power Routing block to be used in calculating the power flow for the next time step. They also record the voltage and current information for these systems, and the power that will be delivered to the bus (which may be less than the requested power if the energy storage devices do not have sufficient SOC to meet the demand). The power information is monitored to assess the performance of the hybrid system – if used in ADVISOR then the power information would be delivered to the motor simulation block and thence to the model of the full vehicle. The power losses in the batteries and supercapacitors are recorded; adding these together gives the total energy losses throughout the drive cycle, allowing the efficiency of the overall energy storage system to be monitored.

The control strategy is implemented inside the power routing block. This block is illustrated in Figure 4.20. In the power routing block, the battery and supercapacitor SOCs are used to calculate the peak power demand that they can supply without dropping below 48V for the batteries or below 37.5V for the supercapacitors. Similarly the charging power is limited to ensure that the supercapacitors are not charged above 75V, nor the batteries above 90V. The batteries' charging current is further limited to 55A, as this is the peak charging current delivered from the EnerSys-Hawker battery charger. This ensures that the batteries do not receive

damaging currents. This block also limits the power based on the capabilities of the motor.

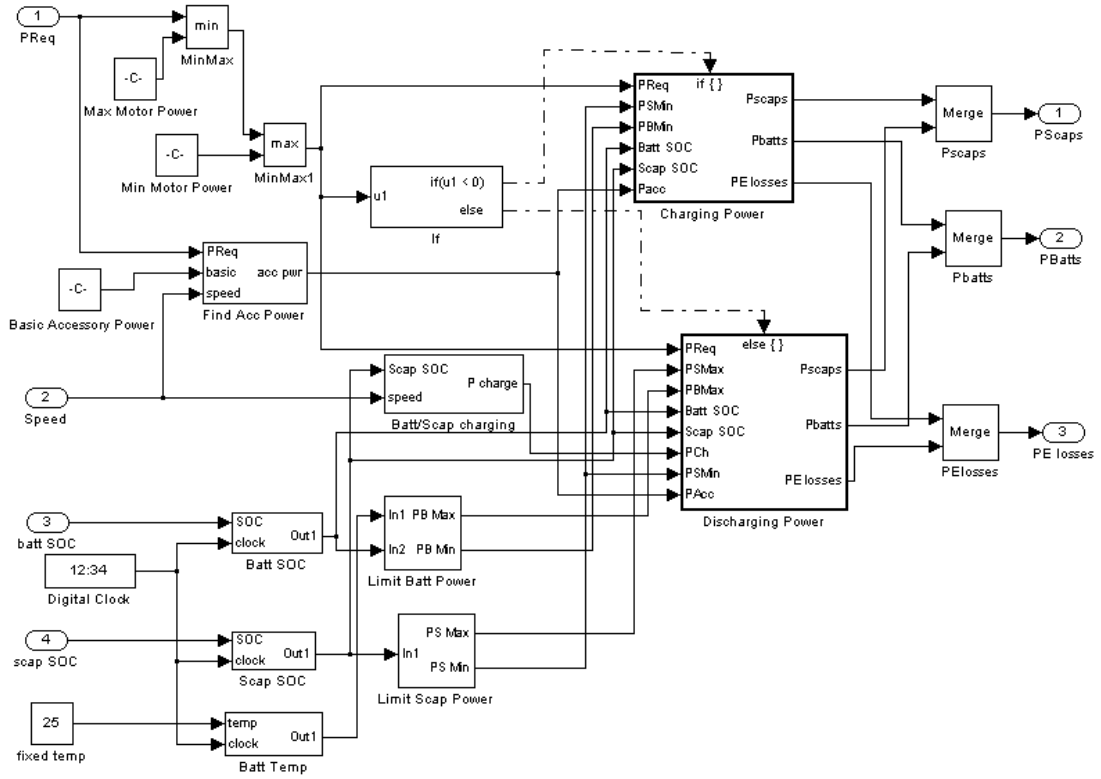

Figure 4.20: Inside the 'Power Routing' block for the author's hybrid batter/supercapacitor model in Simulink. Measurement blocks have been removed for clarity.

The accessory power is also calculated in this block. The accessory power refers to any power demanded by the Cobra for a purpose other than traction: for example the headlights, turn signals and motor cooling fan. The typical accessory demand for the Cobra is 140W and any time the Cobra is moving it is assumed that this 140W draw is being taken directly from the batteries, and is not delivered via the hybridising power electronics. When the Cobra is stationary, the power actually recorded during the drive cycle is assumed to be equal to the accessory demand, and this is drawn from the batteries in place of the standard 140W value. The real accessory power varied from 13W when the inverter cooling fan was off to 275W with the fan working extra following an incident of overheating.

The power routing block is further subdivided into two blocks, one for Charging Power and one for Discharging Power. These blocks assign the power flow to some combination of the batteries and supercapacitors, as described in next section. These blocks also calculate the losses in the power electronics, as defined in the efficiency maps of Figure 4.18. The next section discusses the control strategy that was developed by the author and implemented in the hybrid model.

4.5.1 Control Strategy

Control of the power delivery in the vehicle involves two main elements. First, when power is demanded of the energy storage system the control strategy must determine what portion of the power will come from the batteries and what portion will come from the supercapacitors. This element also determines what happens to power delivered to the hybrid energy storage system during regenerative braking. Second, the control strategy must determine when and how fast the batteries should charge the supercapacitors. This element describes the energy management of the hybrid system. A complete control strategy therefore consists of a power flow management strategy (PFMS) and a supercapacitor management strategy (SMS).

The strategy that has been devised for the Cobra is a tuneable strategy which can be adjusted to optimise for different factors. To get the best results it must be optimised for each drive cycle. The optimisation and development of generic strategies is discussed more fully in sections 5.1.3 and 5.2.3.

The control strategy is useful for assessing different optimisations with a range of supercapacitors and drive cycles. Recall that the different optimisations investigated are: maximising efficiency and minimising peak currents in the batteries, with vehicle performance and cost also considered as factors. By optimising for each situation, the following questions may be answered:

1) Does the quantity of energy available from regenerative braking affect the optimal strategies?
2) Does the size of the supercapacitor pack affect the optimal strategies?
3) Do different optimisations lead to the same strategy, or are the strategies in conflict?

A diagram of the control strategy is shown in Figure 4.21.

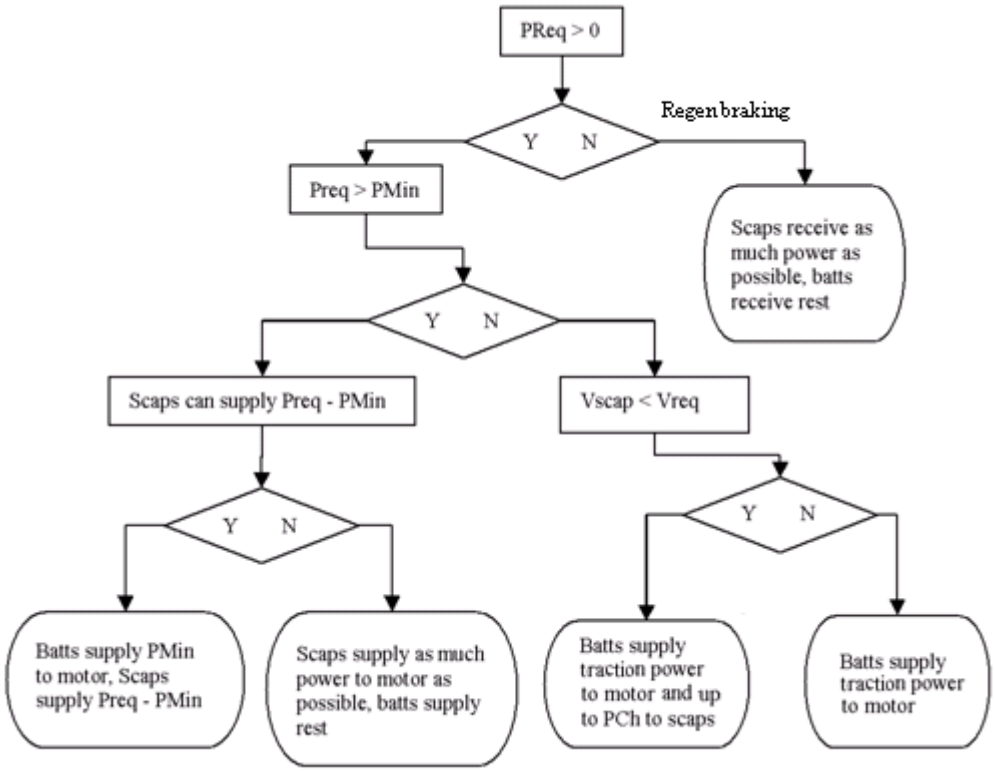

Figure 4.21 Flowchart showing the control strategy for a requested power PReq from the energy storage system. PMin is the minimum power sent by the batteries to the motor, Vscap is the actual supercapacitor voltage, Vreq is the required supercapacitor voltage (based on vehicle speed), and PCh is the charging power sent from the batteries to the supercapacitors.

The strategy specifies two values which can be adjusted to achieve different optimisations. The first value describes the contribution of the batteries to the vehicle power demands. When a request for power, PReq, is made of the energy storage system, the power flow management strategy dictates that a certain minimum power, PMin, should be withdrawn from the batteries. Any remaining power is supplied by the supercapacitors if possible, with the constraint that the supercapacitor voltage is prohibited from dropping below 50% of the maximum. If the full power cannot be supplied by the supercapacitors then the remainder is supplied by the batteries. For example, if the motor demands 10kW and PMin is equal to 4kW, then the batteries will supply 4kW and the supercapacitors will supply 6kW, even if the supercapacitors could supply more. However, if the supercapacitors can only supply

3kW due to a low state of charge (SOC), then the batteries will supply 7kW. The battery power may also be limited by the batteries' SOC. If it is not possible for the batteries and supercapacitors together to supply the power requested, then they will supply as much power as they can and the shortfall is registered. A failure to meet a power demand signifies a drop in the performance capability of the vehicle. Different values of PMin were tested, ranging from 0 to 11.6kW. The peak power required by the drive cycles was 11.5kW, so when PMin was at the maximum tested value, the supercapacitors were not used at all.

The second value is defined by the supercapacitor management strategy is a charging power, PCh, to be sent from the batteries to the supercapacitors. A voltage Vreq was defined for the supercapacitors and related to the speed (mph) of the vehicle, such that:

$$V_{req} = V_{\max} * \sqrt{1 - speed * 3/160}\,. \qquad (4\text{-}18)$$

$V_{\max}$ is 2.5V for the individual supercapacitors, or 75V for a pack of thirty. This relationship was chosen to set the supercapacitor voltage to its minimum value (50% of the maximum) at 40mph, as this is the top speed that the Cobra is expected to reach. The supercapacitor voltage was also set to be at a maximum when the Cobra was stopped. This equation is broadly similar to the relationship between supercapacitor voltage and speed given for the vehicle in [52] and gives good results for efficiency and battery current. By keeping a lower state of charge at higher speeds, the supercapacitors are generally able to receive more energy from regenerative braking. Conversely, at lower speeds the supercapacitors have a high state of charge, ready to provide a high burst of power to accelerate the vehicle.

If the supercapacitor voltage falls below that prescribed by the SMS, then the battery sends a charging power of no more than PCh to the supercapacitors, with the actual value depending on whether the batteries were also required to send power to the motor at that time. The tested values of PCh ranged from 0 to 4kW, where a PCh of 0 meant that the supercapacitors were recharged only via regenerative braking.

Finally, during regenerative braking all power is delivered to the supercapacitors up to full supercapacitor SOC, and any excess power is delivered to the batteries. If this would exceed the batteries' ability to accept a charging current, then the power is not captured and it is assumed that friction brakes are used to slow the car. This is indicated in Figure 4.21 as the case where PReq < 0.

By testing the strategy over a wide range of urban drive cycles, and by altering the values of PCh and PMin, different optimisations could be achieved. The most efficient strategy for each drive cycle was identified and so was the strategy which led to the lowest peak battery currents. In each case the initial supercapacitor SOC was 100%. The initial battery SOC was tested at 100%, 80% and 50%.

4.5.2 Supercapacitor Packs

A range of supercapacitors from two companies were considered for the tests. The capacitors from Nippon Chemi-con were not included as they are much more expensive and have a higher DC ESR than equivalent supercapacitors from other companies – see Section 4.1 for details. The supercapacitors used in the models are available from Maxwell and from Ness, and represent a sample of the available products from the two companies. The chosen supercapacitors are detailed in Table 4.3. Each capacitor has a peak voltage of 2.7V.

Table 4.3: Properties of different commercially available supercapacitors

Company	Cap. (F)	Unit Cost* (£)	ESR (mΩ)	Weight (kg)	Volume (l)
Maxwell	650	22.01	0.8	0.2	0.211
Maxwell	2600	49.50	0.31	0.46	0.439
Maxwell	3000	56.73	0.29	0.55	0.475
Ness	600	31.50	0.83	0.21	0.324
Ness	1700	42.50	0.65	0.385	0.594
Ness	3500	66.50	0.36	0.685	0.594
Ness	5000	86.00	0.33	0.93	0.594

* Cost information from 2007-2008.

At this point it is appropriate to comment on the effects of mass. The addition of a pack of supercapacitors and associated electronics will increase the mass of the vehicle. The weight of the hybrid system will vary depending on the size of the supercapacitors chosen. The capacitors themselves range from 0.2kg to 0.93kg – for a pack of thirty, this gives a pack weight of between 6 and 27.9kg. Additionally, the power electronics are expected to weigh approximately 10kg. Hybrid vehicles in the literature typically compare the hybrid performance and battery-only performance of their vehicles with the mass kept constant – the battery-only vehicle either contains the supercapacitors but has them disconnected [62] or carries sandbags [59] or an additional passenger [51] with an equivalent weight to the supercapacitors and electronics. In this case the Cobra was tested with an additional weight of 22kg, in the form of an empty hydrogen tank. This gives a mid-range weight for a supercapacitor pack, similar to a pack consisting of thirty 1700F or 2600F supercapacitors and their electronics. However, simulations in the full version of ADVISOR revealed that the weight difference does not substantially affect the performance of the vehicle, since the percentage difference is very small. The addition of 30kg of weight to the battery-only Cobra changes the total energy output by less than 1.5%, and peak output and regeneration powers by less than 300W.

4.6 Chapter Summary

Sizing a supercapacitor pack for a battery/supercapacitor hybrid vehicle requires consideration of both the physical constraints of the vehicle and the desired effect of the hybridisation. Physical constraints include the existing battery pack and motor capabilities, and the physical space available in which to place the additional components.

The hybridisation scheme could be geared towards maximising efficiency, in which case a relatively small supercapacitor pack could be added to take advantage of the energy available through regenerative braking while minimising cost. As shown in Table 4.1, given a pack of thirty supercapacitors then each individual supercapacitor would need an individual capacitance of 175-1475F to serve this purpose. However, as shown in Figure 4.1, lower capacitance corresponds to a higher resistance, which would reduce the efficiency of the pack. The trade-off between these aspects is

investigated with simulations of the hybrid system and described in the following chapter.

If the focus is on minimising battery currents, then a large supercapacitor pack may be used to permit the batteries to output only the average power – from Table 4.1, the individual capacitors may be 2051-2211F for the ECE-15 based cycles, or 4017-4691F for the George Square cycles. However, optimal results for battery current minimisation require perfect knowledge of the drive cycle, which is not realistic. Furthermore, a large supercapacitor pack would be very expensive - £1485 for thirty 2600F capacitors or £2580 for thirty 5000F capacitors. The benefits of using smaller supercapacitor packs for battery current minimisation are explored using the hybrid system model and are also described in the following chapter.

A model of the Cobra with both batteries and supercapacitors has been created to assess the benefits of the different optimisations schemes. A range of options have been proposed involving different pack sizes and voltages, and the author's model is therefore flexible and modular to accommodate this.

A number of 650F power type supercapacitors from Maxwell were tested and characterised to form a supercapacitor model. The most accurate supercapacitor model for a drive cycle-like current profile, with an error of less than 1.5%, was found to be one using a fixed value for the capacitance and resistance, characterised using tests over the 1.25V-2.5V per cell range. This is the typical cell voltage range which would be experienced by the supercapacitors in an electric vehicle, making it more suitable for parameter extraction than tests which use the full voltage range of the supercapacitors. Testing also proved that a model created from the nominal voltage and current gave adequate results, with an error of no more than 5%. This shows that different commercially available supercapacitors can be modelled using the nameplate details without needing to purchase and characterise each one.

The integrating power electronics consist of two half bridge converters; these were simulated in the hybrid model using efficiency maps, which in turn were found by

modelling the converters in detail in Matlab/Simulink for a range of power demands to and from the supercapacitors and the batteries over a range of states of charge. The converter model data was extracted from the nominal values for commercially available power semiconductor switches and capacitors, while the parameters for the air core inductors were determined using an analysis of the amount of copper required as the inductor material. Commercially available high current inductors are only produced by a few specialised companies and within a limited range of inductance values. Therefore suitable inductors would ultimately need to be constructed in-house.

The supercapacitor and power electronics models described in this chapter were combined with the battery model from section 3.2 to create a novel hybrid energy storage system model. This model was developed to simulate the behaviour of the battery/supercapacitor hybrid Cobra over the seven previously defined drive cycles using a novel, rule-based control strategy which may be tuned to different optimisations.

The control strategy used two variables for tuning. The first, PMin, defines the minimum power demand for which the supercapacitors would be used. Any discharging power with a value lower than PMin would be provided solely by the batteries. This was tested over a range of values of Pmin from 0 to11.6kW. The second tuneable variable was PCh, the power at which the batteries would charge the supercapacitors. The supercapacitors were controlled to maintain a specified voltage which was related to the speed of the vehicle using Equation 4-18. Any time the supercapacitors fell below the required voltage for a given time step, the batteries would send a charging power of no more than PCh. The charging power would be lower if the batteries were also supplying a traction power demand at the time such that PCh plus the traction power would exceed the batteries capabilities.

Using this control strategy, seven commercially available supercapacitors from two different companies were chosen for simulation in packs of thirty for each of the

defined drive cycles. These results of these simulations are described in detail in the following chapter.

5 Comparing the Optimisation Schemes

Two potential optimisation schemes have been proposed in this thesis for use in a battery/supercapacitor hybrid Cobra. The first is to maximise the overall efficiency of the vehicle, thereby increasing the range. The second is to minimise the peak currents in the battery pack, with the goal of extending their lifespan. Chapters 3 and 4 described the development of the Cobra model used in this investigation, while Section 4.5.1 discussed the tuneable control strategy which will direct the power flow between the energy storage elements. The optimisation schemes also consider the impact of supercapacitor size and cost, considering seven different commercially available supercapacitors. The simulation results can then be used to identify the optimal pack size for the different optimisation strategies.

Two speed cycles have been chosen to compare the relative efficacy of the different strategies. The first cycle is four repetitions of the ECE-15 cycle, which was originally depicted over one cycle in Figure 2.1, with the four repetition variant shown in Figure 3.48. The ECE-15 cycle is a standard test cycle widely used throughout Europe to assess the performance of electric and ICE vehicles. It is therefore ideal for acting as a performance baseline and for comparing results to other vehicles. The drawback to this cycle is that it is not a driving pattern that would typically be seen in real life. The acceleration and deceleration rates are both slower than would be found in a typical drive, and the repetitive pattern could not be replicated in any road situation, which constantly changes due to the presence of traffic signals, other vehicles, pedestrians and so forth. Therefore, a second cycle will be used to provide a real-life driving scenario. This was formed from four separate trips around George Square in the Cobra, performed on July 22, 2009 and on August 4, 2009. The four trips have been joined into a single drive cycle for modelling purposes. Each of the two cycles was studied including a range of regeneration possibilities, representing the amount of energy which could be recovered during braking. The power and speed profiles for the cycles are shown in Section 3.5.

The base results for these cycles are the performance of the Cobra when using its six original batteries with an initial SOC of 100%, and without any assistance from the supercapacitors. This has been simulated with the model described in Section 3.2. Table 5.1 shows the yield and peak battery current for each of these cycles. In each case, the batteries were able to provide the power necessary to complete the cycle. However, in some cycles they were not able to accept all of the regeneration energy that was available, as the charging power was too high. As an example, Figure 5.1 shows the power requested and supplied for the George Square Super Regeneration cycle. The dashed line indicates regeneration power available to the vehicle, while the solid line shows the actual power into and out of the batteries. The charging current is limited to -55A to prevent damage to the batteries, leaving some regeneration power going to waste.

The chosen drive cycles have total discharge energies of 0.52 to 0.61kWh, representing no more than 12% of the total energy stored in the standard battery pack. In order to evaluate the effects that lower battery states of charge might have in making hybridisation more or less effective, the cycles were also modelled with battery initial SOCs of 80% and 50%.

In order to assess the efficacy of the hybridisations, two additional models of the battery-only Cobra have been created. The first adds an additional battery, bringing the pack size to seven batteries and a nominal operating voltage of 84V. The second adds yet another battery, bringing the nominal operating voltage to 96V – bearing in mind that the Cobra motor can accept an input voltage of up to 400V. This allows the battery/supercapacitor hybrid to be compared to simpler and cheaper modifications to the Cobra. If the vehicle with the addition of one or two batteries outperforms the vehicle with added supercapacitors, then the supercapacitors are clearly not a sensible option. These were also modelled across a range of different initial SOCs. Each battery weighs 24kg, approximately equivalent to adding a supercapacitor pack containing 35 of the Ness 3500F supercapacitors, or 26 of the Ness 5000F supercapacitors.

Table 5.1: The base case results: characteristics of the drive cycles as driven by the battery-only Cobra, using a standard pack of 6 batteries with an initial SOC of 100%.

Cycle	Regeneration	Yield (km/kWh)	Maximum Battery Current (A)	Missed Regen. Energy (J)
ECE-15	Medium	7.01	176	0
	High	7.16	176	0
	Super	8.77	179	6119
George Square	Low	5.69	178	0
	Medium	5.87	177	0
	High	6.09	177	5335
	Super	6.65	177	71909

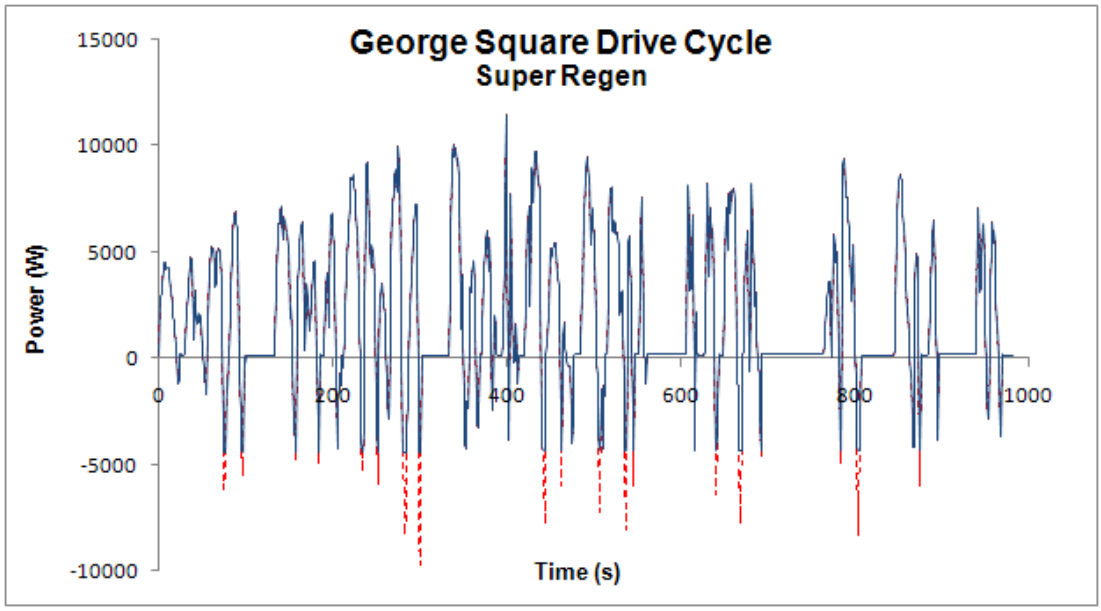

Figure 5.1: Power for the George Square Super Regeneration drive cycle, with regenerated power shown as negative. The solid blue line shows the power into and out of the battery pack with no support from supercapacitors. The dotted line shows the additional power that is available but cannot be accepted by the batteries lest they be damaged by the high currents.

This chapter describes the simulations in more detail, their results and the conclusions that can be drawn.

5.1 Maximising Efficiency

Supercapacitors have the most potential to increase the efficiency of the vehicle during high regeneration cycles. In these cycles, the supercapacitors can capture the

high power without risking damage, while the batteries have more limited current acceptance and higher losses. However, the supercapacitors must receive this power via the power electronics, which have their own losses; furthermore, the supercapacitors must discharge through these same electronics.

Optimising for efficiency can increase the vehicle's range. The supercapacitors can increase the range of the vehicle both by improving the yield, which means that each unit of energy results in further distance travelled, and by increasing the total amount of energy that is stored in the vehicle. The latter point assumes that the supercapacitors are fully charged at the same time that the batteries are charged.

Adding an additional battery to the pack can also increase the yield, as a higher voltage means that lower currents are needed to provide the required power, thereby reducing losses. Much more important to the range of the vehicle is the amount of energy stored in a single battery. Each battery contains 70Ah, thus adding a battery to the pack increases the energy content by 840Wh. The supercapacitors by comparison contain far less energy – the largest capacitance considered was 5000F, and a pack of thirty of these supercapacitors contains only 130Wh. The pack would need to contain 194 supercapacitors in order to have the energy content of just one battery. The range-extending capability of a battery is therefore quite significant.

5.1.1 Optimised Strategy Results for Efficiency

The best performance for the battery/supercapacitor hybrid Cobra on a drive cycle may be found by optimising the control strategy for each individual cycle, in this case to find the highest yield possible for the control strategy. These optimised results will be investigated first, to demonstrate the supercapacitors' potential for increasing the yield of the Cobra. This section will focus only on the efficiency – the impact of this optimisation strategy on battery current is discussed in Section 5.3.

Consider Figure 5.2, which shows the effect of the supercapacitor packs on the yield for the different cycles. The Low and Medium Regeneration cycles offer almost no improvement at all – less than 1% in all cases, with the smallest three supercapacitor packs actually decreasing the efficiency of the vehicle. The High Regeneration

cycles fare a little better, with improvements of up to 1.6% on the George Square cycle, while the Super Regeneration cycle shows improvements for all supercapacitor pack sizes, up to 6.6% for the 5000F supercapacitors on the George Square cycle.

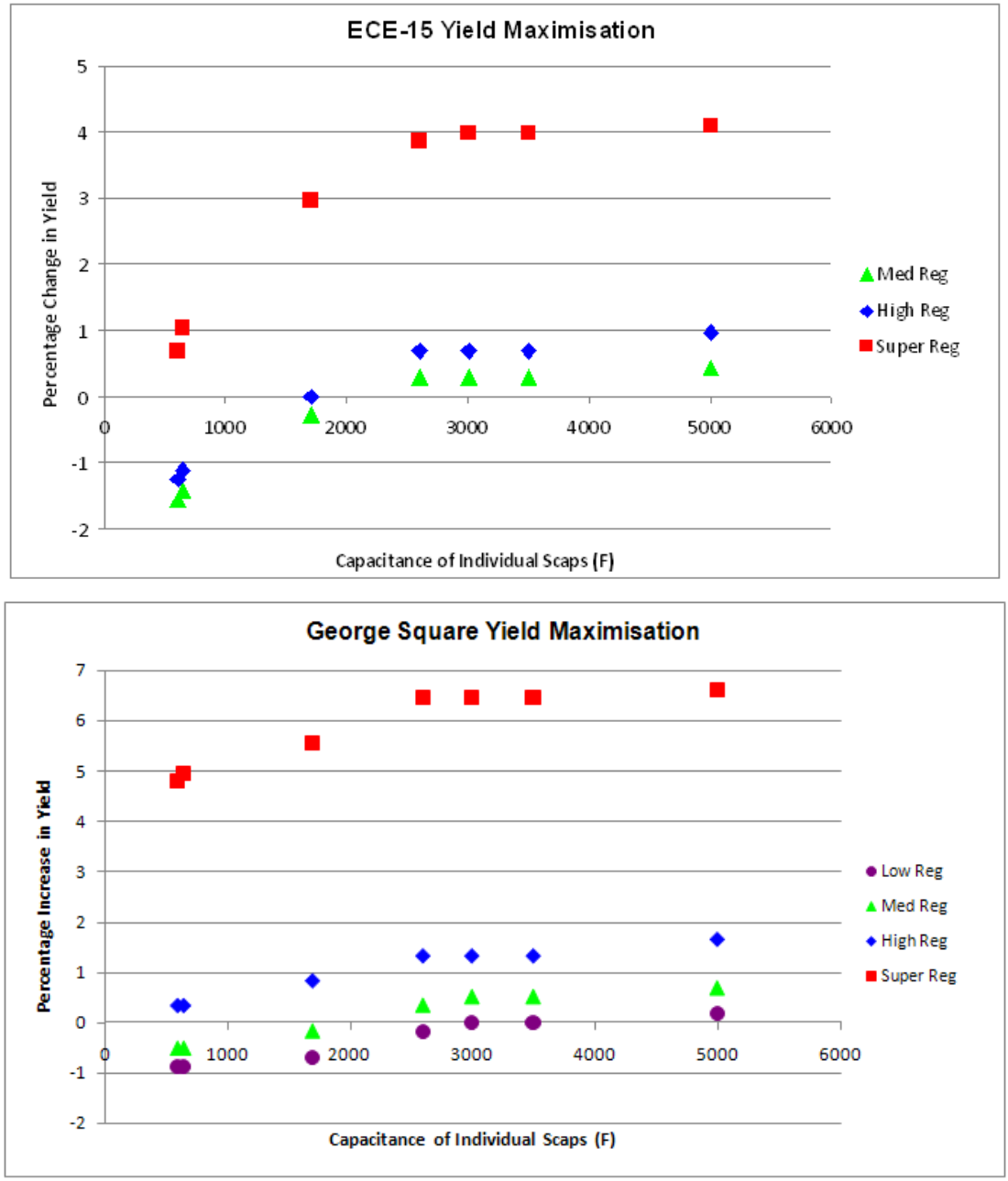

Figure 5.2: Percentage change in yield for different supercapacitor sizes in each cycle when optimised for efficiency, as compared to the performance of the battery-only Cobra in that cycle.

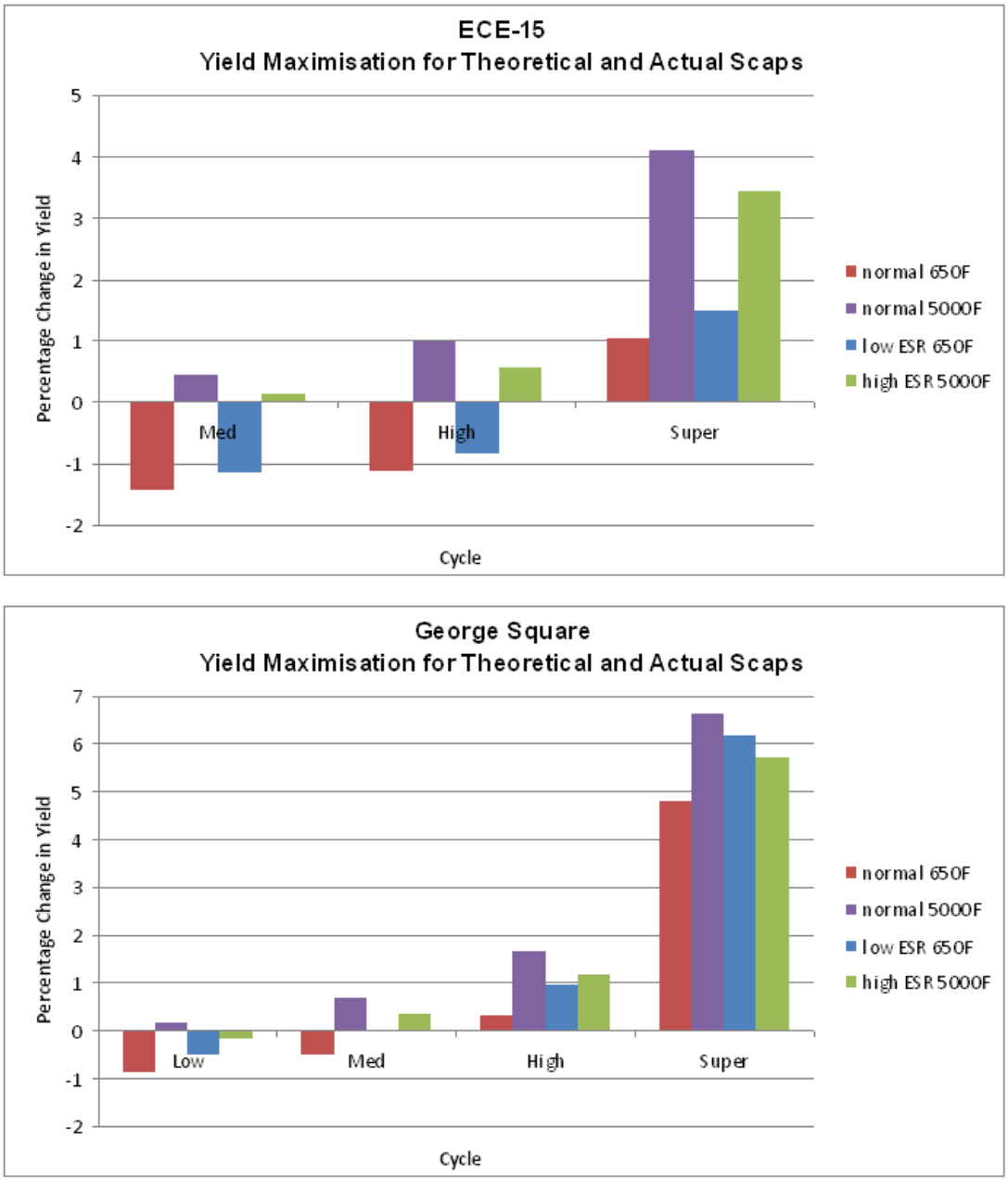

Figure 5.3: Percentage change in yield for different supercapacitor sizes in each cycle: Maxwell 650F, Ness 5000F, theoretical low ESR 650F, and theoretical high ESR 5000F.

Contrary to what was suggested in Section 4.2.2, the larger supercapacitor capacitances are much better at improving the efficiency of the vehicle than the smaller supercapacitors. The reasons for this were investigated by modelling two theoretical capacitors, one with a capacitance of 650F and an internal resistance of 0.33mΩ (the resistance of the Ness 5000F supercapacitors) and the second with a

capacitance of 5000F and an internal resistance of 0.8mΩ (the resistance of the Maxwell 650F supercapacitors). These results are shown in Figure 5.3.

For both cycles, a larger capacitance is helpful to increase the yield of the vehicle. For the ECE-15-based cycle, the energy content of the large supercapacitors makes a larger difference. Both the normal 5000F supercapacitor and the high ESR 5000F supercapacitor outperform both versions of the 650F supercapacitor. Furthermore, in each case the two 650F supercapacitors produce yields which are within 1% of each other, as do the two 5000F supercapacitors. For the George Square cycles, the difference in the internal resistance has more of an impact. In the Super Regeneration cycle, the pack of low ESR 650F supercapacitors outperforms the pack of high ESR 5000F capacitors.

A supercapacitor pack with a larger capacity increases efficiency not only because of the lower resistance, but also because the SOC remains high, resulting in lower currents and lower power electronic losses. In most cases, there are multiple operating points from which the peak yield can be obtained. Nevertheless, smaller supercapacitors are consistently discharged to a lower SOC than larger supercapacitors. Table 5.2 shows the range in the percentage of energy used from each type of supercapacitor in yield-maximising strategies. Recall that the maximum allowable energy usage for a supercapacitor pack is 75%, as the supercapacitor packs are controlled to have a minimum voltage that is ½ the maximum voltage.

This pattern also applies to the theoretical supercapacitors. This can be seen in Figure 5.4 which depicts the supercapacitor voltage for the 650F, 5000F, low ESR 650F and high ESR 5000F supercapacitor packs in the two Super Regeneration cycles. The 5000F supercapacitor pack remains at high voltage, with 30% of the total energy content used on the George Square cycle and only 22% used on the ECE-15 cycle. The High ESR version gets slightly more use, with 32% and 27% of the energy content being used. Meanwhile both the standard and Low ESR 650F supercapacitor packs are fully used, being discharged to the lower limit of 37.5V in the George Square cycle, and 38V in the ECE-15 cycle. This pattern is repeated in the other drive cycles.

Table 5.2: Percentage of supercapacitor energy content used in each cycle for a yield maximising strategy.

SUPERCAP	**ECE-15**			**George Square**			
Regeneration	Med	High	Super	Low	Med	High	Super
Ness 600F	73-74%	68-74%	74%	75%	75%	75%	75%
Max. 650F	73-75%	74%	74%	75%	75%	75%	75%
Ness 1700F	43%	43-65%	50-53%	50-68%	49-59%	54-58%	48-55%
Max. 2600F	39-42%	36-45%	38-44%	42-62%	40-64%	41-58%	38-43%
Max. 3000F	31-47%	33-50%	35-38%	48-65%	56%	37-61%	34-42%
Ness 3500F	27-41%	29-43%	30-33%	42-58%	43-60%	35-54%	34%
Ness 5000F	22-51%	28%	21-27%	38-62%	34-55%	33-48%	26-39%

Recall that the control strategy was optimised by adjusting two values: the minimum power which is to be supplied by the batteries (PMin) and the charging power which is to be sent from the batteries to the supercapacitors (PCh). Several combinations of PMin and PCh were found to produce the maximum yield for a given cycle. The values which were used to create Figure 5.4 are shown in Table 5.3, along with the yields produced by these values. In each column, the number in bold is the maximum yield achieved with the control strategy. Three sets of PMin/PCh values are used because no combination of PMin and PCh produced optimal results for all of the supercapacitor packs. The sub-optimal yield values for supercapacitors using the other two PMin/PCh sets are also shown for comparison.

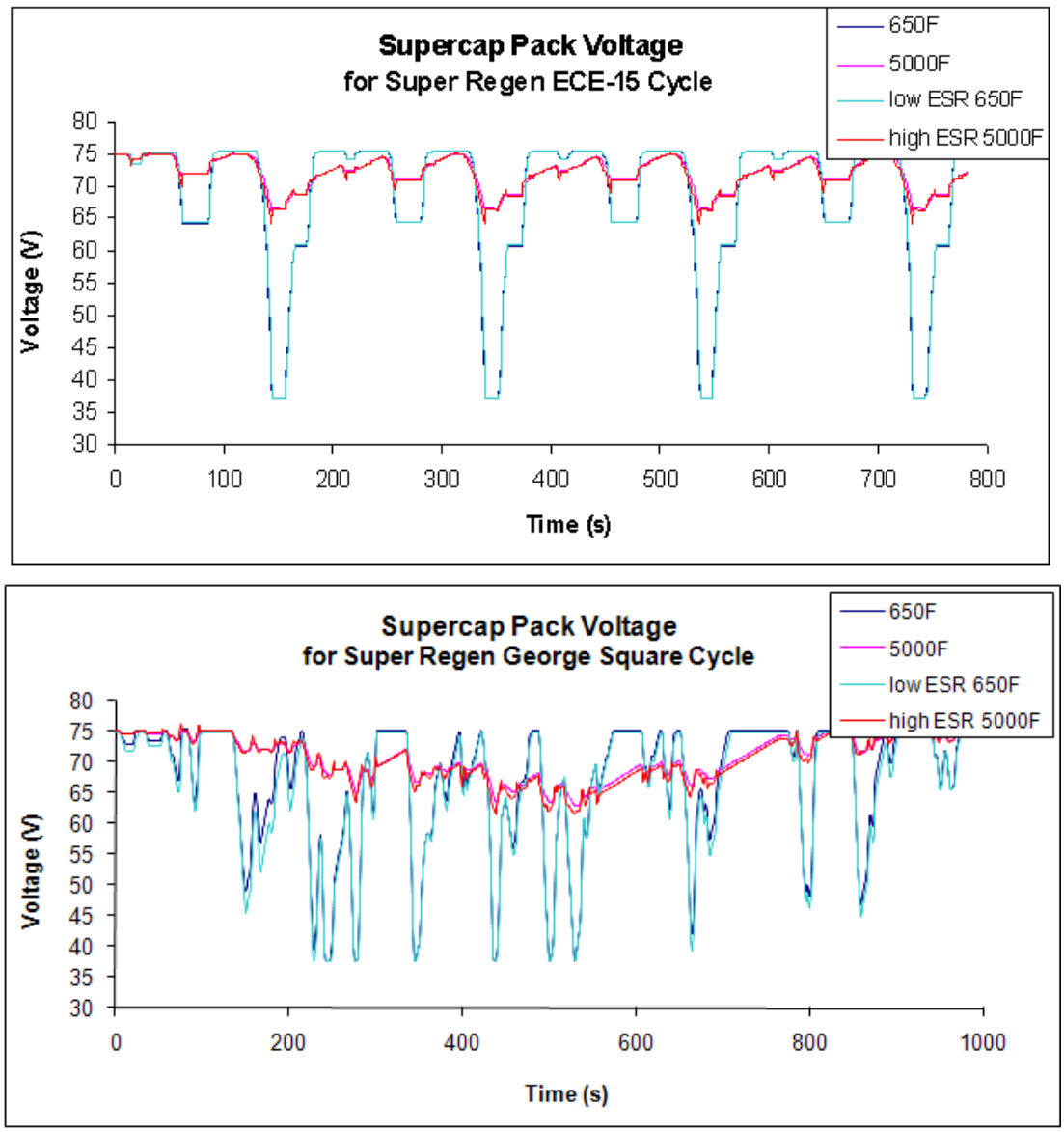

Figure 5.4: Selected supercapacitor packs, optimised for peak yield, on the Super Regeneration drive cycles.

Table 5.3: The optimal points used for the Super Regeneration cycle data shown in Figure 5.4. The yields (km/kWh) for each supercapacitor at the optimal points is shown in bold, while the yields for other supercapacitors' optimal points are also shown for comparison.

	650F		5000F		Low ESR 650F		High ESR 5000F	
	ECE15	**4GSq**	**ECE15**	**4GSq**	**ECE15**	**4GSq**	**ECE15**	**4GSq**
PMin 3600	8.74	6.98	**9.14**	**7.10**	8.8	**7.07**	**9.08**	**7.04**
PCh 1000								
PMin 3800	8.70	**6.99**	9.13	7.09	8.76	7.06	9.08	7.03
PCh 1000								
PMin 6000	**8.87**	6.76	8.91	6.77	**8.91**	6.78	8.89	6.75
PCh 0								

The energy contained in the supercapacitors also has an impact on the range of the vehicle. The battery pack has a nominal capacity of 70Ah and a nominal voltage of 72V, for a total energy content of 5040Wh. In the battery tests described in Section 3.2.4, the batteries showed a voltage collapse at about 25% state of charge. Thus, only 75% of this energy is useable. There are 30 supercapacitors in each pack, for a nominal voltage of 75V. The energy content of supercapacitors is given in Equation 2-5, but since the supercapacitors are discharged to no less than half their peak voltage, again only 75% of this energy is available. Several values of capacitance were modelled, and the additional available energy for the packs ranges from 11.72Wh for the 600F supercapacitors to 97.66Wh for the 5000F supercapacitors.

Taking the effects of both the increased yield and the additional energy into account, the range increase is found to be 9.4% for the Super Regeneration George Square trips, using six batteries and a pack of thirty 5000F supercapacitors. This is the largest range increase for this trip. Similarly, the largest increase for the ECE-15 trips was 6.8% for the Super Regeneration trip and the pack of 5000F supercapacitors. A summary of these results and those for the other cycles is shown in Figure 5.5.

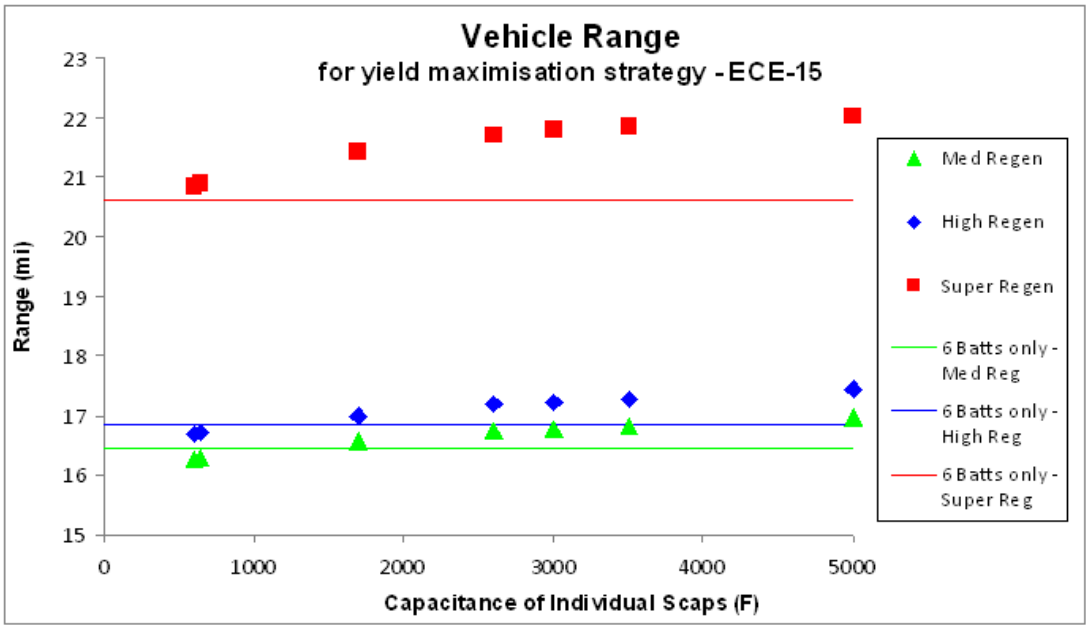

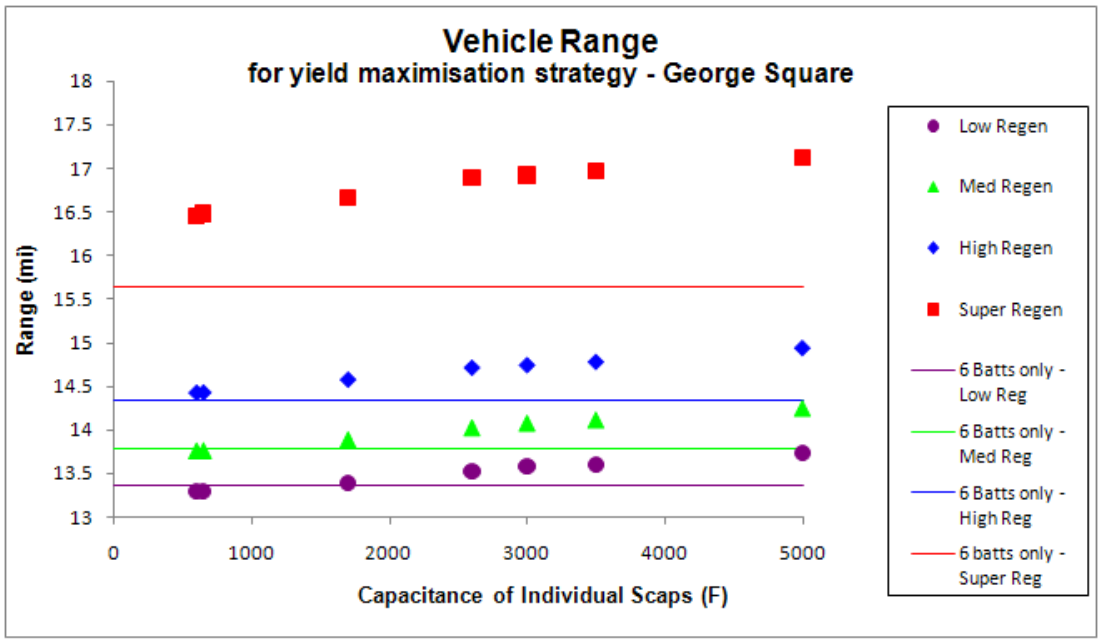

Figure 5.5: Vehicle ranges for the different drive cycles, compared to the range of the battery-only vehicle.

The hybridisation results have been compared to the result for the Cobra with one or two additional batteries. Since this is a low cost and technically straightforward upgrade to the vehicle, it may be preferable to adding a bank of supercapacitors. The simulations showed that if a single battery is added to the Cobra, rather than adding any supercapacitors, then the yield is increased by 1.2-2.4% depending on the amount of regenerated energy available. Similarly, adding a second battery increases

the yield by 2.1-4.4%. However, adding batteries also means adding energy, with a nominal energy content of 840Wh per battery. Assuming that 75% of this energy is useable, then adding a single additional battery to the Cobra would increase the range by at least 18.1%, rising to 19.5% with an efficient full braking control added to take maximum advantage of regenerative braking. The ranges of the Cobra for the different cycles with the addition of one or two batteries are shown in Figure 5.6.

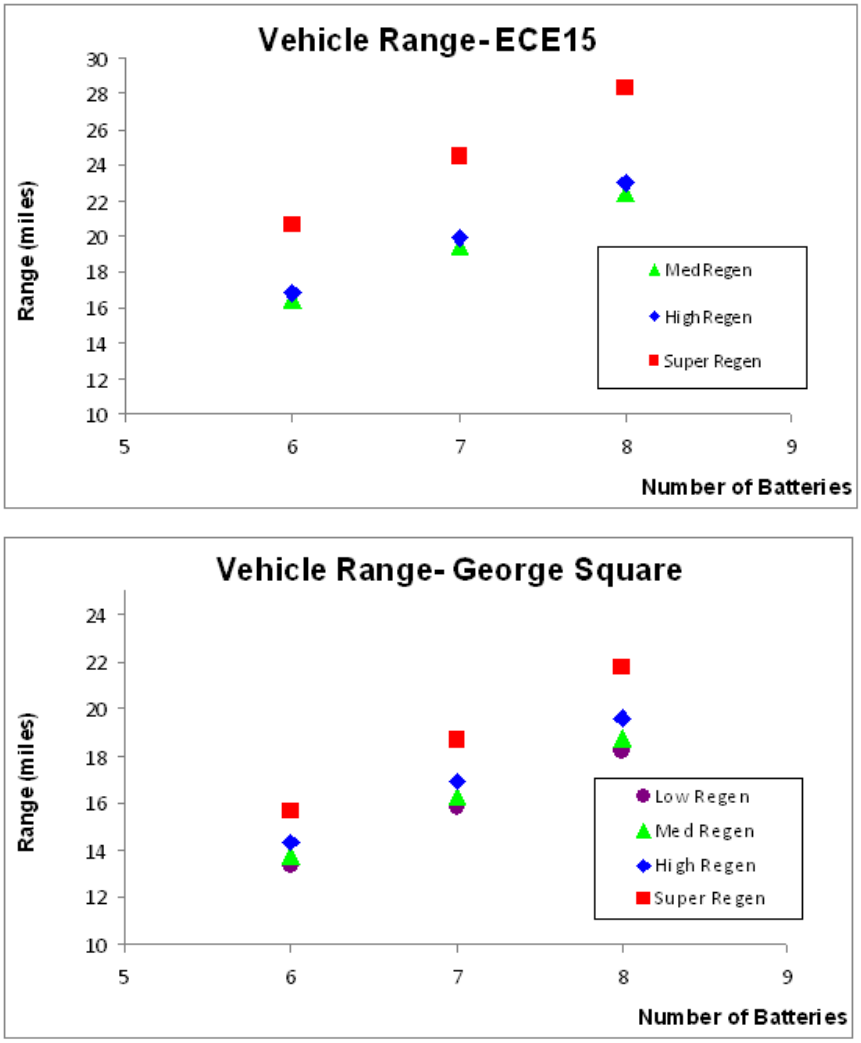

Figure 5.6: Range of Cobra for different battery pack sizes in each cycle.

The range extension provided by the extra batteries far exceeds that provided by the supercapacitors, and the batteries also outperform the supercapacitors in terms of cost, while adding a comparable weight and volume. Each additional battery costs just £154.14, while the supercapacitor pack costs range from £660.30 for the 650F

capacitors from Maxwell, to £2580 for the 5000F capacitors from Ness, plus £252.00 for the integration boards that prevent overcharging and £495.47 for the power electronics. The individual batteries weigh 24.3kg and have a volume of 9.78 litres, while the supercapacitor packs range in size from 6kg and 6.33 litres to 28kg and 17.82 litres, not including power electronics. The power electronics would add approximately 10kg, although the additional volume occupied by the electronics will depend on their physical arrangement within the vehicle.

5.1.2 Maximising Efficiency at Low Battery SOC

Supercapacitors were found to be somewhat more effective at improving vehicle efficiency when the batteries started at a low SOC, especially for the larger supercapacitor packs and for the higher regeneration profiles. These results are shown in Figures 5.7 and 5.8. The 600F and 650F supercapacitors continue to offer no benefit to the vehicle except during the Super Regeneration drive cycles. Yield benefits increase for the larger supercapacitor packs, to a maximum of 8.2% for the 5000F supercapacitor pack in the George Square Super Regeneration cycle and with an initial battery SOC of 50%. This correlates to an increase in range of 11%. However, this continues to be less effective than adding a single battery to the Cobra, as this increases the range of the vehicle on this cycle by 20.1%.

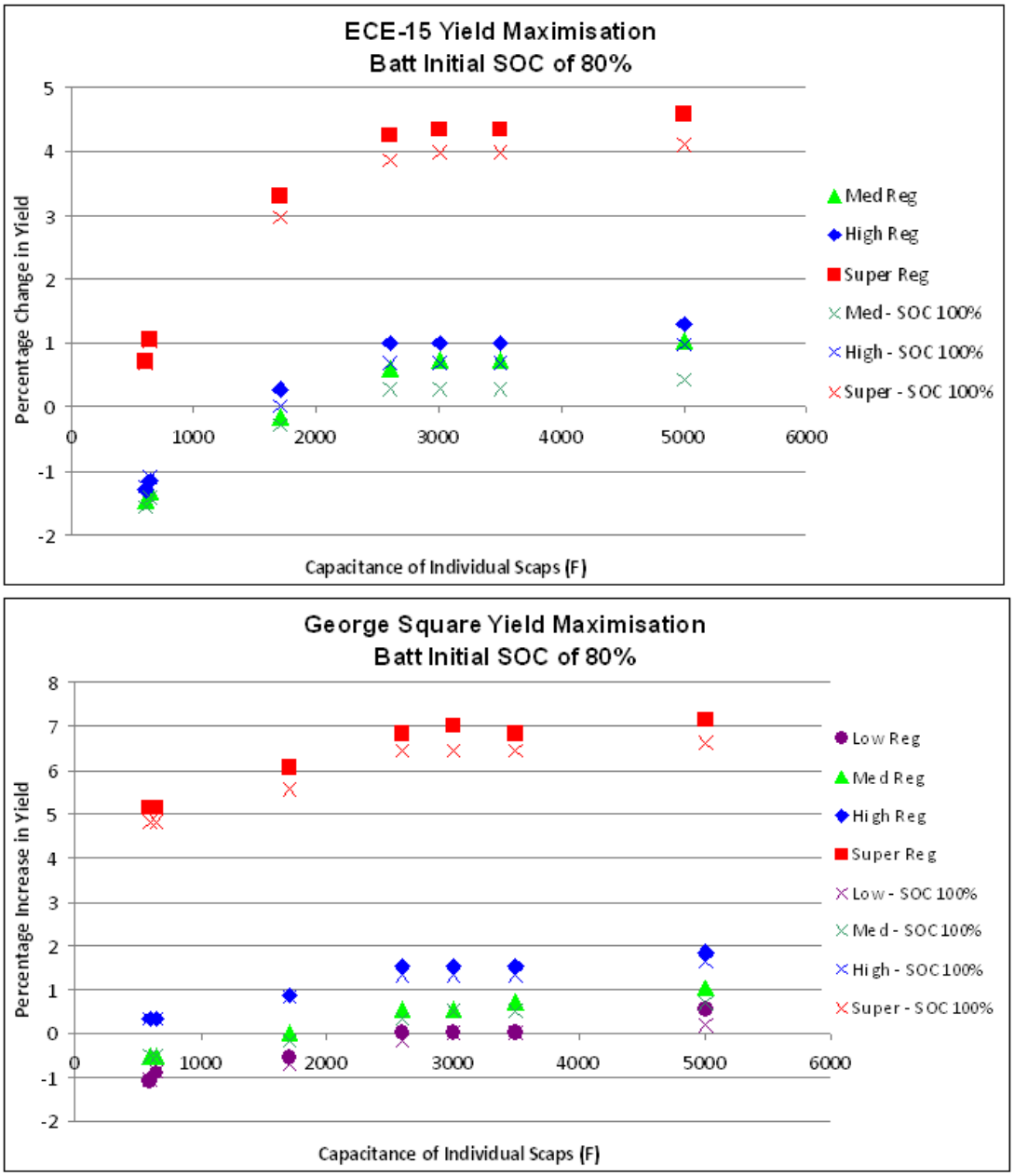

Figure 5.7: Percentage change in yield for different supercapacitor sizes in each cycle when optimised for efficiency with an initial battery SOC of 80%, as compared to the performance of the battery-only Cobra in that cycle with the same SOC. Results for the 100% SOC yield maximisation are also shown for comparison.

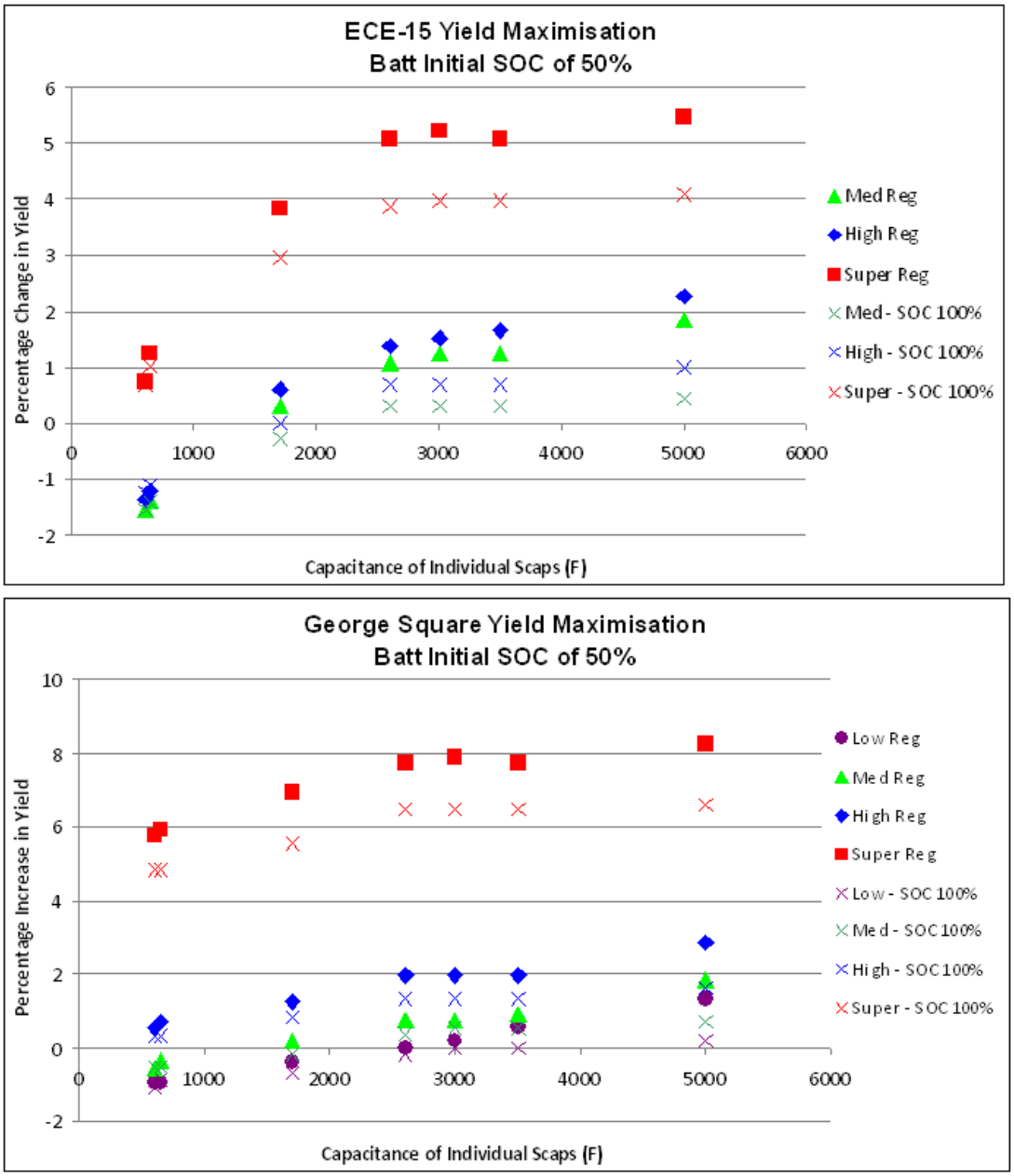

Figure 5.8: Percentage change in yield for different supercapacitor sizes in each cycle when optimised for efficiency with an initial battery SOC of 50%, as compared to the performance of the battery-only Cobra in that cycle with the same SOC. Results for the 100% SOC yield maximisation are also shown for comparison.

5.1.3 Developing a Generic Strategy for Efficiency Maximisation

A generic control strategy for yield maximisation would need to be developed if this strategy was to be used in a practical vehicle. This would require data from a variety of drive cycles, and ideally could be adjusted by the control software while the vehicle was driving. This research focussed on two basic cycles, with a total of

seven variations reflecting different amounts of regenerative braking. This does not provide enough data to make definitive claims about a generic strategy; nevertheless, a study of the results for these drive cycles demonstrates that a useful generic strategy should be possible for effective yield maximisation.

The values of PMin and PCh which produced a yield within 1% of the highest yield value were considered for each supercapacitor in each cycle. These demonstrated a considerable overlap for each supercapacitor over all seven drive cycle variations, with the overlapping region being larger for larger capacitances. Figure 5.9 shows the combinations of PMin and PCh for which the yield was found to be within 1% of the maximum, for the Maxwell 650F and the Ness 5000F supercapacitors in all seven cycles. The optimal PMin and PCh values for the 650F supercapacitor depend on the base cycle more strongly than on the amount of regenerative energy available. The ECE-15 cycle results, represented in Figure 5.9 as coloured diamonds, show overall higher values of PMin than do the George Square cycle results, represented as rings. Conversely, the optimisation points for the large Ness 5000F supercapacitor depend more on the amount of regenerative braking, as the Low and Medium Regeneration values for both base cycles have several points in common for PMin $\geq$ 5000W, while the Super Regeneration values for both base cycles also share several common points. These are shown in Figure 5.9 respectively as the yellow diamonds/pink rings and the brown diamonds/green rings.

To make the regions of overlap clearer, Figure 5.10 shows only the points where all seven tested cycles have optimal points in common, for each of the tested supercapacitor packs.

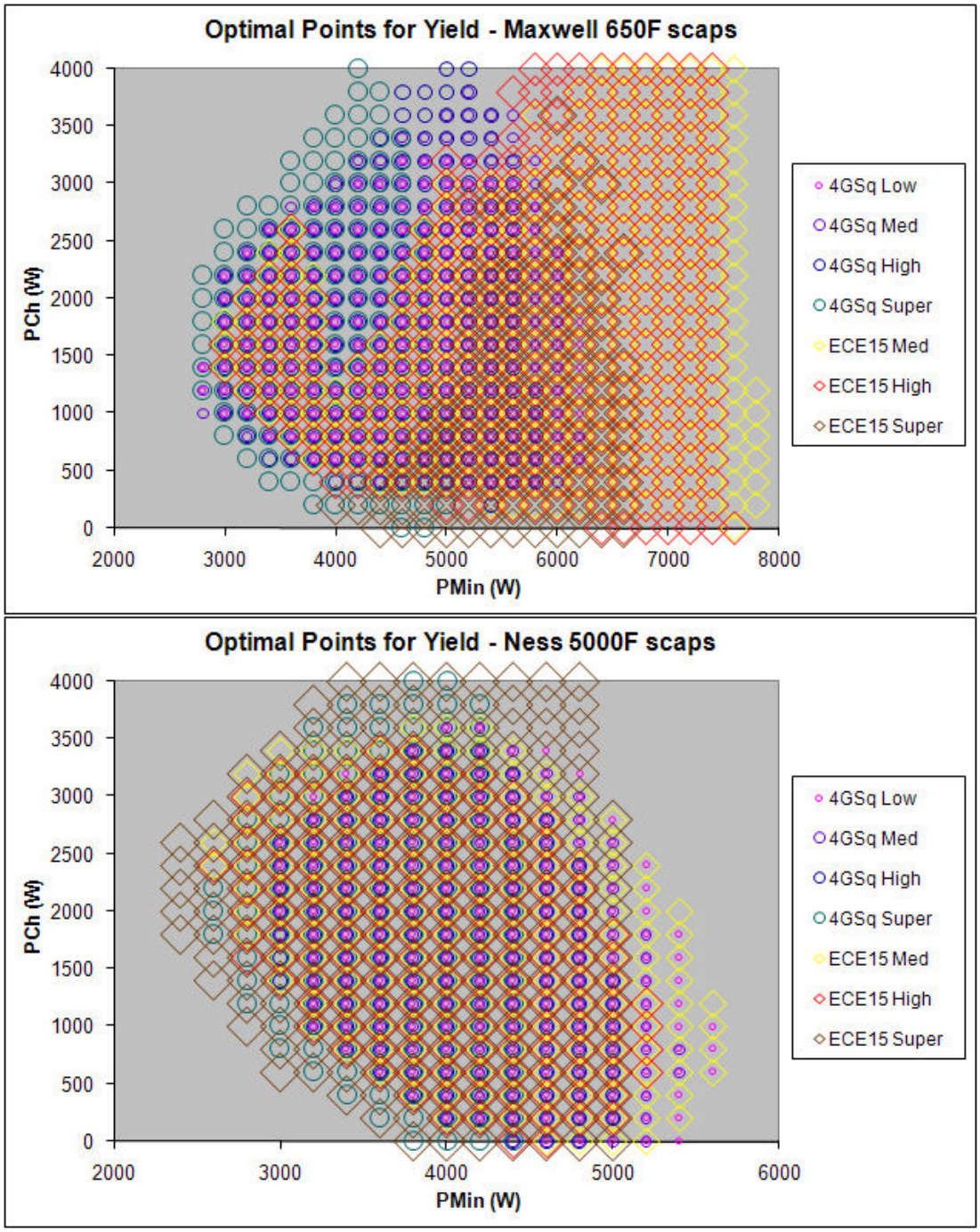

Figure 5.9: Values of PMin and PCh which provide the maximum yield, or a yield within 1% of the maximum. The upper plot shows results for the Maxwell 650F supercapacitors for each of the tested cycles, while the lower plot shows results for the Ness 5000F supercapacitors.

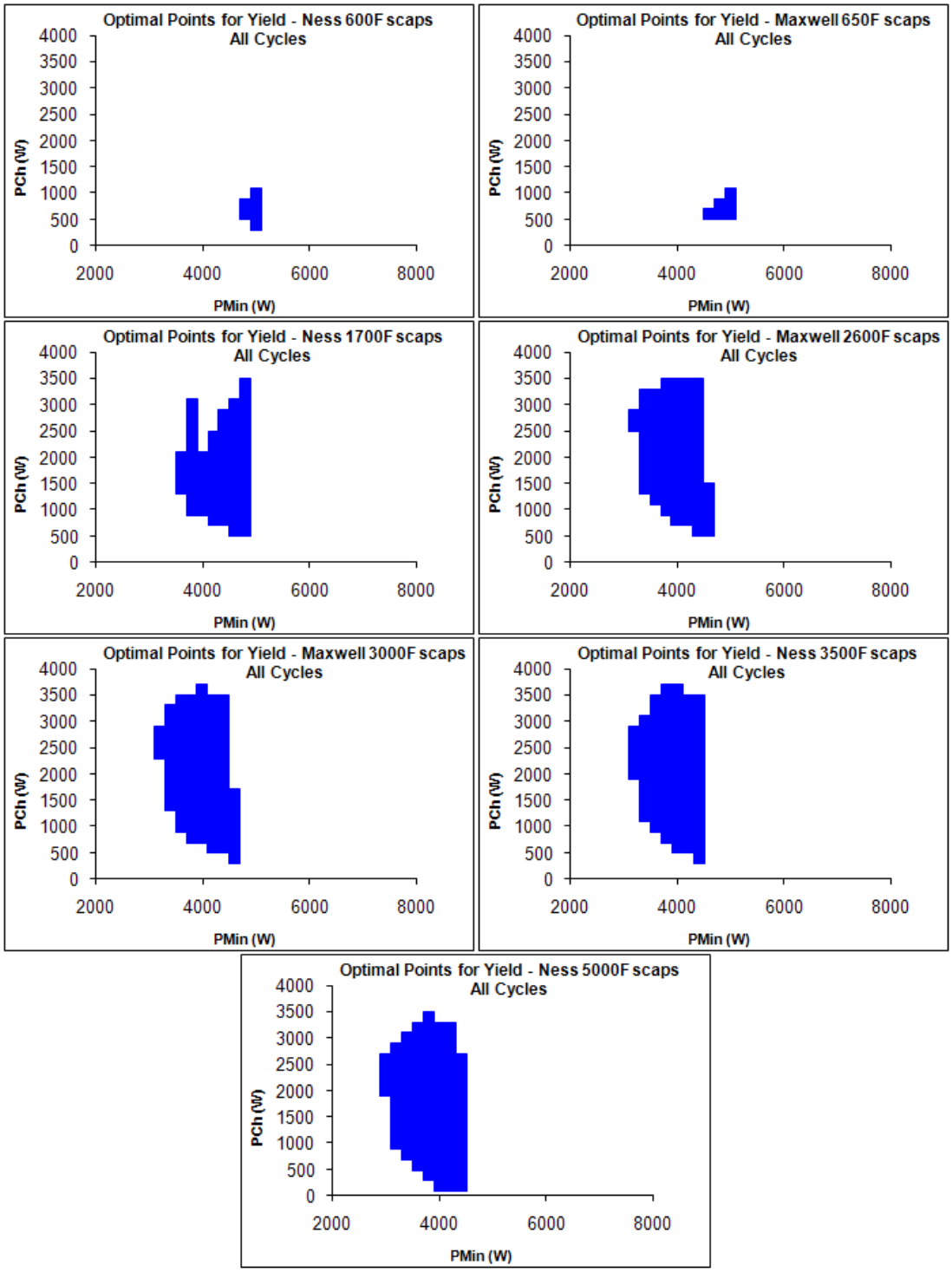

Figure 5.10: Values of PMin and PCh for which yields within 1% of the maximum were achieved for all seven simulated cycles, for each type of supercapacitor. These are the operating regions which are likely to be used in a generic efficiency-maximising control strategy.

In general, achieving a high yield value for the battery/supercapacitor hybrid requires a value of PMin between 3000 and 5000W – this represents the power demands

which will be filled by the batteries. For small 600F or 650F supercapacitor packs, the value of PCh should be 1000W or lower. This represents the rate at which the supercapacitor pack is recharged by the batteries, and the low optimal charging value is indicative of the fact that high charging powers create excessive losses in the power electronics. This is less of an issue for the larger supercapacitor packs, due to the fact that these capacitor packs are not discharged to such low voltages as the smaller packs – see Section **Error! Reference source not found.** for details.

A real-life vehicle will most likely have a fixed regenerative braking algorithm which will not show such wide variation in percentage of energy recovered as is shown in these seven cycles. This will widen the optimal operating region for maximising efficiency somewhat. However, the fact remains that even the optimal results showed lower improvements to vehicle range than would be achievable with the addition of a single extra battery. Since vehicle range extension is the ultimate goal of increasing vehicle efficiency, this means that supercapacitors are not likely to be used in this fashion in commercial EVs.

5.1.4 Comparison to Results from Literature

These simulations assume that two half bridge converters will be used to connect the batteries and supercapacitors to the motor controller. This is not the most efficient architecture possible, but it was chosen to allow a finer control of power flow. It is also possible that other, more efficient strategies could be devised, and perhaps a more efficient architecture or strategy would make the supercapacitors more useful for efficiency maximisation and range extension. A review of the literature shows that this is not the case.

Consider first the electric vehicle constructed at the Catholic University of Chile, and described in Section 2.3.1 [51-53]. This vehicle used a 356V pack of 12V, 50Ah lead acid batteries, giving a total energy of 17.8kWh. To this vehicle was added a 300V, 20F pack of supercapacitors – an additional energy of 0.625kWh, or 3.5% of the battery energy. The batteries and supercapacitors were connected with a single half bridge converter, and a maximum yield increase of 8.9% was achieved, using a control strategy based on an Artificial Neural Net. The total range increase of this

vehicle, counting both added energy and increased yield, would therefore be 12.7% if the supercapacitors were recharged from the grid at the same time as the batteries were recharged.

Costs for this vehicle's batteries and supercapacitors are not given, however a cost analysis is performed in [51] which forecasts costs of $150/kWh for the batteries and $5,160 for the supercapacitor pack and converter. Note that the forecast was performed in 2005 and assumes a cost of $30 for each 2700F cell – a high power 2600F cell from Maxwell cost approximately $90 in 2007. The original battery pack contained 26 batteries, so in order to increase the energy content of the battery pack by at least 12.7% (and neglecting any technical issues or yield effects associated with the increased voltage), one would need to add 4 batteries. Each battery contains 0.6kWh, so based on the cost assumptions made in [51], the four batteries would cost $360 in total. The addition of a supercapacitor pack is therefore more than 14 times more costly than the additional batteries needed to achieve the same benefit to range extension.

Another battery/supercapacitor car, that built by CR-ENEA and collaborators, used the supercapacitors in parallel with the batteries, thus avoiding the converter losses entirely [33]. This vehicle is described in this thesis in Section 2.3.6. The vehicle used eight 6V, 180Ah batteries and added two 48.6V packs of supercapacitors, each with a pack capacitance of 47F. This gave an 11.1% increase in efficiency – the method of calculation was not specified, but for the purpose of this analysis it is assumed to be the yield. The supercapacitors contained an energy of 0.03kWh – just 0.3% of the batteries' energy of 8.6kWh. However, as the supercapacitors were connected in parallel to the batteries, most of their energy would not be used, and the energy content of the supercapacitors would not have a significant impact on the range. Although costs for the batteries and supercapacitor packs are not given, it is worth noting that a single additional battery would increase the range by 16.7%.

Finally, consider the scooter built by the National Science Council of Taiwan, first discussed in Section 2.3.5 [63, 64]. This scooter used four 12V, 15.6Ah batteries,

thus the energy content of the batteries was 748.8Wh. The addition of eleven 1700F supercapacitors added 18.9Wh to the vehicle, 2.5% of the battery energy, and increased the range of the vehicle by 18.5%. Cost information was not available for this vehicle, but note that an additional battery, identical to the others, would have increased the range by 25%.

What of the other vehicles reviewed in Section 2.3? The EVermont battery/supercapacitor vehicle did not find any reliable increase in efficiency or range [57]. The Karlsruhe van could not offer a comparison of battery alone to battery/supercapacitor hybrid, as the battery was too low power to operate on its own [60]. Finally, the Cranfield University researchers did not quantify the efficiencies for their go-kart, as the main focus of their work was the mechanism of controlling the hybrid system [61, 62].

The obvious conclusion for this work is that supercapacitors are not an effective way to increase the range of a vehicle. Their energy content is so low that the additional space and weight that they represent would be far better devoted to an additional battery, if range extension is the goal. This would be true even if the supercapacitors were much cheaper than they are today.

5.2 Minimising Battery Currents

In contrast to their performance as range extenders, the author's investigations show that supercapacitors are very effective at minimising the battery currents. High regeneration energy is not needed for the supercapacitors to reduce battery currents. All that is needed is for the batteries to charge the supercapacitors at a suitable rate, leaving the supercapacitors to supply high power bursts as needed. The supercapacitors may also be recharged by regenerative braking, but this was found to have only a small impact on the usefulness of the capacitors.

Section 4.2.3 described the possibility for a perfectly controlled drive cycle for which the battery has a constant power output throughout the cycle. This represents the minimum peak battery current which can be achieved. These currents, for each of the seven tested cycles, are given in Table 5.4.

Table 5.4: Battery currents given a theoretical, perfectly controlled cycle in which the battery outputs a constant power.

	ECE-15			George Square			
Regeneration	Med	High	Super	Low	Med	High	Super
Battery I (A)	34	34	26	37	29	27	24
Reduction from battery only (%)	81%	81%	85%	79%	84%	85%	86%

5.2.1 Optimised Strategy Results for Peak Battery Current Reduction

The battery current reduction for the different cycles and supercapacitor packs, optimised for minimising peak battery currents for each cycle, is shown in Figure 5.11. The supercapacitors do not need to have a large capacitance to be useful in this regard. Even the smallest tested supercapacitor pack size, thirty 600F capacitors from Ness, can reduce the battery peak currents by up to 49%

By contrast, the addition of further batteries is not particularly helpful in this regard. The batteries do increase the voltage of the pack, and thus reduce the currents, but this benefit is offset somewhat by the additional battery resistance. The highest power demand for the drive cycles was 11.5kW. Using Equation 3-6, the current needed to provide this power from 6 fully charged batteries can be calculated as 176A. Similarly, the required power for 7 batteries is 147A, and for 8 batteries is 126A. These represent improvements of 16.9% and 28.8%, respectively. But the pack voltage has increased by 16.7% in the case of seven batteries and by 33.3% in the case of eight. The benefits of that extra voltage diminish as further batteries are added. In fact, in order to get the same benefit, in terms of peak battery current reduction, as even the smallest pack of supercapacitors, the battery pack size would need to be increased to 10 batteries. This would mean an additional battery weight of almost 100kg.

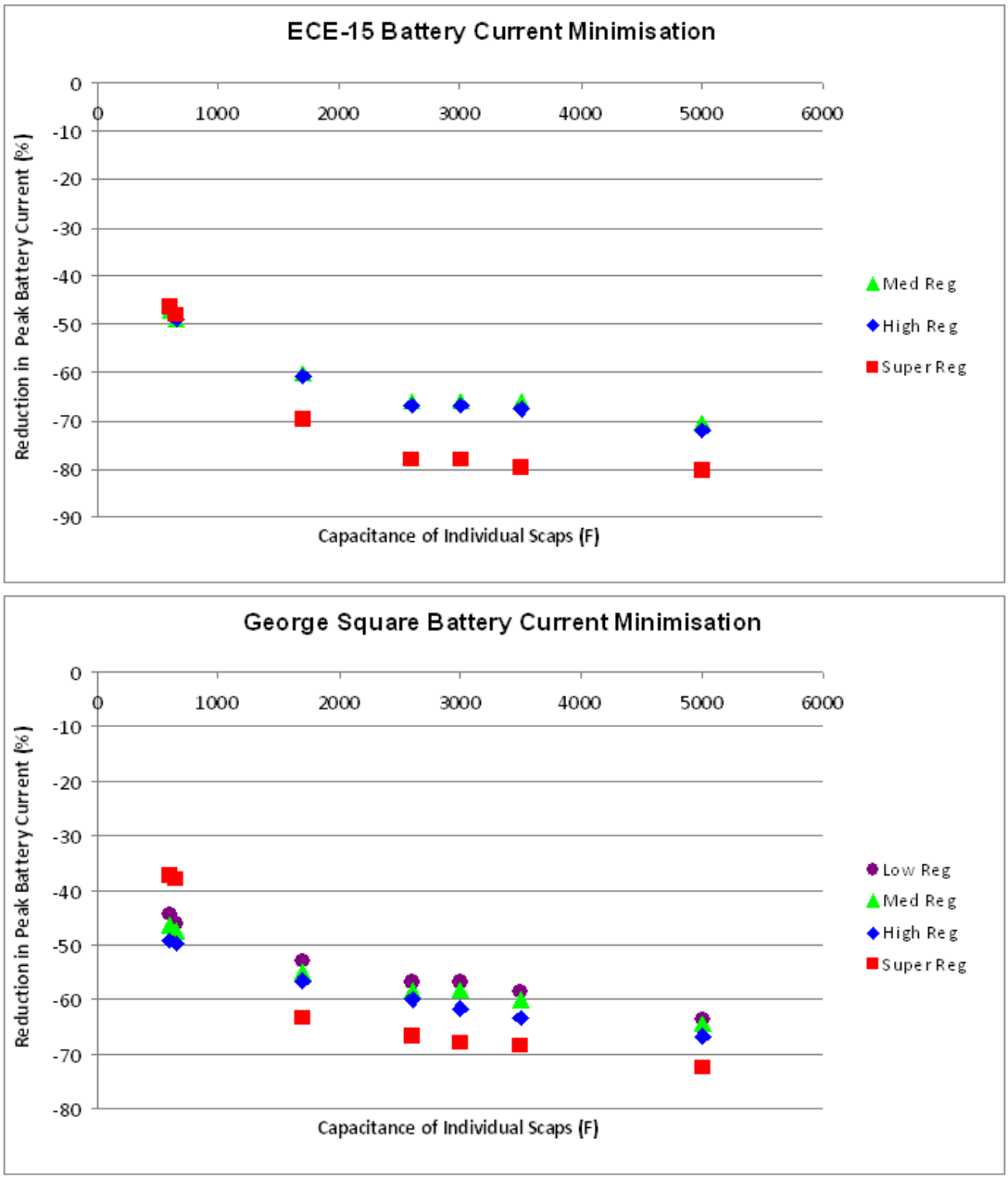

Figure 5.11: Percentage change in peak battery current for different supercapacitor sizes in each cycle, as compared to the performance of the battery-only Cobra in that cycle.

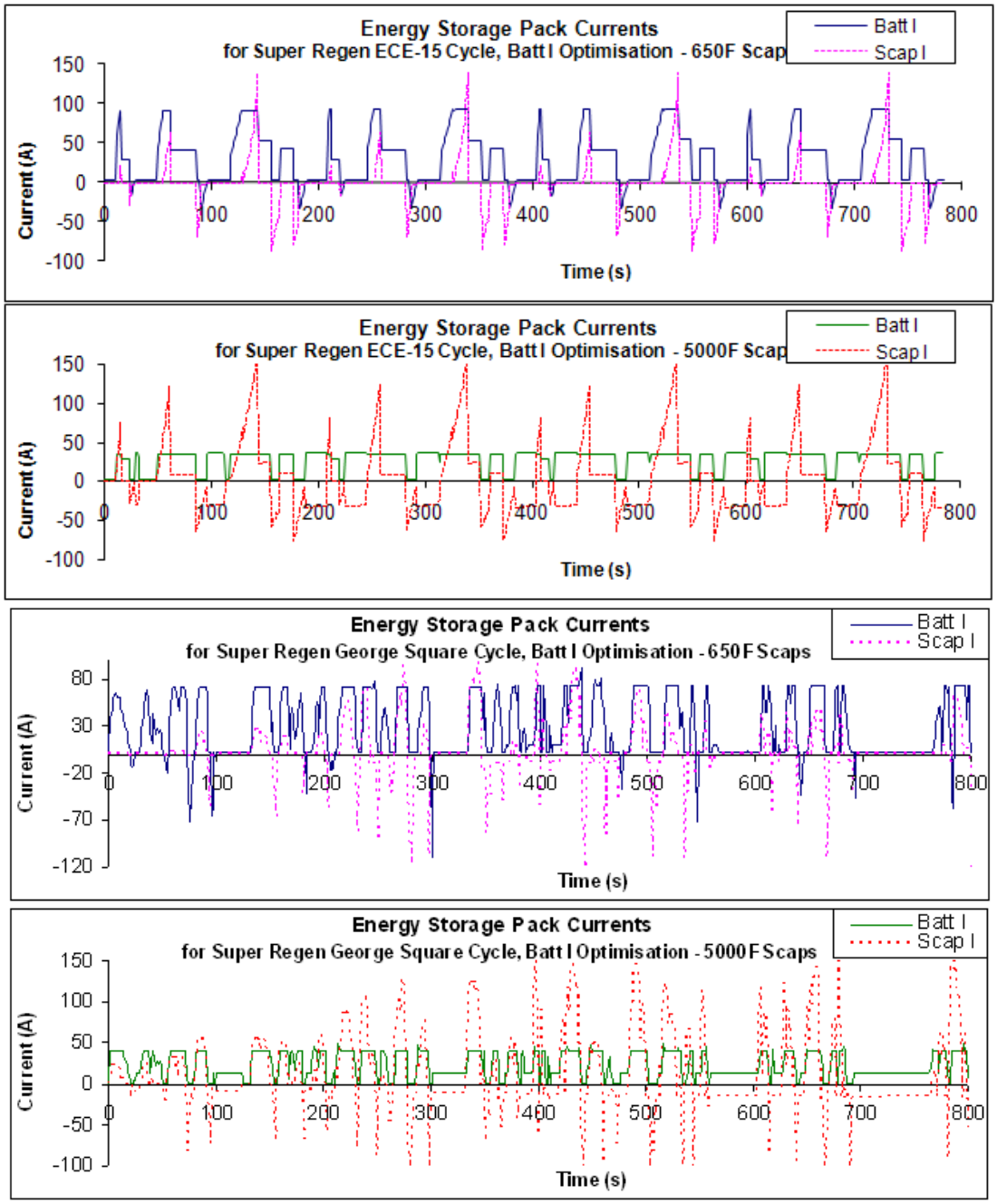

Figure 5.12: Battery and Supercapacitor currents for 650F and 5000F supercapacitors for the Super Regeneration ECE-15 and George Square drive cycles.

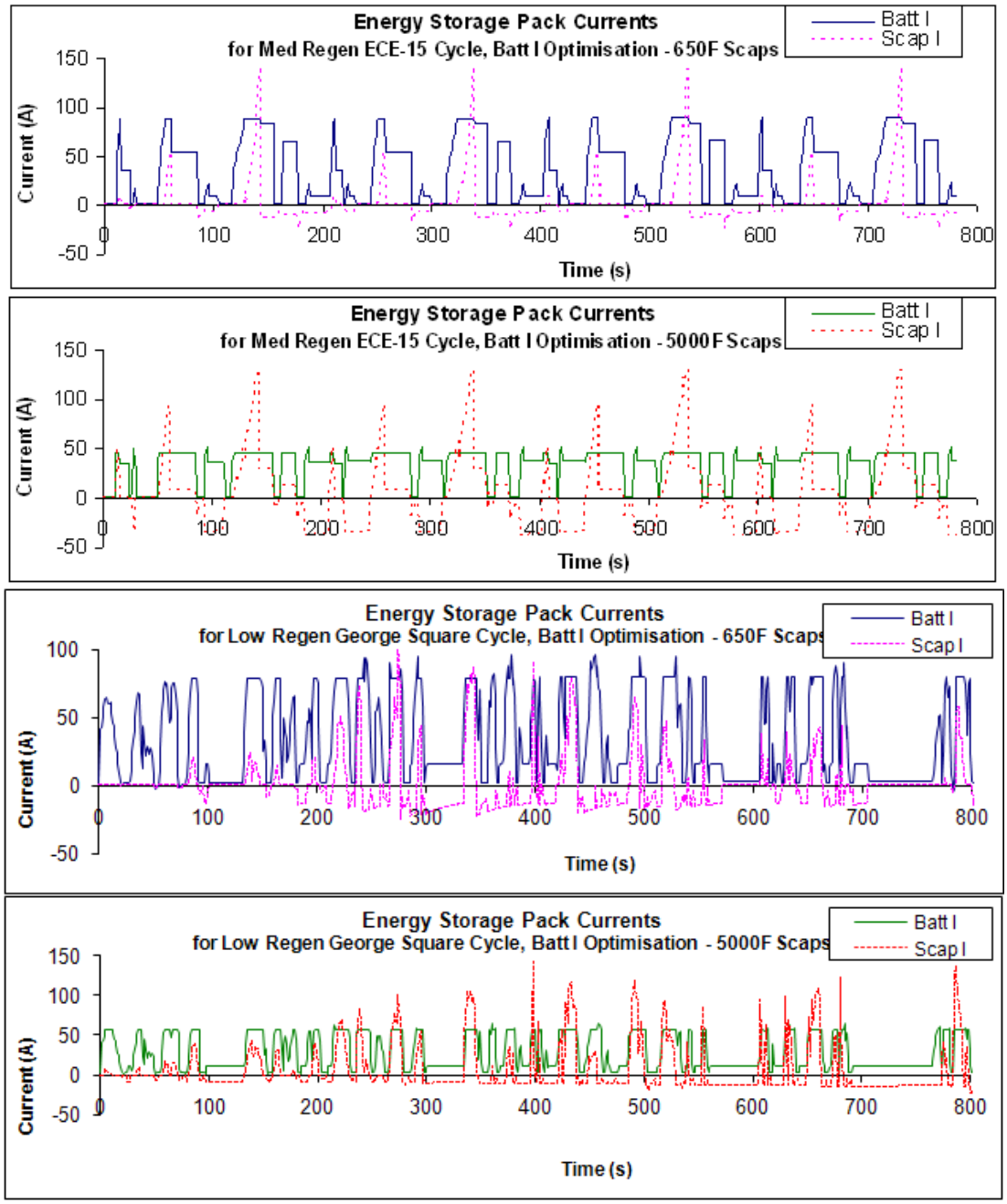

Figure 5.13: Battery and Supercapacitor currents for 650F and 5000F supercapacitors for the Med Regeneration ECE-15 and the Low Regeneration George Square drive cycles.

The typical battery current profile for each cycle shows the batteries discharging at the PMin rate, with occasional spikes upwards as the batteries recharge the supercapacitors. Some examples are shown in Figures 5.12 and 5.13.

The greater battery current reduction for the larger supercapacitors is due primarily to their greater capacitance, and not to their lower resistance. This can be seen in Figure 5.14, which shows the percentage reduction in peak battery current for the Maxwell 650F, Ness 5000F, Low ESR 650F and High ESR 5000F supercapacitor packs.

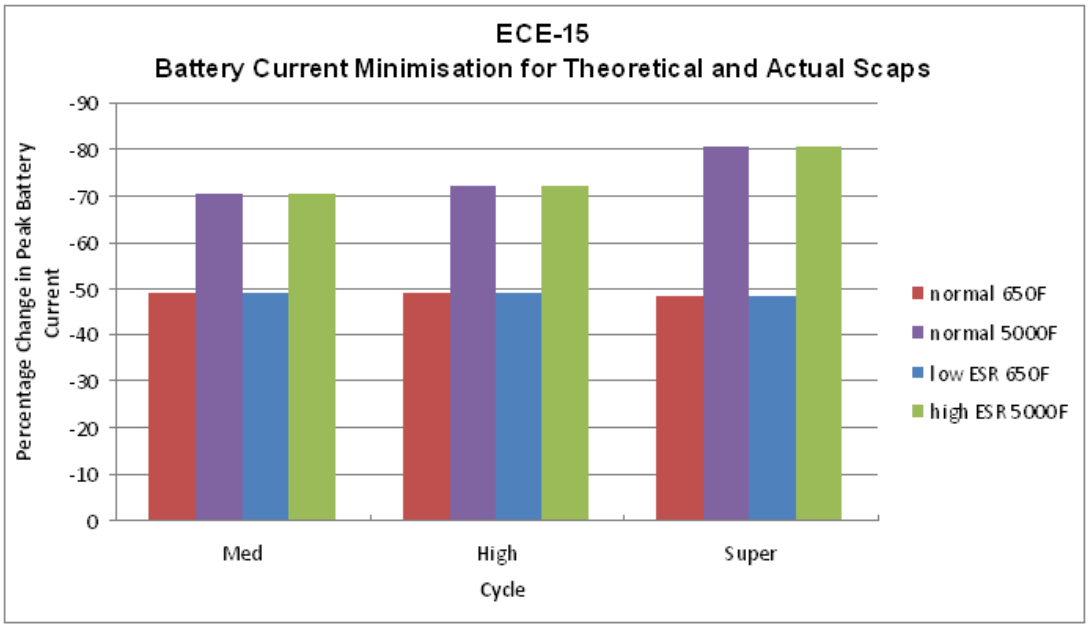

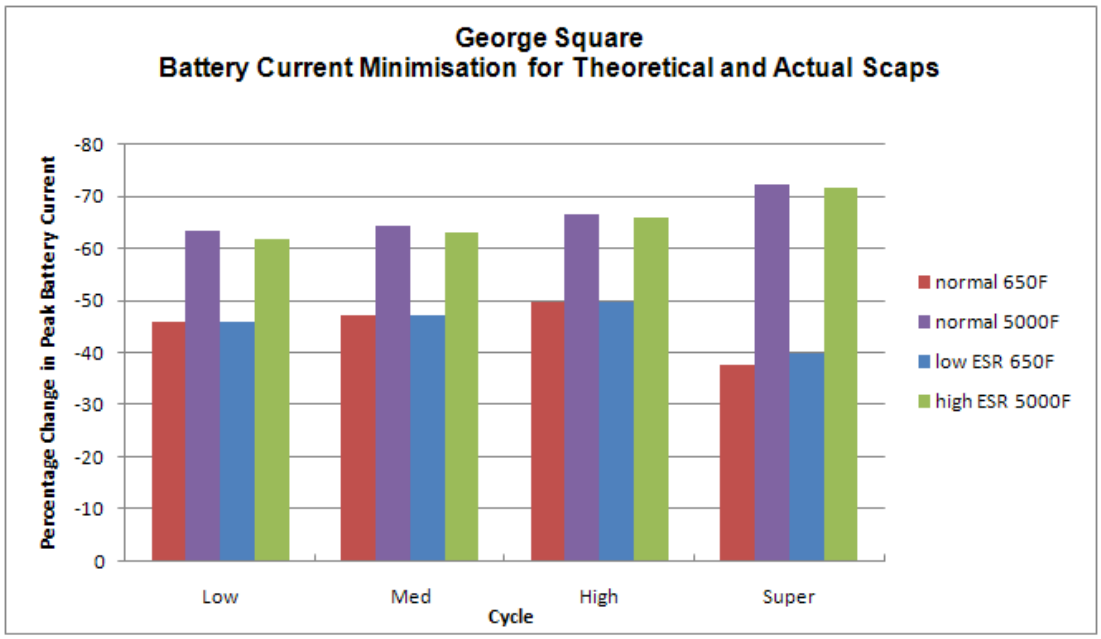

Figure 5.14: Percentage change in peak battery current for different supercapacitor sizes in each cycle: Maxwell 650F, Ness 5000F, theoretical low ESR 650F, and theoretical high ESR 5000F.

Table 5.5: The optimal points used for the cycle data shown in Figures 5.12 and 5.13, plus optimal points for the remaining drive cycles. The peak battery current (A) for each supercapacitor at the optimal points is shown in bold, while the peak battery currents for other supercapacitors' optimal points are also shown for comparison.

	650F ECE-15			5000F ECE-15		
	Med	**High**	**Super**	**Med**	**High**	**Super**
PMin 3200 / **PCh 2600**	198	197	202	**52**	52	45
PMin 3200 / **PCh 2400**	198	197	202	74	**49**	45
PMin 2400 / **PCh 2400**	198	198	202	195	96	**35**
PMin 6000 / **PCh 600**	**90**	**90**	127	90	90	90
PMin 6200 / **PCh 0**	198	197	**93**	93	93	93

	650F George Square				5000F George Square			
	Low	**Med**	**High**	**Super**	**Low**	**Med**	**High**	**Super**
PMin 4000 / **PCh 600**	164	164	164	163	**65**	65	65	60
PMin 3400 / **PCh 1000**	164	164	164	163	118	**63**	63	63
PMin 3200 / **PCh 1000**	164	164	164	163	123	119	**59**	59
PMin 2800 / **PCh 800**	164	164	164	163	159	158	133	**49**
PMin 5400 / **PCh 1000**	**96**	96	96	111	88	80	80	110
PMin 5400 / **PCh 800**	134	**93**	93	111	88	80	80	110
PMin 5400 / **PCh 600**	151	130	**89**	111	85	85	80	110
PMin 5000 / **PCh 600**	164	164	143	**110**	82	82	82	73

The values used for PMin and PCh for each of these plots are shown in Table 5.5. There was considerable variation in the combinations of PMin and PCh which provided the lowest peak battery currents for each cycle and supercapacitor pack. Therefore, 13 value sets are shown. In each column, the value in bold shows the best result achieved for that cycle and supercapacitor type. The peak battery currents for each supercapacitor and cycle using the other 12 PMin/PCh pairs are also shown for comparison.

5.2.2 Minimising Battery Currents at Low Battery SOC

The state of charge of the battery has very little impact on the supercapacitors' effectiveness at reducing peak battery currents. This is illustrated in Figures 5.15 and 5.16. These figures show the percentage reduction in peak battery currents for each drive cycle and supercapacitor pack when optimised for current reduction, and with initial battery SOCs of 80% and 50%, respectively.

The percentage change in the peak battery currents is minimal, in spite of the fact that peak battery currents rise as SOC decreases, due to the lower battery voltage. Figure 5.17 shows the values for the peak battery currents at each tested SOC, for 6, 7 or 8 batteries and without any assistance from supercapacitors. Peak battery currents are the same for each version of the George Square drive cycle and for the Medium and High Regeneration versions of the ECE-15 based cycle. The peak currents for the Super Regeneration ECE-15 cycle are 2-4A higher than those of the lower regeneration cycles.

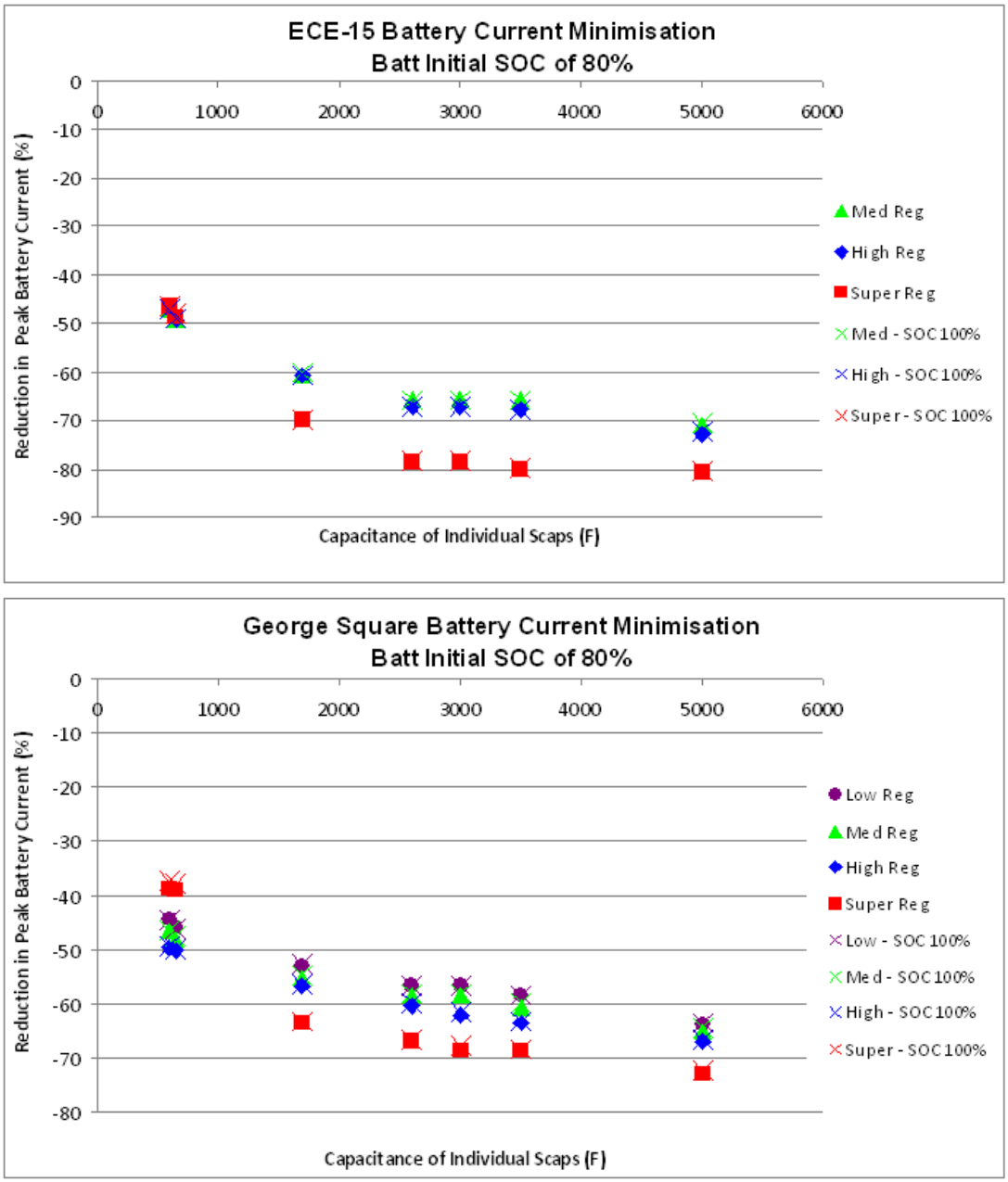

Figure 5.15: Percentage change in peak battery current for different supercapacitor sizes in each cycle, as compared to the performance of the battery-only Cobra in that cycle, for an initial battery SOC of 80%. The results for an initial battery SOC of 100% are also shown for comparison.

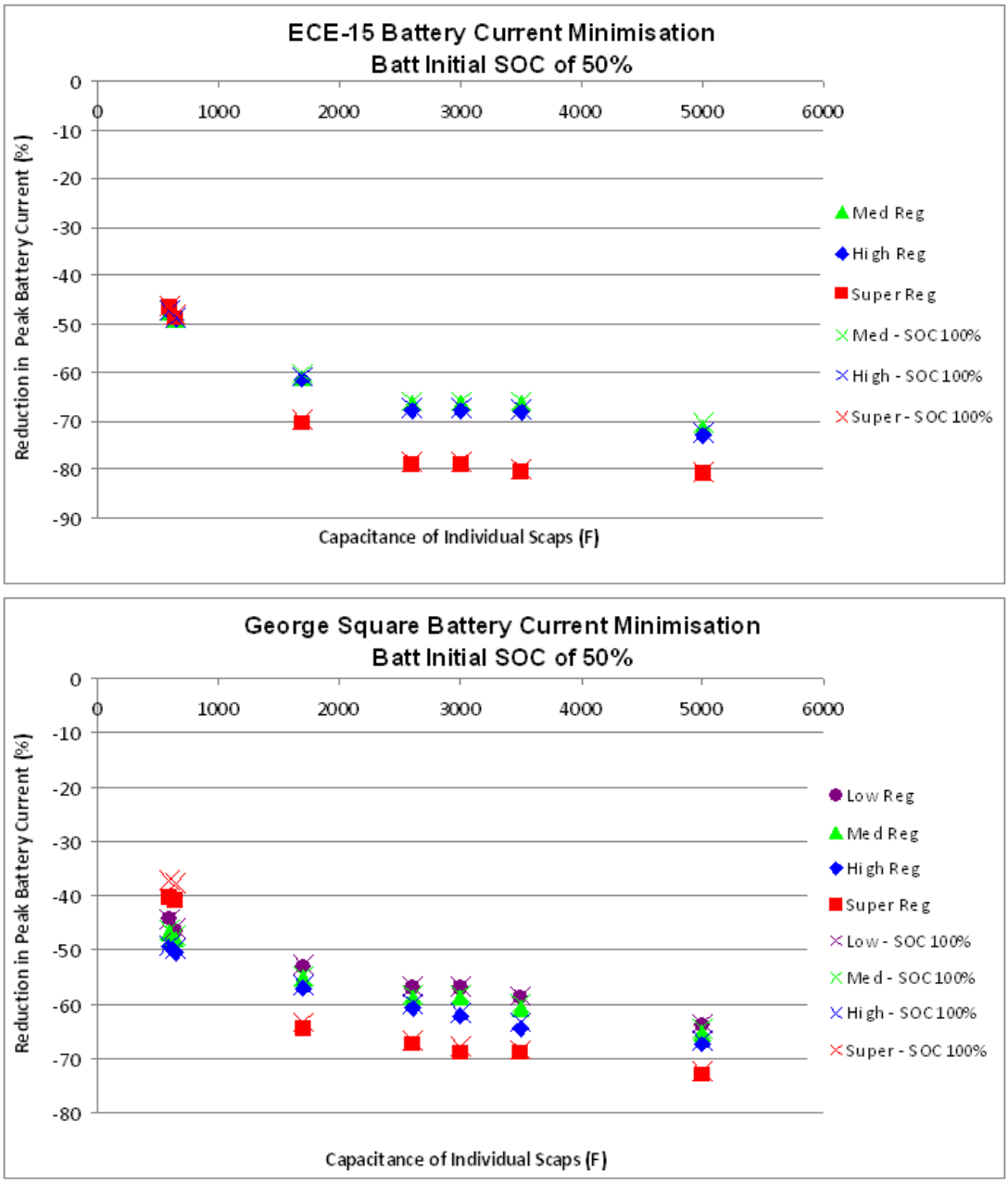

Figure 5.16: Percentage change in peak battery current for different supercapacitor sizes in each cycle, as compared to the performance of the battery-only Cobra in that cycle, for an initial battery SOC of 50%. The results for an initial battery SOC of 100% are also shown for comparison.

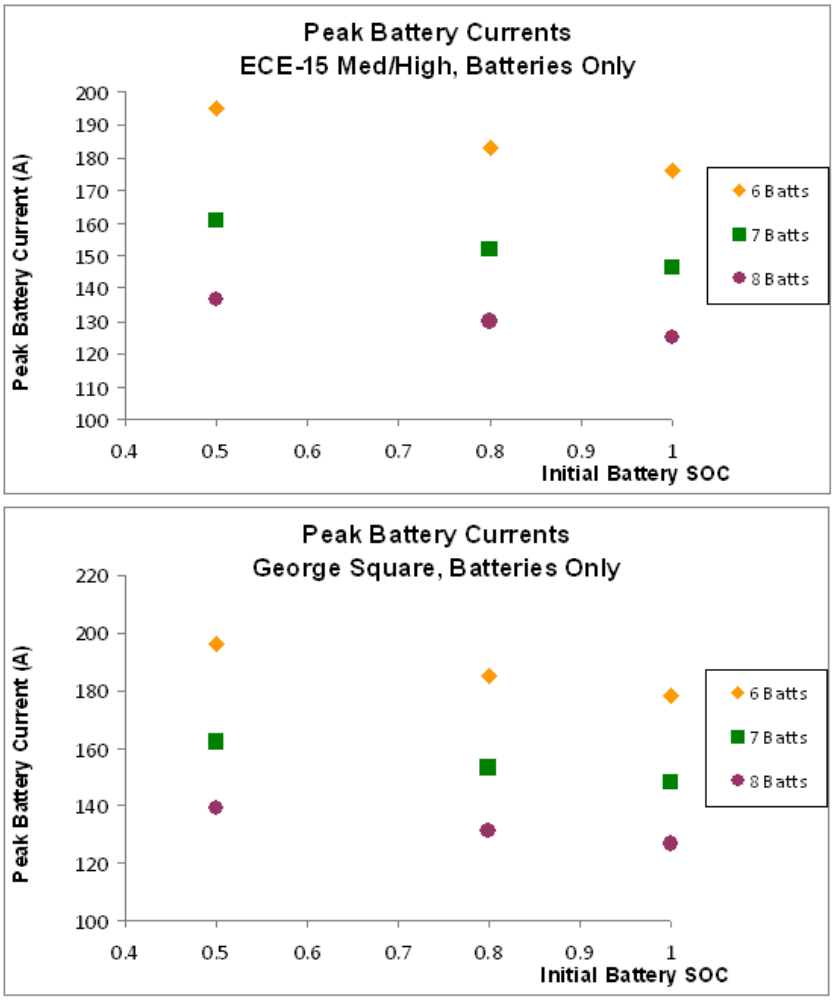

Figure 5.17: Peak battery currents for the battery-only Cobra using a pack of six, seven or eight batteries at different initial SOCs, and without any use of the supercapacitors.

5.2.3 Developing a Generic Strategy for Battery Current Minimisation

A wide range of drive cycles would need to be assessed to ensure that a generic strategy was effective. An investigation of the drive cycles used in this investigation shows that the optimal operating regions for battery current minimisation are narrow for larger supercapacitors and vary from cycle to cycle, complicating any generic strategy development. Smaller supercapacitor packs, on the other hand, have much broader optimal regions and offer a better chance for a generic strategy to have an effectiveness similar to that of the optimised strategy.

The values of PMin and PCh which produced the lowest peak battery current, and those which produced a peak battery current within 10% of the lowest value, were found for each tested supercapacitor in each drive cycle. Results for the Maxwell 650F supercapacitor are shown in Figure 5.18. The ECE-15 cycles have a broad operating region, especially the Super Regeneration cycle, while the George Square operating region is narrower. Only three points produce peak battery currents within 10% of the lowest value achieved for the 650F capacitor pack for all cycles: PMin = 6200W and PCh = 600 or 800W; PMin = 6400W and PCh = 400W.

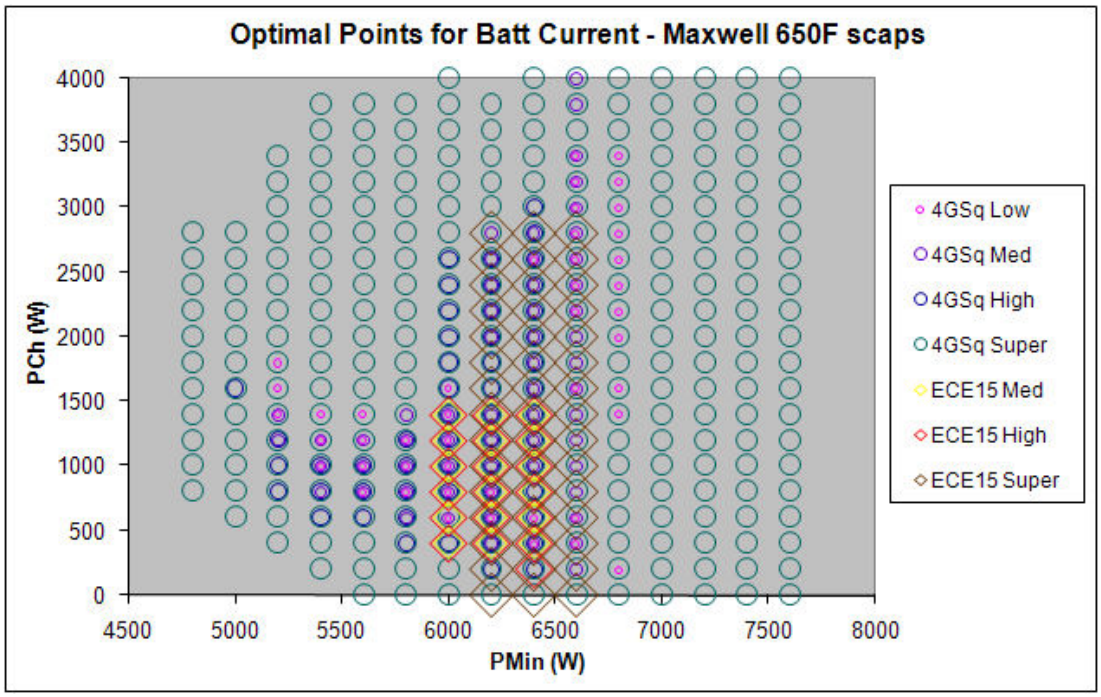

Figure 5.18: Values of PMin and PCh which provide the minimum peak battery currents, or a peak battery current within 10% of the minimum, for the Maxwell 650F supercapacitors in each of the simulated drive cycles.

For the next smallest supercapacitor simulated, the Ness 1700F, each cycle has a more sharply defined optimal operating region, as shown in Figure 5.19. In most cycles the peak battery current is created when the battery outputs both its controlled minimum power (PMin) plus the supercapacitor charging value (PCh). This explains the diagonal shape of the optimal operating regions. For some cycles, high values of PMin create the peak battery current – the battery only charges the supercapacitors during times of low traction power and so many values of PCh may be used during

the cycle to produce similar peak currents. No operating point creates optimal results for all 7 cycles.

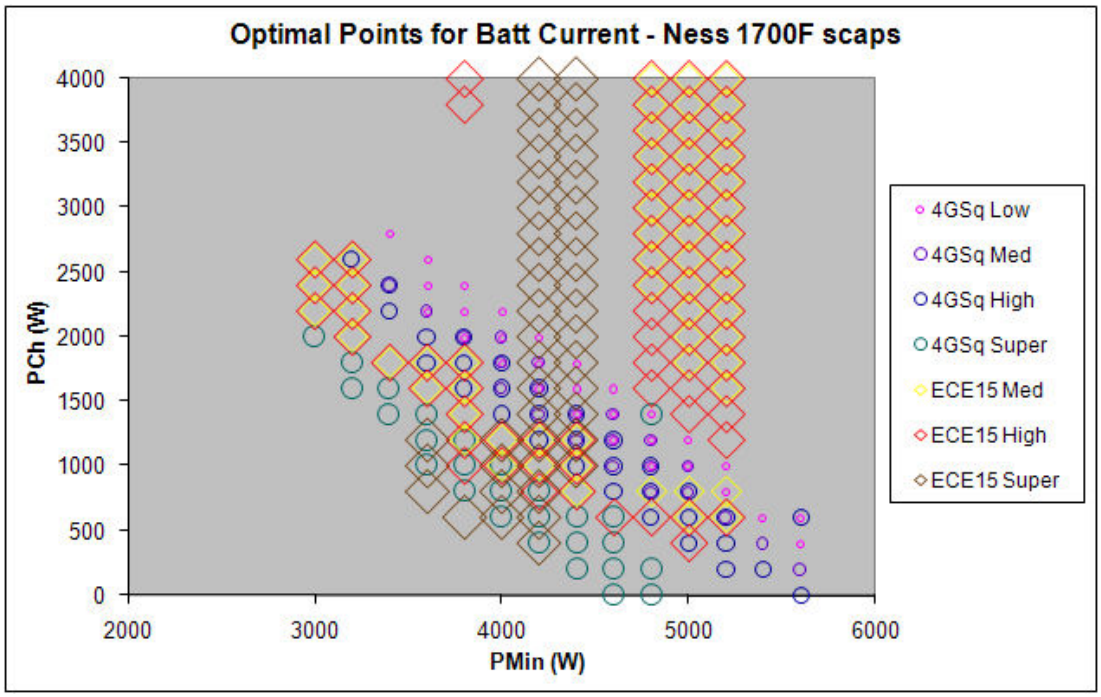

Figure 5.19: Values of PMin and PCh which provide the minimum peak battery currents, or a peak battery current within 10% of the minimum, for the Maxwell 1700F supercapacitors in each of the simulated drive cycles.

As the capacitance of the supercapacitors increases, suitable operating regions for each cycle become smaller and more distinct. Results for the Maxwell 3000F supercapacitors and for the Ness 5000F supercapacitors are shown in Figure 5.20. Note that for the 5000F supercapacitors in the George Square Medium and High Regeneration cycles, there are only three optimal points: the point which created the lowest peak battery current for the cycle and two others which produced peak battery currents within 10% of this value. This indicates that optimising for battery current is not a trivial task, and would require active management during a drive with adjustments to the control strategy being made by the software to adapt to the different driving conditions.

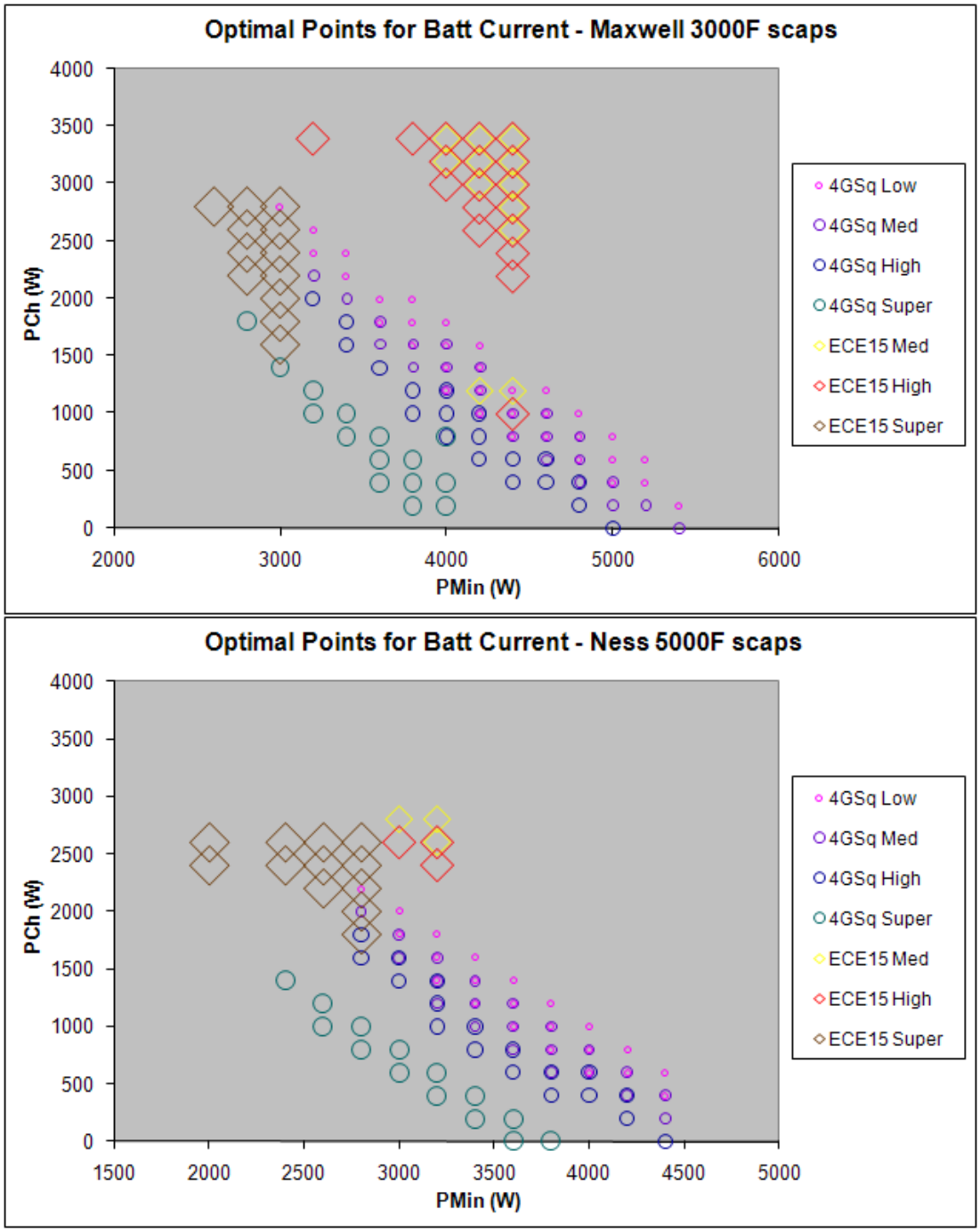

Figure 5.20: Values of PMin and PCh which provide the minimum peak battery currents, or a peak battery current within 10% of the minimum, for the Maxwell 3000F supercapacitors (upper plot) and for the Ness 5000F supercapacitors (lower plot) in each of the simulated drive cycles.

5.2.4 Comparison to Results from Literature

Most existing battery/supercapacitor vehicles do not focus on battery current reduction, although many suggest that battery life will be extended they do not offer

a quantitative analysis [33, 62, 63]. Based on battery current plots, the EVermont vehicle has a current reduction of approximately 25-42%, from peak currents of 200-240A for the battery-only vehicle to peak currents of 140-150A for the hybrid [57, 58]. A single battery current plot shown in [51] shows the battery currents in the Chilean vehicle reduced by approximately 67%, with the vehicle controlled to have a peak battery current of no more than 40A. By contrast, the battery current minimisation strategy described in this thesis is predicted to reduce peak battery currents by 37-80%, depending on the cycle and the supercapacitor pack.

Whether battery current reduction is a worthwhile use for supercapacitors or not hinges on a determination of the extent to which battery life can be extended by this process. Recall that the batteries tested at the University of Hawaii, as described in Section 2.7.4, had a life extension of 253%, 13 cycles to 33 cycles, following a current reduction of 80%. This level of current reduction is possible for some cycles, as shown in Figure 5.11. If typical lead acid batteries in regular use are expected to last for 3 years in an electric vehicle, then an equivalent life extension would mean they would last 7.6 years. Meanwhile, a study of experimental lead-acid battery cells created and tested at the Bulgarian Academy of Sciences [44] found an increased life span of the positive plates by up to 50% for a 33% reduction in peak current density, although some of the plates did not experience a life extension. This same group also found a life extension of approximately 137% for a plate following an 83% reduction in peak current density. This study was based on a current profile derived from an electric vehicle drive cycle, with an original peak current density of 300A/kg, which led to a positive plate life of 400 cycles.

However, the batteries used at the University of Hawaii were regular car starter batteries, not electric vehicle batteries, and thus it cannot be assumed that their performance is directly analogous to that of the Cobra batteries. Certainly a lifetime of 13 or 33 cycles would be a pitiful performance for any electric vehicle. The Bulgarian batteries were experimental traction batteries which focussed on the positive plates alone, and thus can also not be taken as directly analogous to the Cobra batteries. Conducting extensive lifetime testing of a variety of batteries is the

only way to know for certain if the proposed magnitude of current reduction will provide a substantial enough increase to the life of the batteries. As it is inherently expensive and time consuming to carry out such lifetime tests, the literature is critically limited in this regard, and thus the effects of peak current magnitude on battery life cannot be quantified in a statistically significant fashion. Recall, however, that life tests performed on the EVermont batteries with a peak current reduction of approximately 35% did not result in a significant life extension [58].

The financial savings which battery life extension could provide to a vehicle depend both on the battery costs and on the life of the car itself. Life costs for an electric vehicle have previously been considered for a 10 year span [21] and a 12 year span [51]. Another group, arguing that EVs are likely to last much longer than ICE vehicles due to lower vibrations, suggest that a typical vehicle might last as long as 17 years, a value calculated based on the assumption that the vehicle is driven for 165,000 miles in its life [15].

Battery costs for the Cobra for different vehicle and battery life spans are shown in Table 5.6. These costs have been calculated given the original cost of £924.84 for the batteries and assuming a base battery life of 3 years, with additional rules taken from [15], as follows:

- Replacement batteries cost 80% of the original price due to lower overheads, thus £739.87 for replacement Cobra batteries.
- Used batteries which have not reached the end of their life may be resold at 70% of the replacement cost, multiplied by the fraction of life remaining. For example, if the last set of batteries were used for half their total lifespan, they could be resold for 0.5*0.7*739.87, or £258.96.
- Batteries with less than 10% of their life remaining have no resale value.
- If new batteries would be used for less than 15% of their life before the vehicle life ends, then the new batteries are not purchased and instead the old batteries are used for longer than usual.

Table 5.6: Battery costs for different life spans of vehicle and battery.

Car Life (yrs)	Base Case (3 year batt. life)	Battery Life Extension of:				
		10%	20%	50%	100%	253%
9	£2,404.58	£2,263.34	£2,145.63	£1,664.71	£1,405.76	£1,242.21
10	£2,799.18	£2,404.58	£2,289.49	£2,001.76	£1,492.08	£1,310.35
11	£2,971.82	£2,799.18	£2,404.58	£2,116.86	£1,578.39	£1,378.50
12	£3,144.46	£2,956.12	£2,799.18	£2,231.95	£1,664.71	£1,446.64
13	£3,539.05	£3,144.46	£2,943.05	£2,347.04	£1,972.99	£1,514.79
14	£3,711.69	£3,491.97	£3,086.91	£2,404.58	£2,059.31	£1,582.94
15	£3,884.33	£3,648.91	£3,452.74	£2,799.18	£2,145.63	£1,664.71
16	£4,278.93	£3,805.86	£3,596.60	£2,914.27	£2,231.95	£1,664.71
17	£4,451.56	£4,184.76	£3,740.46	£3,029.36	£2,318.27	£2,009.34
18	£4,624.20	£4,341.70	£3,884.33	£3,144.46	£2,404.58	£2,077.48
19	£5,018.80	£4,498.65	£4,250.15	£3,481.51	£2,712.86	£2,145.63
20	£5,191.44	£4,624.20	£4,394.02	£3,596.60	£2,799.18	£2,213.77

As mentioned in the previous section, the supercapacitor packs would cost at least £1,407.77 for the Maxwell 650F supercapacitors, up to £3,327.47 for the Ness 5000F supercapacitors, including power electronics and integration boards. The supercapacitor should last at least 10 years, perhaps longer given the cold climate in Britain [116]. The savings in battery costs based on different life extensions relative to the base cost of a 3-year battery life are shown in Table 5.7. The base cost of the different supercapacitor packs, including power electronics and integration kits, are also shown with colour coding. The battery life extension savings are likewise coloured to indicate which options would be cost-effective for different supercapacitor pack sizes. Note, however, that vehicle life spans in excess of 10 years have an increasing likelihood that the supercapacitors themselves would need to be replaced, incurring additional costs. Some portions of the power electronics might also need replacing during the life of the vehicle, although this would be less problematic for the vehicle owner as these would represent relatively small sums at the time of replacement.

This table indicates that a battery life extension of 50% (to 4.5 years) could be financially viable if this could be achieved with small supercapacitors and if the vehicle has a life span of at least 17 years. This would also require the supercapacitor pack itself to last for the full life of the vehicle. A battery life

extension of 100% offers more possibility for success for the supercapacitors, while the full 253% achieved by the Hawaii battery pack would make a supercapacitor pack worth using for any vehicle life of 10 years or more. Taking a battery life extension of 100%, the supercapacitor pack should consist of 2600F supercapacitors or smaller. As the 2600F capacitor size is no longer available from Maxwell, this leaves three options: 1700F, 650F or 600F. The 1700F supercapacitors were found to reduce the peak battery currents by up to 70%, while the 650F and 600F capacitors reduced currents by up to 50% and 49%, respectively.

Table 5.7: The cost savings of different battery life extension values, relative to the base cost of a 3-year battery life. This is compared to the base cost of the supercapacitor packs with power electronics, and colour-coded to indicate which packs would be affordable.

Car Life	Battery Life Extension of:					S-Cap Type	Pack Cost (w/ PE)
	10%	20%	50%	100%	253%		
9	£141.25	£258.96	£739.87	£998.83	£1,162.38		
10	£394.60	£509.69	£797.42	£1,307.11	£1,488.83		
11	£172.64	£567.24	£854.96	£1,393.43	£1,593.32	M650	£1,407.77
12	£188.33	£345.27	£912.51	£1,479.74	£1,697.81	N600	£1,692.47
13	£394.60	£596.01	£1,192.02	£1,566.06	£2,024.26	N1700	£2,022.47
14	£219.72	£624.78	£1,307.11	£1,652.38	£2,128.75	M2600	£2,232.47
15	£235.41	£431.59	£1,085.15	£1,738.70	£2,219.62	M3000	£2,449.37
16	£473.07	£682.33	£1,364.65	£2,046.98	£2,614.21	N3500	£2,742.47
17	£266.80	£711.10	£1,422.20	£2,133.30	£2,442.23	N5000	£3,327.47
18	£282.50	£739.87	£1,479.74	£2,219.62	£2,546.72		
19	£520.15	£768.64	£1,537.29	£2,305.93	£2,873.17		
20	£567.24	£797.42	£1,594.84	£2,392.25	£2,977.66		

Modest battery life extensions of 10% or 20% would mean that supercapacitors today are not cost-effective. The total cost of supercapacitors, power electronics and integration kits would need to be reduced by an order of magnitude for this to become a worthwhile reason for hybridisation. On the other hand, a single additional battery for the Cobra costs £154.14 and reduces peak battery currents by up to 16.9% - if this is sufficient to extend the battery life by 10%, then this would be a cost-effective addition to the vehicle.

5.3 Combining Strategies for Efficiency and Battery Current Reduction

The author has shown that supercapacitors, as part of a battery hybrid energy source, are very effective at reducing peak battery currents, and ineffective at increasing vehicle range. This shows that the primary goal of a battery/supercapacitor strategy should be current reduction. However, ideally the supercapacitors would reduce the currents while increasing the vehicle range as much as they are able – this would create the maximum benefit. But is this possible?

Strategies which produced the minimum peak battery current and strategies which produced the maximum yield rarely overlapped. Of the 49 cases simulated (seven supercapacitor types in seven drive cycles), only 5 contained such overlaps (one of which had two overlaps). The overlapping points are shown in Table 5.8 – the George Square Low Regeneration cycle features the most overlaps.

Strategies which minimised battery current were generally very efficient. In 43 of the 49 cases simulated, each strategy which produced the minimum peak battery current was within 1% of the maximum yield. The six remaining cases are described in Table 5.9. Battery current optimisation strategies most frequently produced lower yields in the George Square Super Regeneration cycle. The results of Tables 5.8 and 5.9 show that higher levels of regenerative braking are associated with a greater disconnect between battery current and yield optimisation strategies. Also note that for the 600F supercapacitor pack, a battery current optimisation strategy sometimes results in a lower yield than that which is produced by the batteries alone, even when a higher yield is possible through efficiency optimisation. This means that optimising for reduced battery currents may result in a net loss of efficiency for the vehicle.

Strategies which optimised for yield, on the other hand, frequently did not create good results for battery current, although the peak currents were always below those which occurred when the batteries were operating alone. In only two of the 49 simulated cases did every yield optimising point create a peak battery current which was within 10% of the minimum (as found when optimising for battery current),

while 18 more had some of the optimal yield points producing peak battery currents within 10% of the minimum. This leaves 29 cycles for which the optimal yield points had battery currents that were always higher than this. These points are shown in Table 5.10.

Table 5.8: Operating points which provide optimal results for both battery current and yield

Cycle	S-Cap	PMin (W)	PCh (W)	Peak Battery I (A)	Yield (km/kWh)
ECE-15 Med	600F	6200	400	93	6.90
ECE-15 High	1700F	3800	1400	69	7.17
GSq Low	1700F	4600	1200	84	5.65
		4200	1600		
	2600F	4200	1200	77	5.68
	3000F	4200	1200	77	5.69

Table 5.9: Operating points in which optimising for peak battery current produced a yield which was less than 1% of the maximum value achieved by that hybridisation on that cycle.

Cycle	S-Cap	Peak Battery I (A)	Yield Produced (km/kWh)	Best Yield (km/kWh)	Battery-only Yield (km/kWh)
GSq High	600F	90	6.03-6.04	6.12	6.10
GSq Super	600F	111	6.59-6.89	6.98	6.66
	650F	110	6.90-6.92	6.99	
	2600F	59	7.00	7.09	
	3000F	57	6.98-7.00	7.09	
	3500F	56	7.00-7.02	7.09	

Optimising for yield produces a marked increase in peak battery currents for most of the supercapacitor packs and drive cycles simulated, while optimising for minimum battery currents tends to result in only slightly reduced yields. However, this relationship should not be assumed to hold for any drive cycle, and in particular the smallest supercapacitor packs may produce net efficiency losses to the vehicle if used to optimise for reduced peak battery currents.

Table 5.10: Operating points in which optimising for yield produced a peak battery current which was more than 10% of the maximum value achieved by that hybridisation on that cycle.

Cycle	S-Cap	Peak Yield (km/kWh)	Peak Battery I Produced (A)	Min. Peak Battery I (A)	Battery-only Peak Batt. I (A)
ECE-15 Med	1700F	6.99	80	70	176
	2600F	7.03	69-72	60	
	3000F	7.03	69-76	60	
	3500F	7.03	69-79	60	
	5000F	7.04	66-79	52	
ECE-15 High	650F	7.09	124	90	176
	2600F	7.22	66-72	58	
	3000F	7.22	66-76	58	
	3500F	7.22	69-76	57	
	5000F	7.24	72	49	
ECE-15 Super	600F	8.84	129	96	179
	650F	8.87	124	93	
	2600F	9.12	48-54	39	
	3000F	9.13	48-51	39	
	3500F	9.13	48-51	36	
	5000F	9.14	45-60	35	
GSq Low	600F	5.64	164	99	178
	650F	5.64	164	96	
GSq Med	600F	5.84	164	95	177
	650F	5.84	140-164	93	
GSq High	600F	6.12	164	90	177
	650F	6.12	148-164	89	
	5000F	6.20	69-76	59	
GSq Super	600F	6.98	148-163	111	177
	650F	6.99	143-158	110	
	2600F	7.09	69-75	59	
	3000F	7.09	66-75	57	
	3500F	7.09	72	56	
	5000F	7.10	61-69	49	

5.4 Generic Methodology for Assessing Optimisation Schemes

This chapter has so far described a methodology developed by the author for selecting an optimisation strategy for the Cobra, and sizing the supercapacitor pack based on this optimisation. The same methodology could be used for other battery-powered vehicles for which a hybridisation with supercapacitors was being

contemplated as a means of either increasing vehicle range or as a way to minimise peak battery currents.

For a battery/supercapacitor hybridisation to be a cost-effective vehicle design strategy, it must offer greater benefits than operating the vehicle with batteries alone. For the Cobra, the hybridisation option has been compared to the addition of a further lead-acid battery, instead of the supercapacitors. This provides a suitable comparison, as the additional battery adds comparable weight to the vehicle as would a supercapacitor pack, and is much simpler to implement. In general, the comparison between additional batteries and a hybridisation strategy must be made with similar metrics – if the individual batteries are much smaller than the supercapacitors (as for Li-ion batteries, for example), then the comparison should consider the addition of a number of batteries equivalent to the supercapacitor weight. Volume constraints may also be considered.

The comparison between addition of further batteries and hybridisation with supercapacitors serves to determine if hybridisation is a cost-effective adaptation to the vehicle. If the supercapacitors are to act as range extenders, then this means they will need to provide a considerable increase to yield at a low cost. As discussed in Section 5.1.4, this is not currently possible due to the high cost of supercapacitors.; furthermore, the superior energy density of batteries makes them much more effective than supercapacitors at providing range extension.

If the supercapacitors are to minimise battery currents, then this means they will need to provide a significant battery life extension to reduce lifetime vehicle costs. This has been shown to be theoretically possible in Section 5.2.4. For a hypothetical vehicle using this methodology, battery lifetime information would be needed for the battery chemistry used in the vehicle. Lead acid batteries are very cheap compared to other types of battery – sample cost data as shown in Table 1.1 shows NiMH batteries costing 2.4 times more per Wh, and Li-ion batteries more than 7 times more expensive. However, Li-ion batteries also have twice the cycle life of the lead acid batteries, and NiMH batteries almost three times the cycle life. By comparing the

lifetime costs of the battery-supercapacitor hybrid vehicle with the lifetime costs associated with normal vehicle operation, the cost-effectiveness of this strategy can be assessed. The lifetime cost benefits of adding further batteries to the vehicle may also be assessed for comparison.

5.5 Chapter Summary

The Cobra was simulated on each of the drive cycles described in Section 3.5, with a variety of energy storage options. As a base case, the Cobra was modelled with the six batteries comprising its original battery pack. The simulations were performed at different initial battery states of charge: 100%, 80% and 50%. The Cobra was also modelled with somewhat larger battery packs of seven and eight batteries. The performance of the Cobra with these larger battery packs provided a comparison to the performance of the battery/supercapacitor hybrid Cobra. This allowed an assessment of whether the benefits provided by the supercapacitors would be better achieved with the addition of further batteries.

The battery/supercapacitor hybrid Cobra was modelled using six batteries and packs of thirty supercapacitors, with simulations for seven different packs consisting of different commercially available capacitors. Again, the battery pack was modelled as having different initial SOCs. The different values of PMin and PCh allowed the hybrid Cobra to be optimised for either minimum peak battery currents or for maximum yield.

The yield optimisations demonstrated that the supercapacitors could be used to improve the efficiency of the Cobra. These improvements were more effective if the Cobra had higher levels of regenerative braking. Larger supercapacitor packs provided more efficiency gains, partly because commercial supercapacitors have higher internal resistance if the capacitance is lower. For example, 650F supercapacitors from Maxwell have an internal resistance of 0.8mΩ, while the 5000F capacitors from Ness have an internal resistance of just 0.33mΩ. The greater efficiency of the larger supercapacitor packs is also due to the fact that they use less of their stored energy and thus maintain a high voltage. The 600F, 650F and 1700F supercapacitors cause net efficiency losses to the vehicle in Low and Medium

Regeneration cycles and for the High Regeneration ECE-15 cycle, even when optimised for maximum yield. For the remaining supercapacitors, the increase in capacitance from 2600F to 5000F produced little difference in peak yield. Lower battery SOC meant that the supercapacitors provided greater benefits to efficiency in terms of percentage increase in yield.

However, the ultimate purpose for efficiency improvements is to enable the vehicle to travel farther on a single charge. For range increases, it is far more effective to add an additional battery to the vehicle as this both improves the yield of the vehicle and adds to the stored energy. The hybridisation offered a maximum range improvement of 9.4%, using the 5000F supercapacitors on the George Square Super Regeneration cycle, including both yield and additional energy from charging the supercapacitors at the same time as the batteries, and assuming the batteries began at 100% SOC. If the batteries began at 50% then the range improvement increased to a maximum value of 11%. However, adding a single battery to the pack instead of hybridising the vehicle would add a minimum of 18.1% to the vehicle range, rising to 20.1% if the battery began at 50% SOC. Given that a single Cobra battery costs £154.14 while a supercapacitor pack plus power electronics and integration boards costs between £1,407.77 and £3,327.47, it is clear that adding a battery to the Cobra is the best way to increase its range, and this remains the case even with a substantial decrease in supercapacitor price.

The battery current optimisations showed that the supercapacitor packs could be used to reduce battery currents by as much as 80% for the 5000F supercapacitor in the ECE-15 Super Regeneration cycle (not far off the theoretical maximum reduction for that cycle of 85%), while even the smallest supercapacitor pack could reduce battery currents by up to 49%. Larger supercapacitor packs were more effective at reducing battery currents, as a large capacitance is needed to handle the power fluctuations in the vehicle. Increased availability of energy from regenerative braking typically increased the effectiveness of the hybridisation, with the notable exception of the 600F and 650F supercapacitors used on the George Square Super Regeneration cycle.

Hybridisation with supercapacitors offers a much more effective method of reducing battery currents than adding additional batteries. A single additional battery, if added to the Cobra, can reduce battery currents by only 16.9%, while a second added battery would reduce currents by 28.8%. However, the narrow operating region for PMin and PCh values to produce optimal results, and the variability of optimal PMin and PCh values, would make this strategy difficult to implement in a practical setting.

Ultimately the purpose of minimising battery currents is to prolong the battery life. At present there is not enough data in the literature to state conclusively whether or not this is an effective method. Battery life would need to be extended by at least 50% for commercially available supercapacitors to be useful, and this would additionally require the supercapacitors themselves to survive for up to 20 years in the vehicle. A more conservative life extension of 10-20% would require the cost of installing supercapacitors in the Cobra to be reduced by an order of magnitude in order for this to be a cost-effective approach.

For the drive cycles simulated for the Cobra, a battery current minimisation strategy will typically produce yields within 1% of the yields found in the efficiency maximising strategy. However, the 600F supercapacitor packs sometimes saw a net decrease in efficiency when optimised for battery currents. Strategies to optimise efficiency, on the other hand, frequently saw significantly higher battery currents than those to minimise the currents, albeit still below the currents produced when the batteries were used alone. Lower levels of regenerative braking meant the two different optimisation strategies were more likely to be compatible.

6 Conclusions

This thesis has described the development of a model of a battery/supercapacitor hybrid vehicle. The complete hybrid model consisted of three components:

1. a novel battery model
2. a simple supercapacitor model
3. a power electronics efficiency map.

The model power flows were controlled using a novel, tuneable control strategy that allowed for different optimisations. The hybrid model and control strategy are described in Section 4.5.

Two possible optimisations formed the focus of this work, specifically an optimisation to maximise the vehicle's efficiency, and an optimisation to minimise the battery currents. This allowed an assessment of the relative efficacy of these two strategies.

6.1 Model development

The Cobra batteries were simulated using a novel Matlab/Simulink-based model developed by the author and suitable for use within ADVISOR – this model is detailed in Section 3.2 and verified in Section 3.3. This model was created to strike a balance between accuracy and ease of implementation when used in a broader vehicle simulation system. The model calculates the voltage and current in the batteries based on power demand information and demonstrated a peak error of 3.1%. This is a significant improvement on the models provided as standard within ADVISOR, which were reported as having peak errors of 12% for the 'Rint' model and of 4% for the 'RC' model [127]. The model was used to simulate the behaviour of the battery-only Cobra, and was later combined with the supercapacitor and power electronic models to simulate the hybrid Cobra.

The supercapacitors were simulated using a simple Matlab/Simulink model designed to use the nameplate details of a variety of commercial capacitors, as described in Section 4.3. This enabled the hybrid battery/supercapacitor vehicle model to be used to investigate a wide range of hybridisation options. The supercapacitor model was

verified using commercial supercapacitors from Maxwell with a peak error of less than 5%. The supercapacitors and batteries were interfaced to each other using efficiency maps, shown in Section 4.4, representing two half bridge DC/DC converters.

Finally, the model contained a novel control strategy to direct power flow in the hybrid energy storage system. This strategy was designed to be 'tuneable' to optimise for different variables. This work focussed on two options for optimisation: maximising vehicle efficiency and minimising battery currents. The operational details for each optimisation were found through simulation and the efficacy of the optimisations were compared, along with the implementation costs associated with installing the supercapacitors. The results of this study may be found in Chapter 5, with Section 5.1 providing details of the efficiency optimisation strategy and Section 5.2 focussing on the battery current minimisation strategy.

The choice of optimisation strategy was found to have a significant impact on the overall effectiveness of the hybridisation. This is discussed in detail in Section 5.3. Previously constructed battery/supercapacitor hybrid vehicles have mostly focussed on maximising efficiency, with the assumption that battery life will be enhanced as a result. The results of this study have shown that such a strategy will not provide the most effective hybridisation for the vehicle. Using a tuneable control strategy as described in this thesis would provide future experimental vehicles with a means to assess a range of strategies and to confirm that the hybridisation will be used to the best effect. A similar strategy could also be applied to other types of hybrid vehicle which provide a variety of possible hybridisation benefits, and hence a variety of optimisation schemes.

6.2 Optimal Use of Supercapacitors

The author has demonstrated that while supercapacitors may be combined with batteries to improve the efficiency of an electric vehicle, this in itself is not a cost-effective method of hybridisation. This is because while a more efficient vehicle is capable of travelling further on a single charge, directly increasing its range by

installing an additional battery is a far more effective and inexpensive method of achieving range extension.

The addition of a supercapacitor pack was found to increase the range of the Cobra by up to 9.4% for the investigated drive cycles, using a supercapacitor pack containing thirty 5000F supercapacitors in series. Smaller packs produced even smaller gains in range – packs consisting of 1700F supercapacitors or smaller typically resulted in overall efficiency losses and a resultant decreased range. By contrast, a single additional battery added to the Cobra would increase its range by a minimum of 18.1%. The additional battery would cost only £154.14, while the supercapacitors would cost £1407.77 for the cheapest pack (650F capacitors from Maxwell) plus power electronics, and up to £3,327.47 if the most expensive pack, that of the Ness 5000F capacitors, were used instead.

Furthermore, a review of existing battery/supercapacitor vehicles described in the literature has shown that these results would hold true for these vehicles as well. No vehicle achieved an improvement to efficiency or range with the supercapacitors beyond what it could have achieved by increasing the size of its battery pack. The high cost of supercapacitors relative to batteries means that this is not likely to become a cost-effective strategy in the future.

On the other hand, supercapacitors are very effective at reducing battery currents. Battery current minimisation has previously been shown to extend battery life [44, 140], although a specific relationship between peak current and life span for traction batteries has not been established. For the drive cycles investigated in this research, the perfect control of a drive cycle, where the battery produces a constant current output throughout, would result in a 79-86% reduction in the peak battery current. The control strategy developed by the author, when optimised for battery current reduction, has achieved current reductions of up to 80% for the largest investigated pack of thirty 5000F supercapacitors, and up to 49% for the smallest pack of thirty 600F supercapacitors. This has the potential to offer significant extensions to battery life, as comparable reductions in peak current resulted in a life extension of 253% for

lead-acid starter batteries [140], and of 137% for experimental lead-acid traction batteries [44].

For the Cobra, a battery life extension of 100% (to an average of six years) would make a small supercapacitor pack financially viable, and could potentially support a 30-capacitor pack of up to 2600F each based on current costs, assuming the vehicle is used for at least 16 years and the supercapacitors themselves do not require replacement. Note that the 2600F supercapacitor pack was found to be capable of reducing battery currents by up to 78%. As this size of supercapacitor is no longer available from Maxwell, the next lower supercapacitor size of 1700F would need to be used – a pack of 30 of these capacitors was found to reduce battery currents by up to 70%, depending on the amount of regenerative braking. For the current, low regeneration capabilities of the Cobra, the 1700F supercapacitors were found to reduce peak battery currents by 53%, but with a small reduction (<1%) in vehicle efficiency. Battery life extension would need to be at least 50% to make any supercapacitor pack a financially viable option for the Cobra based on current prices.

Optimising for battery current minimisation results in slightly lower efficiencies than the efficiency maximisation strategy, typically by a value of less than 1%. However, the battery current minimisation strategy sometimes results in a net loss of efficiency for the vehicle for small supercapacitor capacitances. Optimising for maximum efficiency usually results in battery currents that are at least 10% higher than those found with the battery current minimisation strategy, up to 84% higher. Such a strategy is much less likely to produce significant battery life extensions. Therefore, the author recommends a battery current minimisation control strategy for the Cobra, with a supercapacitor pack consisting of thirty 1700F supercapacitors from Maxwell. However, if supercapacitor and power electronic costs decrease relative to the cost of batteries, then a larger supercapacitor pack would provide greater battery current reduction.

Again, based on a review of the literature it seems likely that this would be a more effective strategy for battery/supercapacitor hybrid vehicles in general. In particular,

low-cost urban vehicles which use lead-acid batteries are likely to benefit from this strategy as a means to reduce lifetime costs and increase reliability. However, further study is needed to quantify the benefits of battery current reduction to battery life span.

6.3 Summary of Contributions

This thesis has presented four aspects of novelty as accomplished by the author:

1) A methodology for comparing optimisation strategies for a battery/supercapacitor hybrid vehicle. This consists of two elements: to identify the most effective optimisation strategy for an electric vehicle, and to identify a suitable supercapacitor pack size for that strategy from a range of commercially available supercapacitor packs. The different optimisation strategies have different metrics of success, namely the improvement of efficiency and the increase in battery life. A comparison between the efficacy of supercapacitor hybridisation and that of adding an additional battery to the vehicle has been demonstrated as a basis for comparing these disparate metrics. A supercapacitor pack size can then be determined by examining both the effectiveness of the supercapacitors at achieving the desired metric and the cost of installation of the supercapacitor pack and associated equipment.

2) Using this methodology, it has been shown that the most effective hybridisation strategy for the Cobra is to minimise peak battery currents - the optimal pack size will depend on the life extension which can be achieved for the batteries, and the author has demonstrated the relationship between pack size and battery life extension. Meanwhile, the author has shown that optimising for maximised efficiency is not a cost-effective strategy. An examination of the literature shows that these results would hold true for other experimental battery/supercapacitor vehicles.

3) A novel control strategy for managing the power flow in the hybrid system, developed to be ‘tuneable’ to allow the investigation of the different options for optimisation, e.g. increased yield or lower peak battery currents. The simulations of this control strategy have demonstrated that the optimal points

for maximising yield and for minimising peak battery currents are typically not the same, and hence that choice of optimisation strategy has a significant impact on the effectiveness of a hybrid vehicle.

4) A novel battery model for use in the simulations of the hybrid system, created to provide an accurate simulation of the Cobra battery pack while remaining simple to implement within the ADVISOR framework. The model was verified with experimental data and shown to offer an improved performance to that of the standard ADVISOR models.

6.4 Future Work

The next step in this research should be a thorough investigation of battery lifetime and the effects of peak current reduction. This is essential to confirm the usefulness of supercapacitors as energy buffers in battery electric vehicles. The literature on this topic is very limited. This research would require a high power test rig and a large number of batteries to be tested, and thus will require a very large budget. This is doubtless the reason for the limitations of the published literature in this area.

The control strategy described in this thesis should be implemented and tested. It could be implemented with software designed to 'learn' by computing the optimal values for PMin and PCh as the vehicle is driven, perhaps by means of a neural net. This would allow a more practical implementation of the strategy, offering the opportunity to examine a range of drive cycles with the Cobra.

The methodology used in this work to compare an efficiency optimisation strategy with a battery current minimisation strategy could be extended to consider vehicle acceleration as well. This would be suitable for a vehicle with a peak motor power which exceeds the power capabilities of the batteries. The efficacy of the addition of a supercapacitor pack to boost vehicle acceleration would also be comparable to the efficacy of increasing the number of batteries in the pack.

Some other opportunities for future research are enumerated below:

1) Hybridisation of supercapacitors with different battery types, especially lithium-ion batteries.
2) The effects of different types of drive cycle and personal driving styles on the effectiveness of hybridisation.
3) Different types of vehicle, such as sports cars, buses and lorries, which have different needs and thus different possible optimisation strategies.
4) Extension of the battery model to include temperature effects and low SOC behaviour.

References

[1] C. Dore, T. Murrells, N. Passant, M. Hobson, G. Thistlethwaite, A. Wagner, Y. Li, T. Bush, K. King, J. Norris, P. Coleman, C. Walker, R. Stewart, I. Tsagatakis, C. Conolly, N. Brophy, and M. Hann, "UK Emissions of Air Pollutants 1970 to 2006," UK National Atmospheric Emissions Inventory (NAEI), 2008, available at http://www.airquality.co.uk/archive/reports/cat07/0810291043_NAEI_2006_Report_Final_Version(3).pdf, accessed on 15 Feb, 2009.

[2] M. Steinberg, "Fossil fuel decarbonization technology for mitigating global warming," *International Journal of Hydrogen Energy,* vol. 24, pp. 771-777, 1999.

[3] "FY 2002: Annual Progress Report for the Light Vehicle Propulsion & Ancillary Subsystems Program," United States Department of Energy, 2002, available at http://www1.eere.energy.gov/vehiclesandfuels/pdfs/program/2002_vehicle_propulsion.pdf.

[4] J. Van Mierlo, G. Maggetto, and P. Lataire, "Which energy source for road transport in the future? A comparison of battery, hybrid and fuel cell vehicles," *Energy Conversion and Management,* vol. 47, pp. 2748-2760, 2006.

[5] U. Bossel, "Efficiency of Hydrogen Fuel Cell, Diesel-SOFC-Hybrid and Battery Electric Vehicles," European Fuel Cell Forum, 2003, available at http://www.efcf.com/reports/E04.pdf, accessed on 18 Nov. 2009.

[6] M. Eberhard and M. Tarpenning, "The 21st Century Electric Car," Tesla Motors, 2006, available at http://www.teslamotors.com/display_data.php?data_name=21stCentElectricCar, accessed on 2007, no longer available.

[7] "UK Energy in Brief July 2008," Department for Business, Enterprise and Regulatory Reform, 2008, available at http://www.berr.gov.uk/files/file46983.pdf.

[8] Tesla Motors, 2009, available at www.teslamotors.com, accessed on 2 March, 2009.

[9] Going Green Limited, 2009, available at http://www.goingreen.co.uk/, accessed on 2 March 2009.

[10] G. Berdichevsky, K. Kelty, J. B. Straubel, and E. Toomre, "The Tesla Roadster Battery System," 2006, available at http://www.teslamotors.com/display_data/TeslaRoadsterBatterySystem.pdf, accessed on 24 Jan. 2010.

[11] Daimler AG smart fortwo coupé & cabrio data sheet, 2009, available at http://realwww.smart.com/is-bin/intershop.static/WFS/mpc-uk-Site/-/Editions/Root%20Edition/units/mpc-uk/default/Media/images/MPCGallery/smart_pricelist_feb09.pdf.

[12] Group Lotus plc, 2008, available at http://www.lotuscars.com/index.html, accessed on 2 March 2009.

[13] T. Woody, "Have you driven a Fjord lately?," Business 2.0 Magazine, July 31, 2007, available at http://money.cnn.com/magazines/business2/business2_archive/2007/08/01/100138830/index.htm, accessed on 11 June 2009.

[14] S. Silke Carty, "Battery leasing could help ease anxiety about hybrids," USA Today, 22 June, 2008, available at http://www.usatoday.com/money/autos/2008-06-19-hybrid-battery-lease_N.htm, accessed on 11 June 2009.

[15] M. A. Delucchi, A. Burke, T. Lipman, and M. Miller, "Electric and Gasoline Vehicle Lifecycle Cost and Energy-Use Model," University of California, Davis, Report for the California Air Resources Board,, UCD-ITS-RR-99-4, 2000.

[16] C. Lombardi, "Hawaii unveils plans for Better Place," in Planetary Gear, Dec 3, 2008, available at http://news.cnet.com/8301-17912_3-10112095-72.html?tag=mncol;txt, accessed on 18 March 2009.

[17] A. A. Adly, A. F. Zobaa, and G. J. Nolan, "Trends, features and recent research efforts in the field of hybrid electric vehicles," *International Journal of Alternative Propulsion,* vol. 1, pp. 1-5, 2006.

[18] P. Corbo, F. Corcione, F. Migliardini, and O. Veneri, "Experimental assessment of energy-management strategies in fuel-cell propulsion systems," *Journal of Power Sources,* vol. 157, pp. 799-808, 2006.

[19] K.-H. Hauer and B. Narayanan, "Numerical Simulation of Two Different Ultra Capacitor Hybrid Fuel Cell Vehicles," in the Proceedings of Electric Vehicle Symposium 18, 2001, CD-ROM.

[20] J. R. Szczesny, "As Electric Cars Arrive, Where Will They Plug In?," Time Magazine, 2009, available at http://www.time.com/time/business/article/0,8599,1940117,00.html, accessed on 18 Jan. 2010.

[21] A. Baisden and A. Emadi, "ADVISOR-Based Model of a Battery and an Ultra-Capacitor Energy Source for Hybrid Electric Vehicles," *IEEE Transactions on Vehicular Technology,* vol. 53, pp. 199-205, Jan 2004.

[22] P. Van den Bossche, F. Vergels, J. Van Mierlo, J. Matheys, and W. Van Autenboer, "SUBAT: An assessment of sustainable battery technology," *Journal of Power Sources,* vol. 162, pp. 913-919, 2006.

[23] M. Mastragostino and F. Soavi, "Strategies for high-performance supercapacitors for HEV," *Journal of Power Sources,* vol. 174, pp. 89-93, 2007.

[24] P. Lailler, F. Zaninotto, S. Nivet, L. Torcheux, J.-F. Sarrau, J.-P. Vaurijoux, and D. Devilliers, "Study of the softening of the positive active-mass in valve-regulated lead-acid batteries for electric-vehicle applications," *Journal of Power Sources,* vol. 78, pp. 204-213, 1999.

[25] H. Bode, *Lead-Acid Batteries*, ISBN: 0471084557, London, John Wiley & Sons, 1977.

[26] P. Ruetschi, "Aging mechanisms and service life of lead-acid batteries," *Journal of Power Sources,* vol. 127, pp. 33-44, 2004.

[27] A. Burke, "The Present and Projected Performance and Cost of Double-layer and Pseudo-capactive Ultracapacitors for Hybrid Vehicle Applications," in the Proceedings of IEEE Vehicle Power and Propulsion Conference, 2005, pp. 356-366

[28] R. Ball, "Supercapacitors See Growth as Costs Fall," Electronics Weekly, 2006, available at http://www.electronicsweekly.com/Articles/2006/03/01/37810/supercapacitors-see-growth-as-costs-fall.htm, accessed on 23 Feb, 2009.

[29] P. Pereirinha and J. Trovao, "Comparative Study of Multiple Energy Sources in Different Utilizations of a Small Electric Vehicle," in the Proceedings of 3rd European Ele-Drive Transportation Conference (EET-2008), Geneva, Switzerland, 2008, CD-ROM.

[30] R. Carter and A. Cruden, "Strategies for control of a battery/supercapacitor system in an electric vehicle," in the Proceedings of International Symposium on Power Electronics, Electrical Drives, Automation and Motion (SPEEDAM 2008), Ischia, Italy, 2008, pp. 727-732

[31] R. Carter and A. Cruden, "Strategies for maximising battery lifetime in a battery/supercapacitor system for an electric vehicle," in the Proceedings of 3rd European Ele-Drive Transportation Conference (EET-2008), Geneva, Switzerland, 2008, CD-ROM.

[32] T. Markel, A. Brooker, T. Hendricks, V. Johnson, K. Kelly, B. Kramer, M. O'Keefe, S. Sprik, and K. Wipke, "ADVISOR: a systems analysis tool for advanced vehicle modeling," *Journal of Power Sources,* vol. 110, pp. 255-266, 2002.

[33] F. Brucchi, F. Giulii Capponi, F. Smargiasse, and P. Santoro, "High Efficiency-Low Cost Powertrain for Urban Electric Vehicle," in the Proceedings of Electric Vehicle Symposium 24, Stavanger, Norway, 2009, CD-ROM.

[34] L. Gao, A. Dougal, and S. Liu, "Active Power Sharing in Hybrid Battery/Capacitor Power Sources," in the Proceedings of Applied Power Electronics Conference and Exposition, 2003, vol. 1, pp. 497-503

[35] S. Pay and Y. Baghzouz, "Effectiveness of Battery-Supercapacitor Combination in Electric Vehicles," in the Proceedings of Power Technology Conference, 2003, vol. 3,

[36] D. Baert and A. Vervaet, "Lead-acid battery model for the derivation of Peukert's Law," *Electrochimica Acta,* vol. 44, pp. 3491-3504, 1999.

[37] A. Vervaet and D. Baert, "The lead acid battery: semiconducting properties and Peukert's Law," *Electrochimca Acta,* vol. 47, pp. 3297-3302, 2002.

[38] D. Doerffel and A. Sharkh, "A critical review of using the Peukert equation for determining the remaining capacity of lead-acid and lithium-ion batteries," *Journal of Power Sources,* vol. 155, pp. 395-400, 2006.

[39] Compagnone, "A new equation for the limiting capacity of the lead/acid cell," *Journal of Power Sources,* vol. 35, pp. 97-111, 1991.

[40] EnerSys Hawker Genesis EP Lead Acid Batteries data sheet, 2008, available at http://www.enersysreservepower.com/documents/US-EP-RS-001_0406.pdf.

[41] H. Wenzl, I. Baring-Gould, R. Kaiser, B. Yann Liaw, P. Lundsager, J. Manwell, A. Ruddell, and V. Svoboda, "Life prediction of batteries for selecting the technically most suitable and cost effective battery," *Journal of Power Sources,* vol. 144, pp. 373-384, 2005.

[42] Maxwell Technologies MC Power Series supercapacitor data sheet, 2008, available at http://www.maxwell.com/pdf/uc/datasheets/MC_Cell_Power_ 1009361_rev9.pdf.

[43] J. McDowall, "Lies, Damned Lies and Statistics: The Statistical Treatment of Battery Failures," in the Proceedings of Battcon, 2005, pp. 9.1-9.10

[44] G. Papazov and D. Pavlov, "Influence of cycling current and power profiles on the cycle life of lead/acid batteries," *Journal of Power Sources,* vol. 62, pp. 193-199, 1996.

[45] B. Culpin and D. Rand, "Failure modes of lead/acid batteries," *Journal of Power Sources,* vol. 36, pp. 415-438, 1991.

[46] B. Rachmanto, K. Nonami, K. Kuriyama, H. Shimazaki, T. Kagamiishi, and T. Moriya, "A Study on AMB Flywheel Powered Electric Vehicle," *Journal of System Design and Dynamics,* vol. 3, pp. 659-670, 2009.

[47] A. Folkesson, C. Andersson, P. Alvfors, M. Alakula, and L. Overgaard, "Real life testing of a Hybrid PEM Fuel Cell Bus," *Journal of Power Sources,* vol. 118, pp. 349-357, 2003.

[48] L. Egiziano, A. Giustiniani, G. Lisi, G. Petrone, G. Spagnuolo, and M. Vitelli, "Experimental characterization of the photovoltaic generator for a hybrid solar vehicle," in the Proceedings of IEEE International Symposium on Industrial Electronics, ISIE 2007, 2007, pp. 329-334

[49] R. Kotz, M. Bartschi, F. Buchi, R. Gallay, and P. Dietrich, "Hy-Power - A Fuel Cell Car Boosted with Supercapacitors," in the Proceedings of International Seminar on Double Layer Capacitors and Similar Energy Storage Devices, Deerfield Beach, USA, 2002,

[50] S. Nishikawa, M. Sasaki, A. Okazaki, S. Araki, T. Miyata, and M. Nishina, "Development of capacitor hybrid truck," *JSAE Review,* vol. 24, pp. 249-254, 2003.

[51] M. Ortuzar, "Design, Implementation and Evaluation of an Auxiliary Energy System for Electric Vehicles, Based on Ultracapacitors and Buck-Boost Converter," PhD Thesis, Pontificia Universidad Catolica de Chile, 2005.

[52] J. Dixon and M. Ortuzar, "Test Results with Regenerative Braking based on Ultracapacitors and a Buck-Boost Converter," in the Proceedings of Electric Vehicle Symposium 18, 2001, CD-ROM.

[53] J. Moreno, M. Ortuzar, and J. Dixon, "Energy-Management System for a Hybrid Electric Vehicle, Using Ultracapacitors and Neural Networks," *IEEE Transactions on Industrial Electronics,* vol. 53, pp. 614-623, April 2006.

[54] J. Dixon, M. Ortuzar, R. Schmidt, G. Lazo, I. Leal, F. Garcia, M. Rodriguez, A. Amaro, and E. Wiechmann, "Performance Characteristics of the First, State-of-the-art Electric Vehicle Implemented in Chile," in the Proceedings of Electric Vehicle Symposium 17, 2000, CD-ROM.

[55] J. Dixon, M. Ortuzar, E. Arcos, and I. Nakashima, "ZEBRA plus ultracapacitors: A good match for energy efficient EVs," in the Proceedings of Electric Vehicle Symposium 21, 2005, CD-ROM.

[56] B. Arnet and L. Haines, "Combining Ultra-Capacitors with Lead-Acid Batteries," in the Proceedings of Electric Vehicle Symposium 17, 2000, CD-ROM.

[57] G. Wight, H. Garabedian, B. Arnet, and J.-F. Morneau, "Integration and Testing of a DC/DC Controlled Supercapacitor into an Electric Vehicle," in the Proceedings of Electric Vehicle Symposium 18, 2001, CD-ROM.

[58] P. Angers, "Supercapacitors - do they improve battery life?," in the Proceedings of Electric Vehicle Symposium 21, 2005, CD-ROM.

[59] Wight, Jung, and Garabedian, "On-Road and Dynamometer Testing of a Capacitor-Equipped Electric Vehicle," in the Proceedings of Electric Vehicle Symposium 19, 2002, CD-ROM.

[60] J. Lott and H. Spath, "Double Layer Capacitors as additional Power Source in Electric Vehicles," in the Proceedings of Electric Vehicle Symposium 18, 2001, CD-ROM.

[61] L. Rosario and P. Luk, "Implementation of a Modular Power and Energy Management Structure for Battery-Ultracapacitor Powered Electric Vehicles," in the Proceedings of Hybrid Vehicle Conference, 2006, pp. 141-156

[62] L. Rosario, "Power and Energy Management of Multiple Energy Storage Systems in Electric Vehicles," PhD Thesis, Cranfield University, 2007.

[63] Y.-P. Yang, J.-J. Liu, T.-J. Wang, K.-C. Kuo, and P.-E. Hso, "An Electric Gearshift With Ultracapacitors for the Power Train of an Electric Vehicle With a Directly Driven Wheel Motor," *IEEE Transactions on Vehicular Technology,* vol. 56, pp. 2421-2431, Sept 2007.

[64] Y.-P. Yang and T.-H. Hu, "A New Energy Management System of Directly-Driven Electric Vehicle with Electronic Gearshift and Regenerative Braking," in the Proceedings of American Control Conference, New York City, USA, 2007, pp. 4419-4424

[65] S. Colton, "A Simple Series Battery/Ultracapacitor Drive System for Light Vehicles and Educational Demonstration," in the Proceedings of Ecological Vehicles, Renewable Energies: EVER 2009, Monaco, 2009, pp. 1-10

[66] "Electric Green Racing," University of Manchester, online final project video, 2007, available at http://www.eee.manchester.ac.uk/undergraduate/courses/specialfeatures/fourthyearproject/Electric_Green_Racing_medium.wmv, accessed on 15 Jan. 2010.

[67] J.-M. Timmermans, P. Zadora, Y. Cheng, J. Van Mierlo, and P. Lataire, "Modelling and Design of Super Capacitors as Peak Power Unit for Hybrid Electric Vehicles," in the Proceedings of IEEE Vehicle Power and Propulsion Conference, 2005, pp. 701-708

[68] E. Faggioli, P. Rena, V. Danel, X. Andrieu, R. Mallant, and H. Kahlen, "Supercapacitors for the energy management of electric vehicles," *Journal of Power Sources,* vol. 84, pp. 261-269, 1999.

[69] G. Guidi, T. M. Undeland, and Y. Hori, "Effectiveness of Supercapacitors as Power-Assist in Pure EV Using a Sodium-Nickel Chloride Battery as Main Energy Storage," in the Proceedings of Electric Vehicle Symposium 24, Stavanger, Norway, 2009, CD-ROM.

[70] P. Barrade and A. Rufer, "The use of supercapacitors for energy storage in traction systems," in the Proceedings of IEEE Vehicle Power and Propulsion Conference, 2004,

[71] G. Wight, "Integration and Testing of a DC/DC Controlled Supercapacitor into an Electric Vehicle - Final Report," 2002, available at http://www.evermont.org/ProjectReports/ITDCSFinalReport.pdf., accessed on March 27, 2009.

[72] J. Trovao, P. Pereirinha, and H. Jorge, "Design Methodology of Energy Storagr Systems for a Small Electric Vehicle," in the Proceedings of Electric Vehicle Symposium 24, Stavanger, Norway, 2009, CD-ROM.

[73] F. Rafik, H. Gualous, R. Gallay, M. Karmous, and A. Berthon, "Contribution to the sizing of supercapacitors and their applications," in the Proceedings of 1st European Symposium on Supercapacitors and Applications (ESSCAP 2004), Belfort, France, 2004,

[74] J. M. Miller, P. J. McCleer, M. Everett, and E. G. Strangas, "Ultracapacitor Plus Battery Energy Storage System Sizing Methodology for HEV Power Split Electronic CVTs," in the Proceedings of IEEE International Symposium on Industrial Electronics, Dubrovnik, Croatia, 2005, pp. 317-324

[75] S. Bontour, D. Hissel, H. Gualous, F. Harel, and J. M. Kauffmann, "Design of a parallel fuel cell-supercapacitor auxiliary power unit (APU)," in the Proceedings of the Eight International Conference on Electrical Machines and Systems, 2005, vol. 2, pp. 911-915

[76] C. R. Akli, X. Roboam, B. Sareni, and A. Jeunesse, "Energy management and sizing of a hybrid locomotive," in the Proceedings of European Conference on Power Electronics and Applications, 2007, pp. 1-10

[77] D. Rotenberg, A. Vahidi, and I. Kolmanovsky, "Ultracapacitor Assisted Powertrains: Modeling, Control, Sizing, and The Impact on Fuel Economy," in the Proceedings of American Control Conference, Seattle, Washington, USA, 2008, pp. 981-987

[78] R. Schupbach and J. Balda, "Comparing DC-DC Converters for Power Management in Hybrid Electric Vehicles," in the Proceedings of Electric Machines and Drives Conference, 2003, vol. 3, pp. 1369-1374

[79] S. Dwari and L. Parsa, "A Novel High Efficiency High Power Interleaved Coupled-Inductor Boost DC-DC Converter for Hybrid and Fuel Cell Electric Vehicle," in the Proceedings of Vehicle Power and Propulsion Conference, 2007, pp. 399-404

[80] K. Wang, C. Y. Lin, L. Zhu, D. Qu, F. C. Lee, and J. S. Lai, "Bi-directional DC to DC converters for fuel cell systems," in the Proceedings of Power Electronics in Transportation, Dearborn, MI, USA, Oct. 1998, pp. 47-51

[81] R. Sickel, D. Vetters, H. Mehlich, M. Bodach, T. Bocklisch, and J. Lutz, "Modular converter for fuel cell systems with buffer storage," in the Proceedings of 2005 European Conference on Power Electronics and Applications, Dresden, Germany, 2005, pp. P.1-P.9

[82] Z. Cerovsky and V. Pavelka, "DC-DC Converter for charging and discharging super-capacitors used in electric hybrid cars," in the Proceedings of 10th European Conference on Power Electronics and Applications, Toulouse, France, 2003, CD-ROM.

[83] P. Thounthong, S. Rael, and B. Davat, "Utilizing fuel cell and supercapacitors for automotive hybrids electrical system," in the Proceedings of Applied Power Electronics Conference and Exposition (APEC 2005), Austin, TX, 2005, vol. 1, pp. 90-96

[84] B. Taylor, A. Brown, D. Stone, and N. Schofield, "A High Power DC-DC Converter, Employing Synchronous Rectification of Parallel MOSFET Devices, for use as an Electric Vehicle Battery-to-Supercapacitor Interface " in the Proceedings of 10th European Conference on Power Electronics and Applications, Toulouse, France, 2003, CD-ROM.

[85] J. Silvestre, "Half-bridge bidirectional DC-DC converter for small electric vehicle," in the Proceedings of International Symposium on Power Electronics, Electrical Drives, Automation and Motion (SPEEDAM), 2008, vol. Session TA4: Electric Vehicle Drives, pp. 884-888

[86] L. Solero, A. Lidozzi, and J. Pomilio, "Design of Multiple-Input Power Converter for Hybrid Vehicles," *IEEE Transactions on Power Electronics,* vol. 20, pp. 1007-1016, Sept 2005.

[87] D. Heinemann, D. Naunin, and G. Petsch, "Ultracaps in power-assist applications in Battery Powered Electric Vehicles - Implications on Energy Management Systems," in the Proceedings of Electric Vehicle Symposium 18, 2001, CD-ROM.

[88] S. M. Lukic, S. G. Wirasingha, F. Rodriguez, J. Cao, and A. Emadi, "Power Management of an Ultracapacitor/Battery Hybrid Energy Storage System in an HEV," in the Proceedings of Vehicle Power and Propulsion Conference, 2006, pp. 1-6

[89] NREL, "Advisor 2002 - A Powerful Vehicle Simulation Tool Gets Better," 2002, available at http://www.nrel.gov/news/press/2002/2102_advisor_tool .html, accessed on 25 May 2010.

[90] K. Wipke, M. Cuddy, and S. Burch, "ADVISOR 2.1: A User-Friendly Advanced Powertrain Simulation Using a Combined Backward/Forward Approach," *IEEE Transactions on Vehicular Technology,* vol. 48, pp. 1751-1761, 1999.

[91] A. Burke and M. Miller, "Electrochemical Capacitors as Energy Storage in Hybrid-Electric Vehicles: Present Status and Future Prospects," in the Proceedings of Electric Vehicle Symposium 24, Stavanger, Norway, 2009, CD-ROM.

[92] R. Schupbach and J. Balda, "The Role of Ultracapacitors in an Energy Storage Unit for Vehicle Power Management," in the Proceedings of Vehicular Technology Conference, 2003, vol. 5, pp. 3236-3240

[93] C. Maxoulis, D. Tsinoglou, and G. Koltsakis, "Modeling of automotive fuel cell operation in driving cycles," *Energy Conversion and Management,* vol. 45, pp. 559-573, 2004.

[94] M. Panagiotidis, G. Delagrammatikas, and D. Assanis, "Development and Use of a Regenerative Braking Model for a Parallel Hybrid Electric Vehicle," in the Proceedings of Society of Automotive Engineers 2000 World Congress, Detroit, MI, March 2000, SAE Technical Paper Number 2000-01-0995.

[95] J. Van Mierlo and G. Maggetto, "Innovative Iteration Algorithm for a Vehicle Simulation Program," *IEEE Transactions on Vehicular Technology,* vol. 53, March 2004.

[96] L. U. Gokdere, K. Benlyazid, R. A. Dougal, E. Santi, and C. W. Brice, "A virtual prototype for a hybrid electric vehicle," *Mechatronics,* vol. 12, pp. 575-593, 2002.

[97] A. Schneuwly, V. Hermann, and R. Gallay, "High Performance Double-layer Capacitor for Automotive Applications," in the Proceedings of Electric Vehicle Symposium 18, 2001, CD-ROM.

[98] J. Schiffer, D. Linzen, and D. Sauer, "Heat generation in double layer capacitors," *Journal of Power Sources,* vol. 160, pp. 765-772, 2006.

[99] F. Belhachemi, S. Rael, and B. Davat, "A physical based model of power electric double-layer supercapacitors," in the Proceedings of Industry Applications Conference, 2000, vol. 5, pp. 3069-3076

[100] R. De Levie, "On Porous Electrodes in Electrolyte Solutions," *Electrochimica Acta,* vol. 8, pp. 751-780, 1963.

[101] W. Pell, B. Conway, W. Adams, and J. de Oliveira, "Electrochemical efficiency in multiple discharge/recharge cycling of supercapacitors in hybrid EV applications," *Journal of Power Sources,* vol. 80, pp. 134-141, 1999.

[102] R. Bonert and L. Zubieta, "Measurement Techniques for the Evaluation of Double-Layer Power Capacitors," in the Proceedings of Industry Applications Conference, 1997, pp. 1097-1100

[103] J. R. Miller and A. F. Burke, "Electric Vehicle Capacitor Test Procedures Manual," U.S. Department of Energy, DOE/ID-10491, 1994, available at http://avt.inl.gov/battery/pdf/ultracap_test_procedures_manual_10_94.pdf.

[104] L. Zubieta and R. Bonert, "Characterization of Double-Layer Capacitors for Power Electronics Applications," *IEEE Transactions on Industry Applications,* vol. 36, pp. 199-205, Jan/Feb 2000.

[105] H. Gualous, D. Bouquain, A. Berthon, and J. Kauffman, "Experimental study of supercapacitor serial resistance and capacitance variations with temperature," *Journal of Power Sources,* vol. 123, pp. 86-93, 2003.

[106] R. A. Dougal, L. Gao, and S. Liu, "Ultracapacitor model with automatic order selection and capacity scaling for dynamic system simulation," *Journal of Power Sources,* vol. 126, pp. 250-257, 2004.

[107] W. Lajnef, J.-M. Vinassa, S. Azzopardi, O. Briat, E. Woirgard, C. Zardini, and J. L. Aucouturier, "Ultracapacitors Modeling Improvement Using an Experimental Characterization Based on Step and Frequency Responses," in the Proceedings of Power Electronics Specialist Conference, 2004, pp. 131-143

[108] S. Buller, E. Karden, D. Kok, and R. W. DeDoncker, "Modeling the Dynamic Behavior of Supercapacitors Using Impedance Spectroscopy," in the Proceedings of Industry Applications Conference, 2001, vol. 4, pp. 2500-2504

[109] S. Buller, E. Karden, D. Kok, and R. W. DeDoncker, "Simulation of Supercapacitors in highly dynamic Applications," in the Proceedings of Electric Vehicle Symposium 18, 2001, CD-ROM.

[110] P. J. Mahon, G. L. Paul, S. M. Keshishian, and A. M. Vassallo, "Measurement and modelling of the high-power performance of carbon-based supercapacitors," *Journal of Power Sources,* vol. 91, pp. 68-76, 2000.

[111] R. L. Spyker and R. M. Nelms, "Classical Equivalent Circuit Parameters for a Double-Layer Capacitor," *IEEE Transactions on Aerospace and Electronic Systems,* vol. 36, pp. 829-836, July 2000.

[112] W. Lajnef, J.-M. Vinassa, S. Azzopardi, O. Briat, A. Guedon-Gracia, and C. Zardini, "First step in the reliability assessment of ultracapacitors used as power source in hybrid electric vehicles," *Microelectronics Reliability,* vol. 44, pp. 1769-1773, 2004.

[113] J.-N. Marie-Francoise, H. Gualous, and A. Berthon, "Supercapacitor thermal- and electrical-behaviour modelling using ANN," *IEE Proceedings - Electric Power Applications,* vol. 153, pp. 255-262, March 2006.

[114] F. Rafik, H. Gualous, R. Gallay, A. Crausaz, and A. Berthon, "Frequency, thermal and voltage supercapacitor characterization and modeling," *Journal of Power Sources,* 2007.

[115] R. Kotz, M. Hahn, and R. Gallay, "Temperature behavior and impedance fundamentals of supercapacitors," *Journal of Power Sources,* vol. 154, pp. 550-555, 2006.

[116] Epcos supercapacitor information data sheet, 2006, available at http://www.epcos.com/web/generator/Web/Sections/ProductCatalog/Capacitors/Ultracapacitors/PDF/PDF__UltraCapTechnology,property=Data__en.pdf;/PDF_UltraCapTechnology.pdf, accessed in 2006. No longer available.

[117] W. Lajnef, J.-M. Vinassa, O. Briat, and E. Woirgard, "Specification and use of pulsed current profiles for ultracapacitors power cycling," *Microelectronics Reliability,* vol. 45, pp. 1746-1749, 2005.

[118] N. Rizoug, P. Bartholomeus, B. Vulturescu, P. L. Moigne, and X. Pierre, "Voltage sharing in supercapacitor modules: experimental study," in the Proceedings of Power Electronics Specialists Conference, Aachen, Germany, 2004, vol. 1, pp. 690-696

[119] D. Linzen, S. Buller, E. Karden, and R. W. DeDoncker, "Analysis and Evaluation of Charge-Balancing Circuits on Performance, Reliability, and Lifetime of Supercapacitor Systems," *IEEE Transactions on Industry Applications,* vol. 41, pp. 1135-1141, Sept/Oct 2005.

[120] R. L. Spyker and R. M. Nelms, "Analysis of Double-Layer Capacitors Supplying Constant Power Loads," *IEEE Transactions on Aerospace and Electronics Systems,* vol. 36, pp. 1439-1443, Oct 2000.

[121] R. L. Spyker and R. M. Nelms, "Optimization of Double-Layer Capacitor Arrays," *IEEE Transactions on Industry Applications,* vol. 36, pp. 194-198, Jan/Feb 2000.

[122] R. G. Wiegers, D. M. Blackketter, and H. L. Hess, "Modelling performance of ultracapacitor arrays in hybrid electric vehicles," *International Journal of Alternative Propulsion,* vol. 1, pp. 32-46, 2006.

[123] T. R. Crompton, *Battery Reference Book: Third Edition*, ISBN: 978-0-7506-4625-3, Oxford, Newnes, 2000.

[124] M. Fogiel, *Basic Electricity*, 2004 ed., ISBN: 0-87891-420-X, Piscataway, New Jersey, Research and Education Association, 2002.

[125] S.-i. Tobishima, K. Takei, Y. Sakurai, and J.-i. Yamaki, "Lithium ion cell safety," *Journal of Power Sources,* vol. 90, pp. 188-195, 2000.

[126] S. W. Moore and P. J. Schneider, "A Review of Cell Equalization Methods for Lithium Ion and Lithium Polymer Battery Systems," Society of Automotive Engineers, SAE 2001-01-0959, 2001.

[127] V. H. Johnson, "Battery performance models in ADVISOR," *Journal of Power Sources,* vol. 110, pp. 321-329, 2002.

[128] H. L. Chan and D. Sutanto, "A new battery model for use with battery energry storage systems and electric vehicles power systems," in the Proceedings of Power Engineering Society Winter Meeting, 2000, vol. 1, pp. 470-475

[129] M. Durr, A. Cruden, S. Gair, and J. McDonald, "Dynamic model of a lead acid battery for use in a domestic fuel cell system," *Journal of Power Sources,* vol. 161, pp. 1400-1411, 27 Oct 2006.

[130] M. Pasquali, M. Ceraolo, and V. Sglavo, "Modeling and Test on E.V. Lead-Acid Batteries," in the Proceedings of Electric Vehicle Symposium 18, 2001, CD-ROM.

[131] E. Karden, P. Mauracher, and F. Schope, "Electrochemical modelling of lead/acid batteries under operating conditions of electric vehicles," *Journal of Power Sources,* vol. 64, pp. 175-180, 1997.

[132] E. Barsoukov, J. H. Kim, C. O. Yoon, and H. Lee, "Universal battery parameterization to yield a non-linear equivalent circuit valid for battery simulations at arbitrary load," *Journal of Power Sources,* vol. 83, pp. 61-70, 1999.

[133] A. J. Salkind, "Lead-Acid Batteries," in *Handbook of Batteries: Third Edition*, D. Linden and T. Reddy, Eds. London: McGraw-Hill, 2002, pp. 23.6-23.7.

[134] B. S. Bhangu, P. Bentley, D. A. Stone, and C. M. Bingham, "Nonlinear Observers for Predicting State-of-Charge and State-of-Health of Lead-Acid Batteriers for Hybrid-Electric Vehicles," *IEEE Transactions on Vehicular Technology,* vol. 54, pp. 783-794, May 2005.

[135] J. Schiffer, D. U. Sauer, H. Bindner, T. Cronin, P. Lundsager, and R. Kaiser, "Model prediction for ranking lead-acid batteries according to expected lifetime in renewable energy systems and autonomous power-supply systems," *Journal of Power Sources,* vol. 168, pp. 66-78, 2007.

[136] S. Drouilhet and B. L. Johnson, "A Battery Life Prediction Method for Hybrid Power Applications," in the Proceedings of 35th AIAA Aerospace Sciences Meeting and Exhibit, 1997, pp. NREL/CP-440-21978

[137] C. C. Chan, E. W. C. Lo, and S. Weixiang, "The available capacity computation model based on artificial neural network for lead-acid batteries in electric vehicles," *Journal of Power Sources,* vol. 87, pp. 201-204, 2000.

[138] D. U. Sauer, "Modelling of local conditions in flooded lead/acid batteries in photovoltaic systems," *Journal of Power Sources,* vol. 64, pp. 181-187, 1997.

[139] P. Singh, C. Fennie, and D. Reisner, "Fuzzy logic modelling of state-of-charge and available capacity of nickel/metal hydride batteries," *Journal of Power Sources,* vol. 136, pp. 322-333, 2004.

[140] G. Randolf, "Final Report of the Battery Life Extension Experiment," University of Hawaii and Hawaii Electric Vehicle Demonstration Project, Honolulu, HI, , Spring 1999.

[141] MES-DEA AC Induction Motor data sheet, 2006, available at http://www.atea.it/pdf/AC-Induction-motors.pdf.

[142] "AC Induction Motor Drive Type VPA 200-400 User Manual," MES-DEA, April 1999.

[143] M. Kiel, O. Bohlen, and D. U. Sauer, "Harmonic analysis for identification of nonlinearities in impedance spectroscopy," *Electrochimca Acta,* vol. 53, pp. 7367-7374, 2008.

[144] EnerSys-Hawker Lifeplus TC3 Battery Charger data sheet, 2010, available at http://www.enersys-hawker.com/pdf/td/hf_e_td.pdf.

[145] R. Kaushik and I. G. Mawston, "Coulombic efficiency of lead/acid batteries, particularly remote-area power-supply (RAPS) systems," *Journal of Power Sources,* vol. 35, pp. 377-383, 1991.

[146] Testec Elektronik GmbH 25MHz Differential Probe data sheet, 2003, available at http://www.testec.de/DL/TT/MA/SI9002_EN.PDF.

[147] Tenma AC/DC Current Clamp data sheet, 2000, available at http://www.farnell.com/datasheets/80732.pdf.

[148] Tektronix TDS2000B Series Digital Storage Oscilloscopes data sheet, 2009, available at http://www2.tek.com/cmsreplive/psrep/13295/3GW_19558_2_2009.10.13.16.21.12_13295_EN.pdf.

[149] J. M. Miller, *Propulsion Systems for Hybrid Vehicles*, ISBN: 0-86341-336-6, Bodmin, Cornwall, MPG Books Limited, 2004.

[150] Y. Gao, L. Chen, and M. Ehsani, "Investigation of the Effectiveness of Regenerative Braking for EV and HEV," Society of Automotive Engineers, SAE 1999-01-2910, 1999.

[151] C. Ashtiani, R. Wright, and G. Hunt, "Ultracapacitors for automotive applications," *Journal of Power Sources,* vol. 154, pp. 561-566, 2006.

[152] Nesscap Co., Ltd. Ultracapacitor Products data sheet, 2008, available at http://www.nesscap.com/.

[153] batScap Supercapacitors data sheet, 2007, available at www.batscap.com (upon request from company).

[154] Nippon Chemi-Con Corporation DLCAP: Electric Double Layer Capacitors data sheet, 2006, available at http://www.chemi-con.co.jp/e/catalog/dl.html.

[155] Epcos UltraCap data sheet, 2006, no longer available.

[156] Delucchi and Lipman, "An analysis of the retail and lifecycle cost of battery-powered electric vehicles," *Transportation Research Part D,* vol. 6, pp. 371-404, 2001.

[157] Vishay BC Components Aluminum Capacitors: Power High Ripple Current Screw Terminals data sheet, 2010, available at http://www.farnell.com/datasheets/314432.pdf.

[158] Farnell UK Vishay Electrolytic Capacitor, 4700uF, 200V, Part no. 8820970 data sheet, 2009, available at http://uk.farnell.com/vishay-bc-components/222210222472/capacitor-4700uf-200v/dp/8820970?Ntt= 8820970.

[159] RS Components Dual IGBT 300A, 600V, 2MBi300U2B-060-50 data sheet, 2009, available at http://uk.rs-online.com/web/search/searchBrowseAction .html?method=getProduct&R=0462871.

[160] Planet Engineers Flat Magnet Wire, AWG 128x256H data sheet, 2009, available at http://www.planetengineers.com/product.asp?pid=916.

[161] H. A. Wheeler, "Simple Inductance Formulas for Radio Coils," *Proceedings of the Institute of Radio Engineers,* vol. 16, pp. 1398-1400, 1928.

[162] B. W. Williams, *Principles and Elements of Power Electronics: Devices, Drivers, Applications, and Passive Components* ISBN: 978-0-9553384-0-3, available at http://homepages.eee.strath.ac.uk/~bwwilliams/Book/Title%20 page,%20toc,%20and%20preface.pdf, 2006.

Appendix A: The Operation of Half Bridge Converters

This appendix will briefly describe the operation and control of a half-bridge DC-DC converter, as shown in Figure A.1. Details of half-bridge converter operation may be found in reference [162], and descriptions of the use of such converters in battery/supercapacitor electric vehicles may be found in references [51, 62].

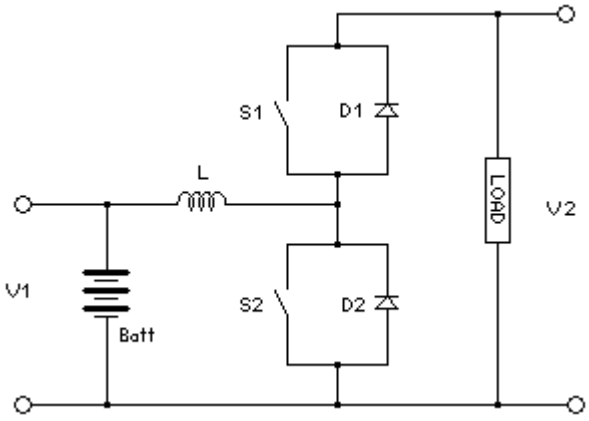

Figure A.1: A half-bridge DC-DC converter.

The half-bridge converter is also known as a 'buck-boost' converter, because power may flow either from V1 to V2 (boost) or from V2 to V1 (buck). When operating in boost mode, switch S1 remains open while switch S2 is operated to control the current flow, as illustrated in Figure A.2.

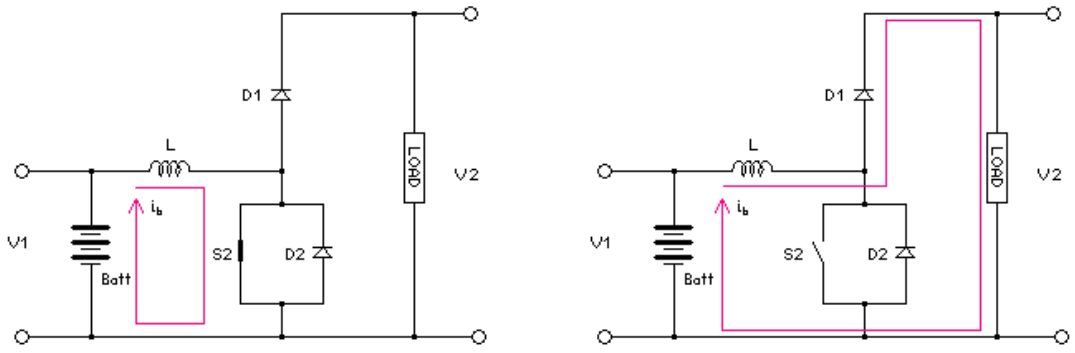

Figure A.2: Current flow in the half-bridge converter in boost mode as switch S2 is closed and opened.

When switch S2 is closed:

$$V1 = L\frac{di_b}{dt} \tag{A-1}$$

S2 will switch at a certain frequency f, and during each time period $1/f$ it will have a duty cycle δ_{S2}, which is a number between 0 and 1, representing the fraction of the time that the switch is shut. Thus the switch will be closed for a time period of δ_{S2}/f, and Equation A-1 may be rewritten as:

$$\begin{aligned} &V1 = L\frac{\Delta i_b}{\delta_{S2}} f \\ &\Rightarrow V1 * \delta_{S2} = L * \Delta i_b * f \end{aligned} \tag{A-2}$$

When switch S2 is open, then:

$$V1 + L\frac{di_b}{dt} = V2 \tag{A-3}$$

Since the switch will be open for a time period of $(1-\delta_{S2})/f$, Equation A-3 may be expressed as:

$$\begin{aligned} &V1 + L\frac{\Delta i_b}{(1-\delta_{S2})} f = V2 \\ &\Rightarrow (V2 - V1) * (1-\delta_{S2}) = L * \Delta i_b * f \end{aligned} \tag{A-4}$$

Assuming the inductor current is continuous (which is to say that the current is always greater than 0), then Δi_b in equations A-2 and A-4 are equivalent, and the two equations may be set equal to each other:

$$\begin{aligned} &V1 * \delta_{S2} = (V2 - V1) * (1-\delta_{S2}) \\ &\Rightarrow \frac{V2}{V1} = \frac{1}{1-\delta_{S2}} \end{aligned} \tag{A-5}$$

Similarly, when operating in buck mode, switch S1 is used and switch S2 is kept open, as illustrated in Figure A.3.

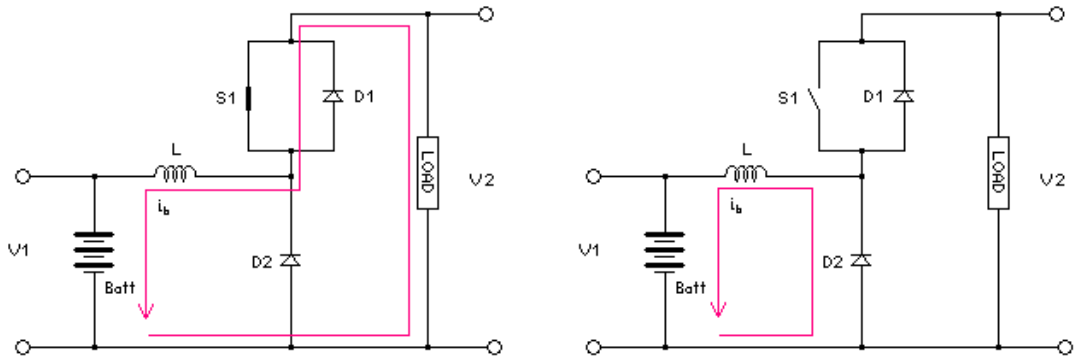

Figure A.3: Current flow in the half-bridge converter in buck mode as switch S1 is closed and opened.

When switch 1 is closed:

$$V2 = L\frac{di_b}{dt} + V1 \tag{A-6}$$

Switch 1 will typically operate at the same frequency f as switch 2, with duty cycle δ_{S1}. Therefore:

$$V2 = L\frac{\Delta i_b}{\delta_{S1}} f + V1$$

$$\Rightarrow (V2 - V1) * \delta_{S1} = L * \Delta i_b * f \tag{A-7}$$

Similarly, when S1 is open:

$$V1 = L\frac{di_b}{dt} \tag{A-8}$$

Given that the switch will be open for a time period $(1-\delta_{S1})/f$, Equation A-8 becomes:

$$V1 = L\frac{\Delta i_b}{(1-\delta_{S1})} f$$

$$\Rightarrow V1 * (1-\delta_{S1}) = L * \Delta i_b * f \tag{A-9}$$

As with the boost case, Equations A-7 and A-9 may be equated to give the relationship between V1 and V2:

$$V1*(1-\delta_{S1}) = (V2-V1)*\delta_{S1}$$

(A-10)

$$\Rightarrow \frac{V2}{V1} = \frac{1}{\delta_{S1}}$$